SITE-SPECIFIC PHOSPHORYLATION OF HISTONE H1 ASSOCIATED WITH CELL CYCLE PROGRESSION AND TRANSCRIPTION

BY

YUPENG ZHENG

DISSERTATION

Submitted in partial fulfillment of the requirements
for the degree of Doctor of Philosophy in Cell and Developmental Biology
in the Graduate College of the
University of Illinois at Urbana-Champaign, 2010

Urbana, Illinois

Doctoral Committee:

Professor Andrew Belmont, Chair
Assistant Professor Craig Mizzen, Director of Research
Associate Professor Michel Bellini
Assistant Professor Peter Jones
Professor David Shapiro

ABSTRACT

Histone H1 phosphorylation is thought to affect chromatin condensation and function, but few details are known about the impact of H1 variant-specific phosphorylation in higher eukaryotes. Using novel proteomic approaches, we directly demonstrate that specific sites in the two dominant H1 variants of HeLa S3 cells are phosphorylated either exclusively during mitosis or during both interphase and mitosis. Interphase H1 phosphorylation in HeLa S3 cells is abundant and remarkably hierarchical, contrary to evidence that sites are used fortuitously during the cell cycle. Analyses with antisera to individual H1.2 and H1.4 interphase phosphorylations reveal that they are distributed throughout nuclei but appear to be particularly enriched in nucleoli. Chromatin immunoprecipitation analyses reveal that interphase phosphorylated H1.4 is enriched at active rDNA promoters and is rapidly induced at steroid hormone response elements by hormone treatment. Our results imply that site-specific interphase H1 phosphorylation facilitates transcription by RNA polymerases I and II, and has an unanticipated function in ribosome biogenesis and the control of cell growth. In contrast to histone modifications enriched at gene regulatory regions, site-specific interphase H1 phosphorylation is enriched within the body and the regulatory elements of transcribed genes. Our data suggest CDK8 and CDK9, kinases with known association with the transcriptional machinery, as candidates that could account for this distribution of interphase H1 phosphorylation. Comparative analyses of H1 variant expression and phosphorylation in different human cell lines reveal that H1.3 is significantly less phosphorylated during interphase relative to other H1 variants in the cell lines tested. Analyses of the phosphorylation of site-specific H1 mutants ectopically expressed in human cells identified features of H1.3 that lead to its underphosphorylation. Together these results suggest that differences in interphase phosphorylation may contribute to the functional diversity of H1 variants.

I dedicate the work described herein to my beloved wife and son, Fang and Ethan.
Their unfaltering encouragement makes all of this possible.

ACKNOWLEDGEMENTS

First, I would like to express m gratitude to my thesis advisor, Dr. Craig Mizzen, for his constant support, encouragement and being a great mentor to me over my graduate career. I would also like to thank him for giving me the opportunity to pursue a very interesting question using an interdisciplinary approach. Without his insightful advice and invaluable guidance, my graduate study would not have been as satisfying or as productive.

I would like to thank the members of my thesis committee. First, Dr. Andrew Belmont for his advice, discussion and help, and the remainder of my committee, Dr. Michel Bellini, Dr. Peter Jones and Dr. David Shapiro for their advice, guidance and encouragement throughout my graduate studies. I am also grateful for the generosity of Dr. Neil Kelleher for providing access to his lab's FTMS instrument and training in mass spectrometry.

I am also deeply indebted to the members of the Mizzen Lab, past and present, for their friendship and support. I would like express my gratitude to Dr. James Pesavento, Dr. Hongbo Yang and Kuei-Yang Hsiao for their support, critical discussion, sharing ideas and reagents, and above all for their friendship.

Finally, I would especially like to thank my family for their love, support, faith, and endless patience throughout my graduate study. I could not have accomplished this work without them.

TABLE OF CONTENTS

CHAPTER 1

INTRODUCTION

1.1 Nucleosome

Eukaryotic cells are faced with the challenge of packing their genomic DNA, more than a meter long in the case of humans, into nuclei with average diameters of only a few microns. The association of DNA with histones in nucleosomes and the higher order folding of nucleosomal filaments in chromatin provides the degree of compaction necessary to achieve this and constitutes the basis by which portions of the genome are selectively made accessible for transcription and other DNA-templated processes. The nucleosome is composed of 146 bp DNA wrapped in 1.7 left-handed superhelical turns around an octamer formed by two histone H2A-H2B heterodimers and one H3-H4 tetramer. A molecule of histone H1, also termed as linker histone, binds DNA on the outer surface of the nucleosome at the point where the entering and exiting strands meet. The binding of H1 is thought to both "seal" the nucleosome and to enable the reversible folding of extended 10 nm or "beads-on-a-string", transcriptionally active chromatin fibers into the 30 nm, transcriptionally inactive chromatin fibers that comprise the bulk form of chromatin in interphase nuclei (Khorasanizadeh, 2004; Oudet et al., 1975).

Members of the H1 family in higher eukaryotic cells, including extreme variants such as H5 found in avian erythrocytes, possess a tripartite structure with a globular domain flanked by less structured N- and C-terminal tails. In particular, the vey long C-terminal tail comprising almost half of the protein is highly basic with abundant lysines and arginines. Unlike the conserved core histones, histone H1 is more divergent across species. The putative H1 called Hho1p in *s. cerevisiae* possesses two globular domains whereas H1 in *tetrahymena* lacks globular domain (Mizzen et al., 1999; Schafer et al., 2005). This structure discrepancy leads to the debate that whether there is H1 counterparts in these two organisms.

Several crystal structures of nucleosome core particles have been obtained from reconstituted nucleosome containing human α-satellite DNA, which are able to form homogenous nucleosome particle (Harp et al., 2000; Luger et al., 1997). From these structure studies, we have learned that the core particles are formed by "handshake arrangement" through interaction between histone fold domains, consisting of three helix core domains. Besides the histone fold core, there are disordered N-terminal and C-terminal tails for each histone, which protrude beyond the nucleosome disk. Very importantly, these tails are ideal for numerous covalent modifications, also called post-translational modification (PTM), such as methylation, acetylation, ADP-ribosylation, ubiquitination and phosphorylation. As pointed out by Khorasanizadeh, the PTMs in the histones seem have no effect in the structure of nucleosome in higher eukaryotic cells (Khorasanizadeh, 2004). Interestingly, crystal structure of *s. cerevisiae* nucleosome core particle reveals yeast nucleosomes are likely to be subtly destabilized as compared with higher eukaryotic cells since the stabilizing interactions between H2A-H2B are absence in the H2A L1 loops area, which is consistent with the idea that much of the yeast genome remains open through much of its life cycle (White et al., 2001). It is worth noting that this weaker organization of nucleosomes in yeast might require the extra globular domain in putative linker histone for the properly compacting of 30 nm fiber.

1.2 30 nm Chromatin Filament

The 30 nm chromatin fiber is the secondary structure proposed for the hierarchy folding into the large scale configuration for the entire chromosome. Although the 30 nm fiber structure has not been seen in the whole nuclei, the facts that it can be assembled in vitro and visualized when chromatin is released from the nuclei by MNase (Micrococcal nuclease) digestion argue that the 30 nm fiber is a distinct secondary higher-order chromatin structure. Despite several models have been proposed for 30 nm folding, its

structure still remains elusive (Robinson and Rhodes, 2006; Staynov, 2008; Tremethick, 2007). As discussed by Dorigo *et al* (Dorigo et al., 2004), these models can be grouped into two classes: 1) the one-start helix, with the bent linker DNA connecting consecutive nucleosomes arranged in the same helix path, and 2) the two-start helix, based on straight linker DNA connecting between two adjacent stacks of helically arranged nucleosomes. Solenoid and zigzag are examples for one-start and two-start helix respectively. In solenoid model, six consecutive nucleosomes are arranged in a turn of a helix with a pitch of 11 nm (Finch and Klug, 1976). In zigzag model, histone H1 directs the formation of stem-like organization by juxtaposing the entering and exiting linker DNA segments, which in turn directs the arrangement of two rows of nucleosomes and the subsequent folding into the helix with linker DNA crisscrosses between each stack of nucleosomes (Bednar et al., 1998). In another word, consecutive nucleosomes are physically closer to each other in the one-start helix whereas alternative nucleosomes are closer to each other in the two-start helix.

To overcome the obstacle of structure determination for 30 nm fiber caused by the heterogeneity of native chromatin fiber, Richmond's lab reconstituted highly regular arrays on repeats of DNA sequence having nucleosome-positioning properties and has demonstrated two rows of 6 nucleosomes instead of a single stack of 12 nuclesomes were obtained from protein-protein crosslinked 12 nucleosome repeats, which supports the zigzag model (Dorigo et al., 2004). In addition, the crystal structure of the tetranucleosome they obtained further supports the zigzag conformation and demonstrated the axis of two rows of nucleosome stacks are not parallel but rotated by -71.3 degrees with each other and only the central linker DNA is straight (Schalch et al., 2005). More importantly, the same zigzag conformation was also demonstrated for the H1 containing nucleosome arrays by crosslinking and electron microscopy study (Dorigo et al., 2004). However, the diameter of chromatin fiber calculated from the model

building by stacking the tetranucleosome crystal structure is about 25 nm, which is smaller than expected for the 30 nm fiber. Rhodes' Lab has taken different approach to determine the structure of 30 nm fiber (Robinson et al., 2006; Routh et al., 2008). They also reconstituted nucleosome arrays on nucleosome-positioning sequence, but, in contrast to Richmond's lab, contained specialized chicken linker histone H5 and used different length of linker DNA. They proposed the interdigitated solenoid model based on the tight constraints obtained from the physical dimension and compact ratios measured in the EM images of series of arrays having different nucleosomal repeats lengths ranging from 177 to 237 bp with 10 bp increment. Very importantly, they found the diameter of folded fiber does not increase linearly with the length of the linker DNA as expected from the zigzag model. Fibers folded from 177-207 bp nucleosomal repeat length have diameter of 33-34 nm and compact ration of 11 nucleosomes per 11 nm, which are more closer to the native chromatin fiber (Woodcock et al., 1984). The authors suggested the different structure models reported from these two labs are likely caused by the presence of the linker histone. In addition, Staynov pointed out the zigzag conformation reported from Richmond lab might represent a special kind of chromatin structure originated from the telomeric yeast chromatin (Staynov, 2008). In summary, among several structures proposed for 30 nm chromatin fiber, interdigitated solenoid fiber is the only structure constructed so far with addition of histone H1, hence should more closely resemble its native structure.

1.3 Roles of Histone H1 in the Organization of 30 nm Chromatin Fiber

The idea of histone H1 facilitating the folding of 10 nm filament into 30 nm higher order structure has been suggested by numerous studies (Allan et al., 1981; Finch and Klug, 1976; Thoma et al., 1979). On the contrary, the fact that 30 nm fiber can also be achieved without the H1 to form the crystal seems argue against the essential role of H1 in the 30 nm fiber compaction (Dorigo et al., 2004; Schalch et al., 2005). However, it

has also been clearly demonstrated that inorganic cations and histone H1 are required to achieve full stability of condensed nucleosomal arrays (Carruthers et al., 1998).

The position of the H1 on the nucleosome has not been fully determined over the past three decades despite numerous efforts. DNase I footprinting results indicate H1 binds directly to the minor grove in the dyad and symmetrically protects the 10 bp linker DNA in the entering and exiting strands (Staynov, 2008; Staynov and Crane-Robinson, 1988). However this symmetric model proposed by Allan *et al*. (Allan et al., 1980) has been challenged by the crystal structure study of the globular domain of chicken histone H5 (GH5), which demonstrates globular domain is a three-helix bundle sharing structure homology with helix-turn-helix DNA-binding domain and there is only two instead of three DNA binding sites one would predict from symmetric model (Ramakrishnan et al., 1993). Fluorescence recovery after photobleaching (FRAP) is an invaluable technique to dissect the dynamic behavior of chromatin-binding proteins *in vivo*, the observed fluorescence recovery rate is a direct reflection of their chromatin interactions. Combined FRAP with systematic mutagenesis, Brown *et al.* have found globular domain of mouse histone $H1^0$ interacts with the nucleosomes through two distinct binding sites formed by several spatially clustered positively charged residues. By theoretical modeling, they further proposed that one site interacts with the major groove near the dyad axis and the second site interacts with the minor groove on the linker DNA (Brown et al., 2006). This slightly off-axis location reconciles the binding of minor grove predicted by DNAse I footprinting with binding of major groove in the DNA by helix-turn-helix domain. However, it can not explain the MNase digest experiment. If there are only two DNA binding sites in the globular domain, only one of the 10 bp linker DNA is bound and protected by globular domain in H1 while the other 10 bp linker should become accessible to the enzyme. Then why does MNase digestion of native chromatin only generate 147 and 168 bp without intermediate size fragment? The

answer might lie in the C-terminal domain (CTD) in H1. Biophysical analysis with series of CTD deletion mutants of mouse $H1^0$ using analytical ultracentrifugation has identify two specific subdomains in the CTD, which can stabilize the tertiary structure of reconstituted 12-nucleosome arrays (Lu and Hansen, 2004). Interestingly, both subdomains encompass one out of three cyclin-dependent kinase (CDK) phosphorylation motifs (S/TPXK) within the CTD and such S/TPXK motif can form a β-turn to bind the minor DNA groove (Lu and Hansen, 2004). Similar results have been obtained *in vivo* by FRAP techniques. The deletion of the entire CTD resulted in severe decrease of residence time of human H1.1, which suggests CTD also promotes H1-nucleosome binding. Interestingly, a single substitution of Thr152 (residing in S/TPXK motif) with glutamic acid reduced the affinity of H1 to chromatin to the same extent as deletion of all 70 CTD residues, whereas substitution of Ser183 with glutamic acid (residing in S/TPXK motif) elicited less dramatic effect (Hendzel et al., 2004). This result indicates the S/TPXK motifs in different part of molecule contribute differently to the binding of H1. Since serine and threonine in the S/TPXK motifs are the phosphorylation sites in H1, it is very likely that phosphorylation at different sites can modulate binding of H1 to chromatin differently. Taken these together, Brown *et al*. proposed a model for H1 binding in 30 nm fiber (Brown et al., 2006): First, the disordered H1 CTD captures linker DNA through efficient but nonspecific binding to linker DNA; second, this binding places the globular domain near the nucleosome and, perhaps promotes the stable and specific binding through one-dimensional scanning; third, stable globular binding then facilitate the acquisition of structure within the CTD, such as adopting an α-helical structure (Vila et al., 2001). However, more work has to be done in order to fully understand how H1 promotes the folding of chromatin.

1.4 H1 Variants and Potential Specific Roles

Multiple H1 family members are expressed in diverse organisms. Both human and mouse genomes contain up to 11 variants, including five DNA replication-dependent, non-allelic variants of H1 (H1.1, H1.2, H1.3, H1.4 and H1.5), together with the DNA replication-independent variant ($H1^0$, H1x), the testicular specific variants (H1t, H1T2 and HILS1) and the oocytic H1oo (Brown, 2003; Happel and Doenecke, 2009). The somatic variants of H1 (H1.1-H1.5) from mouse and human have been intensively studied. Among them, H1.1 is only found in thymus, testis, spleen, lymphocytic and neuronal cells in human (Parseghian and Hamkalo, 2001). In a survey for expression of variants in several human cell lines, no H1.1 mRNA was detected in most of the cell lines except a low level of H1.1 mRNA in human testis whereas H1.2 and H1.4 in all cells are expressed at a high level, indicating these two variants might be more important for human cells (Meergans et al., 1997).

Despite the heterogeneity of histone H1 in the same species, which mainly resides in the tails, the same variant among mammals is surprisingly conserved in both the globular domain and the tails. From evolution point of view, the sequence of H1 variants is moderately conserved among animal species with H1.4 possessing the most conserved structure (Ponte et al., 1998). More specifically, sequence comparison by ClustalW program finds 94% identity for H1.4 between human and mouse H1.4 compared with only 87% identify between H1.2 and H1.4 in human, two closest sequence-related variants. There is some evidence to support the idea that heterogeneity sequence of H1 variants result in some extent of functional distinction among them. For example, H1.5 but not H1.4 can be specifically recruited by interacting with Msx1, a key regulatory element of myogenic determination factor MyoD, and cooperate to inhibit muscle differentiation by turning off the expression of MyoD gene (Lee et al., 2004). In addition, both H1.5 and *Xenopus* H1C can repress Xmyf5, XmyoDa, and XmyoDb,

which is consistent with previous studies (Steinbach et al., 1997). Additional evidence for H1 variant specific function comes from the finings that H1.2 but not other variant is able to serve as cytochrome c-releasing factor which can transmit apoptotic signals arising from DNA damage to mitochondria (Konishi et al., 2003). It is remained puzzling that how cells distinguish newly synthesized H1.2 in cytoplasm from H1.2 leaking from DNA. One possibility is through the different modification, such as methylation, acetylation, ubiqutination and formylation, which has been identified through proteomic approach (Wisniewski et al., 2007).

One approach to study how H1 is associated with nucleosomal DNA is to compare the mononucleosome/chromatin binding affinity and chromatin compacting ability for different H1 variants. Although significant studies have been dedicated to answer this question, the conclusion remained elusive due to the discrepancies among different experiment schemes and labs as described below. First, comparison of various H1 variants purified from rat liver using gel retardation classified H1 variants into groups of high (H1.2, H1.3 and H1.4), intermediate (H1.1) and low (H1.5) binding affinity to mononucleosome (Talasz et al., 1998). Second, another *in vitro* study estimating the relative affinity between H1 variants purified from rat brain and SAR (scaffold-associated region) or the chromatin classified them into groups of high affinity (H1.3, H1.4 and $H1^0$), intermediate affinity (H1.5 and H1.2) and low affinity (H1.1) (Orrego et al., 2007). Third, the *in vivo* binding characteristic of H1 variants by FRAP study classified them into three groups of tight binding (H1.4 and H1.5), intermediary binding ($H1^0$ and H1.3) and weaker binding (H1.1 and H1.2) (Th'ng et al., 2005). Fourth, the comparison of H1-GFP variants ($H1^0$, H1.2, H1.3 and H1.5) in untreated and differentiated MEL cells demonstrated increase of residence time for all tested variants in differentiated cells and the H1.2 is the most weaker binding variants with residence time roughly half of other variants whereas no discernable difference been seen among other variants (Yellajoshyula

and Brown, 2006). Fifth and the most recent study of H1-mononucleosome affinity by band shift assay distinguishes three subgroups: high affinity variants, H1.5 and H1.4; intermediate affinity variants: H1.2, H1.3 and $H1^0$; and low affinity variants: H1.1 and H1x (Clausell et al., 2009).

In general, H1 variants' affinity for mononucleosome/chromatin correlates with their chromatin compacting properties. However, some exceptions exist and the difference among literature makes the conclusion elusive again. For example, H1.2 is reported as weakly aggregating variant in dinucleosome (Liao and Cole, 1981) and also shown as poorer condenser of chromatin compared to H1.1, H1.3, H1.4 and H1.5 (Khadake and Rao, 1995). In contrast, H1.5 was determined as the least whereas H1.1 as the strongest condenser for inducing aggregation of polynucleosome reconstituted from MMTV LTR promoter (Talasz et al., 1998). Moreover, the most recent study by atomic force microscopy has classified H1 variants as weak condenser (H1.1 and H1.2), intermediate condensers (H1.3) and strong condensers ($H1^0$, H1.4, H1.5 and H1x), which is more consistent with the findings from FRAP study (Clausell et al., 2009). Despite the discrepancies, all studies agree that H1.2 has low or intermediate while H1.4 has strongest affinity. Considering H1.2 and H1.4 are the most ubiquitous expressed forms in human cells, it suggests the different H1 variants might play some specific roles based in their affinity to chromatin and cells require at least two H1 variants with very different affinity to chromatin. Another approach to decipher the specific roles of H1 variants *in vivo* is to investigate the subnuclear localization of H1 variants (Parseghian et al., 1993). However it is impeded by the lack of H1 variant-specific antibodies. An alternative approach using GFP tagging has demonstrated $H1^o$, H1.1, H1.2 and H1.3 are commonly enriched in euchromatic regions, whereas H1.4 and H1.5 are preferentially localized to hetrochromatic regions (Th'ng et al., 2005).

1.5 H1 Phosphorylation

Cell Cycle Regulated H1 Phosphorylation

Histone H1 phosphorylation has been studied in various model organisms for over 40 years. Histone H1 purified from synchronized CHO cells were separated by ion exchange column. Incorporated rate of [^{32}P] phosphate / [^{3}H] lysine or electrophoresis was used to calculate how many phosphate per molecule and it has been determined that 1 phosphorylation in late G1, 3 phosphorylations in S/G2, and up to 6 phosphorylations in M phase (Hohmann et al., 1976). All of the phosphorylations in H1 are lost to the level below detectable level during telophase, thus resetting H1 to an unphosphorylated state at the beginning of the next cell cycle (Gurley et al., 1978). The more recent effort to compare the HPLC profile of tryptic phosphopeptides of H1 from synchronized CHO cells found three phosphopeptides in G1/S sample. Since only 1 phosphorylation has been observed at this cell cycle stage, it indicates that it is added to any one of the three interphase phosphorylation sites seen in S and G2. Thus, it does not appear to be an absolute order for which site is phosphorylated first, second and third during interphase (Gurley et al., 1995). This random phosphorylation is contradictory to the hierarchy of H1 phosphorylation discovered from phosphorylation sites mapping in ciliated protozoan *Tetrahymena thermophila*, where phosphorylation in H1 is added in a sequential fashion, first at Thr46, then at Ser42, and last at Ser44, (Mizzen et al., 1999).

How H1 phosphorylation progresses through cell cycle has also been investigated in HeLa S3 cells by metabolic labeling of synchronized cells with ^{32}P-orthophosphate. Both the percentage of phosphorylated H1 and the amount of phosphorylation sites increase from G1 to M phase. For major phosphorylation sites in H1.2, it starts from 0 in G1 phase, increases to 1 in S phase and reaches 3 or 4 in M phase; for major phosphorylation sites in H1.4, it starts from 1 in G1, increases to 2 in S and reaches to 5 or 6 in M (Ajiro et al., 1981a; Ajiro et al., 1981b). In short, phosphorylation in H1 starts

from G1/S boundary, steadily increases over S and G2 and reaches its maximum level during M. Similar to H1 in CHO, random phosphorylation had also been suggested for H1 in M phase HeLa cells. The number of phosphopeptides found in mitosis was more than the phosphorylation number achieved in mitosis, which suggests the candidate of H1 phosphorylation might exceed the phosphorylation number found in mitosis and there is no molecules can achieve all the possible candidate sites simultaneously (Ajiro et al., 1981b). The association of hyperphosphorylation with metaphase is not limited to mammalian cells, H1 in *Physarum polycephalum*, a slime mold, can obtain 20-24 phosphates per molecule in metaphase (Mueller et al., 1985).

CDK1 and CDK2 Are H1 Kinase

Identifying the kinase for H1 phosphorylation is critical for understanding how phosphorylations in H1 are regulated. CDK1 has been implicated as the major M phase kinase for H1 based on comparison of phosphopeptide generated from H1 purified from mitotic enriched cells with *in vitro* phosphorylation of H1 by CDK1 (Langan et al., 1989). More refined study has demonstrated that all four tested CDK/cyclin complexes are able to phosphorylate H1 to the same extent as achieved in mitosis by comparing HPLC profile of tryptic phosphopeptides generated from *in vitro* phosphorylation with those from mitotic enriched CHO cells. These four tested kinases are interphase-specific CDK2/cyclin A, the late interphase CDK1/cyclin A, mitotic-specific CDK1/cyclin B, and the CDK1/unknown cyclin (Swank et al., 1997). This result raise another question: why are there only 3 phosphorylations in CHO H1 during S phase when the active S-phase CDK2/cyclin A can phosphorylate all 6 sites in free H1? The authors speculate that H1, when bound to chromatin, is locked into a structure that allows only limited accessibility to such kinases (Swank et al., 1997). This notion has been further supported by the observation that CDK1 isolated from mitotic HeLa cells, capable of phosphorylating H1 to the maximum extent, does not significantly phosphorylate chromatin-bound H1 *in*

vitro (Jerzmanowski and Cole, 1992). However, this explanation was proposed before the dynamic feature of H1 has been fully appreciated through FRAP studies. To reconcile the fact that chromatin-bound H1 is constantly exchanging with the pool of free H1 and the fact that H1 is not fully phosphorylated in interphase, we speculate phosphorylation of H1 during interphase might only happen when they are bound with chromatin and it requires CDKs being targeted to chromatin to phosphorylate H1 with limited accessibility to all candidate sites.

Besides the *in vitro* data to support CDK1 and CDK2 are the kinases for H1, *in vivo* studies have corroborated these findings. When CDK1 was inactivated at the non-permissive temperature in FT210 cells harboring a temperature sensitive mutation of CDK1, cells were blocked in early G2 phase and H1 did not undergo mitosis-related phosphorylations, suggesting that H1 is an *in vivo* substrate for the CDK1 kinase (Guo et al., 1995). The correlation between higher CDK2 activity in the oncogene transformed cells and more abundance of H1 interphase phosphorylation suggests CDK2 is H1 kinase responsible for the interphase phosphorylation (Chadee et al., 1995; Herrera et al., 1996).

Model for Reconciling the Paradox of H1 Phosphorylation

Considering that the positively charged lysine-rich N and C-terminal tail domains of H1 are involved in neutralizing the negative charge associated with DNA phosphates, one might predict that H1 phosphorylation should counteract this charge, neutralization and promote chromatin decondensation. Why then, does hyperphosphorylation of H1 at mitosis correlate with chromosome condensation? To reconcile this paradox, Roth and Allis have proposed that H1 phosphorylation causes transient decondensation of chromatin which in turn allows specific chromosome condensation factors to gain access to specific DNA regions and condense the chromatin subsequently (Roth and Allis, 1992). However, no such factor has been identified yet, thus this paradox remains elusive.

Effect of H1 Phosphorylation on H1-Chromatin Interactions

Although the function of H1 phosphorylation is not understood, a significant amount of progress has been obtained through continuing research. Determining how H1 phosphorylation affects its binding to chromatin and its effect in chromatin structure is a key step toward deciphering the function of H1 phosphorylation. The correlation between increased H1 phosphorylation and the relaxation of chromatin structure suggests phosphorylated H1 binds more loosely to chromatin and in turn causes the chromatin become more accessible to MNase digestion (Chadee et al., 1995; Herrera et al., 1996). Early reconstitution experiments show that H1 phosphorylation diminishes its ability to condense chromatin (Langan and Chambers, 1987). The chromatography purified naturally occurring H1 from early G1, S phase and M phase, representing none-, medium- and hyper-phosphorylation respectively, were used to compare how phosphorylation affects the ability of H1 to bind mononucleosome or promote the aggregation of polynucleosome. It turns out the ability of H1 to bind mononucleosome was not affected by phosphorylation, but the ability to aggregate polynucleosomes was reduced when H1 was hyperphosphorylated (Talasz et al., 1998). This result indicates the medium phosphorylation which H1 received in interphase doesn't change H1-chromatin interaction but the hyperphosphorylated H1 in mitosis actually binds chromatin more loosely.

Although there is no easy way to tag the phosphorylated H1 with GFP, several FRAP experiments were able to provide indirect evidence to infer how phosphorylation influences H1-chromaitn interaction *in vivo*. Lever *et al.* showed a kinase inhibitor staurosporine can greatly increase the recovery time of mouse GFP-H1.1 (GFP fused with N-terminal of H1) in the stable cell line, which suggest phosphorylation decrease the H1-chromatin interactions thus recovery time increase once phosphorylation of H1 is inhibited. However, from the same report, no decrease of recovery time was observed

in early G1 phase cells when phosphorylation level in H1 is lowest (Lever et al., 2000). This discrepancy can be either explained by the indirect effect resulted from wide spectrum kinase inhibitory action by staurosporine or the simply fact that H1.1 phosphorylation is not cell cycle regulated like other H1 variants despite it also possesses multiple CDK motifs in the CTD. Similar to H1.1, no change of recovery time was found for stable integrated mouse GFP-$H1^{o}$ (GFP fused with C-terminal of H1) in the different cell cycle stages in synchronized embryonic stem cells (Meshorer et al., 2006). By contrast, Contreras *et al*. found the recovery time for human H1.4-GFP (GFP fused with C-terminal of H1) were fast, intermediate and slowest for asynchronous, late G1 and G0 respectively (Contreras et al., 2003). Since we don't know whether and how H1.1 and $H1^{0}$ phosphorylation change during cell cycle, whereas the dynamic of human H1.4 phosphorylation has been well documented by Ajiro (Ajiro et al., 1981a), it is likely that the discrepancies are just the result of phosphorylation of H1.1 and $H1^{0}$ not cell cycle regulated or existing at low abundance that not able to influence the dynamic of H1. In addition, Contreras *et al*. compared the recovery time of human H1.4-GFP with H1.4-M1-5-GFP, five CDK phosphorylation consensus sites mutated from serine or threonine residues into alanines, in several cell lines by transient transfection. Decrease of recovery time was observed for mutants, which suggests phosphorylation increase the dynamic of H1. Interestingly, the levels of recovery of the fusion proteins are directly correlated with CDK2 activity in three different cell lines. When CDK2 activity is low, moderate, or high, the difference in levels of recovery between H1.4-GFP and H1.4-M1-5-GFP is correspondently low, moderate, or high, respectively. This result not only corroborates the effect of H1 phosphorylation in increasing their dynamic but also indicates CDK2 is the kinase for H1 (Contreras et al., 2003).

The finding of phosphorylated H1 being more dynamic than unphosphorylated H1 is also consistent with earlier immuno-electron microscopy data, which suggests that

unphosphorylated H1 is only found on nuclear chromatin/chromosomes, but phosphorylated H1 localizes to both nuclear chromatin/chromosomes and the cytoplasm in S and M phase cells (Bleher and Martin, 1999).

1.6 Roles of Histone H1 in Transcription

Is H1 a General or Gene-Specific Transcription Repressor?

Histone H1 has been shown to be able to repress transcription by all three eukaryotic polymerase (reviewed in (Paranjape et al., 1994; Workman and Buchman, 1993)). Direct evidence supporting the repression effect of H1 in pol II gene transcription came from in vitro chromatin reconstitution experiment, which found transcription from chromatin with H1 incorporated reduces dramatically to 1~4% of that with only core nucleosomes incorporated (Laybourn and Kadonaga, 1991). The idea widely accepted is that histone H1 is a general transcription repressor and sequence-specific transcription factors and/or basal transcription factors are required to displace H1 during transcription activation. However, a couple lines of evidence are against the general repressor model. First, all the H1 deletion or overexpression experiments, as will be discussed later, found out only small amount of genes are affected in either up- or down-regulation manners. Second, the general repressor model predicts a depletion of H1 in the activated gene, which has been disproved by multiple ChIP experiments showing H1 only partially rather than completely depleted upon transcriptional activation (see review in (Paranjape et al., 1994; Zlatanova and Van Holde, 1992)). Third, the more direct approach to address whether histone H1 is present in transcriptionally active chromatin has been achieved by studying the effect of specific anti-H1 antibodies on *in vitro* transcription in isolated nuclei. The anti-H1 antibodies significantly and reproducibly inhibited the transcriptional activity in isolated nuclei, which indicating that active gene chromatin does contain histone H1 (Srebreva and Zlatanova, 1992). Fourth, H1 was observed to localize to both fully extended, actively transcribed genes and repressed 30-nm chromatin

fiber in Balbiani ring genes in the salivary glands of *Chironomus tentans* (Ericsson et al., 1990). Similar, H1 was also found in all regions of polytene chromosomes, regardless of their transcriptional status (the H1 specific antibody bound to bands, interbands and puffs) (Hill et al., 1989). All these data has clearly demonstrated that complete depletion of H1 is not observed for active transcription.

The transcription inhibitory mechanism of H1 has been further reveled by recent studies. The *in vitro* transcription from HTLV-1 reconstituted chromatin demonstrated transcription repression effect of H1 relies on the inhibiting the acetyltransferase activity of p300. Interestingly, the inhibitory effect of H1 on p300 acetyltransferase activity is alleviated when Tax is present during chromatin assembly, but the activation effect of Tax is not achieved by histone H1 displacement (Konesky et al., 2006). This result actually corroborates the finding that H1 acts as a specific repressor of core histone acetylation in chromatin, which suggests the repression of PCAF acetyltransferase activity by H1 is caused by the steric hindrance of H3 N-terminal tail accessibility from the H1 tails (Herrera et al., 2000). Contradicting previous findings that H1 interferes with transcription factor binding to the DNA (Juan et al., 1994), the repressive effects of H1 do not result from inhibition CREB or Tax binding to chromatin (Konesky et al., 2006).

The regulation mechanism is not limited to virus gene transcription. Two recent independent studies have identified H1 as a component in a complex that is required to repress p53-mediated transcription. Both PURα and YB1, identified in the H1.2 complex purified from tagged H1.2, are required for H1.2 to inhibit both the transcription from reconstituted chromatin containing p53 regulated promoter and the acetylation of core histones by p300 (Kim et al., 2008). Importantly, knockdown any of these three proteins results in the de-repression of p53-dependent gene, which demonstrates that histone H1 itself is not enough to repress transcription from specific gene and it requires

additional cofactors to achieve the repression. More intriguingly, the isolated H1.2 complex also contains cofactors (e.g. CAPERα and nucleolin) that are known to activate transcription. It will be very interesting to investigate further to see whether H1.2 can activate transcription when bound with activating cofactor. Shortly after, Nishiyama *et al.* provided the *in vivo* evidence that H1-p53-CHD8 complex is necessary for the suppression of p53 mediated transcription. Three different approaches to decrease the amount of H1, including triple H1 knockout mouse ES cells, RNAi depletion of all H1 variants, dominant-negative mutant of histone H1, all results in de-repression of genes as indicated by the increase in the abundance of p21 or cell proliferation (Nishiyama et al., 2009).

Several insights regarding the mechanism of transcription repression effects of H1 can be implied from theses studies. First, how H1 variants can repress a specific genes without specific sequence recognition? It is very likely that H1 variants rely on the sequence specific factors to target them to a specific gene. In the case of p53 targeting H1.2 together with the repressive cofactors to Bax gene, no comparison of other H1 variants has been analyzed but in the Msx1 targeting H1.5 to MyoD gene, some evidences were provided that H1.5 is the only variant able to repress the MyoD gene (Lee et al., 2004). Second, it shed some light on how H1 represses the transcription by blocking the HAT accessibility to core histones. Third, it is possible that recruitment of Tax might activate the transcription by phosphorylating H1 first, which in turn loosen up the chromatin and enable the access of H3 by HAT.

Differential effects of histone H1 in transcription are first discovered in the study of *Xenopus* oocyte 5S rRNA gene, a pol III transcribed gene. The oocyte 5S rRNA genes are active in growing oocytes but become progressively repressed after mid-blastula transition (MBT) and are repressed in somatic cells. In contrast, somatic 5s rRNA genes

are active in all these stages. It has been revealed that histone B4, *Xenopus* oocyte H1 variant, is replaced by H1 somatic variant H1A during embryogenesis, which results in specific repression of *Xenopus* oocyte 5S rRNA gene (Bouvet et al., 1994; Kandolf, 1994). It is believed that H1 in the nucleosome containing H1 blocks TFIIA from accessing the oocyte 5S rRNA gene but not the somatic 5S rRNA gene (Howe et al., 1998; Sera and Wolffe, 1998). Mapping of the core particle positioning on oocyte 5S rRNA gene found little or no phasing (i.e. was randomly positioned). With addition of H1, a unique phasing was observed to cover all the sequence required for binding of transcription factor TFIIA. In contrast, the chromatosome position (with H1) in the somatic 5S rRNA gene does not occlude the critical sequence element for TFIIA binding (Sera and Wolffe, 1998). However, the inhibitory effect of H1 in oocyte 5S rRNA genes is not simply the result of transcription factor binding site occlusion. When the oocyte 5S rRNA coding sequence was placed at positions 546 bp or 1,237 bp upstream of its wild type position, H1 suppression of pol III transcription was lost. When however one 5S rRNA was left at wild type position with another sequence inserted at 546 bp, both copies are subjected to H1 suppression. It clearly indicated the large scale chromatin reorganization mediated by H1 play some roles in controlling differential inactivation of 5S rRNA (Tomaszewski and Jerzmanowski, 1997). The fact that the vast majority of genes whose expressions are necessary for *Xenopus* embryo development are not inhibited by H1A also challenges the notion of H1 as general transcription repressor.

Lessons Learned from H1 Deletion in Unicellular Organisms

It is unexpected that the complete knockout of H1 gene in several unicellular organisms, including *Tetrahymena thermophila* (Shen et al., 1995), *Saccharomyces cerevisiae* (Patterton et al., 1998), *Aspergillus nidulans* (Ramon et al., 2000) and *Ascobolus immerses* (Barra et al., 2000), all reveal H1 is not essential for viability or growth. If H1 were a general transcription repressor, a global transcription upregulation of transcription

would be expected. However, elimination of H1 does not affect transcription globally in *Tetrahymena* and only causes up- or downregulation of specific genes (Shen and Gorovsky, 1996). Similarly, no derepression of transcription is seen in yeast when H1 is removed. Only 27 genes are downregulated 2-fold or more in the whole genome transcription analysis, with less than 0.5% of total genes in this organisms affected (Hellauer et al., 2001).

Since H1 in both *Tetrahymena* and yeast lack the canonical tripartite structure, whether what we have learned from deletion in these two organisms can be readily generalized has been in debate for a while. Levy *et al.* have summarized several evidences to support the yeast Hho1p is a true functional homologues to histone H1 in other species, including: 1) HHO1 is transcribed during the S phase as seen in mammalian H1; 2) Hho1p generates the most similar chromatin immunoprecipitation (ChIP) pattern to the four core histones in a high-throughput screen; 3) Hho1p is present in a complex together with the core histones in immunoprecipitation (Levy et al., 2008).

Although Hho1p is not essential in yeast, closer examinations reveal roles in fine tuning gene transcription or maintaining genome stability. As an example of fine tuning transcription: Hho1p is required for maximal pol I processivity during rDNA transcription (Levy et al., 2008). An example of maintaining genome stability: Hho1p is shown to inhibit DNA repair by homologous recombination, thus loss of H1 lead to an increase in the propensity to undergo DNA repair and decrease in the life span (Downs et al., 2003); Hho1p hinders the de novo establishment of silent chromatin but does not affect the stability of preexistent silent chromatin (Yu et al., 2009). The effect of H1 in genome stability is not limited in yeast, removal of H1 in *Ascobolus* also caused increase of accessibility of chromatin to nuclease digestion and shortening of lifespan (Barra et al., 2000).

Lessons Learned from H1 Depletion in Higher Eukaryotes

Since all of the lower eukaryotes described above each has only one H1 gene, deletion and the subsequent interpretation of phenotype is straightforward. However, the multiple H1 variants in animals, up to 11 variants in human and mouse, makes this approach very challenging.

The first attempt of knockout was the most divergent of the H1 variants, $H1^0$, with a rationale of minimum possible compensation effect. However, $H1^0$ knockout mice can develop normally (Sirotkin et al., 1995). Similarly, mice have single (H1.2, H1.3, H1.4) knockout or even the combinatory knockout with $H1^0$ are all viable with no obvious defect (Fan et al., 2001) and mice lacking the testis-specific linker histone H1t has no defect in spermatogenesis (Lin et al., 2000). However the careful examinations have identified subtle defects in these knockout mice: it has been demonstrated $H1^0$ is required for terminal differentiation in dendritic cells (Gabrilovich et al., 2002) and less abundant testis-specific H1, H1T2 is critical in spermiogenesis (Martianov et al., 2005; Tanaka et al., 2005). In addition, an interesting analysis of position effect in the single H1 variants knockout background demonstrated both positive and negative effects of specific H1 variants. Absence of H1.3 or H1.4, but not H1.1, H1.2, or $H1^0$ is found to attenuate the rate of age-dependent silencing of a multicopy globin transgene. Similarly, different H1 variants also have different effects on expressing a variegating YAC transgene. These results strongly suggest that the other variants do not fully compensate for the loss of a specific variant in the null mice although compensation effect keeps the H1-to-core ratio in null mice similar to the wild type mice (Alami et al., 2003).

Despite no global effects in the single knockout of H1 in mice, a triple knockout of the H1c,d,e (H1.2, H1.3 and H1.4) genes in mice results in embryonic lethality, and a 20~50% reduction in H1-to-core ratio, shorter nucleosome repeat lengths, global

alterations in chromatin structure in ES cells recovered from null animals (Fan et al., 2003). It is surprisingly similar to deletion experiment in unicellular organisms in a way that only small amount of transcription is affected: only 29 genes are significantly altered. Interestingly, one third of these are known to be regulated by DNA methylation, suggesting links between the function H1 and DNA methylation (Fan et al., 2005).

The recent efforts to deplete a single H1 variant ($H1^0$, H1.2, H1.3, H1.4 and H1.5) by shRNA in human cell lines have demonstrated different results for different variants and some results are cell line specific. More specifically, only depletion of H1.2 and H1.4 affects cell survival with depletion of H1.2 causes G1 arrest in T47D and MCF10A breast epithelial cell lines and apoptosis in MCF7 cells, whereas depletion of H1.4 causes cell death in T47D cells. The effect of H1.2 depletion in cell cycle arrest is probably the results of more than 20 cell cycle regulated genes are significantly downregulated in H1.2 depletion cells. Moreover, only small subset of gene is altered with 2.4% of genes upregulated and 3.7% of genes downregulated (Clausell et al., 2009). Very interestingly, the three groups classified by ratio of downregulated : upregulated for each H1 variant depletion (high: 2.7 for H1.2; intermediate: 2.1 for H1.3 and 1.9 for $H1^0$; low: 1.4 for H1.4 and 1.0 for H1.5) are surprisingly correlative with their ability to condense the chromatin as discussed before. In other word, depletion of a weak condenser like H1.2 tends to cause more downregulation of genes, suggesting it is acting as an activator in more cases, whereas depletion of a stronger condenser like H1.4 tends to cause less downregulation of genes, suggesting it is more so a repressor. It is worth noting that most of the genes are affected by a single H1 variant while a portion of genes are altered by more than one H1 variants, which indicate specific roles and some extent of redundancy of H1 variants in transcription regulation.

Lessons Learned from Overexpression of H1

Interesting results on the selective effect of histone H1 on transcription of individual genes were also obtained using a stably integrated inducible expression system for different histone H1 variants in cultured mouse 3T3 cells. Overproduction of $H1^0$, which increase H1-to-core ratio from 0.8 to 1.3, exhibits transient inhibition of both G1 and S phase progression from a quiescent state and a reduced transcription for all genes tested. On the contrary, overproduction of H1.2 to comparable levels of 1.1 H1-to-core ratio, has no effect on cell cycle and results in either a negligible effect or dramatic increase of some tested genes (Brown et al., 1996). Moreover, these variant specific effects were shown to be due to differences in the structure of the globular domains (Brown et al., 1997). Very surprisingly, overproduction of either $H1^0$ or H1.2 result in a dramatic increase rather than a repression in basal and hormone-induced expression from integrated MMTV promoter (Gunjan and Brown, 1999), which seems to contradict the previous observation that decreased amounts of H1 are associated with activated MMTV promoter stimulated by hormone (Bresnick et al., 1992). To reconcile this contradiction, it has been postulated that H1 affects nucleosome positioning or other aspects of MMTV promoter chromatin architecture to facilitate the binding of liganded nuclear hormone receptors, their synergism with transcription factors such as NF1 and AP-1, and the recruitment or activation of kinases which phosphorylate and facilitate H1 displacement following hormone stimulation (Vicent et al., 2002a).

In summary, all sorts of H1 perturbations result in different effects in different genes, which suggest different H1 variants might play different roles in chromatin structure. However, what exact roles are still remaining in the shadow.

1.7 Evidence That H1 Stoichiometry is Inversely Correlated With Global Transcriptional Activity

The concept of each nucleosome having one H1 has turned out to be oversimplified. By comparing the data from literature, Woodcock found a nice correlation between H1 stoichiometry and transcription inactivation. In another word, the ratio of H1-to-core increases when cells turn off some transcription during differentiation. The stoichiometry in normal mouse ES cells is only 0.5 (1 H1 in every 2 nucleosomes), but increase to 0.8 in 3T3, a mouse embryonic fibroblast cells (Brown et al., 1996; Woodcock et al., 2006). Surprisingly, mouse cells can tolerate as low as 0.25 of H1-to-core stoichiometry as seen in H1 triple knockout ES cells mentioned above (Fan et al., 2005). Similarly, H1 content also differs among different tissues. For example, H1 stoichiometry is 0.79 in liver and 0.83 in thymus, but is as high as 1.3 in chicken erythrocyte (0.9 H5 + 0.4 H1) (Fan et al., 2003; Fan et al., 2005; Woodcock et al., 2006). It is also worth mentioning the H1 stoichiometry in yeast. The first estimation of H1 stoichiometry in *S. cerevisiae* is very low, only 1 Hho1p per 37 nucleosomes (Freidkin and Katcoff, 2001). More recent study reports the stoichiometry of 0.25 and suggests the first study did not measure the abundance of core histones and could therefore have underestimated the ratio of Hho1p to nucleosomes (Downs et al., 2003).

1.8 Roles of H1 Phosphorylation in Transcription

Chromatin immunoprecipitation (ChIP) has become a powerful tool for mapping protein interactions along genomic DNA *in vivo*, and thus has been the most informative assay in providing where the specific histone variants or modifications are associated within the genome. However a specific antibody is necessary for every histone variant or specific modification to be studied by this approach. One can circumvent such limitation by putting a epitope tag in the interested histone variants and using the available tag antibody, however, no similar alternative can be readily applied to histone modification study for

now. A novel non-antibody based technique, aptamer, which is very promising to exceed the antibody in both affinity and specificity, will be an excellent alternative for modification specific antibody in the near future (Williams et al., 2009). For now, we must rely on phosphor-specific antibody to study the function of H1 phosphorylation and the only such antibody is the antisera raised against hyperphosphorylated *Tetrahymena* (Lu et al., 1994). We will call this antisera pTetH1 hereafter, which has been proven to be able to cross-react with phosphorylated H1 from multiple species. Moreover, it is the only available H1 phosphor specific antibody used in most H1 phosphorylation related research in the literature.

Despite the distal relationship between metazoan H1 and *Tetrahymena* H1, what we have learned in *Tetrahymena* might still be able to translate into metazoan and thus it is worth mentioning the important works that have been done in this model organism. With five phosphorylation sites in *Tetrahymena* H1 mapped (Mizzen et al., 1999), two *Tetrahymena* strains were created by gene replacement with alanine or glutamic acid mutations to prevent or mimic phosphorylation respectively. Phosphorylation-mimicking H1 caused activating or repressing specific genes in the same manners as H1 deletion. It leads to the first well known working model for H1 phosphorylation: regulating transcription by mimicking the partial removal of H1 (Dou et al., 1999). Improved model claims that phosphorylation of H1 is acting by changing the overall charge of a small domain, not by phosphate recognition or by creating a site-specific charge, and these charged patches can be moved around without losing their phosphorylation mimicking effects (Dou and Gorovsky, 2000; Dou and Gorovsky, 2002). Work from the same lab, further identified a positive feedback mechanism between H1 phosphorylation and CDC2 expression and an interesting enrichment of dephosphorylated H1 in the CDC2 promoter when gene expression is low after starvation. The authors proposed the localization of unphosphorylated H1 in the CDC2 promoter during starvation is achieved by the

targeting of the catalytic and/or a regulatory subunit of an H1 phosphatase (Dou et al., 2005; Song and Gorovsky, 2007).

It has been demonstrated that, in culture cells carrying a stable integration of ~300 copies MMTV (Mouse Mammary Tumor Virus) LTR (long terminal repeat) linked to CAT gene, enrichment of phosphorylated H1 on the MMTV promoter adjacent to the hormone response element (HRE) was lost when transcription from MMTV is inhibited upon prolonged hormone treatment by pTetH1 ChIP (Lee and Archer, 1998). Further investigation showed CDK2 specific inhibitor CVT-313 can also inhibit both the transcription from MMTV and the enrichment of phosphorylated H1 in the promoter, which implies H1 phosphorylation is necessary for MMTV activation (Bhattacharjee et al., 2001). It is known that MMTV promoter exhibits positioned nucleosomes which cover the five hormone-responsive elements (HREs) and the binding site for nuclear factor 1 (NF1) so that only two of the five HREs can be bound by hormone receptors and the binding site for NF1 is not accessible. The activating process involves a two-step synergism. First, the hormone receptor binds to the exposed HREs and triggers a chromatin-remodeling event that facilitates the access of NF1. Second, bound NF1 in turn stabilizes an open nucleosomal conformation required for efficient binding of further receptor molecules to the hidden HREs and full transactivation (Di Croce et al., 1999). Addition of H1 to the chromatin reconstitution system using minichromosomes containing MMTV leads to tightening and stabilization of the nucleosome covering the regulatory elements of the MMTV promoter, which reduces accessibility for NF1. However, incorporation of histone H1 by ~1 H1-to-core stoichiometry leads to a better binding of progesterone receptor (PR) and improved synergism between PR and NF1, resulting in enhanced transcription initiation. Moreover, phosphorylated H1 association increased while total H1 loading was maintained at the same level over MMTV promoter after addition of PR; both phosphorylated H1 and total H1 association greatly reduced

after addition of both PR and NF1 (Koop et al., 2003; Vicent et al., 2002b). Here are a couple of interesting conclusions from these studies: 1) PR might be able to recruit or activate a kinase to locally phosphorylate H1; 2) H1 phosphorylation is not sufficient to activate the transcription in the presence of PR alone; 3) since total H1 loading does not change while phosphorylation increase in the presence of PR alone, phosphorylation itself might not be enough to induce the displacement of H1; 4) upon full activation of transcription initiation in the presence of PR and NF1, the majority of histone H1 leaves the promoter (Koop et al., 2003; Vicent et al., 2002b). It is worth emphasizing that final depletion of H1 from promoter after activation might be the result of chromatin remodeling but not be the direct consequence of H1 phosphorylation. It actually has been reported that histone H1 can inhibit SWI/SNF chromatin remodeling activity and this inhibition can be relieved after H1 is phosphorylated by Cdc2/Cyclin B in chromatin reconstitution experiment (Horn et al., 2002).

In vivo assembly experiment using microinjection of different amount of mRNA for histone H1 into *Xenopus* oocyte has found addition of H1 to ~ 1 H1-to-core stoichiometry results in maximum effects on enhancing hormone-induced binding of glucocorticoid receptor (GR) and stimulating the transcription from MMTV. A loss of H1 from MMTV promoter and the absence of H1-dependent increase of NRL in MMTV promoter was observed after hormone induction (Belikov et al., 2007). These results corroborate the mechanism proposed by Beato lab that H1 can enhance the hormone receptor binding to the HRE and subsequent activation will displace the H1 from the promoter. The findings described here also shed some light on why overexpression of H1 to 1.2~1.3 H1-to-core stoichiometry actually increases the induction of MMTV transcription (Gunjan and Brown, 1999), possible by increasing the binding affinity with hormone receptor.

However, opposite effect of histone H1 on transcription activation has also been reported in similar experiments scheme with minichromosomes assembled on a synthetic promoter consisting of two estrogen-responsive elements (ERE). In this system, addition of histone H1 leads to a dramatic decrease in the activation of transcription induced by addition of estrogen receptor α (ERα), which is proved to be caused by the inhibition of ERα binding to ERE in the presence of H1 (Cheung et al., 2002). More research is required to clarify such discrepancies, taking into account of the caveats of using a synthetic promoter in ER experiment or representing the differential regulatory effects of H1 in different genes. In summary, the effects of H1 in the binding of transcription factor can be classified into three groups: no inhibition of the binding as seen in Tax/CREB with HTLV-1; enhance of the binding as seen in GR/PR with MMTV, inhibition of the binding as seen in ERα with synthetic ERE.

1.9 Histone H1 and Replication

The cell cycle regulated dynamic of H1 phosphorylation, lowest phosphorylation state in G1, increasing amount of phosphorylation during S-phase, reaching a maximum in mitosis, has led to the speculation that H1 phosphorylation might play some roles in DNA replication (Ajiro et al., 1981a; Ajiro et al., 1981b). In fact, several lines of evidence have suggested the correlation between H1 and replication. H1 added to *X. laevis* extracts is capable of inhibiting DNA replication *in vitro*, by limiting the assembly of prereplicaiton complex (Lu et al., 1997; Lu et al., 1998). By contrast, a higher replication efficiency for SV40 minichromosomes has been observed for reconstitution with S-phase histone H1, which has medium level of phosphorylation, compared with G0- or M-phase histone H1 (Halmer and Gruss, 1996). In addition, artificial recruitment of LacI-Cdc 45 to the loci containing lacO/DHFR tandem repeats in CHO cells was demonstrated to cause these loci to decondense in association with H1 phosphorylation by recruitment of Cdk2 by Cdc45 (Alexandrow and Hamlin, 2005). It

has also been reported that genomic DNA in knockdown of H1 in *Physarum* is more rapidly replicated by disruption of the native timing of replication fork firing (Thiriet and Hayes, 2009). In addition, *Physarum* H1 is transiently lost from replicating chromatin facilitated by phosphorylation of H1 (Thiriet and Hayes, 2009).

1.10 Histone H1 and Chromatin Condensation

Initially, H1 was shown dispensable in chromatin condensation when chromosome can be assembled from unreplicated sperm chromatids in CSF-arrested *Xenopus* egg extract without H1(Ohsumi et al., 1993). Soon this conclusion was put to rest by careful examination. Significant structure defects were detected when replicated chromosome were assembled from H1-depleted "cycled" egg extract. An interesting hypothesis was proposed by authors that the reason H1 requires passage through interphase to become sufficiently enriched in chromosome is that H1 deposition to chromatin is a DNA replication-dependent or assisted process (Maresca et al., 2005). In addition, H1 knockout in both *Tetrahymena* and *Physarum* exhibit larger nuclear volume, indicating that requirement of H1 in chromatin compaction is not limited in *Xenopus* (Shen et al., 1995; Thiriet and Hayes, 2009). More recent study has demonstrated that depletion of H1x, a H1 variant accumulating in the nucleolus during interphase and is distributing at the chromosome periphery during mitosis, induces aberrant spindle formation, indicating H1x is required for chromosome alignment and segregation (Takata et al., 2007).

1.11 H1 and the Histone Code

The histone code hypothesis predicts that the post-translational modifications (PTM) of histones, alone or in combination can function to direct specific and distinct DNA-templated programs (Jenuwein and Allis, 2001; Strahl and Allis, 2000). The tails of histones have many sites where covalent chemical modifications can take place, including acetylation, phosphorylation and methylation. For example, the acetylation of

key lysine residues of histone H3 and H4 by histone acetyltransferases (HATs) was believed to play important roles in transcriptional activation. In addition, crosstalk between two or even three modifications have been reported, for example, phosphorylation at ser10 in H3 and acetylation at lys16 in H4 have been shown to mediate transcription elongation (Zippo et al., 2009) and preferentially deubiquitination of lys119 in H2A in hyperacetylated nucleosomes has been demonstrated to facilitate dissociation of H1 by increase of H1 phosphorylation in response to hormone stimulation in androgen receptor targeted gene (Zhu et al., 2007).

Izzo *et al.* proposed that each H1 variant could be considered as an epigenetic mark, since each individual H1 variant can regulate a subset of specific genes in either negative or positive fashion (Izzo et al., 2008). Besides transcription, H1 has also been shown to play roles in replication, recombination, apoptosis and even senescence (Funayama et al., 2006). However, compared with abundant knowledge of core histone and despite the significant amount of investigation for deciphering the enigmatic histone H1 code, we still do not quite understand even the most abundant modifications of H1, which is phosphorylation, no mention several other less abundant forms of modifications (Wisniewski et al., 2007). I hope the study in this thesis can contribute to the knowledge of how H1 phosphorylation modulates gene transcription.

1.12 References

Ajiro, K., T.W. Borun, and L.H. Cohen. 1981a. Phosphorylation states of different histone 1 subtypes and their relationship to chromatin functions during the HeLa S-3 cell cycle. *Biochemistry*. 20:1445-1454.

Ajiro, K., T.W. Borun, B.S. Shulman, G.M. McFadden, and L.H. Cohen. 1981b. Comparison of the structures of human histone 1A and 1B and their intramolecular phosphorylation sites during the HeLa S-3 cell cycle. *Biochemistry*. 20:1454-1464.

Alami, R., Y. Fan, S. Pack, T.M. Sonbuchner, A. Besse, Q. Lin, J.M. Greally, A.I. Skoultchi, and E.E. Bouhassira. 2003. Mammalian linker-histone subtypes differentially affect gene expression in vivo. *Proc Natl Acad Sci U S A.* 100:5920-5.

Alexandrow, M.G., and J.L. Hamlin. 2005. Chromatin decondensation in S-phase involves recruitment of Cdk2 by Cdc45 and histone H1 phosphorylation. *J. Cell Biol.* 168:875-886.

Allan, J., G.J. Cowling, N. Harborne, P. Cattini, R. Craigie, and H. Gould. 1981. Regulation of the higher-order structure of chromatin by histones H1 and H5. *J Cell Biol*. 90:279-88.

Allan, J., P.G. Hartman, C. Crane-Robinson, and F.X. Aviles. 1980. The structure of histone H1 and its location in chromatin. *Nature*. 288:675-9.

Barra, J.L., L. Rhounim, J.L. Rossignol, and G. Faugeron. 2000. Histone H1 is dispensable for methylation-associated gene silencing in Ascobolus immersus and essential for long life span. *Mol Cell Biol*. 20:61-9.

Bednar, J., R.A. Horowitz, S.A. Grigoryev, L.M. Carruthers, J.C. Hansen, A.J. Koster, and C.L. Woodcock. 1998. Nucleosomes, linker DNA, and linker histone form a unique structural motif that directs the higher-order folding and compaction of chromatin. *PNAS*. 95:14173-14178.

Belikov, S., C. Astrand, and O. Wrange. 2007. Mechanism of histone H1-stimulated glucocorticoid receptor DNA binding in vivo. *Molecular and Cellular Biology*. 27:2398-2410.

Bhattacharjee, R.N., G.C. Banks, K.W. Trotter, H.L. Lee, and T.K. Archer. 2001. Histone H1 phosphorylation by Cdk2 selectively modulates mouse mammary tumor virus transcription through chromatin remodeling. *Mol Cell Biol*. 21:5417-25.

Bleher, R., and R. Martin. 1999. Nucleo-cytoplasmic translocation of histone H1 during the HeLa cell cycle. *Chromosoma*. 108:308-16.

Bouvet, P., S. Dimitrov, and A.P. Wolffe. 1994. Specific regulation of Xenopus chromosomal 5S rRNA gene transcription in vivo by histone H1. *Genes Dev*. 8:1147-59.

Bresnick, E.H., M. Bustin, V. Marsaud, H. Richard-Foy, and G.L. Hager. 1992. The transcriptionally-active MMTV promoter is depleted of histone H1. *Nucleic Acids Res*. 20:273-8.

Brown, D.T. 2003. Histone H1 and the dynamic regulation of chromatin function. *Biochem Cell Biol*. 81:221-7.

Brown, D.T., B.T. Alexander, and D.B. Sittman. 1996. Differential effect of H1 variant overexpression on cell cycle progression and gene expression. *Nucleic Acids Res*. 24:486-93.

Brown, D.T., A. Gunjan, B.T. Alexander, and D.B. Sittman. 1997. Differential effect of H1 variant overproduction on gene expression is due to differences in the central globular domain. *Nucleic Acids Res*. 25:5003-9.

Brown, D.T., T. Izard, and T. Misteli. 2006. Mapping the interaction surface of linker histone H1(0) with the nucleosome of native chromatin in vivo. *Nat Struct Mol Biol*. 13:250-5.

Carruthers, L.M., J. Bednar, C.L. Woodcock, and J.C. Hansen. 1998. Linker histones stabilize the intrinsic salt-dependent folding of nucleosomal arrays: mechanistic ramifications for higher-order chromatin folding. *Biochemistry*. 37:14776-87.

Chadee, D.N., W.R. Taylor, R.A. Hurta, C.D. Allis, J.A. Wright, and J.R. Davie. 1995. Increased phosphorylation of histone H1 in mouse fibroblasts transformed with oncogenes or constitutively active mitogen-activated protein kinase kinase. *J Biol Chem*. 270:20098-105.

Cheung, E., A.S. Zarifyan, and W.L. Kraus. 2002. Histone H1 represses estrogen receptor alpha transcriptional activity by selectively inhibiting receptor-mediated transcription initiation. *Mol Cell Biol*. 22:2463-71.

Clausell, J., N. Happel, T.K. Hale, D. Doenecke, and M. Beato. 2009. Histone H1 subtypes differentially modulate chromatin condensation without preventing ATP-dependent remodeling by SWI/SNF or NURF. *PLoS One*. 4:e0007243.

Contreras, A., T.K. Hale, D.L. Stenoien, J.M. Rosen, M.A. Mancini, and R.E. Herrera. 2003. The dynamic mobility of histone H1 is regulated by cyclin/CDK phosphorylation. *Mol Cell Biol*. 23:8626-36.

Di Croce, L., R. Koop, P. Venditti, H.M. Westphal, K.P. Nightingale, D.F. Corona, P.B. Becker, and M. Beato. 1999. Two-step synergism between the progesterone receptor and the DNA-binding domain of nuclear factor 1 on MMTV minichromosomes. *Mol Cell*. 4:45-54.

Dorigo, B., T. Schalch, A. Kulangara, S. Duda, R.R. Schroeder, and T.J. Richmond. 2004. Nucleosome arrays reveal the two-start organization of the chromatin fiber. *Science*. 306:1571-3.

Dou, Y., and M.A. Gorovsky. 2000. Phosphorylation of linker histone H1 regulates gene expression in vivo by creating a charge patch. *Mol Cell*. 6:225-31.

Dou, Y., and M.A. Gorovsky. 2002. Regulation of transcription by H1 phosphorylation in Tetrahymena is position independent and requires clustered sites. *Proc Natl Acad Sci U S A*. 99:6142-6.

Dou, Y., C.A. Mizzen, M. Abrams, C.D. Allis, and M.A. Gorovsky. 1999. Phosphorylation of linker histone H1 regulates gene expression in vivo by mimicking H1 removal. *Mol Cell*. 4:641-7.

Dou, Y., X. Song, Y. Liu, and M.A. Gorovsky. 2005. The H1 Phosphorylation State Regulates Expression of CDC2 and Other Genes in Response to Starvation in Tetrahymena thermophila. *Mol. Cell. Biol.* 25:3914-3922.

Downs, J.A., E. Kosmidou, A. Morgan, and S.P. Jackson. 2003. Suppression of homologous recombination by the Saccharomyces cerevisiae linker histone. *Mol Cell*. 11:1685-92.

Ericsson, C., U. Grossbach, B. Bjorkroth, and B. Daneholt. 1990. Presence of histone H1 on an active Balbiani ring gene. *Cell*. 60:73-83.

Fan, Y., T. Nikitina, E.M. Morin-Kensicki, J. Zhao, T.R. Magnuson, C.L. Woodcock, and A.I. Skoultchi. 2003. H1 Linker Histones Are Essential for Mouse Development and Affect Nucleosome Spacing In Vivo. *Mol. Cell. Biol.* 23:4559-4572.

Fan, Y., T. Nikitina, J. Zhao, T.J. Fleury, R. Bhattacharyya, E.E. Bouhassira, A. Stein, C.L. Woodcock, and A.I. Skoultchi. 2005. Histone H1 depletion in mammals alters global chromatin structure but causes specific changes in gene regulation. *Cell*. 123:1199-212.

Fan, Y., A. Sirotkin, R.G. Russell, J. Ayala, and A.I. Skoultchi. 2001. Individual somatic H1 subtypes are dispensable for mouse development even in mice lacking the H1(0) replacement subtype. *Mol Cell Biol*. 21:7933-43.

Finch, J.T., and A. Klug. 1976. Solenoidal model for superstructure in chromatin. *Proc Natl Acad Sci U S A*. 73:1897-901.

Freidkin, I., and D.J. Katcoff. 2001. Specific distribution of the Saccharomyces cerevisiae linker histone homolog HHO1p in the chromatin. *Nucleic Acids Res*. 29:4043-51.

Funayama, R., M. Saito, H. Tanobe, and F. Ishikawa. 2006. Loss of linker histone H1 in cellular senescence. *J. Cell Biol.* 175:869-880.

Gabrilovich, D.I., P. Cheng, Y. Fan, B. Yu, E. Nikitina, A. Sirotkin, M. Shurin, T. Oyama, Y. Adachi, S. Nadaf, D.P. Carbone, and A.I. Skoultchi. 2002. H1(0) histone and differentiation of dendritic cells. A molecular target for tumor-derived factors. *J Leukoc Biol*. 72:285-96.

Gunjan, A., and D.T. Brown. 1999. Overproduction of histone H1 variants in vivo increases basal and induced activity of the mouse mammary tumor virus promoter. *Nucleic Acids Res*. 27:3355-63.

Guo, X.W., J.P. Th'ng, R.A. Swank, H.J. Anderson, C. Tudan, E.M. Bradbury, and M. Roberge. 1995. Chromosome condensation induced by fostriecin does not require p34cdc2 kinase activity and histone H1 hyperphosphorylation, but is associated with enhanced histone H2A and H3 phosphorylation. *Embo J*. 14:976-85.

Gurley, L.R., J.A. D'Anna, S.S. Barham, L.L. Deaven, and R.A. Tobey. 1978. Histone phosphorylation and chromatin structure during mitosis in Chinese hamster cells. *Eur J Biochem*. 84:1-15.

Gurley, L.R., J.G. Valdez, and J.S. Buchanan. 1995. Characterization of the Mitotic Specific Phosphorylation Site of Histone H1. *J. Biol. Chem.* 270:27653-27660.

Halmer, L., and C. Gruss. 1996. Effects of cell cycle dependent histone H1 phosphorylation on chromatin structure and chromatin replication. *Nucleic Acids Res*. 24:1420-7.

Happel, N., and D. Doenecke. 2009. Histone H1 and its isoforms: Contribution to chromatin structure and function. *Gene*. 431:1-12.

Harp, J.M., B.L. Hanson, D.E. Timm, and G.J. Bunick. 2000. Asymmetries in the nucleosome core particle at 2.5 A resolution. *Acta Crystallogr D Biol Crystallogr*. 56:1513-34.

Hellauer, K., E. Sirard, and B. Turcotte. 2001. Decreased expression of specific genes in yeast cells lacking histone H1. *J Biol Chem*. 276:13587-92.

Hendzel, M.J., M.A. Lever, E. Crawford, and J.P. Th'ng. 2004. The C-terminal domain is the primary determinant of histone H1 binding to chromatin in vivo. *J Biol Chem*. 279:20028-34.

Herrera, J.E., K.L. West, R.L. Schiltz, Y. Nakatani, and M. Bustin. 2000. Histone H1 is a specific repressor of core histone acetylation in chromatin. *Mol Cell Biol*. 20:523-9.

Herrera, R.E., F. Chen, and R.A. Weinberg. 1996. Increased histone H1 phosphorylation and relaxed chromatin structure in Rb-deficient fibroblasts. *Proc Natl Acad Sci U S A*. 93:11510-5.

Hill, R.J., F. Watt, C.M. Wilson, T. Fifis, P.A. Underwood, G. Tribbick, H.M. Geysen, and J.O. Thomas. 1989. Bands, interbands and puffs in native Drosophila polytene chromosomes are recognized by a monoclonal antibody to an epitope in the carboxy-terminal tail of histone H1. *Chromosoma*. 98:411-21.

Hohmann, P., R.A. Tobey, and L.R. Gurley. 1976. Phosphorylation of distinct regions of f1 histone. Relationship to the cell cycle. *J. Biol. Chem.* 251:3685-3692.

Horn, P.J., L.M. Carruthers, C. Logie, D.A. Hill, M.J. Solomon, P.A. Wade, A.N. Imbalzano, J.C. Hansen, and C.L. Peterson. 2002. Phosphorylation of linker histones regulates ATP-dependent chromatin remodeling enzymes. *Nat Struct Biol*. 9:263-7.

Howe, L., T. Itoh, C. Katagiri, and J. Ausio. 1998. Histone H1 binding does not inhibit transcription of nucleosomal Xenopus laevis somatic 5S rRNA templates. *Biochemistry*. 37:7077-82.

Izzo, A., K. Kamieniarz, and R. Schneider. 2008. The histone H1 family: specific members, specific functions? *Biol Chem*. 389:333-43.

Jenuwein, T., and C.D. Allis. 2001. Translating the histone code. *Science*. 293:1074-1080.

Jerzmanowski, A., and R.D. Cole. 1992. Partial displacement of histone H1 from chromatin is required before it can be phosphorylated by mitotic H1 kinase in vitro. *J Biol Chem*. 267:8514-20.

Juan, L.J., R.T. Utley, C.C. Adams, M. Vettese-Dadey, and J.L. Workman. 1994. Differential repression of transcription factor binding by histone H1 is regulated by the core histone amino termini. *Embo J*. 13:6031-40.

Kandolf, H. 1994. The H1A histone variant is an in vivo repressor of oocyte-type 5S gene transcription in Xenopus laevis embryos. *Proc Natl Acad Sci U S A*. 91:7257-61.

Khadake, J.R., and M.R. Rao. 1995. DNA- and chromatin-condensing properties of rat testes H1a and H1t compared to those of rat liver H1bdec; H1t is a poor condenser of chromatin. *Biochemistry*. 34:15792-801.

Khorasanizadeh, S. 2004. The Nucleosome: From Genomic Organization to Genomic Regulation. *Cell*. 116:259-272.

Kim, K., J. Choi, K. Heo, H. Kim, D. Levens, K. Kohno, E.M. Johnson, H.W. Brock, and W. An. 2008. Isolation and characterization of a novel H1.2 complex that acts as a repressor of p53-mediated transcription. *J Biol Chem*. 283:9113-26.

Konesky, K.L., J.K. Nyborg, and P.J. Laybourn. 2006. Tax Abolishes Histone H1 Repression of p300 Acetyltransferase Activity at the Human T-Cell Leukemia Virus Type 1 Promoter. *J. Virol.* 80:10542-10553.

Konishi, A., S. Shimizu, J. Hirota, T. Takao, Y. Fan, Y. Matsuoka, L. Zhang, Y. Yoneda, Y. Fujii, A.I. Skoultchi, and Y. Tsujimoto. 2003. Involvement of histone H1.2 in apoptosis induced by DNA double-strand breaks. *Cell*. 114:673-88.

Koop, R., L. Di Croce, and M. Beato. 2003. Histone H1 enhances synergistic activation of the MMTV promoter in chromatin. *Embo J*. 22:588-99.

Langan, T.A., and T.C. Chambers. 1987. H1 histone phosphorylation, cell cycle progression and chromatin structure. *Prog Clin Biol Res*. 249:215-23.

Langan, T.A., J. Gautier, M. Lohka, R. Hollingsworth, S. Moreno, P. Nurse, J. Maller, and R.A. Sclafani. 1989. Mammalian growth-associated H1 histone kinase: a homolog of cdc2+/CDC28 protein kinases controlling mitotic entry in yeast and frog cells. *Mol Cell Biol*. 9:3860-8.

Laybourn, P.J., and J.T. Kadonaga. 1991. Role of nucleosomal cores and histone H1 in regulation of transcription by RNA polymerase II. *Science*. 254:238-45.

Lee, H., R. Habas, and C. Abate-Shen. 2004. MSX1 cooperates with histone H1b for inhibition of transcription and myogenesis. *Science*. 304:1675-8.

Lee, H.L., and T.K. Archer. 1998. Prolonged glucocorticoid exposure dephosphorylates histone H1 and inactivates the MMTV promoter. *Embo J*. 17:1454-66.

Lever, M.A., J.P. Th'ng, X. Sun, and M.J. Hendzel. 2000. Rapid exchange of histone H1.1 on chromatin in living human cells. *Nature*. 408:873-6.

Levy, A., M. Eyal, G. Hershkovits, M. Salmon-Divon, M. Klutstein, and D.J. Katcoff. 2008. Yeast linker histone Hho1p is required for efficient RNA polymerase I processivity and transcriptional silencing at the ribosomal DNA. *Proc Natl Acad Sci U S A*. 105:11703-8.

Liao, L.W., and R.D. Cole. 1981. Condensation of dinucleosomes by individual subfractions of H1 histone. *J Biol Chem*. 256:10124-8.

Lin, Q., A. Sirotkin, and A.I. Skoultchi. 2000. Normal spermatogenesis in mice lacking the testis-specific linker histone H1t. *Mol Cell Biol*. 20:2122-8.

Lu, M.J., C.A. Dadd, C.A. Mizzen, C.A. Perry, D.R. McLachlan, A.T. Annunziato, and C.D. Allis. 1994. Generation and characterization of novel antibodies highly selective for phosphorylated linker histone H1 in Tetrahymena and HeLa cells. *Chromosoma*. 103:111-21.

Lu, X., and J.C. Hansen. 2004. Identification of specific functional subdomains within the linker histone H10 C-terminal domain. *J Biol Chem*. 279:8701-7.

Lu, Z.H., D.B. Sittman, D.T. Brown, R. Munshi, and G.H. Leno. 1997. Histone H1 modulates DNA replication through multiple pathways in Xenopus egg extract. *J Cell Sci*. 110 (Pt 21):2745-58.

Lu, Z.H., D.B. Sittman, P. Romanowski, and G.H. Leno. 1998. Histone H1 reduces the frequency of initiation in Xenopus egg extract by limiting the assembly of prereplication complexes on sperm chromatin. *Mol Biol Cell*. 9:1163-76.

Luger, K., A.W. Mader, R.K. Richmond, D.F. Sargent, and T.J. Richmond. 1997. Crystal structure of the nucleosome core particle at 2.8 A resolution. *Nature*. 389:251-60.

Maresca, T.J., B.S. Freedman, and R. Heald. 2005. Histone H1 is essential for mitotic chromosome architecture and segregation in Xenopus laevis egg extracts. *J. Cell Biol.* 169:859-869.

Martianov, I., S. Brancorsini, R. Catena, A. Gansmuller, N. Kotaja, M. Parvinen, P. Sassone-Corsi, and I. Davidson. 2005. Polar nuclear localization of H1T2, a histone H1 variant, required for spermatid elongation and DNA condensation during spermiogenesis. *Proc Natl Acad Sci U S A*. 102:2808-13.

Meergans, T., W. Albig, and D. Doenecke. 1997. Varied expression patterns of human H1 histone genes in different cell lines. *DNA Cell Biol*. 16:1041-9.

Meshorer, E., D. Yellajoshula, E. George, P.J. Scambler, D.T. Brown, and T. Misteli. 2006. Hyperdynamic plasticity of chromatin proteins in pluripotent embryonic stem cells. *Dev Cell*. 10:105-16.

Mizzen, C.A., Y. Dou, Y. Liu, R.G. Cook, M.A. Gorovsky, and C.D. Allis. 1999. Identification and Mutation of Phosphorylation Sites in a Linker Histone. PHOSPHORYLATION OF MACRONUCLEAR H1 IS NOT ESSENTIAL FOR VIABILITY IN TETRAHYMENA. *J. Biol. Chem.* 274:14533-14536.

Mueller, R.D., H. Yasuda, and E.M. Bradbury. 1985. Phosphorylation of histone H1 through the cell cycle of Physarum polycephalum. 24 sites of phosphorylation at metaphase. *J Biol Chem*. 260:5081-6.

Nishiyama, M., K. Oshikawa, Y. Tsukada, T. Nakagawa, S. Iemura, T. Natsume, Y. Fan, A. Kikuchi, A.I. Skoultchi, and K.I. Nakayama. 2009. CHD8 suppresses p53-mediated apoptosis through histone H1 recruitment during early embryogenesis. *Nature Cell Biology*. 11:172-U139.

Ohsumi, K., C. Katagiri, and T. Kishimoto. 1993. Chromosome condensation in Xenopus mitotic extracts without histone H1. *Science*. 262:2033-5.

Orrego, M., I. Ponte, A. Roque, N. Buschati, X. Mora, and P. Suau. 2007. Differential affinity of mammalian histone H1 somatic subtypes for DNA and chromatin. *BMC Biol*. 5:22.

Oudet, P., M. Gross-Bellard, and P. Chambon. 1975. Electron microscopic and biochemical evidence that chromatin structure is a repeating unit. *Cell*. 4:281-300.

Paranjape, S.M., R.T. Kamakaka, and J.T. Kadonaga. 1994. ROLE OF CHROMATIN STRUCTURE IN THE REGULATION OF TRANSCRIPTION BY RNA-POLYMERASE-II. *Annual Review of Biochemistry*. 63:265-297.

Parseghian, M.H., R.F. Clark, L.J. Hauser, N. Dvorkin, D.A. Harris, and B.A. Hamkalo. 1993. Fractionation of human H1 subtypes and characterization of a subtype-specific antibody exhibiting non-uniform nuclear staining. *Chromosome Res*. 1:127-39.

Parseghian, M.H., and B.A. Hamkalo. 2001. A compendium of the histone H1 family of somatic subtypes: an elusive cast of characters and their characteristics. *Biochem Cell Biol*. 79:289-304.

Patterton, H.G., C.C. Landel, D. Landsman, C.L. Peterson, and R.T. Simpson. 1998. The biochemical and phenotypic characterization of Hho1p, the putative linker histone H1 of Saccharomyces cerevisiae. *J Biol Chem*. 273:7268-76.

Ponte, I., J.M. Vidal-Taboada, and P. Suau. 1998. Evolution of the vertebrate H1 histone class: evidence for the functional differentiation of the subtypes. *Mol Biol Evol*. 15:702-8.

Ramakrishnan, V., J.T. Finch, V. Graziano, P.L. Lee, and R.M. Sweet. 1993. Crystal structure of globular domain of histone H5 and its implications for nucleosome binding. *Nature*. 362:219-223.

Ramon, A., M.I. Muro-Pastor, C. Scazzocchio, and R. Gonzalez. 2000. Deletion of the unique gene encoding a typical histone H1 has no apparent phenotype in Aspergillus nidulans. *Mol Microbiol*. 35:223-33.

Robinson, P.J., L. Fairall, V.A. Huynh, and D. Rhodes. 2006. EM measurements define the dimensions of the "30-nm" chromatin fiber: evidence for a compact, interdigitated structure. *Proc Natl Acad Sci U S A*. 103:6506-11.

Robinson, P.J.J., and D. Rhodes. 2006. Structure of the '30 nm' chromatin fibre: A key role for the linker histone. *Current Opinion in Structural Biology*. 16:336-343.

Roth, S.Y., and C.D. Allis. 1992. Chromatin condensation: does histone H1 dephosphorylation play a role? *Trends Biochem Sci*. 17:93-8.

Routh, A., S. Sandin, and D. Rhodes. 2008. Nucleosome repeat length and linker histone stoichiometry determine chromatin fiber structure. *Proc Natl Acad Sci U S A*. 105:8872-7.

Schafer, G., E.M. Smith, and H.G. Patterton. 2005. The Saccharomyces cerevisiae linker histone Hho1p, with two globular domains, can simultaneously bind to two four-way junction DNA molecules. *Biochemistry*. 44:16766-75.

Schalch, T., S. Duda, D.F. Sargent, and T.J. Richmond. 2005. X-ray structure of a tetranucleosome and its implications for the chromatin fibre. *Nature*. 436:138-41.

Sera, T., and A.P. Wolffe. 1998. Role of histone H1 as an architectural determinant of chromatin structure and as a specific repressor of transcription on Xenopus oocyte 5S rRNA genes. *Mol Cell Biol*. 18:3668-80.

Shen, X., and M.A. Gorovsky. 1996. Linker histone H1 regulates specific gene expression but not global transcription in vivo. *Cell*. 86:475-83.

Shen, X., L. Yu, J.W. Weir, and M.A. Gorovsky. 1995. Linker histones are not essential and affect chromatin condensation in vivo. *Cell*. 82:47-56.

Sirotkin, A.M., W. Edelmann, G. Cheng, A. Klein-Szanto, R. Kucherlapati, and A.I. Skoultchi. 1995. Mice develop normally without the H1(0) linker histone. *Proc Natl Acad Sci U S A*. 92:6434-8.

Song, X., and M.A. Gorovsky. 2007. Unphosphorylated H1 Is Enriched in a Specific Region of the Promoter when CDC2 Is Down-Regulated during Starvation. *Mol. Cell. Biol.* 27:1925-1933.

Srebreva, L.N., and J.S. Zlatanova. 1992. Antibodies specific to histone H1 inhibit in vitro transcription in isolated mammalian nuclei. *Mol Cell Biochem*. 110:91-100.

Staynov, D.Z. 2008. The controversial 30 nm chromatin fibre. *Bioessays*. 30:1003-1009.

Staynov, D.Z., and C. Crane-Robinson. 1988. Footprinting of linker histones H5 and H1 on the nucleosome. *Embo J*. 7:3685-91.

Steinbach, O.C., A.P. Wolffe, and R.A. Rupp. 1997. Somatic linker histones cause loss of mesodermal competence in Xenopus. *Nature*. 389:395-9.

Strahl, B.D., and C.D. Allis. 2000. The language of covalent histone modifications. *Nature*. 403:41-45.

Swank, R.A., J.P.H. Th'ng, X.W. Guo, J. Valdez, E.M. Bradbury, and L.R. Gurley. 1997. Four Distinct Cyclin-Dependent Kinases Phosphorylate Histone H1 at All of Its Growth-Related Phosphorylation Sites. *Biochemistry*. 36:13761-13768.

Takata, H., S. Matsunaga, A. Morimoto, R. Ono-Maniwa, S. Uchiyama, and K. Fukui. 2007. H1.X with different properties from other linker histones is required for mitotic progression. *FEBS Lett*. 581:3783-8.

Talasz, H., N. Sapojnikova, W. Helliger, H. Lindner, and B. Puschendorf. 1998. In vitro binding of H1 histone subtypes to nucleosomal organized mouse mammary tumor virus long terminal repeat promotor. *J Biol Chem*. 273:32236-43.

Tanaka, H., N. Iguchi, A. Isotani, K. Kitamura, Y. Toyama, Y. Matsuoka, M. Onishi, K. Masai, M. Maekawa, K. Toshimori, M. Okabe, and Y. Nishimune. 2005. HANP1/H1T2, a novel histone H1-like protein involved in nuclear formation and sperm fertility. *Mol Cell Biol*. 25:7107-19.

Th'ng, J.P., R. Sung, M. Ye, and M.J. Hendzel. 2005. H1 family histones in the nucleus. Control of binding and localization by the C-terminal domain. *J Biol Chem*. 280:27809-14.

Thiriet, C., and J.J. Hayes. 2009. Linker histone phosphorylation regulates global timing of replication origin firing. *J Biol Chem*. 284:2823-9.

Thoma, F., T. Koller, and A. Klug. 1979. Involvement of histone H1 in the organization of the nucleosome and of the salt-dependent superstructures of chromatin. *J Cell Biol*. 83:403-27.

Tomaszewski, R., and A. Jerzmanowski. 1997. The AT-rich flanks of the oocyte-type 5S RNA gene of Xenopus laevis act as a strong local signal for histone H1-mediated chromatin reorganization in vitro. *Nucleic Acids Res*. 25:458-66.

Tremethick, D.J. 2007. Higher-order structures of chromatin: the elusive 30 nm fiber. *Cell*. 128:651-4.

Vicent, G.P., R. Koop, and M. Beato. 2002a. Complex role of histone H1 in transactivation of MMTV promoter chromatin by progesterone receptor. *J Steroid Biochem Mol Biol*. 83:15-23.

Vicent, G.P., R. Koop, and M. Beato. 2002b. Complex role of histone H1 in transactivation of MMTV promoter chromatin by progesterone receptor. *The Journal of Steroid Biochemistry and Molecular Biology*. 83:15-23.

Vila, R., I. Ponte, M. Collado, J.L. Arrondo, and P. Suau. 2001. Induction of secondary structure in a COOH-terminal peptide of histone H1 by interaction with the DNA: an infrared spectroscopy study. *J Biol Chem*. 276:30898-903.

White, C.L., R.K. Suto, and K. Luger. 2001. Structure of the yeast nucleosome core particle reveals fundamental changes in internucleosome interactions. *EMBO J*. 20:5207-18.

Williams, B.A.R., L. Lin, S.M. Lindsay, and J.C. Chaput. 2009. Evolution of a Histone H4-K16 Acetyl-Specific DNA Aptamer. *Journal of the American Chemical Society*. 131:6330-6331.

Wisniewski, J.R., A. Zougman, S. Kruger, and M. Mann. 2007. Mass spectrometric mapping of linker histone H1 variants reveals multiple acetylations, methylations, and phosphorylation as well as differences between cell culture and tissue. *Mol Cell Proteomics*. 6:72-87.

Woodcock, C.L., L.L. Frado, and J.B. Rattner. 1984. The higher-order structure of chromatin: evidence for a helical ribbon arrangement. *J Cell Biol*. 99:42-52.

Woodcock, C.L., A.I. Skoultchi, and Y. Fan. 2006. Role of linker histone in chromatin structure and function: H1 stoichiometry and nucleosome repeat length. *Chromosome Res*. 14:17-25.

Workman, J.L., and A.R. Buchman. 1993. MULTIPLE FUNCTIONS OF NUCLEOSOMES AND REGULATORY FACTORS IN TRANSCRIPTION. *Trends in Biochemical Sciences*. 18:90-95.

Yellajoshyula, D., and D.T. Brown. 2006. Global modulation of chromatin dynamics mediated by dephosphorylation of linker histone H1 is necessary for erythroid differentiation. *Proc Natl Acad Sci U S A*. 103:18568-73.

Yu, Q., H. Kuzmiak, Y. Zou, L. Olsen, P.A. Defossez, and X. Bi. 2009. Saccharomyces cerevisiae linker histone Hho1p functionally interacts with core histone H4 and negatively regulates the establishment of transcriptionally silent chromatin. *J Biol Chem*. 284:740-50.

Zhu, P., W.L. Zhou, J.X. Wang, J. Puc, K.A. Ohgi, H. Erdjument-Bromage, P. Tempst, C.K. Glass, and M.G. Rosenfeld. 2007. A histone H2A deubiquitinase complex coordinating histone acetylation and H1 dissociation in transcriptional regulation. *Molecular Cell*. 27:609-621.

Zippo, A., R. Serafini, M. Rocchigiani, S. Pennacchini, A. Krepelova, and S. Oliviero. 2009. Histone Crosstalk between H3S10ph and H4K16ac Generates a Histone Code that Mediates Transcription Elongation. *Cell*. 138:1122-1136.

Zlatanova, J., and K. Van Holde. 1992. Histone H1 and transcription: still an enigma? *J Cell Sci*. 103 (Pt 4):889-95.

CHAPTER 2*
HISTONE H1 PHOSPHORYLATION SITES MAPPING AND CELL CYCLE REGULATED DYNAMICS IN HELA S3 CELLS

*: Some material was adapted from manuscript:
Histone H1 Phosphorylation is Associated with Transcription by RNA Polymerases I and II
Yupeng Zheng, Sam John, James J. Pesavento, Jennifer R. Schultz-Norton, R. Louis Schiltz, Sonjoon Baek, Ann M. Nardulli, Gordon L. Hager, Neil L. Kelleher and Craig A. Mizzen

2.1 Introduction

Previous investigations have utilized metabolic labeling of synchronized cells with ^{32}P-orthophosphate to detect H1 phosphorylation during the cell cycle (Ajiro et al., 1981a; Ajiro et al., 1981b; Gurley et al., 1995). This approach provides a measure of the net rate of H1 phosphorylation, i.e. the balance between ongoing phosphorylation and dephosphorylation over the interval monitored, that may reveal the true abundance of different phosphorylated forms. Generally, it was found that ^{32}P incorporation into H1 was progressive during the cell cycle: it was low or undetectable in G1 phase, increased moderately during S and G2 phases, peaked sharply near the G2/M transition to attain a maximum during mitosis, and then fell sharply near the end of mitosis. Several studies suggested that interphase phosphorylation occurred preferentially in the C-terminal domain of H1. However, individual sites were not identified and H1 phosphorylation sites being used randomly or hierarchically has not been fully resolved.

The mapping of phosphorylation sites in H1 is not only able to clarify the controversy between sequential and random phosphorylation discussed in the chapter 1.5.1 but also able to greatly benefit the H1 phosphorylation function study. When this project started, the only known H1 phosphorylation sites were obtained from *Tetrahymena* by microsequencing of tryptic phosphopeptides (Mizzen et al., 1999). However, *Tetrahymena* H1, lacking the globular domain, is very different from mammalian H1 and thus is not very useful for the further investigation of the mammalian H1 phosphorylation.

In addition, two mapping results for H1 phosphorylation have been published during our efforts (Garcia et al., 2004; Wisniewski et al., 2007). The novel mass spectrometry technique we adopted allows us to analyze an intact protein. Such technique is called top-down mass spectrometry (TDMS) compared to the conventional bottom-up approach which requires digesting proteins into small peptides before analyzing (Garcia et al., 2007; Pesavento et al., 2004). There are at least there disadvantage of the bottom-up approach: first, it cannot always assign the observed phosphopeptides to five conserved H1 subtypes unambiguously; second, it lost the abundance information of different phosphorylated forms; third, it cannot address whether all the phosphorylation sites are localized to one molecule simultaneously or not.

2.2 The Expression and Phosphorylation of Histone H1 in HeLa S3 Cells

We used Top Down Mass Spectrometry (TDMS) to analyze H1 phosphorylation since it has been shown previously that this approach can be used to characterize the expression and posttranslational modification of histone variants present in mixed samples (Pesavento et al., 2008b; Phanstiel et al., 2008; Thomas et al., 2006). The typical broadband mass spectra of crude H1 prepared from asynchronous HeLa cells was shown in Figure 2.1 A for three selected charge states. The relative abundance for each component was very similar among different charges. As shown in Figure 2.1 B, the spectra from a single charge state was remarkably simple: a total of eight species with distinct molecular weights were readily apparent above background noise. Four of these were clustered between 21200 and 21400 Da (group 1), the other three were clustered between 21700 and 22000 Da (group 2). The last small peak falling between these two clusters had higher charge of +26, thus its molecular mass is actually larger than those in group 2. The molecular mass of the smallest component in group 1, 21261 Da, closely matched the 21262.7 Da predicted for human H1.2 from Genbank NP_005310, assuming the loss of Met residue 1 and acetylation of the newly exposed α-amino group of residue

2 during protein maturation (Polevoda and Sherman, 2003). Further analyses confirmed that this form is mature H1.2 lacking posttranslational modifications (see below). The next largest component in the group 1, 21291 Da, was approx. 30 Da larger than expected for mature H1.2, suggesting either that it was dimethylated (Δm = + 28 Da) or an allelic variant of H1.2 containing one or more amino acid substitutions. Further analyses revealed that this form is a novel A142T substitution allelic variant of H1.2 (H1.2-T142). The 21342 Da component closely matched the molecular mass expected for monophosphorylated mature H1.2 (21342.7 Da), and we shown below that this component is monophosphorylated H1.2 (1p-H1.2-A142). The 21372 Da component was approx. 80 Da larger than expected for unmodified mature H1.2-T142 (21292.7 Da). Further analyses confirmed that this component is monophosphorylated H1.2-T142 (1p-H1.2-T142).

The molecular weights determined for the three components in group 2, 21762 Da, 217842 Da and 21922 Da, closely matched those predicted from Genbank NP_005312 for the unmodified, mono- and diphosphorylated forms of mature H1.4 (21763.0 Da, 21842.9 Da, and 21922.9 Da), respectively. Further analyses confirmed these identifications as shown in Figure 2.1 B. Relative quantification of the allelic and phosphorylated forms of H1.2 in the mass spectrum revealed that monophosphorylation of the A142 and T142 allelic forms was proportional to their expression, and that approx. 28 % of total H1.2 was monophosphorylated in asynchronously growing HeLa S3 cells. The extent of H1.4 monophosphorylation was quite similar to that of H1.2, affecting approx. 29 % of total H1.4, with diphosphorylation affecting approx. 12 % of total H1.4 (Table 2.2).

The third H1 variants detected in TDMS was H1.5 with very low abundance and its phosphorylation levels was lower than the sensitivity limit of FTMS. Previous analyses

have detected the presence of additional H1 variants including $H1^0$, H1.3 and H1.X in adherent HeLa cells (Garcia et al., 2004; Happel et al., 2005; Meergans et al., 1997). However, given the sensitivity limits of TDMS, our data implies that the levels of these proteins are lower than those of H1.2, H1.4 and H1.5, and reveals that H1.2 and H1.4 are expressed in markedly greater amounts than other variants in HeLa S3 cells growing in suspension. The relatively minor amounts of H1.5 is further confirmed by chromatographic and electrophoretic analyses as shown later, which suggest that H1.5 is the third most abundant variant in HeLa cells. Since fewer than approx. 5 % of the cells in asynchronously growing cultures are expected to be in mitosis at a given time, our findings that nearly a third of all H1.2/H1.4 is monophosphorylated and roughly a sixth of all H1.4 is diphosphorylated under these conditions is consistent with previous chromatographic and electrophoretic evidence that interphase H1 phosphorylation is moderately abundant in mammalian cells (Ajiro et al., 1981a; Gurley et al., 1975; Lennox et al., 1982; Talasz et al., 1996).

2.3 H1 is Progressively Phosphorylated during Interphase

As discussed in the introduction, H1 phosphorylation levels are cell cycle regulated. Our TDMS approach is particularly well suited for analyzing both the expression and phosphorylation levels of H1 variants from the crude H1 in a semi-quantitative manner. H1 from cells arrested at G1 by butyrate, G1/S by mimosine and M phase by colchicine were analyzed [21-23]. As shown in Figure 2.2 A, B, the abundance of 1p-H1.4 was barely detectable whereas 1p-H1.2 and 2p-H1.4 fell below the detection limit in the HeLa cells arrested in G1 by 20 mM sodium butyrate treatment for 24 hrs. In addition, H1 phosphorylation levels were also greatly decreased in cells arrested in G1/S by 0.5 mM mimosine treatment for 24 hrs (Krude, 1999). Theses results suggest H1 phosphorylation levels are lowest at G1 and start to increase before cells enter S phase.

To investigate H1 phosphorylation levels during S phase, we analyzed samples prepared at different times after releasing HeLa cells from synchronization at the G1/S boundary by double thymidine blocks. The same seven ion species apparent for samples from asynchronous cells were also observed for post-released samples, but their relative abundances varied after releasing (Figure 2.3). 2p-H1.4, 1p-H1.4 and 1p-H1.2 were increased initially and decreased later in abundance as cells progressed from early S phase to G1 phase of the next cell cycle (i.e., from 2 h to 15 h post-release). Interestingly, both the increase of 1p-H1.4 when cells progressed toward G2/M and decrease of 1p-H1.4 when cells reenter G1 are not as dramatic as seen for 2p-H1.4 and 1p-H1.2. This observation of rapid phosphorylation/dephosphorylation versus slower phosphorylation/dephosphorylation is also seen in the HIC study described below and will be discussed in more details with more frequently sampling data.

For the cells arrested in mitosis by 1 μM colchicine treatment for 18 hrs, maximum of six phosphorylations were added to H1.4 and maximum of four were added to H1.2, which agrees with early biochemistry analysis (Ajiro et al., 1981a; Ajiro et al., 1981b). We also detected unphosphorylated and intermediate phosphorylated H1 forms. Among them, the presence of 0p- 1p- 2p-H1.4 and 0p-, 1p-H1.2 can be explained by the presence of interphase cells (suspension HeLa S3 culture treated with colchicine harvested for this analysis had ~20% of cells remaining outside G2/M based on FACS). It remains unresolved whether these 3p-, 4p-, 5p-H1.4 and 2p-, 3p-H1.4 forms are the existing forms in cells or just simply the degradation forms of 6p-H1.4 and 4p-H1.2 during sample handling. However, the fact that less intermediate phosphorylation forms were observed for the fresh prepared sample analyzed by HIC described later suggests these intermediate phosphorylation forms were more likely introduced during sample handling.

Although intact H1.2 and H1.4 species were observed when crude H1 was analyzed (Figure 2.1), residues 2-5 were missing from most ion species when mild OCAD (Collisionally Activated Dissociation) was applied in FTMS to improve the resolution (Figure 2.2). Similar residue loss was more prominent when homogenous individual HIC peaks was analyzed using the conditions that maintained the intact H1 forms for crude total H1 sample. Loss of these same residues (typically SETA) in histone H1 during electrospray ionization has been reported previously (Wang et al., 1997), and other proteins are also known to be preferentially fragmented at specific peptide bonds during this process (Carroll et al., 2006; Grandori, 2003).

In sum, these TDMS studies of total H1 in HeLa cells have unequivocally determined the 1p-H1.4, 2p-H1.4 and 1p-H1.2 are present in interphase while 6p-H1.4 and 4p-H1.2 are achieved in M phase. In addition, it also demonstrated that the percentage of mono-/di-phosphorylated H1 in interphase starts to increase from G1, keeps progressively increasing when cells traverse S phase and reaches the maximum level in G2/M.

2.4 Resolution of Phosphorylated H1 Variants by HIC

We attempted to directly identify phosphorylation sites in crude H1 using the TDMS approach. However, the fragmentation of phosphorylated H1 achieved by ECD was not sufficient enough for phosphorylation sites identification by this approach due to ion suppression effect (Ouvry-Patat et al., 2008). We have employed RP-HPLC to separate core histones to individual variants for successful characterizing expression and modifications by TDMS in our lab. Unfortunately, we were unable to resolve H1.2 from H1.4 by RP-HPLC (see Appendix 6.1).

There is at least three reasons motivated us to develop a chromatography method to resolve H1 forms differing in either amino acid sequence or degree of phosphorylations.

First, we had trouble to obtain high quality fragments ions by ECD for the MS/MS analysis to map the phosphorylation sites from crude H1, which could be very likely overcome by just using more homogenous fraction. Second, chromatography is more ideal than TDMS for quantification of single form of modification(s) relative to the total pool of that variant and the relative abundance among variants since some ion species will be underrepresented in the TDMS due to ion suppression effect (Pesavento et al., 2006). Third, the ability to purify naturally occurred phosphorylated H1 forms will enable us to do some biophysical studies for H1 phosphorylation in the future, such as how specific phosphorylation in H1 could affect its binding with chromatin or the rate of transcription from reconstituted chromatin.

Similar to RP-HPLC, hydrophobic interaction chromatography (HIC) separates proteins based on surface hydrophobicity. However selectivity is generally superior to that of RP-HPLC for proteins large enough to have significant secondary or tertiary structure. Particularly, HIC has greater sensitivity than other chromatography method to the location of a modification or residue difference, especially if it involves a nonpolar group. Despite this interaction mode does not predict the separation of phosphorylation, we successfully resolve H1 heterogeneity due to both non-allelic amino acid sequence variation and to phosphorylations. As shown in Figure 2.4 A, five major components for H1 prepared from asynchronously growing HeLa cells was resolved. Essentially, these were the same components observed by TDMS except that the A142 and T142 allelic forms of H1.2 were not separated from each other by HIC. Compared to two dimensional approaches using RP-HPLC first to resolve non-allelic H1 variants irrespective of modification, followed by hydrophilic interaction chromatography (HILIC) to resolve phosphorylated forms for each variant fraction individually (Lindner et al., 1997), the HIC approach simplifies comparison of the expression and phosphorylation of H1 variants in different crude samples.

2.5 Mapping H1 Phosphorylation Sites by TDMS

The chromatography purified fraction was desalted, dissolved and then sprayed into the source of FT-ICR via direct infusion mode by ESI. The microdroplets consisting of variably-protonated H1 molecules then pass through a heated metal capillary and skimmer, become desolvated, multiply charged protein ions in the quadrupole region. Specific protein ion charge states can be selected and accumulated before entry into the trapped-ion cell by mass filtering of quadrupole. A typical broadband mass spectrum of HIC purified fraction (peak 1) from crude H1 in mid S HeLa cells was shown in Figure 2.4 B. Many charges states were observed and those ranging from +32 to +25 were shown. Two species were present in most charge states with +160 Da molecular mass shift from either intact mature H1.4 with N-terminal acetylation (purple) or H1.4 losing the residue 2 to 4 (-SETA, green), which suggests peak 1 in HIC is a homogenous diphosphorylated H1.4. The quadrupole was used to select the +28 charge state (inset), eliminating all others from being sent to the ICR cell. The mass spectrum of quadrupole having the same m/z range as the broadband shown in Figure 2.4 C indicates only little amount of ions other than +28 was not eliminated. After a stored waveform inverse Fourier transform (SWIFT) was used to select and accumulate ion specie, all other species were ejected out of the ICR cell and the pure 21492 Da ion specie was ready for the tandem mass analysis (Figure 2.4 C). Tandem mass spectrometry (MS/MS), which consists of the activation of primary ("precursor") ions, dissociation or reaction, followed by mass analysis of the resulting secondary ("product") ions, is useful for sequencing fragment ions that provide detailed structural analysis of modifications (Marshall et al., 1998). Electron capture dissociation (ECD), which is a gentler and more fragment-ion rich method for ion dissociation, is used as our main tools for generating fragment ions for H1 phosphorylation sites mapping. The advantage of ECD is that it only break precursor ion once, which produce one N-terminal fragment called C ion and one C-terminal fragment called Z ion (Cooper et al., 2005). In addition, Infrared

multiphoton dissociation (IRMPD) was used as a supplemental fragmentation method to generate B and Y ions. ECD spectrum of a pure 21492 Da ion specie was shown in Figure 2.5 D. The mass for each fragment ions in the ECD spectrum was manually assigned using MIDAS software and compared with the theoretical mass generated for H1.4-SETA by ProSightPTM ion predictor software (https://prosightptm.scs.uiuc.edu/ionpredictor/) to map two phosphorylation sites predicted from +160 Da mass shift. Series of Z ions, from small to large, can be divided into three groups. First, no mass difference was seen for all the Z ions from Z5 to Z33; second, a +80 Da mass difference was present in all the Z ions from Z34 to Z46, which indicates one phosphorylation is in position 34 counting from C-terminal (i.e. S187); third, a +160 Da mass difference appeared in all the Z ions from Z52, which indicates the second phosphorylation is localized within the 6 residue between position 47 to 52 counting from C-terminal. The reason that the first phosphorylation can be mapped to a single residue whilst the second can only be mapped to a 6 residue stretch is the fragment coverage. However we can take advantage from the fact that phosphorylation only occurs in three amino acid residues: serine, threonine and tyrosine. Since there is only one such phosphorylatable residue among the 6 residues stretch, we can unequivocally assigned second phosphorylation to S172. By contrast, all C ions indicated there is no modification in the rest part of molecule. A graphical fragment ions map covered from residue 158 (Z ions and Y ions) is depicted to show the backbone cleavages that leads to the fragment ions observed in ECD/IRMPD spectra and the phosphorylation sites mapped was indicated as circled residue (Figure 2.4 E). In sum, the phosphorylation sites in the diphosphorylated H1.4 was mapped to S172 and S187 (counting methionine as the first residue) by MS/MS analysis. Very importantly, this top down approach analysis unequivocally proves that peak 1 is homogeneous of diphosphorylated H1.4 with phosphorylation localized to both S172 and S187 but not other sites.

2.6 H1 is Phosphorylated at a Specific Subset of Sites during Interphase

We chose to identify interphase phosphorylation sites in H1 recovered from HIC fractions from 4 hour post-release cells (mid-S). Although phosphorylation levels were clearly rising at this time, there was little possibility of contamination by hyperphosphorylated H1 from mitotic cells compared to later time points (Figure 2.8 A). SDS gel electrophoresis confirmed that peaks 1-3 and peaks 4-5 were essentially homogenous fractions of H1.4 and H1.2, respectively, at this time point (Figure 2.8 B). We also confirmed that several minor peaks which eluted prior to peak 1 contained H1.5, but did not characterize these further.

Mass spectra for HIC peaks 1-5 from the 4 hour post-release sample are shown in Figure 2.5. Consistent with the presence of a single band for peak 3 in SDS gels (Figure 2.8 B), TDMS detected a single major component with molecular mass of 21333.1 Da for peak 3. This closely matched the 21332.8 Da molecular weight predicted for residues 6-219 of human H1.4 lacking any post-translational modifications. MS/MS analyses by ECD confirmed that it matched unmodified H1.4 missing residues 1-5. Analysis of HIC peak 2 detected a single major component with mass of 21412.3 Da, matching the mass predicted for residues 6-219 of H1.4 modified by monophosphorylation (21412.8 Da). Strikingly, MS/MS analyses localized this phosphorylation exclusively to serine 187 located within one of several cyclin-dependent kinase (CDK) substrate consensus motifs commonly found in the C-terminal domain of H1 variants of metazoans. A single major component was also detected for HIC peak 1. This had a molecular mass of 21491.6 Da, closely matching the 21492.7 Da mass predicted for residues 6-219 of H1.4 modified by two phosphorylations. MS/MS analyses revealed that in this case, phosphorylation occurred exclusively on serines 172 and 187, the former residue also occurring within a C-terminal domain CDK substrate consensus motif. Thus, the H1 kinase(s) active during interphase appear to generate predominantly just two phosphorylated forms of

H1.4: pS187-H1.4 and pS172+pS187-H1.4. Moreover, the data also suggest that interphase phosphorylation of H1.4 proceeds in hierarchical fashion, with preferential modification of S187 prior to that of S172 since phosphorylation at S172 alone was not detected. As shown in Figure 2.11, S187 and S172 lie within the most C-terminal and second most C-terminal CDK substrate consensus motifs of human H1.4, respectively.

Two major components were detected by TDMS in each of HIC peaks 4 and 5 (Figure 2.5). The molecular mass of the smaller component in peak 5, 20832.3 Da, matched that predicted for residues 6-213 of H1.2 lacking any modifications (20832.5 Da). The bigger component (20862.2 Da) was 29.9 Da larger and less abundant. MS/MS analyses revealed many peptides in common with H1.2 and localized the +29.9 Da mass difference to a fragment spanning H1.2 residues K127-K159 (data not shown). This difference is consistent with one of several amino acid substitutions which results in a mass change of approx. +30 Da (G>S, A>T, V>E, Thr>Met, Arg>Trp), and also with modifications other than phosphorylation that are common to histones such as dimethylation (+28 Da) or oxidation (+16 Da, +32 Da). However, we were unable to determine directly whether specific residues were substituted or modified since ECD did not fragment this peptide further under the conditions employed. Hence, we used gene-specific primers to amplify the H1.2 coding region from HeLa S3 cell genomic DNA, ligated the products into the pcDNA3.1 vector, and then sequenced plasmids recovered from multiple transformants. This approach detected two polymorphisms in the H1.2 gene that have not been described previously. The first, a T>C substitution at nucleotide 108 (TCT > TCC in the codon for Ser36), does not alter the H1.2 amino acid sequence and was observed in 30/30 clones analyzed (Figure 2.18). The second, a G>A substitution at nucleotide 424 (GCT > ACT in the codon for Ala142), results in an Ala>Thr substitution at residue 142 of the H1.2 protein. This corresponds to a 30.01 Da increase in the predicted molecular weight of the protein, closely matching both the +29.9

Da difference between the minor and major components observed for peak 5 and the +29.7 Da difference from the 20832.5 Da predicted for unmodified H1.2 residues 6-213 based on the gene sequence deposited in Genbank (Table 2.1). This polymorphism was observed in 8/30 of the H1.2 clones analyzed, a frequency similar to the relative abundances of the 20862.2 Da and 20832.3 Da forms observed by MS for peak 5 (Figure 2.5) and the corresponding components in the broadband mass spectrum for crude H1 (Figure 2.1) (i.e. between 1/3 and 1/4). Thus, HeLa S3 cells can express at least two different alleles of H1.2: H1.2-A142 corresponding to Genbank NP_005310, and the novel H1.2-T142 allele described here. Our analyses also suggest that all copies of the H1.2 gene expressed in these cells contain the silent T108C nucleotide polymorphism.

Similarly, analyses of HIC peak 4 also revealed two major components (Figure 2.5). The smaller more abundant species with molecular mass 20912.1 Da closely matched the 20912.5 Da predicted for residues 6-213 of H1.2-A142 with one phosphorylation. The larger less abundant species with molecular mass 20941.7 Da closely matched the 20942.5 Da predicted for residues 6-213 of H1.2-T142 with one phosphorylation. ECD fragmentation and MS/MS analyses localized this phosphorylation exclusively to S173 in both forms. Remarkably, even though H1.2-S173 is homologous with H1.4-S172, the second most C-terminal CDK substrate consensus motif in H1.4, the H1.2-S173 CDK is the most C-terminal such motif in H1.2 since the H1.4-S187 motif (SPAK) is not conserved in H1.2 (SAAK, see Figure 2.11). Thus, despite the presence of several similar motifs elsewhere in these proteins (Figure 2.11), H1.2 and H1.4 are both preferentially phosphorylated at their hindmost CDK substrate consensus motifs during interphase in HeLa S3 cells.

Our TDMS and HIC analyses of total H1 described above have demonstrated phosphorylation in H1 is remarkably simple in HeLa: 1p-H1.2, 1p-H1.4 and 2p-H1.4 in

interphase, 4p-H1.2 and 6p-H1.4 in M phase, no other forms of phosphorylation are observed. However, as discussed in chapter 1.5.1, it has been proposed H1 phosphorylation in interphase (G1, S and G2) is random based on peptide mapping. This hypothesis predicts the existence of isoforms for phosphorylated H1. For example the monophosphorylated H1.4 might be the mixture of forms having one phosphorylation at any site of T18, S27, T146, T154, S172 and S187 (phosphorylation sites occurred in M phase, will be described later) or even any of 16 serines, 10 threonines and 1 tyrosine residues in H1.4. Fortunately, these isoforms can be revealed by MS/MS analysis although they are indistinguishable in the broadband spectrum. During manual comparison of observed fragment ions mass against theoretical C/Z ions mass, once the 80 Da shift appeared in C_n or Z_n fragment ion, the observation of any 0 Da shift in C_{n+i} or Z_{n+i} fragment indicates the existence of isoform, otherwise there is no isoforms. Special cautions have been exercised to search for the indication of isoforms and nothing was detected in our MS/MS analyses for 1p-H1.2, 1p-H1.4 and 2p-H1.4.

The caveat in our conclusion that interphase H1 phosphorylations occur in the specific sites comes from our MS/MS analysis is limited to HIC fractions. There is a small chance that the isoforms of phosphorylated H1 containing other phosphorylation sites reported in bottom-up study (Garcia et al., 2004; Wisniewski et al., 2007) are eluted far away from peaks we analyzed. To confirm our conclusion, we tried to establish ion exchange chromatograph (IEC) for H1 variants and phosphorylation separation. We theorized that binding of H1 with weak cation exchange column are solely governed by charge under the denature condition of 8 M urea and thus isoforms of 1p-H1.2, 1p-H1.4 and 2p-H1.4 having phosphorylation at different sites will bind column equally since they all have the same charge. As shown in Figure 2.6, five peaks were resolved in IEC and the first four peaks have been analyzed by TDMS. It turns out the elution order was the same as predicted by the charge. Assuming free amino- and carboxyl-termini, assigning

+1 for all lysine and arginine residues, -1 for all aspartate and glutamate residues and -1.5 for one phosphate at pH 7 (pKa for HPO_4^{2-} is 7), the predicted net charge at pH 7.0 will be 1p-H1.2: +53.5, 0p-H1.2: +56, 2p-H1.4: +55, 1p-H1.4: +57.5 and 0p-H1.4: +59. The MS/MS analysis was performed for 1p-H1.2 and 2p-H1.4 and no isoform was found as indicated in the ECD map shown in Figure 2.6 C. Taken together, the interphase H1 phosphorylation only occurs in a specific subset of M phase phosphorylation. However, we were unable to rule out the existence of the very low abundant random phosphorylation due to limited sensitivity of TDMS.

2.7 H1 Phosphorylation is Reduced during G1 Phase

The TDMS analyses of crude H1 from different cell cycle stages have found levels of phosphorylation in H1 are lowest in G1 phase and highest in M phase cells. After the identity of five major peaks in HIC from H1 in HeLa S3 were revealed by TDMS, we can use it to analyze the expression and phosphorylation levels of H1 in different samples. First, HIC was utilized to confirm the phosphorylation levels of H1 in HeLa S3 from butyrate arrested G1 phase, asynchronous growing and colchicine arrested M phase. As shown in Figure 2.7 A, B, HIC peaks representing 1p-H1.2, 1p-H1.4 and 2p-H1.4 were less abundant in H1 prepared from cultures arrested in G1 comparing with H1 prepared from asynchronous growing cultures. More specifically, 1p-H1.2 decreased from 18% of total H1 to 4%, 1p- and 2p-H1.4 decreased from 17% and 13% to 8% and undetectable, respectively.

In addition, it has also been reported that expression patterns of H1 variants changed when HeLa cells were arrested in G1 by butyrate treatment (Happel et al., 2009). As shown in Figure 2.7 A, induction of $H1^0$ variants was observed and expression of H1.4 slightly increased relative to H1.2 in G1 arrested cells (elution order of $H1^0$ in HIC will be described in chapter 3).

2.8 H1 Hyperphosphorylation during M Phase

In TDMS study, we have already demonstrated the histone H1 are highly phosphorylated in the mitotic cells with hexaphosphorylated H1.4 (6p-H1.4) and tetraphosphorylated H1.2 (4p-H1.2) as major forms. Compared with five major peaks in HIC chromatograph of H1 from interphase, two additional major peaks were observed and labeled as peak 1 and peak 2 (Figure 2.7 A) when crude H1 purified from colchicine arrested sample was analyzed by HIC. Based on the fact that H1.4 is eluted earlier than H1.2 and addition of phosphorylation weakens the binding of H1 in the HIC column, peak 1 and peak 2 were predicated as 6p-H1.4 and 4p-H1.2.

Using the mapping scheme described before, six phosphorylations in H1.4 were localized to T18, S27, T146, T154, S172 and S187 as indicated in ECD map (counting Met as residue 1, Figure 2.7 D). We only analyzed H1.4 losing the first 4 residues by MS/MS since it is the major form. In addition, we also observed intact H1.4 as minor form in the broadband spectra of HIC fractions and its mass indicated it is also hexaphosphorylated, which excludes the possibility that there is addition phosphorylation localized in the first four residues. Interestingly, five phosphorylatable residues in H1.4, except S27, are found in CDK substrate motif. A sixth phosphorylatable residue, S27, is present in an RKS motif resembling that of aurora kinase substrate which is unique to H1.4 (Figure 2.11). Together with immunochemical analyses (chapter 4), our results suggest that T18, S27, T146, T154, S172 and S187 of H1.4 are phosphorylated exclusively during mitosis, and we refer to them as M sites. In contrast, we refer to H1.4-S172 and H1.4-S187 as I site since it can be phosphorylated during both interphase and mitosis (Table 2.3).

Similarly, four phosphorylations in H1.2 were localized to T31, a fragment spanning residues A134-A151 (either T146 or S150), T154 and a fragment spanning residues

K160-P174 (one of T165, T167 and S173). Unfortunately, due to ion suppression from the presence of H1.4 in HIC fraction, no enough ECD fragments was generated to undoubtedly assign the phosphorylation to residues A134-A151 and residues K160-P174. Based on the observation that all sites containing CDK substrate motif are phosphorylated in H1.4 and the fact that there is only four CDK substrate motifs in H1.2 (Figure 2.11), we conclude the four phosphorylations in H1.2 were localized to T31, T146, T154 and S173 (Table 2.3). Based on our TDMS and immunochemical analyses, we consider T31, T146 and T154 of H1.2 to be M sites whereas S173 is I site (Figure 2.11).

When the relative abundance of different phosphorylation forms was quantified, it turned out the less phosphorylated forms, including 0p-H1.2, 1p-H1.2. 0p-H1.4 and 2p-H1.4, were roughly 20% of total H1 (Figure 2.7 B). Since it was estimated that around 20% of cells remaining outside G2/M in our colchicine enriched mitosis HeLa S3 cells (FACS, data not shown), this data suggests majority of H1 in mitosis achieve the maximum level of phosphorylation (4p-H1.2 and 6p-H1.4).

2.9 I Sites May Differ in Their Phosphorylation Dynamics

We used HIC to analyze H1 from HeLa cells at different times after release from synchronization at the G1/S boundary by double thymidine blocks. The same five major peaks apparent for samples from growing asynchronous cells were also resolved for post released samples, but their relative abundance varied at different sampling points (Figure 2.8 A). The proportion of 2p-H1.4 and 1p-H1.2 (HIC peaks 1 and 4) increased as cells went from early S phase through G2 and M phases of the cell cycle (1 h to 11 h post-release) and then became less abundant as cells entered G1 phase of the next cell cycle (11 h to 19 h post-release). Intriguingly, the abundance of 1p-H1.4 (HIC peak 2) changed by only a small amount between 1 and 19 hours post-release compared to

2p-H1.4 and 1p-H1.2 (HIC peaks 1 and 4) (Figure 2.8 C). In addition, the slower phosphorylation and dephosphorylation of 1p-H1.4 compared with 2p-H1.4 and 1p-H1.2 is also observed in the crude H1 analyzed by TDMS (chapter 2.3). This is consistent with the proposal, based on evidence that ^{32}P incorporation is disproportionately lower than the abundance of phosphorylated H1 in early G1 phase, that some H1 phosphorylation in G1 phase cells may perdure from the preceding cell cycle (Ajiro et al., 1981a). However, why phosphorylation dynamic at Ser187 of H1.4 is different than other sites? The sequence in these interphase phosphorylation sites might offer some explanation. As described in chapter 1.5.2, multiple evidences have indicated CDK2 is the kinase for H1 interphase phosphorylation whereas CDK1 is the kinase for H1 mitosis phosphorylation. In fact, all there sites we investigated here all have CDK motif (S/TPXK/R) but S187 of H1.4 also has Erk motif (P-X-S/T-P), which raise the possibility that less phosphorylation dynamic at Ser187 of H1.4 during cell cycle is the result of double kinase actions from cell cycle regulated CDK together with constant active Erk. The global analysis of temporal dynamics of phosphopeptides after stimulation of HeLa cells with epidermal growth factor (EGF) have identified a slight increase of pS187-H1.4 peptide but no increase of phosphopeptides representing other sites in H1 (Olsen et al., 2006). However, further investigations are required to explore this possibility.

2.10 Hierarchical Phosphorylation of S187 is Not Required for S172 Phosphorylation in H1.4

One approach to study the function of phosphorylation is to mimic unphosphorylated or phosphorylated forms by introducing alanine or glutamic acid in the position of serine/threonine (Dou et al., 1999). We tried to establish stable cell lines with H1.4 carrying S187A point mutation fused with FLAG tag in the C-terminus (H1.4-S187A-FLAG) driven by CMV promoter in HeLa S3 cells. The expression level of H1.4-S187A-FLAG analyzed by SDS-PAGE of acid extraction of whole histones from

isolated nuclei (AEWH) estimated near 1:1 ratio of mutant H1.4 compared to total endogenous H1 (H1.2 plus H1.4). Further quantification indicated H1-to-core ratio increased from ~0.8 in HeLa S3 cells to ~1.3 in H1.4-S187A-FLAG stable cell line with the endogenous H1.2 plus H1.4 slightly decreased to 0.7 H1-to-core ratio. Similar H1-to-core ratio of 1.3 has been reported in the overproduction of $H1^0$ in NIH 3T3 cell line under the inducible promoter (Brown et al., 1996). However, it has been reported that overproduction of H1.2 can only reach ~1.1 H1-to-core ration and the importance of maintaining overproduction at the low level has been emphasized (Brown et al., 1996). This might explain our difficulties in obtaining H1.4-WT-FLAG (wild type) stable cell line using the same approach, i.e. cells can tolerate the overproduction of H1.4-S187A better than H1.4-WT. Nonetheless, the toxicity caused by overproduction of H1.4-S187A became obvious when cells were continuingly cultured for a month. The phenotype included abnormality of genome copies (FACS, data not shown), change of nuclear morphology (IF, data not shown) and loss of H1.4-S187A expression in one month (SDS-PAGE, data not shown).

Despite the toxicity problem, it is ideal to test the stringent of the hierarchy of phosphorylation in the H1.4 molecule is in these stable cell lines. As shown in Figure 2.9 B, the H1.4 molecule having S187A mutation could still be phosphorylated at S172 based on the result from western blot of pTetH1 antibody, which recognizes pS172-H1.4 as described in chapter 3. To further determine the abundance of phosphorylation between H1.4 and H1.4-S187A molecules, we use the HILIC established in chapter 3 to analyze the crude H1 purified from HeLa S3 cells and stable cell lines respectively. The identity of peaks for crude H1 from HeLa cells in HILIC was labeled as the result described in chapter 3 and the appearance of two new peaks were further analyzed by TDMS. Both unphosphorylated H1.4-S187A-FLAG and monophosphorylated H1.4-S187A-FLAG were observed in mass spectrum. The quantification of HILIC

chromatography revealed no significant change in abundance of phosphorylation for all endogenous H1 variants, namely H1.2, H1.4 and H1.5, was observed in H1.4-S187-FLAG stable cell line compared with parental HeLa cells. The relative abundance of monophosphorylation in H1.4-S187A-FLAG, presumably at S172 as indicated by pTetH1, was approx 1/3. Surprisingly, approx 1/3 of H1.2 is monophosphorylated and same amount of H1.4 is phosphorylated when both mono- and di-phosphorylated forms were counted (Figure 2.9 D). These results suggested phosphorylation of H1 is more stringently regulated at the abundance of phosphorylation than how many sites are phosphorylated. In another perspective, H1.4-S187A is similar to H1.2 which is not phosphorylated at the position of S188 (SAAK) due to lack of CDK substrate motif (S/TPXK) but still phosphorylated at S173. The lack of CDK motif at both S188 in human H1.2 or S187/S189 in mouse H1.2 might evolve to serve a specific purpose (Figure 2.11). It would be interesting to see whether insertion of a proline to restore a CDK substrate motif in this portion of H1.2 will cause phosphorylation in this site.

2.11 Sequence Variation at S172 Affects Phosphorylation at S187 and Abundant H1 Phosphorylation Is Not Critical For Cell Survival

Among several other mutant stable cell lines we established, H1.4-S172A was very interesting in a way that the overproduction of this mutant greatly suppressed the expression of endogenous H1.2 and H1.4 to less than 5% (Figure 2.9 E). Such effect has been observed in two different clones, which suggests such high level of overproduction is related to some unknown features of this molecule. Further analysis of this mutant protein by TDMS demonstrate it still can obtain monophosphorylation but in a surprisingly low abundance. By contrast, the abundance of mono- and di-phosphorylation in endogenous H1.4 in the same spectrum remained the same as that those in parental HeLa S3 cells (Figure 2.9 F). Several implications can be inferred

from this interesting result: first, the relative abundant H1 phosphorylation (~30% for H1.2 and H1.4) found in HeLa is not critical for cell survival; second, cells have mechanism to monitor H1 protein level, very likely through proteosome pathway as suggested by (Ryan, 1999); third, phosphorylation at S173 or S187 regions might have distinct function; fourth, the most intriguing observation is that the phosphorylation pattern of H1.4-S172A resembles to human H1.3, which was phosphorylated at very low abundance (described in chapter 3). The lost of CDK motif in S174 (SAKK) of H1.3 or S173 (APKK) of H1.4-S173A resulted in the low abundance of phosphorylation despite the next more C-terminal Ser-containing CDK motif is present in both H1.3 and H1.4-S173A (S189PAK in H1.3 and S187PAK in H1.4-S173A, Figure 2.11). However, determining the mechanism that sequence variation at S172 affecting the phosphorylation at S187 requires further investigation.

2.12 Conclusions and Discussions

Previous efforts to map the phosphorylation sites in H1 from asynchronous cells did not reveal the extent to which the sites identified are phosphorylated in interphase (Garcia et al., 2004; Wisniewski et al., 2007). Earlier analyses of synchronized animal cells established that H1 phosphorylation occurs during interphase and changes in abundance during cell cycle progression (reviewed in (Gurley LR, 1978), (Ajiro et al., 1981a; Ajiro et al., 1981b; Hohmann et al., 1983; Talasz et al., 1996)) but did not identify individual sites of phosphorylation. This has complicated efforts to understand differences in interphase phosphorylation between individual H1 variants, whether sites are phosphorylated in hierarchical or random fashion during interphase, and whether specific functions can be ascribed to any interphase phosphorylations. The novel data described here allows us to clarify some of these issues.

All of the interphase phosphorylation we detected in H1.2 is mapped to S173, implying that this is the sole site of phosphorylation in this variant outside of mitosis (Figure 2.5 and Table 2.3). This finding is further supported by our immunochemical analyses (chapter 4), the stoichiometry of interphase phosphorylation reported previously for H1.2 in several species (Sarg et al., 2005; Talasz et al., 1996; Wang et al., 1997), and much of the data reported for the "H1A" (name by the order of elution in chromatography, not the nomenclature used formally in the literature, see Table 2.1) fraction resolved by cation exchange chromatography for synchronized HeLa cells (Ajiro et al., 1981a; Ajiro et al., 1981b). Thus, modulation of H1.2 function via phosphorylation outside of mitosis is limited to changing the abundance and distribution of pS173-H1.2 in human cells.

Our combined data on H1.4 suggest it is phosphorylated at a maximum of two sites during interphase, consistent with estimates of H1.4 interphase phosphorylation stoichiometry reported previously for several species (Sarg et al., 2005; Talasz et al., 1996; Wang et al., 1997). Our HIC analyses showing that the relative abundance of pS172+pS187-H1.4 increases as cells traverse S and G2 phases (Figure 2.8) also confirm previous work (Talasz et al., 1996). However, our analyses are the first to reveal that this phosphorylation occurs hierarchically at S187 followed by S172. The absence of detectable amounts of pS172-H1.4 further suggests that dephosphorylation of pS172+pS187-H1.4 follows the reverse hierarchy, or occurs in an "all or none" fashion that precludes the accumulation of detectable amounts of the pS172-H1.4 form.

The finding that phosphorylation of S187 precedes that of S172 in H1.4 suggests that features of H1.4 or the respective kinase(s) impart a C>N directionality to interphase phosphorylation, consistent with previous evidence that interphase phosphorylation occurs predominantly at Ser residues in the C-terminal domain, and that N-terminal domain sites are generally not phosphorylated until just prior to mitosis (Ajiro et al.,

1981a; Ajiro et al., 1981b; Gurley LR, 1978). However recent evidence suggests the opposite directionality for H1.5 interphase phosphorylation in human cells, starting at S18 in early G1 followed by S172 and S188 (Talasz et al., 2009). Notably, H1.5 is the only somatic variant in humans with a Ser-containing CDK motif in the N-terminal domain (Figure 2.11). Taken together, the available data suggest that interphase H1 phosphorylation is specific for Ser-containing CDK motifs and proceeds hierarchically in variants with multiple SPKK/SPAK motifs, although the C>N directionality of multi-site interphase phosphorylation may be variant-specific. Currently, there is no data to exclude the possibility that the accessibility of tails is the determining factor for interphase phosphorylation, swapping the Ser-containing I site to the threonine and analyzing the phosphorylation pattern of the mutant protein will help to further clarity these possibilities.

2.13 Materials and Methods

HeLa / HeLa S3 Cell Culture

HeLa S3 cells (ATCC) were grown in suspension in Joklik's modified minimal essential medium supplemented with 10% (v/v) newborn calf serum (NCS) in spinner flask at 37 ℃ and 2% CO_2. HeLa cells were also obtained from ATCC and maintained as a monolayer in Dulbecco's modified Eagle's medium (DMEM) supplemented with 10% NCS at 37 ℃ and 5% CO_2. Asynchronous cultures were maintained in logarithmically growing phase by controlling density under 3×10^5 to 3.5×10^5 cells/ml.

Stable Cell Line Cloning

Plasmids of Histone H1.4-WT and H1.4-M5 (T18, T146, T154, S172 and S187 all mutated to alanine) with FLAG (sequence: DYKDDDDK) fused with the C-terminus through six amino acid linker (STDPLP) in pcDNA3.1 hygo(+) were the gift from Herrera (Contreras et al., 2003). Point mutations of S172A and S187A were introduced

by site-directed mutagenesis at A(514)GC->GCC and A(559)GC->GCC respectively (primer: 5'-GGAGCCAAAAAAGCGAAAGCCCCGAAAAAGGCGAAAGC, 5'-GGCGCCCAAGGCCCCAGCGAAGGCCAAAG). For Ser->Glu substitutions, underline nucleotides were mutated to GAG. Dosage of hygromycin B for HeLa S3 was established at 300 μg/ml, which was the minimum dosage able to kill >95% cells in 2 weeks. Cells were transfected with 4.0 μg plasmid with 10 μl lipofectamine 2000 in 6-well plate format according to manufacture protocol and were subcultured to P100 dish with selection of 300 μg/ml hygromycin B at day 3. Clones appeared after ~3 weeks of selection were picked up by localized trypsin digestion under phase-contrast microscope using p200 pipette and further cloned by limited serial dilution in a 96-well plate.

Cell Synchronization and FACS

Cells were synchronized by double thymidine block as described previously (Knehr et al., 1995). Briefly, cells were blocked in 2 mM thymidine for 16 hrs, released into fresh Joklik for 9 hrs, blocked in 2 mM thymidine for another 16 hrs to synchronize in G1/S boundary. Cells at different stages of the cell cycle were obtained by harvesting them at different time after releasing from second thymidine block. Cells were collected by centrifugation, quickly washed twice with cold Tris-buffered saline (TBS; 20 mM Tris, 150 mM NaCl, pH 7.5), and the cell pellets were flash frozen in liquid N_2 and stored at –80 ℃ prior to nuclei isolation. The degree of synchrony was assessed by Fluorescence-Activated Cell Sorting (FACS) analysis of propidium iodide stained cells fixed by 70% ethanol, which was taken hourly after release. Colchicine-arrested samples were also prepared by adding 1 μM colchicine to growing asynchronous cultures (3×10^5 to 3.5×10^5 cells/ml) for 18 h before harvesting.

Histone Extraction

HeLa S3 nuclei were isolated with NIB buffer (15 mM Tris, 60 mM KCl, 15 mM NaCl, 5 mM $MgCl_2$, 1 mM $CaCl_2$, 250 mM Sucrose, pH 7.5) containing 0.5 mM 4-(2-aminoethyl)benzenesulfonyl fluoride hydrochloride (AEBSF), 5 nM microcystin, and 10 mM Na butyrate and extracted with 0.4 N H_2SO_4. Crude histone H1 was prepared by selective precipitation of other proteins with 5% (w/v final) perchloric acid (PCA) from 0.4 N H_2SO_4 acid extraction. This fraction was called PCA-Soluble (PCAS) and is mostly consisting of histone H1 and the precipitated fraction was called PCAI and is mostly consisting of core histones. H1 remained in PCAS was recovered by precipitation with 20% (w/v, final) trichloroacetic acid (TCA). The precipitation was washed with 0.1% HCl acetone once followed with twice wash of acetone.

HPLC (RP, HIC and HILIC)

Beckman System Gold Programmable Solvent Module 126 and Detector Module 166/168 were controlled by the 32 karat software. Absorbance was monitored at 214 nm.

Reverse phase high performance liquid chromatography (RP-HPLC): Column used included ES industries Chromega MC18 analytical column, 25 cm x 4.6 mm, 1000 Å diam. pores, Vydac C_4, C_8 and C_{18} column (4.6 mm [inside diameter] by 250 mm). Multistep linear gradient from buffer A (0.1% v/v trifluoroacetic acid (TFA) in 5% v/v CH_3CN) to buffer B (0.094% TFA in 90% CH_3CN) with flow rate of 0.8 ml/min was used to purify PCA extracted H1. Collected fractions were recovered by Speed-Vacuum.

Hydrophobic Interaction Chromatography (HIC): PolyPROYL A column (PolyLC Inc., 4.6 mm [inside diameter] by 100 mm, 3 μm spherical silica with 150 nm diam. pores) with a multistep linear gradient from buffer A (2.5 M $(NH)_2SO_4$, 50 mM ethylenediamine, pH7.0) to buffer B (1.0 M $(NH)_2SO_4$, 50 mM ethylenediamine, pH7.0). Collected fractions were recovered by RP-HPLC. Chromatograph was exported as

ASCII file from 32 Karat and replot in Excel. The slop was calculated from the beginning to the end of peaks and used to subtract the baseline.

Hydrophilic Interaction Chromatrography (HILIC): polyCAT A column (PolyLC Inc., 4.6 mm [inside diameter] by 200 mm, 5 um spherical silica with 100 nm diam. pores) with a multistep linear gradient from buffer A (70% CH_3CN, 15mM triethylamine/H_3PO_4, pH3.0) to buffer B (70% CH_3CN, 0.68M $NaClO_4$, 15mM triethylamine/H_3PO_4, pH3.0). The volatile organic content of fractions was removed by Speed-Vacuum and histone H1 was recovered from aqueous parts by 20% TCA precipitation.

Mass Spectrometry

All data were acquired on a custom 8.5 T quadrupole Fourier transform ion cyclotron resonance mass spectrometer with an ESI source operated in positive-ion mode as described previously(Patrie et al., 2004; Pesavento et al., 2008b). Desalted HIC/HILIC fractions or crude PCAS were dissolved in 50% methanol + 1% formic acid and introduced into the mass spectrometer by continuous infusion using a syringe pump or a NanoMate 100 (Advion) with low-flow nanospray chips. Targeted ion species were externally accumulated in an octopole ion trap, transferred to the ion cyclotron resonance (ICR) cell, isolated by Stored Waveform Inverse Fourier Transform (SWIFT), and then fragmented by Electron Capture Dissociation (ECD). Data were collected using the modular ICR data acquisition system (MIDAS). The mass values for individual ion fragments were manually determined and compared with theoretical C and Z ion mass values. The mass differences were used to assign the modifications to specific sites. ProSight PTM, a Web-based software and database suite, was used to augment the manual identification and characterization of histone H1 post-transcriptional modifications (https://prosightptm.scs.uiuc.edu). Masses are reported as neutral, monoisotopic species.

2.14 References

Ajiro, K., T.W. Borun, and L.H. Cohen. 1981a. Phosphorylation states of different histone 1 subtypes and their relationship to chromatin functions during the HeLa S-3 cell cycle. *Biochemistry*. 20:1445-1454.

Ajiro, K., T.W. Borun, B.S. Shulman, G.M. McFadden, and L.H. Cohen. 1981b. Comparison of the structures of human histone 1A and 1B and their intramolecular phosphorylation sites during the HeLa S-3 cell cycle. *Biochemistry*. 20:1454-1464.

Albig, W., E. Kardalinou, B. Drabent, A. Zimmer, and D. Doenecke. 1991. Isolation and characterization of two human H1 histone genes within clusters of core histone genes. *Genomics*. 10:940-8.

Brown, D.T., B.T. Alexander, and D.B. Sittman. 1996. Differential effect of H1 variant overexpression on cell cycle progression and gene expression. *Nucleic Acids Res*. 24:486-93.

Carroll, J., I.M. Fearnley, and J.E. Walker. 2006. Definition of the mitochondrial proteome by measurement of molecular masses of membrane proteins. *Proc Natl Acad Sci U S A*. 103:16170-5.

Contreras, A., T.K. Hale, D.L. Stenoien, J.M. Rosen, M.A. Mancini, and R.E. Herrera. 2003. The dynamic mobility of histone H1 is regulated by cyclin/CDK phosphorylation. *Mol Cell Biol*. 23:8626-36.

Cooper, H.J., K. Hakansson, and A.G. Marshall. 2005. The role of electron capture dissociation in biomolecular analysis. *Mass Spectrom Rev*. 24:201-22.

Dou, Y., C.A. Mizzen, M. Abrams, C.D. Allis, and M.A. Gorovsky. 1999. Phosphorylation of linker histone H1 regulates gene expression in vivo by mimicking H1 removal. *Mol Cell*. 4:641-7.

Drabent, B., K. Franke, C. Bode, U. Kosciessa, H. Bouterfa, H. Hameister, and D. Doenecke. 1995. Isolation of two murine H1 histone genes and chromosomal mapping of the H1 gene complement. *Mamm Genome*. 6:505-11.

Garcia, B.A., S.A. Busby, C.M. Barber, J. Shabanowitz, C.D. Allis, and D.F. Hunt. 2004. Characterization of phosphorylation sites on histone H1 isoforms by tandem mass spectrometry. *J Proteome Res*. 3:1219-27.

Garcia, B.A., J.J. Pesavento, C.A. Mizzen, and N.L. Kelleher. 2007. Pervasive combinatorial modification of histone H3 in human cells. *Nat Methods*. 4:487-9.

Grandori, R. 2003. Origin of the conformation dependence of protein charge-state distributions in electrospray ionization mass spectrometry. *J Mass Spectrom*. 38:11-5.

Gurley, L.R., J.G. Valdez, and J.S. Buchanan. 1995. Characterization of the Mitotic Specific Phosphorylation Site of Histone H1. *J. Biol. Chem.* 270:27653-27660.

Gurley, L.R., R.A. Walters, and R.A. Tobey. 1975. Sequential phsophorylation of histone subfractions in the Chinese hamster cell cycle. *J. Biol. Chem.* 250:3936-3944.

Gurley LR, W.R., Barham SS, Deaven LL. 1978. Heterochromatin and histone phosphorylation. *Exp Cell Res.* 111:373-383.

Happel, N., E. Schulze, and D. Doenecke. 2005. Characterisation of human histone H1x. *Biol Chem*. 386:541-51.

Happel, N., J. Warneboldt, K. Hanecke, F. Haller, and D. Doenecke. 2009. H1 subtype expression during cell proliferation and growth arrest. *Cell Cycle*. 8:2226-32.

Hohmann, P.G., D.X. He, and T.B. Shows. 1983. Relationship between H1 histone phosphorylation and genome replication in a mouse-Chinese hamster somatic cell hybrid. *Exp Cell Res*. 143:207-16.

Knehr, M., M. Poppe, M. Enulescu, W. Eickelbaum, M. Stoehr, D. Schroeter, and N. Paweletz. 1995. A critical appraisal of synchronization methods applied to achieve maximal enrichment of HeLa cells in specific cell cycle phases. *Exp Cell Res*. 217:546-53.

Krude, T. 1999. Mimosine arrests proliferating human cells before onset of DNA replication in a dose-dependent manner. *Exp Cell Res*. 247:148-59.

Lennox, R.W., and L.H. Cohen. 1984. The alterations in H1 histone complement during mouse spermatogenesis and their significance for H1 subtype function. *Dev Biol*. 103:80-4.

Lennox, R.W., R.G. Oshima, and L.H. Cohen. 1982. The H1 histones and their interphase phosphorylated states in differentiated and undifferentiated cell lines derived from murine teratocarcinomas. *J Biol Chem*. 257:5183-9.

Lindner, H., B. Sarg, and W. Helliger. 1997. Application of hydrophilic-interaction liquid chromatography to the separation of phosphorylated H1 histones. *J Chromatogr A*. 782:55-62.

Marshall, A.G., C.L. Hendrickson, and G.S. Jackson. 1998. Fourier transform ion cyclotron resonance mass spectrometry: a primer. *Mass Spectrom Rev*. 17:1-35.

Meergans, T., W. Albig, and D. Doenecke. 1997. Varied expression patterns of human H1 histone genes in different cell lines. *DNA Cell Biol*. 16:1041-9.

Mizzen, C.A., Y. Dou, Y. Liu, R.G. Cook, M.A. Gorovsky, and C.D. Allis. 1999. Identification and Mutation of Phosphorylation Sites in a Linker Histone. PHOSPHORYLATION OF MACRONUCLEAR H1 IS NOT ESSENTIAL FOR VIABILITY IN TETRAHYMENA. *J. Biol. Chem.* 274:14533-14536.

Olsen, J.V., B. Blagoev, F. Gnad, B. Macek, C. Kumar, P. Mortensen, and M. Mann. 2006. Global, in vivo, and site-specific phosphorylation dynamics in signaling networks. *Cell*. 127:635-48.

Ouvry-Patat, S.A., M.P. Torres, C.A. Gelfand, H.H. Quek, M. Easterling, J.P. Speir, and C.H. Borchers. 2008. Top-Down Proteomics on a High-field Fourier Transform Ion Cyclotron Resonance Mass Spectrometer. Vol. 492. 215-231.

Patrie, S.M., J.P. Charlebois, D. Whipple, N.L. Kelleher, C.L. Hendrickson, J.P. Quinn, A.G. Marshall, and B. Mukhopadhyay. 2004. Construction of a hybrid quadrupole/Fourier transform ion cyclotron resonance mass spectrometer for versatile MS/MS above 10 kDa. *J Am Soc Mass Spectrom*. 15:1099-108.

Pesavento, J.J., C.R. Bullock, R.D. LeDuc, C.A. Mizzen, and N.L. Kelleher. 2008a. Combinatorial modification of human histone H4 quantitated by two-dimensional liquid chromatography coupled with top down mass spectrometry. *J Biol Chem*. 283:14927-37.

Pesavento, J.J., Y.B. Kim, G.K. Taylor, and N.L. Kelleher. 2004. Shotgun Annotation of Histone Modifications: A New Approach for Streamlined Characterization of Proteins by Top Down Mass Spectrometry. *J. Am. Chem. Soc.* 126:3386-3387.

Pesavento, J.J., C.A. Mizzen, and N.L. Kelleher. 2006. Quantitative analysis of modified proteins and their positional isomers by tandem mass spectrometry: human histone H4. *Anal Chem*. 78:4271-80.

Pesavento, J.J., H. Yang, N.L. Kelleher, and C.A. Mizzen. 2008b. Certain and progressive methylation of histone H4 at lysine 20 during the cell cycle. *Mol Cell Biol*. 28:468-86.

Phanstiel, D., J. Brumbaugh, W.T. Berggren, K. Conard, X. Feng, M.E. Levenstein, G.C. McAlister, J.A. Thomson, and J.J. Coon. 2008. Mass spectrometry identifies and quantifies 74 unique histone H4 isoforms in differentiating human embryonic stem cells. *Proc Natl Acad Sci U S A*. 105:4093-8.

Polevoda, B., and F. Sherman. 2003. N-terminal acetyltransferases and sequence requirements for N-terminal acetylation of eukaryotic proteins. *J Mol Biol*. 325:595-622.

Ryan, C.A. 1999. Phosphorylation of Histone H1 During S Phase in Human Cells. *In* Department of Biology. Vol. Doctor of Philosophy. Boston College.

Sarg, B., W. Helliger, H. Talasz, B. Forg, and H.H. Lindner. 2005. Histone H1 phosphorylation occurs site-specifically during interphase and mitosis. Identification of a novel phosphorylation site on histone H1. *J Biol Chem*.

Talasz, H., W. Helliger, B. Puschendorf, and H. Lindner. 1996. In Vivo Phosphorylation of Histone H1 Variants during the Cell Cycle. *Biochemistry*. 35:1761-1767.

Talasz, H., B. Sarg, and H.H. Lindner. 2009. Site-specifically phosphorylated forms of H1.5 and H1.2 localized at distinct regions of the nucleus are related to different processes during the cell cycle. *Chromosoma*. 118:693-709.

Thomas, C.E., N.L. Kelleher, and C.A. Mizzen. 2006. Mass spectrometric characterization of human histone H3: a bird's eye view. *J Proteome Res*. 5:240-7.

Wang, Z.F., A.M. Sirotkin, G.M. Buchold, A.I. Skoultchi, and W.F. Marzluff. 1997. The mouse histone H1 genes: gene organization and differential regulation. *J Mol Biol*. 271:124-38.

Wisniewski, J.R., A. Zougman, S. Kruger, and M. Mann. 2007. Mass spectrometric mapping of linker histone H1 variants reveals multiple acetylations, methylations, and phosphorylation as well as differences between cell culture and tissue. *Mol Cell Proteomics*. 6:72-87.

2.15 Tables and Figures

Table 2.1

Histone H1 Nomenclature

	I	II	accession number	GenBank Official Symbol	average MW	monoisotopic MW	MW losing 1~4 residues	aa
human	hH1.1		NM_005325	HIST1H1A	21710.9	21697.826	21281.635	214
	hH1.2	H1d	NM_005319	HIST1H1C	21233.5	21220.706	20832.547	212
	hH1.3	H1c	NM_005320	HIST1H1D	22218.7	22205.278	21817.119	220
	hH1.4	H1b	NM_005321	HIST1H1E	21734.0	21720.963	21332.804	218
	hH1.5	H1a	NM_005322	HIST1H1B	22580.1	22566.468	22047.268	225
	hH10		NM_005318		20731.7	20719.154		193
	hH1x		NM_006026		22355.9	22342.492		212

	III	IV	accession number	GenBank Official Symbol	average MW	monoisotopic MW	-SETA MW	aa
mouse	mH1.1	H1a	NM_030609	Hist1h1a	21653.9	21640.866	21252.706	212
	mH1.2	H1c	NM_015786	Hist1h1c	21235.4	2122.681	20764.532	211
	mH1.3	H1d	NM_145713	Hist1h1d	21968.3	21955.085	21566.925	220
	mH1.4	H1e	NM_015787	Hist1h1e	21846.1	21832.975	21444.816	218
	mH1.5	H1b	NM_020034	Hist1h1b	22444.9	22431.395	22043.235	222
	mH10		NM_008197		20729.7	20717.15		193
	mH1x		NM_198622		20019.9	2008.059		187

Nomenclature proposed (I) for human H1 based on gene sequence (Albig et al., 1991), (II) for human H1 based on protein sequence [34, 35], (III) for mouse H1 based on gene sequence (Drabent et al., 1995), (IV) for mouse H1 based on 2-D gel separation (Lennox and Cohen, 1984)

Table 2.2

The Relative Abundance of Phosphorylated H1.2 and H1.4 in Asynchronously Growing HeLa S3 Cells

	H1.2		H1.4		
	0p	1p	0p	1p	2p
A142	48%	20%	59%	29%	12%
T142	23%	8%			
Total	72%	28%			

Phosphorylated and nonphosphorylated forms of H1.2 and H1.4 in crude H1 are expressed as a percentage of the total of the respective variant detected by Top Down mass spectrometry according to the method described in (Pesavento et al., 2008a).

Table 2.3

Sites Phosphorylated in H1.2 and H1.4 during Interphase and Mitosis in HeLa S3 cells

		Molecular weight[a] (Da)				
	HIC peak[b]	Measured	Predicted[c]	Δ*m*	Variant[d]	Modifications[e]
Interphase	1	21491.6	21332.8	+160	H1.4	pS172, pS187
	2	21412.3	21332.8	+80	H1.4	pS187
	3	21333.1	21332.8	0	H1.4	none
	4	20912.1	20832.6	+80	H1.2 (A142)	pS173
		20941.7	20832.6	+110	H1.2 (T142)	pS173
	5	20832.3	20832.6	0	H1.2 (A142)	none
		20862.2	20832.6	+30	H1.2 (T142)	none
Mitosis	6p-H1.4	21813.9	21332.8	+480	H1.4	pT18, pS27, pT146, pT154, pS172, pS187
	4p-H1.2	21153.3	20832.6	+320	H1.2 (A142)	pT31, pT146, pT154, pS173
		21182.9	20832.6	+350	H1.2 (T142)	pT31, pT146, pT154, pS173

[a] Reported as neutral monoisotopic species.

[b] HIC peaks are labeled as in Fig. 1B.

[c] Predicted from Genbank accession numbers NP_005312 (H1.4) and NP_005310 (H1.2) assuming the loss of Met1 during protein maturation *in vivo* and residues 2-5 during electrospray ionization.

[d] Peak identifications are based on MS/MS sequencing of multiple ECD fragment ions. The A142 and T142 allelic variants of H1.2 were detected initially by mass spectrometry and confirmed by genotyping as described in Supp. Fig. 1.

[e] Phosphorylated residues were identified by MS/MS sequencing of ECD fragment ions. Analyses of the H1.2(T142) forms indicated that phosphorylated residues were identical to those determined for the H1.2 (A142) forms.

Figure 2.1

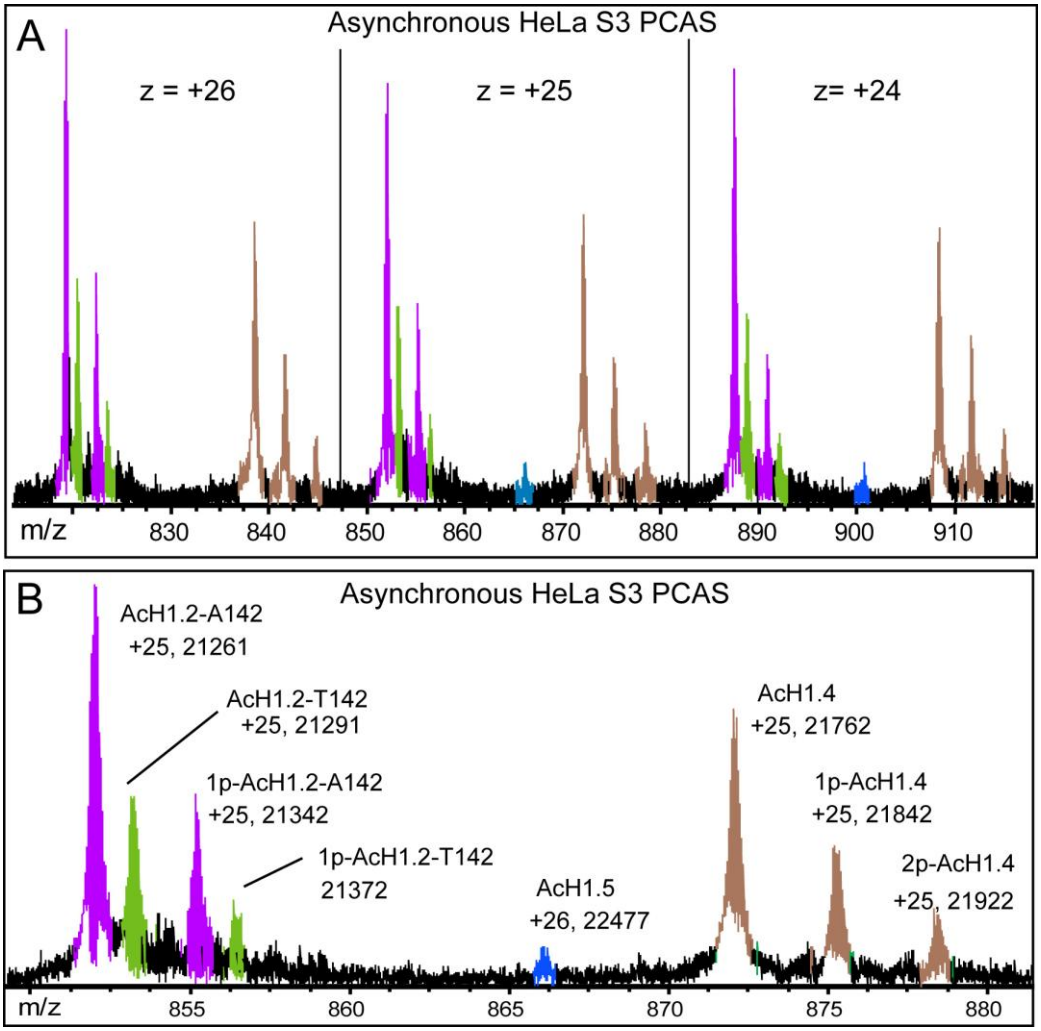

H1 Variant Expression and Phosphorylation in HeLa S3 Cells

The presence of H1 variants shown were confirmed by intact mass and/or gas phase fragmentation during MS/MS analysis. Phosphorylation levels were inferred from the difference between the molecular mass measured for each component and the value predicted for the respective unmodified H1 variant. Molecular masses are reported for the neutral monoisotopic species. PCAS = perchloric acid extracted crude H1

(A) The mass spectrum of crude H1 purified from asynchronously growing HeLa S3 cells. Three charge states are shown here and the relative abundances of H1.2 cluster and H1.4 cluster are similar in three charge sates. The charge for the H1.5 is one more than labeled.

(B) Z= +25 in the H1.2/H1.4 cluster and Z= +26 for H1.5. H1.2 and H1.4 are major variants with minor variant of H1.5. Percentage of phosphorylation for H1.2 and H1.4 is relative high. The Ala142Thr polymorphism in H1.2 was confirmed by genotyping (see text). All forms were missing Met1 and α-N-acetylated at Ser2.

Figure 2.2

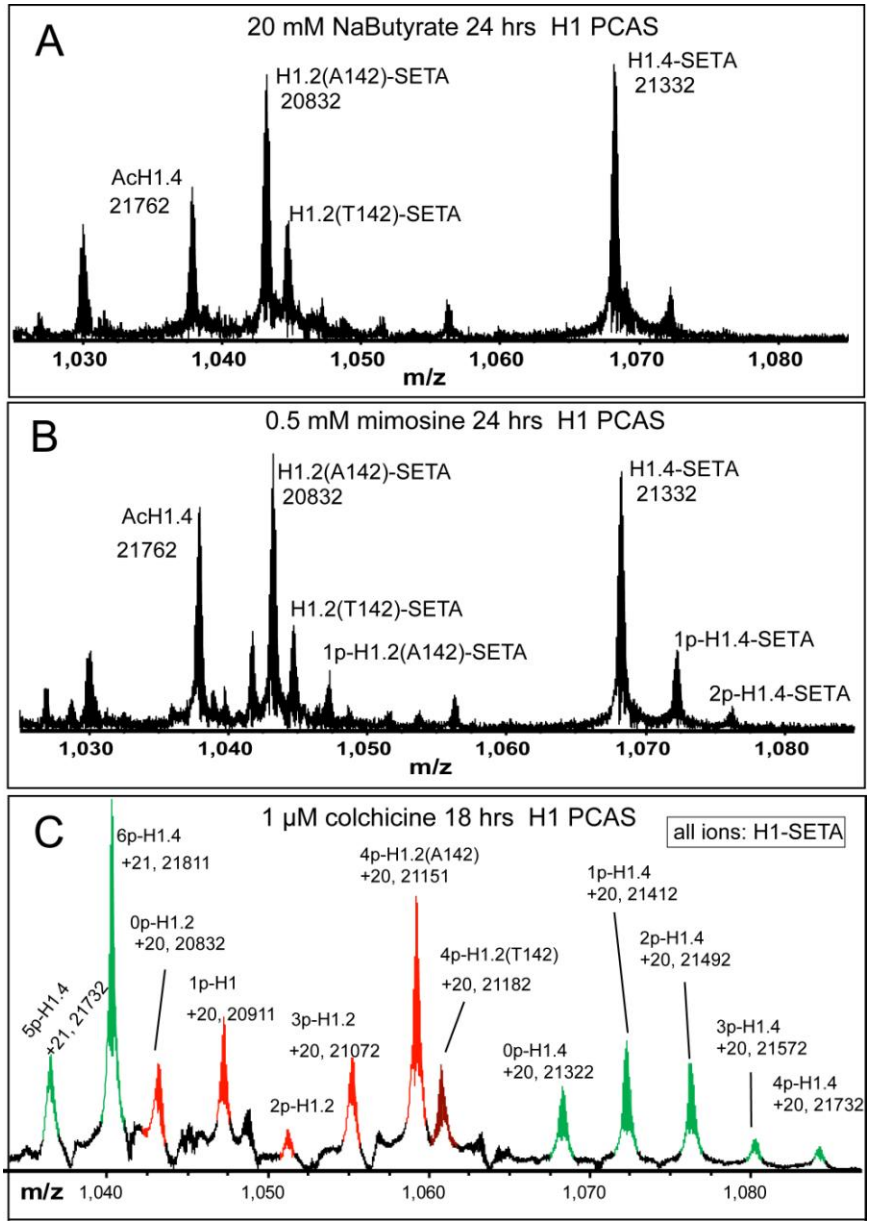

The Levels of Phosphorylated H1.2/H1.4 Are Low in G1 Phase but High in M Phase

Phosphorylation levels were inferred from the difference between the molecular mass measured for each component and the predicted mass for the unmodified H1 variants. Molecular masses are reported for the neutral monoisotopic species. Only the spectrum of the most abundant charge state is shown. Both forms missing Met1 and α-N-acetylated at Ser2 and missing residues 2-5 (SETA) during electrospray ionization (see text) were observed. PCAS = crude H1

The mass spectrum of crude H1 purified from HeLa S3 cells arrested in G1 by sodium butyrate (A), cells arrested in late G1 by mimosine (B) and cells arrested in M phase by colchicine (C).

Figure 2.3

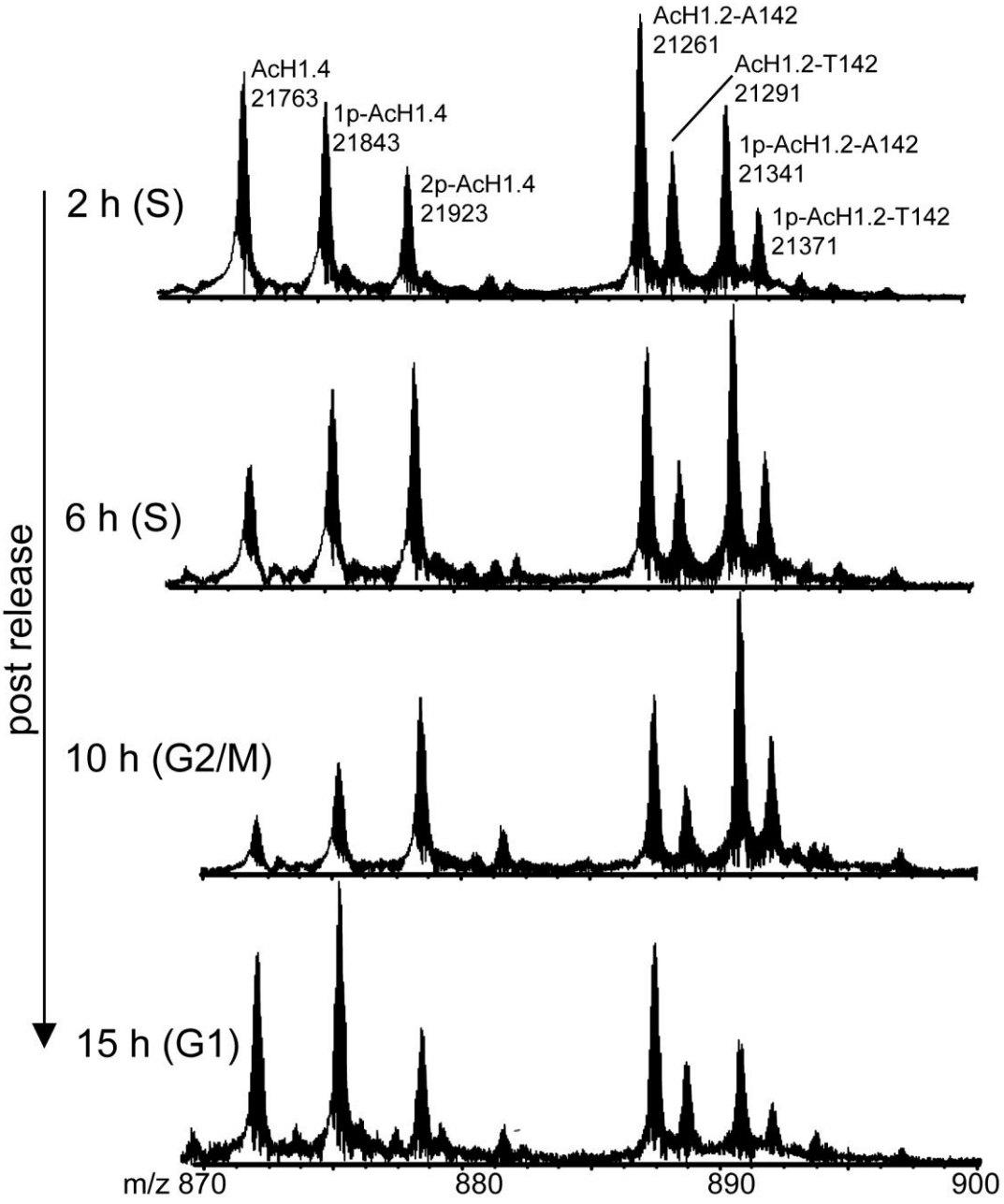

FTMS Analyses of H1 Phosphorylation during the Cell Cycle

The mass spectra of crude H1 prepared from HeLa S3 cells at selected times after release from double thymidine block synchronization. The time point of release and the cell cycle stages it represents is labeled in the left of each spectrum. The identities of each peak in the spectrum were determined by the intact mass or MS/MS analysis as described in the text and are labeled in the top of figure. Molecular masses are reported for the neutral monoisotopic species. Only the spectrum of the most abundant charge state is shown. All forms were missing Met1 and α-N-acetylated at Ser2.

Figure 2.4

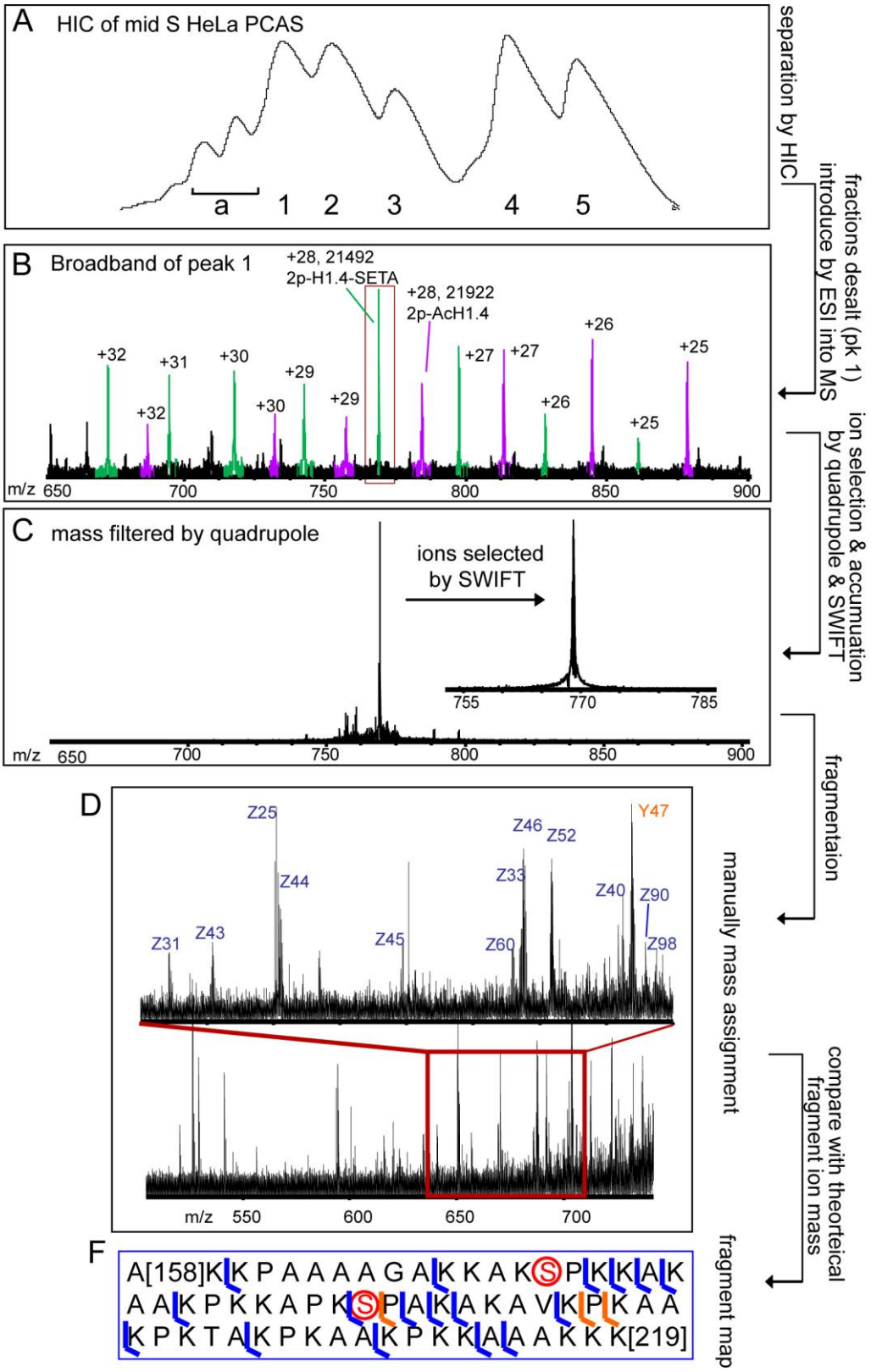
A
HIC of mid S HeLa PCAS
a
1
2
3
4
5
separation by HIC
fractions desalt (pk 1)
introduce by ESI into MS
B
Broadband of peak 1
+28, 21492
2p-H1.4-SETA
+28, 21922
2p-AcH1.4
+32
+31
+30
+29
+27
+26
+25
m/z 650 700 750 800 850 900
ion selection & accumuation
by quadrupole & SWIFT
C
mass filtered by quadrupole
ions selected
by SWIFT
755 770 785
m/z 650 700 750 800 850 900
fragmentaion
D
Z25
Z44
Z31
Z43
Z45
Z46
Z52
Z33
Z60
Y47
Z40
Z90
Z98
m/z 550 600 650 700
manually mass assignment
compare with theorteical
fragment ion mass
F
A[158]KKPAAAAGAKKAKSPKKAK
AAKPKKAPKSPAKAKAVKPKAA
KPKTAKPKAAKPKKAAAKKK[219]
fragment map

Figure 2.4 (cont.)

H1 Variant Identification and Phosphorylation Site Mapping

(A) Crude H1 prepared from HeLa S3 cells was analyzed by Hydrophobic Interaction Chromatography (HIC). PolyPROPYL A column (PolyLC), 100 x 4.6 mm, base = 3 μm spherical silica with 1500 Å diam. pores. Buffer A: 2.5 M $(NH_4)_2$ SO_4 + 50 mM ethylendiamine pH 7.0, Buffer B: 1.5 M (NH_4) $_2SO_4$ + 50 mM ethylendiamine pH 7.0. Column eluate absorbance at 214 nm is plotted for equivalent portions of each separation. Peaks are numbered according to elution order. Each peak was desalted by RP-HPLC and recovered by Speed-Vacuum, then identified by mass spectrometry. (B) ESI-FT mass spectrum (28 scans) of intact H1 purified from HIC peak 1. Intact ions with charges ranging from +25 to +32 are shown. Both intact form of 2p-H1.4 with N-terminal acetylation and the form losing the first 4 residues (2p-H1.4-SETA) are observed in most charge states. (C) The most abundant form with +28 charge and losing SETA residues were selected by quadrupole and further accumulated by SWFT. (D) ECD spectrum of fragment ions from isolated ion species, only part of spectrum is shown here. (E) ECD and IRMPD fragmentation map was generated by comparing the manually assigned mass value for ions in the ECD and IRMPD MS/MS spectrum with theoretical fragment mass value to map the phosphorylation sites. Blue " ⌊" represents Z ions from ECD, orange " ⌊" represents Y ions from IRMPD and the circle around a residue represents phosphorylation in this site.

Figure 2.5

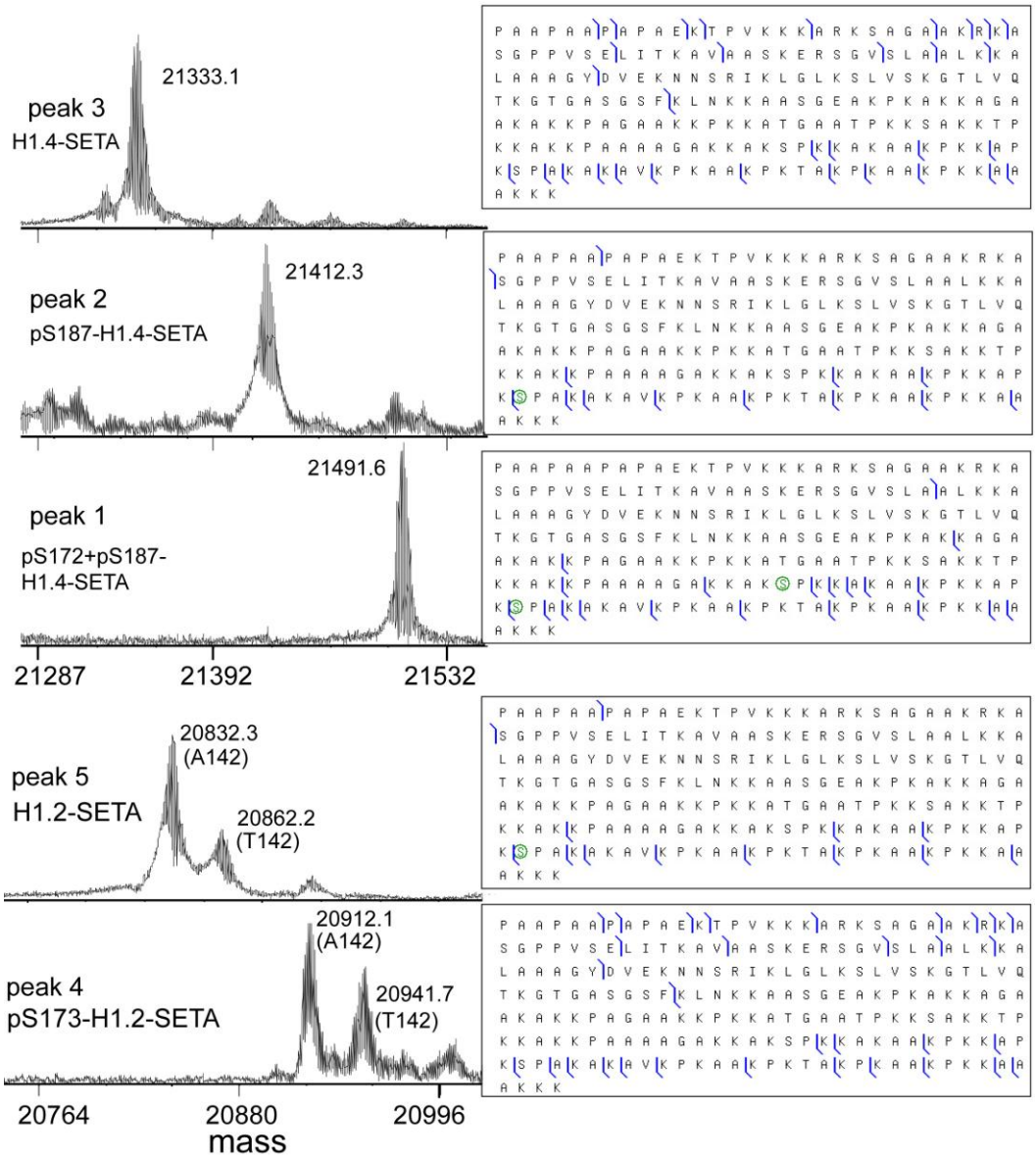

Interphase Phosphorylation of H1 Variants is Unexpectedly Homogenous

The mass spectra of H1 sample recovered from HIC peaks 1-5 of the 4 hour post-release from double thymidine block synchronization (mid-S phase). Molecular masses are reported for the neutral monoisotopic species. The sites of phosphorylation identified by direct MS/MS analysis are indicated. The Ala142Thr polymorphism of H1.2 in peaks 4 and 5 was confirmed by genotyping (see text). Residues 2-5 (SETA) were lost from all of the forms during electrospray ionization (see text). Molecular masses are reported for the neutral monoisotopic species. Only the spectrum of the most abundant charge state is shown in each case. Blue "┗" represents Z ions from ECD, blue "┓" represents C ions from ECD, and the circle around a residue represents phosphorylation in this residue.

Figure 2.6

A

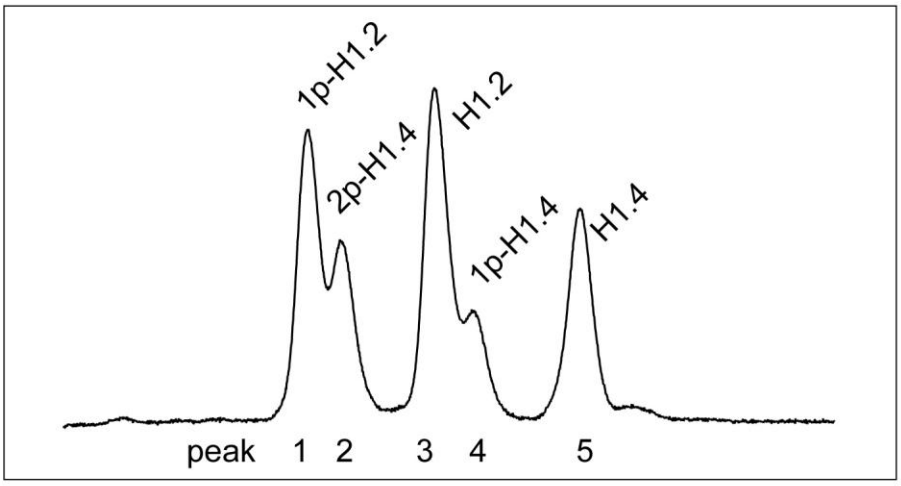

B FTMS broadband intact mass

	Molecular weight (Da)				
peak	Measured	Predicted	∆m	Variant	Modifications
1	20913	20832.6	80	H1.2 -SETA	1 phos
	20941	20862.5	79	H1.2(A141T)-SETA	1 phos
2	21492	21332.8	159	H1.4 -SETA	2 phos
3	20832	20832.6	0	H1.2 -SETA	0 phos
	20861	20862.5	0	H1.2(A141T)-SETA	0 phos
4	21412	21332.8	79	H1.4 -SETA	1 phos
5	n.d.	n.d.	n.d.	H1.4 -SETA	n.d.

C

peak 1
ECD map

H1.2-SETA:
pS173

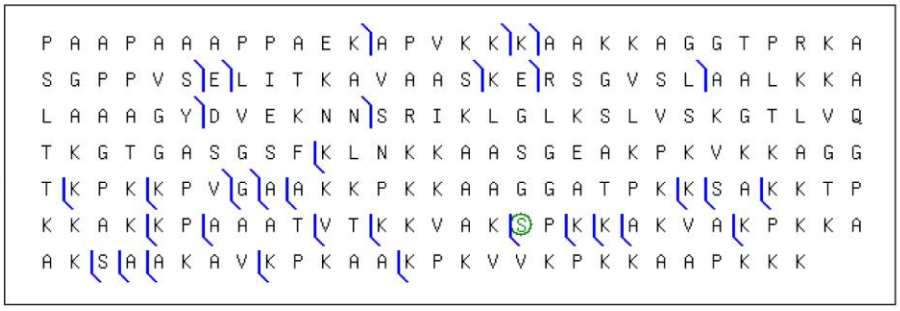

peak 2
ECD map
H1.4-SETA:
pS172
pS187

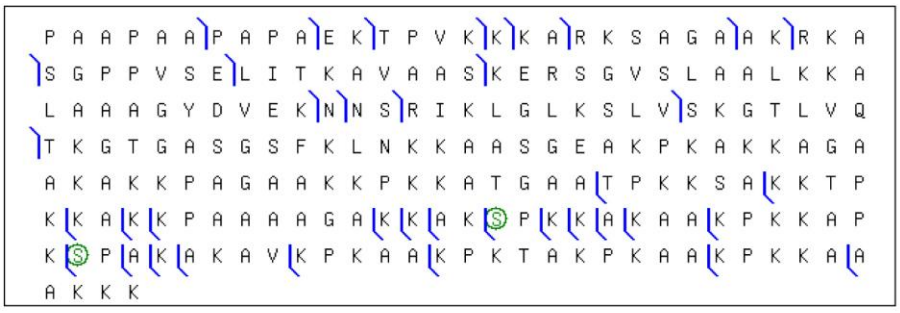

Figure 2.6 (cont.)

Identification of Phosphorylation Sites in H1 Purified by Cation Exchange Chromatography from Mid-S Phase Cells

(A) Crude H1 prepared from HeLa S3 cells was separated by Synchropack CM300 analytical (250 x 4.6 mm, 6 μm spherical silica) cation exchange column using 100 to 300 mM NaCl gradient in 23 mM sodium phosphate pH 7.0, 8 M freshly deionized urea. Column eluate absorbance at 214 nm is plotted for equivalent portions of each separation. Peaks are numbered according to elution order. Each peak was desalted by RP-HPLC and recovered by Speed-Vacuum, then identified by mass spectrometry.

(B) Intact mass of the components from IEC peaks in broadband FT-MS was used to infer the variants identity and phosphorylation levels. Molecular masses are reported for the neutral monoisotopic species.

(C) The sites of phosphorylation identified by direct MS/MS analysis are indicated in the ECD map. Blue "└" represents Z ions from ECD, blue "┐" represents C ions from ECD, the circle around a residue represents phosphorylation in this site.

Figure 2.7

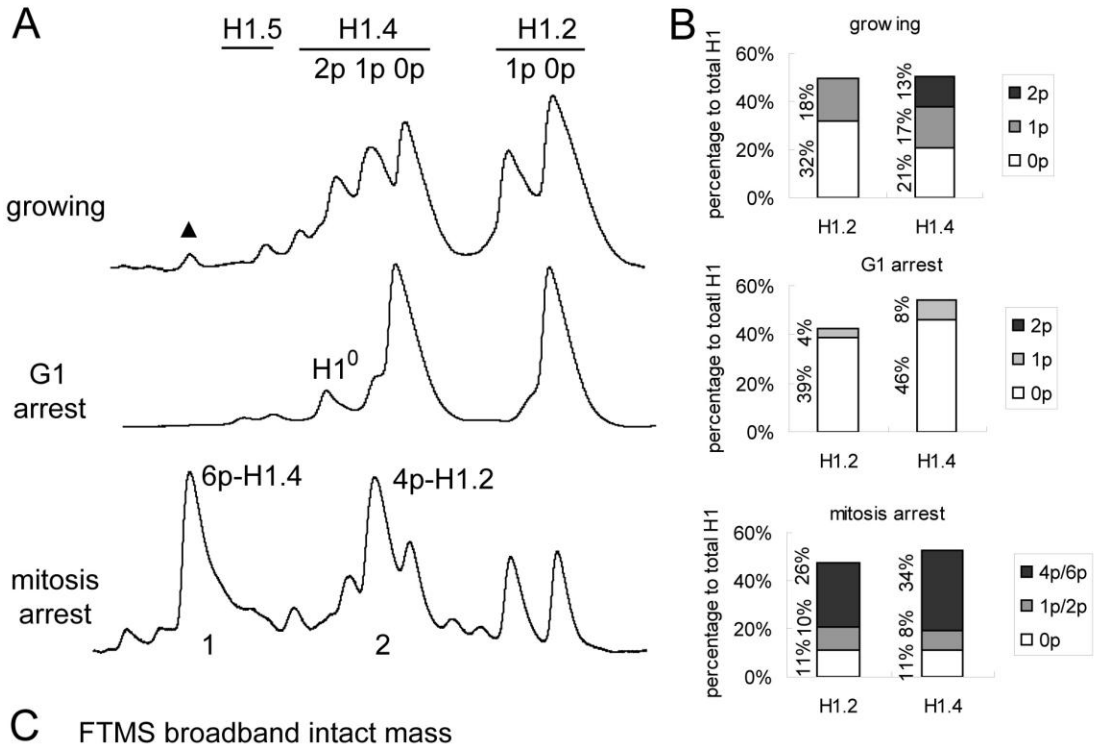

C FTMS broadband intact mass

	Molecular weight (Da)				
Peak	Measured	Predicted	Δm	Variant	Modifications
1	21813	21332.8	480	H1.4 -SETA	6 phos
2	21153	20832.6	320	H1.2 -SETA	4 phos

D

peak 1
ECD fragments
H1.4-SETA:
pT18
pS27
pT146
pT154
pS172
pS187

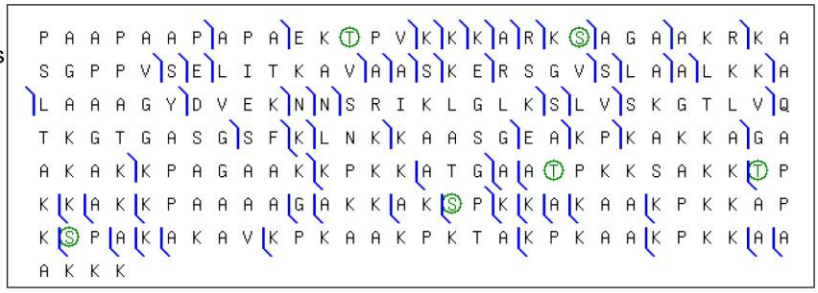

peak 2
ECD fragments
H1.2-SETA:
pT31
pT146 (?)
pT154
pS173 (?)

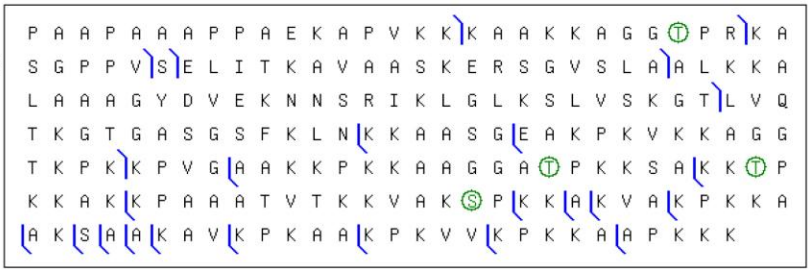

Figure 2.7 (cont.)

Identification of H1 Phosphorylation Sites in M Phase

(A) The hydrophobic interaction chromatography (HIC) profiles of crude H1 prepared from HeLa cells arrested in G1, asynchronously growing, and mitosis arrested (1 μM colchicine 20 hrs). Column eluate absorbance at 214 nm is plotted for equivalent portions of each separation. Peaks for the stationary phase and growing samples are numbered and identified as in Figure 2. The peaks corresponding to hexaphosphorylated H1.4 (6P) and tetraphosphorylated H1.2 (4P) in the colchicine-arrested sample were identified by MS/MS. The elution order of induced $H1^0$ in HIC was demonstrated in the further analysis described later (Figure 3.1). Black triangular indicates the presence of hexaphosphorylated H1.4 in the asynchronous sample.

(B) Quantification of the relative abundance of unphosphorylated and phosphorylated H1.2 and H1.4 to total pool of H1.2 and H1.4. Note: percentage of 1p-H1.4 and 2p-H1.4 were slightly overestimated due to the presence of low level of $H1^0$.

(C) Intact mass of the components from HIC peaks in broadband FT-MS was used to infer the variants identity and phosphorylation levels. Molecular masses are reported for the neutral monoisotopic species.

(D) The sites of phosphorylation identified by direct MS/MS analysis are indicated in the ECD map. Blue "└" represents Z ions from ECD, blue "┐" represents C ions from ECD, the circle around a residue represents phosphorylation in this residue.

Figure 2.8

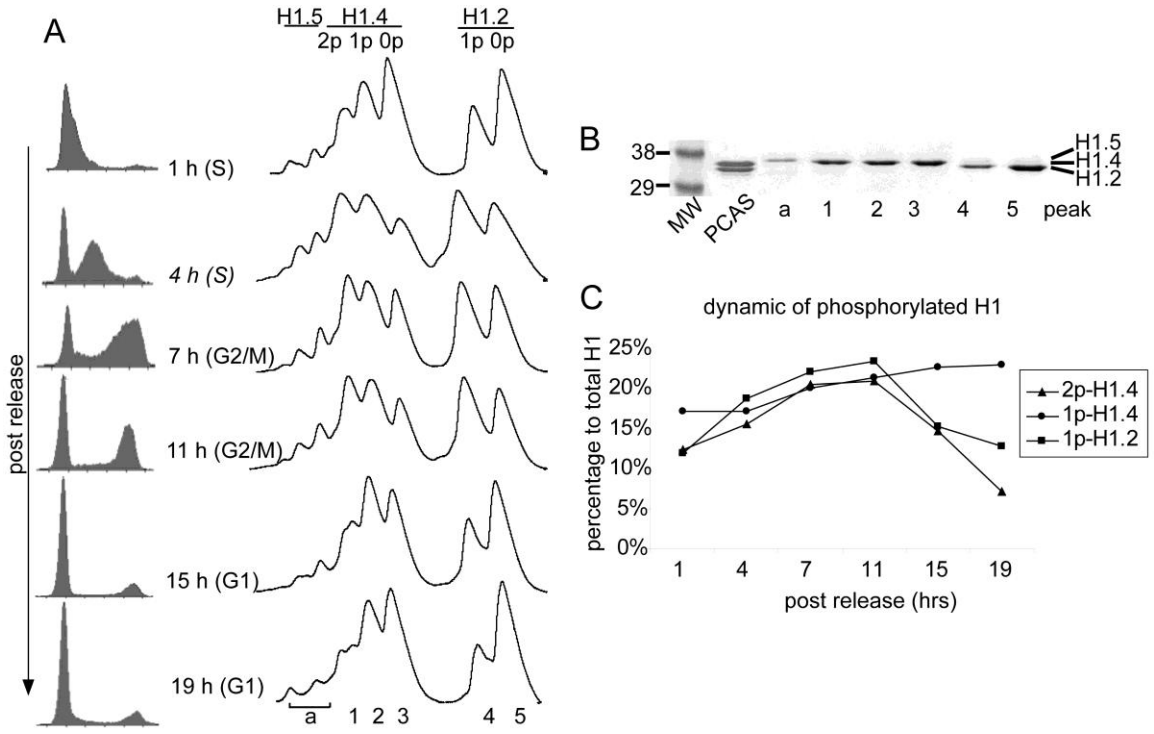

HIC Analyses of H1 Phosphorylation during the Cell Cycle

(A) Crude H1 prepared from HeLa S3 cells at selected times after release from double thymidine block synchronization was analyzed by HIC. Column eluate absorbance at 214 nm is plotted for equivalent portions of each separation. The cell cycle profile from flow cytometry is shown in the left and the approximate cell cycle stage determined by each sample is noted. Peaks are numbered according to elution order and identified based on SDS gel analysis (panel B) and mass spectrometry (Figure 2.6).

(B) SDS polyacrylamide gel analysis of HIC fractions from mid-S phase cells (4 hours post-release). Lanes are identified by the peak numbers shown in (A). The relative mobilities of H1.5 (peaks a), H1.4 (peaks 1-3), and H1.2 (peaks 4 & 5) are shown on the right. Molecular weight standards (MW) in kilodaltons are shown on the left. PCAS = crude H1 from asynchronously growing cells.

(C) The quantification of HIC chromatography is showing the different phosphorylation dynamic of three phosphorylated H1 forms (pS173-H1.2, pS172-H1.4 and pS172+pS187-H1.4).

Figure 2.9

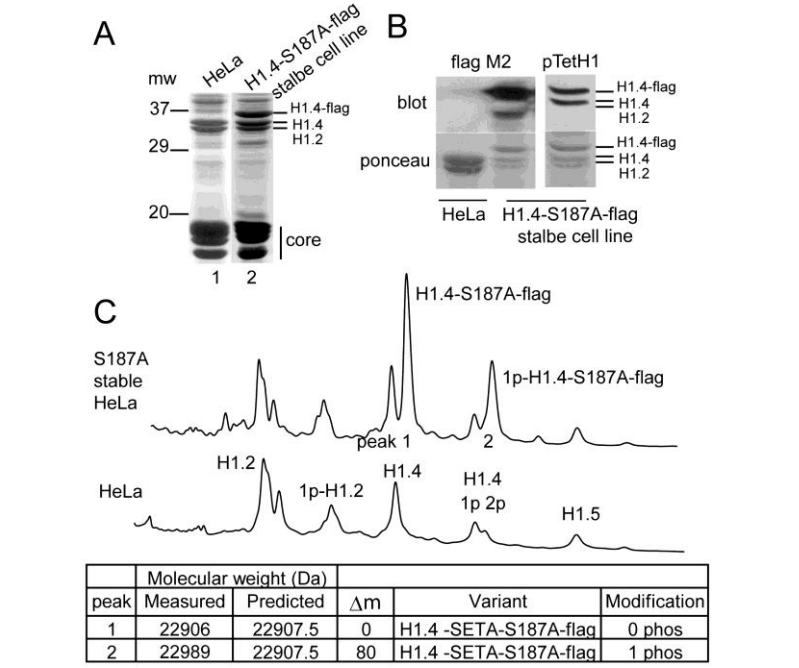

	Molecular weight (Da)				
peak	Measured	Predicted	Δm	Variant	Modification
1	22906	22907.5	0	H1.4 -SETA-S187A-flag	0 phos
2	22989	22907.5	80	H1.4 -SETA-S187A-flag	1 phos

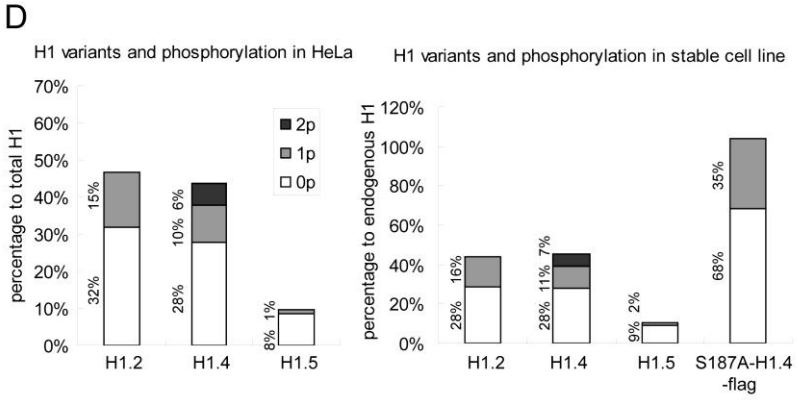

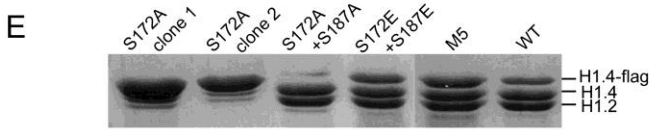

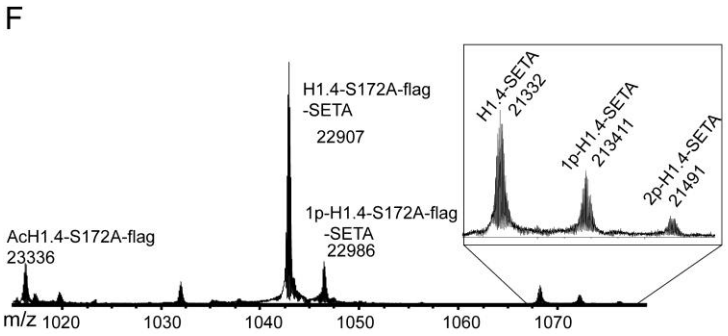

Figure 2.9 (cont.)

Hierarchical Phosphorylation of S187 Is Not Required for S172 Phosphorylation in H1.4 but S172 Mutagenesis affects S187 Phosphorylation

(A) Crude H1 prepared from asynchronous HeLa S3 and H1.4-S187A-flag stable cell line was analyzed by SDS polyacrylamide gel analysis. Appearance of more slowly migrated band above the H1 doublet is the flag tagged H1.4 S187A mutation.

(B) Expression of H1.4-S187A-flag was confirmed by blot with flag M2 antibody and phosphorylation levels of both endogenous H1.4 and overproduced H1 was tested by pTetH1.

(C) HILIC analysis of phosphorylation levels of both endogenous H1.4 and overproduced H1 mutant.

(D) Relative abundances of phosphorylated and unphosphorylated H1 to the pool of total endogenous H1 were quantified from HILIC chromatography. Increase of H1-to-core ratio due to the overproduction is normalized for the relative abundance in H1.4-S187A overproduction cell line (see text).

(E) SDS-PAGE of crude H1 purified from stable cell lines expressing different H1.4 mutants. H1 purified from similar amount of cells were loaded in each lane.

(F) Mass spectrum of crude H1 prepared from H1.4-S172A-flag stable cell line. Substitution of S172A reduced the phosphorylation abundance of H1.4.

Figure 2.10

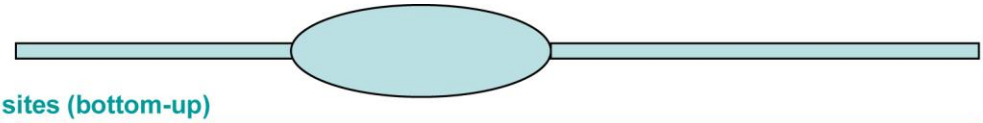

Garcia's sites (bottom-up)

H1.2 (5p)	T31 S36$^{(2,3,4)}$ T146 T154$^{(2,4)}$ S173
H1.3 (5p)	S36$^{(2,3,4)}$ T147 T155 T180 S189
H1.4 (9p)	S2 T4 T18 S27 S36$^{(2,3,4)}$ T146 T154$^{(2,4)}$ T172 pS187
H1.5 (2p)	T138 T155
H1.x (1p)	S31

Wisniewski's sites (bottom-up)

H1.1 (2p)	S2 S43
H1.2 (7p)	S2 S36$^{(2,3,4)}$ S41$^{(2,3)}$ S86$^{(2,3,4)}$ T146 T165 S173
H1.3 (5p)	T18 S36$^{(2,3,4)}$ S41$^{(2,3)}$ S86$^{(2,3,4)}$ T147
H1.4 (9p)	S2 T4 T18 S27 S36$^{(2,3,4)}$ S41 S86$^{(2,3,4)}$ T146 S187
H1.5 (4p)	S2 T4 S18 T138
H1.x (1p)	S31

Sarg's sites

	interphase	M
H1.5	1p: pS18 or pS173 2p: pS18 + pS173 3p: pS18 + pS173 + pS189	4p: 3p + pT138 or 3p + pT155 5p: 3p + pT138 + pT11 or 3p + pT155 + pT11

Our sites (top-down)

	interphase	M
H1.2	1p: pS173	4p: pT31 + pT146 + pT154 + pS173
H1.4	1p: pS187 2p: pS172 + pS187	6p: pT18 + pS27 + pT146 + pT154 + pS172 + pS187

Summary of H1 Phosphorylation Sites

The superscript indicates the peptides detected are conserved among variants and underline indicates the peptides are detected from tissues, otherwise from cell lines (Garcia et al., 2004; Sarg et al., 2005; Wisniewski et al., 2007). The cartoon of H1 molecule is not drawn with the scale to its tripartite structure but just the indication of where the mapped sites located within the molecule.

Figure 2.11

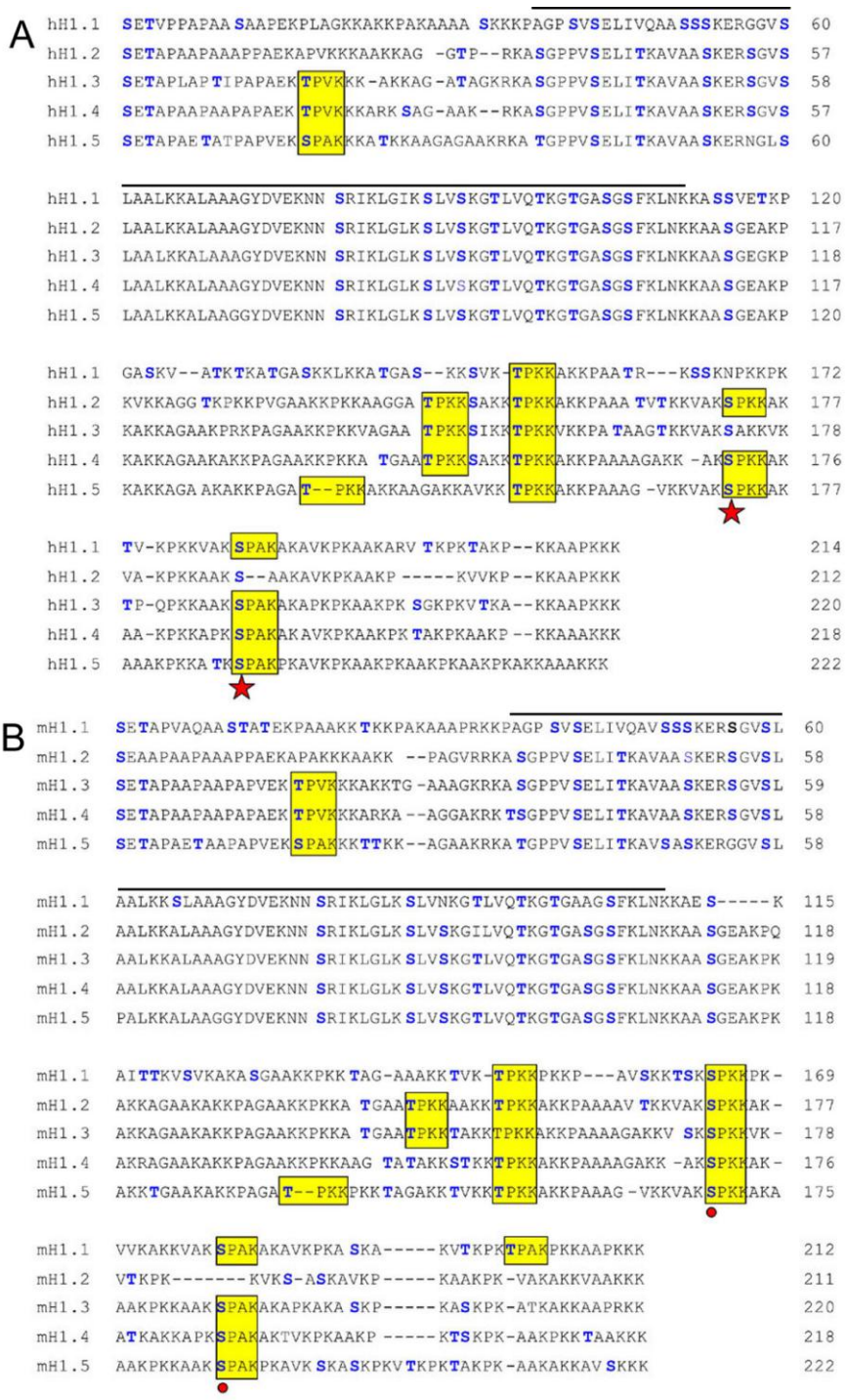

Alignment of Human and Mouse H1 Variants by ClustalW

All serine and threonine are indicated as blue. All CDK motifs (S/TPXX) are indicated by yellow box. The interphase phosphorylation sites we identified are indicated by red start (human) and red dot (mice). Global domain is indicated with black line.

CHAPTER 3

H1 VARIANT EXPRESSION AND PHOSPHORYLATION IN DIFFERENT CELL LINES

3.1 Introduction

As discussed in chapter 1, there is five DNA replication-dependent, non-allelic variants (H1.1, H1.2, H1.3, H1.4 and H1.5), together with the DNA replication-independent variants ($H1^0$ and H1x). Two reports have demonstrated all five somatic H1 variants were expressed in mouse cells. The first report, all five somatic variants were found in several mouse tissues being tested (liver, lung, spleen and thymus) whereas $H1^0$ was present in liver and lung but not in spleen and thymus using 2D gel separation (SDS-PAGE and acid urea gel) (Lennox and Cohen, 1983). The second one demonstrated all H1.2-H1.5 and $H1^0$ were expressed in roughly equal amount with minor amount of H1.1 in NIH 3T3 cells using RP-HPLC separation followed by SDS-PAGE analysis (Talasz et al., 1993). On the opposite hand, survey for the expression of variants in mRNA levels by RNase protection in several human cell lines has demonstrated that only H1.2 and H1.4 are expressed in all cells at a high level and no H1.1 mRNA was detected in most of the cell lines except testis (Meergans et al., 1997). Similar results have also been shown by comparing variants at protein levels using capillary zone electrophoresis (CZE) separation (Kratzmeier et al., 1999). These observations have indicated the H1 variants expression pattern in human cells is not as uniform as that in mouse cells.

In addition, the phosphorylation levels have also been analyzed for mouse H1 in 3T3 cells by acid urea gel analysis of RP-HPLC purified H1 fraction (Talasz et al., 1996). Interestingly, the maximum phosphorylation sites achieved for H1 variants, including H1.1, H1.3, H1.4 H1.5 and $H1^0$, in colcemid treated 3T3 cells are exactly the same as the number of CDK substrate motif whereas maximum phosphorylation sites for H1.2 is one

more than its three CDK substrate motifs (Figure 2.11). In addition, the interphase phosphorylation sites mostly follow the rule of Ser-containing CDK motif as discussed in chapter 2, which proposed phosphorylation only occurs in the Ser-containing CDK motifs during interphase. However, three exceptions have been observed: only monophosphorylation is observed for H1.1 which has 2 Ser-containing CDK motifs; a possible triphosphorylation is observed for H1.4 which possesses only 2 Ser-containing CDK motifs (the 3p-H1.4 might actually be 2p-H1.3) and monophosphorylation for $H1^0$ which lacks such motif (Talasz et al., 1996).

We have found phosphorylation of both H1.2 and H1.4 is rather abundant in HeLa (~30%). However, the stable cell line carrying H1.4-S172A mutation generated from HeLa S3 cells can survive with extreme low abundance of phosphorylation, which suggests this abundant phosphorylation might be just the result of abnormal high level of kinase activity in the HeLa cells (Contreras et al., 2003) and might not necessary for cell survival. In this chapter, I will describe our efforts to answer this question by expanding our analysis to different cell lines.

3.2 H1 Variant Expression and Phosphorylation in Different Cell Lines

As shown in Figure 3.1, three H1 variants, major forms of H1.2 and H1.4 and minor forms of H1.3, were observed from the crude H1 in asynchronous human fibroblasts, VA13 transformed WI-38 cells. Similar to the results described in chapter 2, most ion species lost the first four residues (-SETA). Three interesting results have been observed from TDMS analysis. First, the number of phosphorylation in H1.4 achieved in asynchronous WI-38 VA13 is three instead two in HeLa S3 cells as indicated by triphosphorylated H1.4 in the broadband spectra (Figure 3.1 A); second, abundances of phosphorylation in both H1.2 and H1.4 were slightly higher than those in HeLa S3. Third and most unexpectedly, no apparent phosphorylation was observed in the

broadband spectra for H1.3 (the mass for several small peaks indicated by the question marks does not match to H1.3 with phosphorylation or the combination of modifications). Moreover, the relative abundant phosphorylation in H1.2/H1.4 and the underdetectable phosphorylation in H1.3 were confirmed by HIC (Figure 3.2). For colon adenocarcinoma HT-29 cells, three H1 variants, H1.2, H1.4 and H1.5 with very low abundances of phosphorylation were observed. In addition, the polymorphism of H1.2 identified in HeLa S3 is not seen in WI-38 VA13 and HT-29. These data indicates both the expression and phosphorylation levels of H1 variants vary in different cell lines. However, differences in the efficiency of electrospray ionization between non-allelic H1 variants complicates the quantification of distinct forms of one variant relative to mixtures containing multiple variants, i.e. total H1 (Pesavento et al., 2006). To circumvent this problem, we decide to use the HIC chromatography reported in chapter 2 for better comparison.

The identify of major peaks for total H1 from HeLa S3 cells has been determined by TDMS and gel analysis as described in chapter 1 and labeled in the top of Figure 3.2 A. The identity of each peak in the HIC chromatograph from the new cell lines was determined by aligning them with the HIC from HeLa S3 cells. The identity of the new cluster of peaks eluted later than H1.2, which was not present in HeLa S3 and thus was not identified by TDMS so far, was deduced as H1.3 from the commercial available H1 variant specific antibody (Figure 3.2 C). In addition, the SDS-PAGE analysis of peaks recovered from HIC of WI-38 VA13 cells clearly demonstrated which variants is present in the peak by gel mobility difference (H1.5/H1.4 slowest with H1.5 slightly slower than H1.4, H1.2 fastest, H1.3 in the between of H1.2 and H1.4, $H1^0$ faster than H1.2), which confirms the determination of identity of peaks in new cells line by aligning with those have been identified. One small unsatisfactory fact for HIC is the overlapping of $H1^0$ with H1.5, which limits its ability to measure the amount of H1.5 correctly.

Several interesting patterns can be observed from this comparison: (1) H1.2 and H1.4 are the only two variants that expressed in all 6 cell lines and with roughly equaled expression levels except HepG2 in which expression of H1.4 is twice as much as H1.2 (2) H1.5 is not expressed or expressed in low abundance except in neuroblastoma cell line IMR32; (3) H1.3 is not expressed or only expressed as minor form (all <15% of total) and phosphorylation abundance is very low in this variant; (4) the relative abundances of phosphorylation vary quite a lot for different cell lines, the abundances of phosphorylation in two hematopoietic cell lines (HL-60 and U937) is surprisingly low whereas the abundance of monophosphorylated H1.2 in HepG2 is even higher than unphosphorylated H1.2. The extreme low abundances of phosphorylation in hematopoietic cell lines suggest either H1 phosphorylation is not necessary for these cells or the function of this modification can be substituted by other modification. Interestingly, H4-K16 acetylation is substantially higher in hematopoietic cells (Pesavento et al., 2008b), which might substitute the roles of H1 phosphorylation in opening chromatin. In addition, it is highly impossible that histone H1 kinase, CDK2, is inactive in hematopoietic cells since CDK2 is an essential kinase in dividing cells. Thus, the extreme low abundances of phosphorylation in H1 imply that phosphorylation of H1 is a highly regulated process and therefore H1 phosphorylation is not dispensable and simply the byproduct of CDK2 kinase activity.

As mentioned in introduction, Doenecke group has surveyed H1 variants expression pattern for several human cell lines using capillary zone electrophoresis (CZE) (Kratzmeier et al., 1999). The expression levels of H1 variants in HeLa were reported as 48%, 6%, 26%, 17% and 3% for H1.2, H1.3, H1.4, H1.5 and $H1^0$, respectively. Comparing this expression pattern with our HIC result from HeLa S3 culture, it seems the disappearing of H1.3 and significant decrease of H1.5 are compensated by the increase of H1.4 in the HeLa S3 suspension culture. In fact, the similar expression

pattern difference between HeLa and the suspension adapted S3 has been documented before (Meergans et al., 1997). However, expression pattern do not switch back when HeLa S3 cells was grown as attached instead of in suspension (Meergans et al., 1997) and thus such change of variants expression pattern might be the result of selection during suspension adaption.

Doenecke group has also reported that the expression level of H1.5 in HL-60 and U937 is high whilst H1.3 is low (Kratzmeier et al., 1999), which is quite opposite with what we found in HIC. To exclude the possibility of misalignment of H1 variants in the HIC, we analyzed H1 variants composition in different cell lines by immunoblot, gel electrophoresis and RP-HPLC. First, western blot with H1.5-specific antibody, which was able to detect fairly low abundant H1.5 from HeLa (5%), indicated H1.5 expression in HL-60 is way below 5%. Second, intermediate format gel, which was longer than mini-gel and thus separated H1 variants better, was used to show the expression of H1.3 in HL-60. Moreover, H1.3 was visible as the middle band appearing between H1.2 and H1.4 in both IMR-32 and HL-60 cells (Figure 3.3 A). RP-HPLC has been used to separate H1.5 from other H1 variants by several groups (Kratzmeier et al., 2000; Sarg et al., 2005). The peaks in RP-HPLC were collected and recovered for subsequent analysis by SDS-PAGE. Based on the gel mobility, three resolved RP-HPLC peaks for H1 from WI-38 VA13 were identified as $H1^0$, H1.5 and H1.2/H1.3/H1.3. When RP-HPLC chromatography from different cell lines were aligned together, it clearly demonstrated there was no detectable peak in the elution position of H1.5 in both HL-60 and U937 (Figure 3.3 B), which suggest the expression level of H1.5 was very low in this two cell lines. Taken together, these analyses using alternative techniques have corroborated our conclusion drawn from HIC. The variants composition and extents of phosphorylation in different cell lines with varied analysis techniques have been summarized in Table 3.1.

3.3 Resolving Phosphorylated H1 Variants by HILIC

Although the condition we developed for HIC has successfully resolve all five H1 somatic variants and their phosphorylation forms, we were not satisfied with the fact they elute in broad peaks. How broad peak shape affecting the resolution was very obvious in the HepG2 separation, where it was impossible to determine whether 0p-H1.4 or 1p-H1.4 was the major form of H1.4 (Figure 3.2). Therefore we tried to improve the peak shape by changing pH, solvent or column, but noting worked so far (Appendix 6.2). Since the tertiary structure also affects HIC, it is likely that H1 is conformationally labile and tends to elute in a broad peak. Therefore such broad peak is the characteristic of H1 itself and thus it might be futile to try to improve it.

Mizzen and Lindner have developed Hydrophilic Interaction Liquid Chromatograph (HILIC) to separate H1 variants (Mizzen et al., 2000) or phosphorylation forms from a single H1 variant (Lindner et al., 1997). Ionization of the polyCAT A (weak cation-exchange column) support is suppressed under high percentage of acetonitrile, thus the hydrophilic interaction between the stationary phase and tails of histone becomes dominant. Since the heterogeneity due to both non-allelic amino acid sequence variation and to phosphorylation mostly lies within the tails, this technique should be a good choice for H1 separation. For the purpose of comparing variants expression and phosphorylation levels in different samples, it is very important to be able to separate total H1 in one single chromatography. For this reason, we analyzed total H1 from HeLa cells directly by HILIC, instead of resolve non-allelic H1 variants irrespective of modification by RP-HPLC first and then separate phosphorylated forms for each variant fraction individually by HILIC (Lindner et al., 1996). Total of 6 peaks were resolved in HILIC for H1 samples from asynchronous growing or double thymidine release at 4 hrs and 14 hrs (Figure 3.4 A). The identity of HILIC peak 1~3 for mid S phase sample (post release 4 h) were identified by TDMS as unphosphorylated H1.2,

monophosphorylated H1.2 at S173 and unphosphorylated H1.4 respectively using the procedure described in chapter 2 (Figure 3.4 B, C). Our previous HIC study has clearly demonstrated that abundance of 2p-H1.4 decreases faster than 1p-H1.4 when cells enter next G1 (Figure 2.8 A, C). According to this finding, the peak 4 and 5 in HILIC was inferred as 1p-H1.4 and 2p-H1.4 since abundance of peak 5 decrease faster than peak 4 when comparing post release 14 h (G1) sample with post release 4 h (mid S) sample. The last peak was inferred as H1.5 since the relative abundance of this peak to total H1 match the observation from HIC study. In addition, all the peaks were further confirmed by their mobility on SDS-PAGE and by their reactions with phosphor-specific antibody in western blot (data not shown).

3.4 Major and Rare Forms of Hyperphosphorylated H1.4

The mass spectrum analyses of tryptic H1 peptide using the bottom up approach have identified as much as 9 phosphorylation sites in H1.4 (Figure 2.10) (Garcia et al., 2004; Wisniewski et al., 2007). It is reasonable to believe some of these sites identified in bottom-up were rare and thus below our detection limit. Our lab has successfully use chromatograph to enrich the rare forms of histones for the analyzing by TDMS (Pesavento et al., 2008a). However, HIC does not suit well for this purpose since the condition we used to resolve H1 caused significant change in baseline (Appendix 6.2), which affect our ability to detect low abundant protein.

With the HILIC separation condition established for crude H1 from HeLa, we decided to pursuit the rare form of H1.4 having more than 6 phosphorylation sites. The HILIC chromatograph of crude H1 purified from colchicine arrest HeLa S3 cells was shown in Figure 3.5. Based on the peak assignment analysis we described in section 3.3 and the fact that 4p-H1.2 and 6p-H1.4 was accounting near ~80% of total H1 in the HIC analysis, we can infer the first major peak appearing in the HILIC is 4p-H1.2 while the second is

6p-H1.4. The peak appearing at the beginning of HILIC was due to the overlapping of 0p-H1.2 with some other components which have been carried to this place with starting gradient set too high for this separation. However, there was no obvious peak after 6p-H1.4 looking like a valid candidate for H1.4 having more than 6 phosphorylation sites.

To test the possibility that the rare form of H1.4 having more than 6 phosphorylation sites might accumulated after prometaphase, we set up a procedure to enrich cells after prometaphase. In order to decrease the adverse effect of long exposure to tubulin drug, cells were first synchronized at G2 by releasing 8 h from double thymidine block, and then treated with 0.5 μg/ml of nocodazole for 4.5 hr before they were released to fresh medium to allow the progress of the mitosis for 30 min (TdR-Noc 30 min). When such sample was analyzed by HILIC (Figure 3.5), a tiny peak, which represented roughly 3% of total H1, was appeared after 6p-H1.4 (peak 6). We then used TDMS to analyze all the peaks from TdR-Noc 30 min sample, the phosphorylation levels was determined from the intact molecule mass in the broadband spectra but no sites were further mapped by MS/MS. Series of intermediate phosphorylation forms were identified. As we have discussed in the chapter 2, it was not easy to determine such intermediate phosphorylation forms were just the degradation products during sample handling or the real existing forms in the cells. However, the existence of 7p-H1.4 is clearly demonstrated by the TDMS broadband spectra with +560 Da mass. Since the main ion species for this study were all lost first residues, such 7^{th} site was very likely to be S37, which was the only left candidate in H1.4 (not counting the first five residues) for phosphorylation sites mapped in cell lines (Figure 2.11). In addition, the elution distance between 6p-H1.4 and peak 6 is clearly larger than one phosphorylation can cause (Figure 3.5) as evidence by smaller distance between peak 5 (4p-H1.4) and 6p-H1.4. It suggests this rare hyperphosphorylated form of H1.4 is very likely phosphorylated in all

the 9 sites that have been mapped by bottom-up approach. Taken together, the major form of hyperphosphorylated H1.4 in the M phase is hexaphosphorylated whilst approx 1% of H1.4 can achieve even higher phosphorylation levels, which is very likely to be nonaphosphorylated.

3.5 H1 Variant Expression and Phosphorylation in Mouse 3T3 Cells

As discussed in the introduction, the previous report has indicated the H1 variants except H1.1 in the mouse 3T3 fibroblast are expressed in a roughly equal fashion. We felt there might be some advantages to use this cells line as the model to study H1 phosphorylation, thus we decided to analyze H1 from this cell line.

As shown in Figure 3.6, 15 peaks were resolved in HILIC for crude H1 purified from asynchronous growing 3T3 cells. These peaks were recovered by TCA precipitation and analyzed by both SDS-PAGE and TDMS. Peak 4 was very likely a HMG protein by the gel mobility and thus excluded from TDMS analysis. Based on the intact mass measured in the broadband spectra, identity for all other peaks except peak 5~7 were determined. H1.3 and H1.5 was not resolved in HILIC, but they are expressed at similar level as indicted by FTMS spectrum in the inset. Combining the HILIC and TDMS, our data indicated the expression levels for all H1 variant except H1.1 in the 3T3 were similar, which agrees with previous finding (Talasz et al., 1993). For the phosphorylation levels, H1.2 only gets monophosphorylation while H1.3, H1.4 and H1.5 all get both mono- and diphosphorylation. Thus, our results showed the number of phosphorylation sites in H1.2, H1.3 and H1.4 variants from 3T3 is the same as the number of Ser-containing CDK motif. For H1.5, two monophosphorylated forms were observed in HILIC (peak 10 and peak 11) but only one diphosphorylated form was observed, which agrees with the recent report (Sarg et al., 2005). The triphosphorylated H1.5 reported in 3T3 by AU gel in the previous report might represent a very low

abundant form. When the relative abundance of 3p-H1.5 in CCRF-CEM analyzed by HILIC in a recent paper was quantified, it turned out only account for approx. 5% of total H1.5. To detect such low abundant forms of H1.5 in HILIC will require purified H1.5 first to eliminate the interference from other protein which might coelute in the same place as 3p-H1.5.

When crude H1 purified from contact inhibited culture of 3T3 was analyzed in HILIC, the peaks representing the phosphorylation forms were mostly disappeared with little of monophosphorylated H1 left but no diphosphorylated H1 at all. This observation of the lost of H1 phosphorylation was also confirmed by the western blot using pS187-H1.4 antibody (described in chapter 4).

3.6 Disruption of Three H1 Variants in Mouse ES Cells Does Not Affect Phosphorylation of the Remaining H1 or Core Histone Modifications

Skoultchi Lab has taken great efforts to generate mouse embryonic stem cells null for three H1 genes (H1.2, H1.3 and H1.4) (Fan et al., 2005). The characterization of this H1 triple knockout ES cells (3KO-H1 ES) revealed a 50% reduction of H1 expression level comparing to the normal ES cells (WT ES) and dramatic chromatin structure changes, including decreased global nucleosome spacing and reduced local chromatin compaction (Fan et al., 2005).

We were very interested in how the phosphorylation in histone H1 and some modifications in core histones might change in the 3KO-H1 ES cells. Total H1 purified from WT ES and 3KO-H1 ES were separated in HILIC and some of the peaks were further analyzed by TDMS. As shown in Figure 3.7 A, H1.5 and H1.3 were resolved in HILIC when a new column was used, indicating the lost of resolution for H1.5 and H1.3 seen in 3T3 separation (Figure 3.6) was due to column deterioration. We identified two

monophosphorylated forms of H1.5 (peak 8 & 9 in WT ES and peak 6 & 7 in 3KO-H1) and localized the phosphorylation in first eluted form to S18 for H1.5 by MS/MS study (peak 8 in WT and peak 6 in 3KO). In addition, the first eluted 1p-H1.5 is more abundant than second eluted 1p-H1.5, which was consistence with previous report (Sarg et al., 2005). Very likely, the second eluted 1p-H1.5 was phosphorylated at S173 according to previous mapping result (Sarg et al., 2005). Then the relative abundance of phosphorylated and unphosphorylated H1 variants was quantified from HILIC for wild type and 3KO-H1 and the number for 3KO-H1 was corrected for the 50% decrease of H1 stoichiometry. The relative abundance of both H1.1 and H1.5 increase but the percentage of phosphorylated H1.5 remains the same while some small increase was seen for H1.1 (Figure 3.7 C). Similar to the effects on remaining H1 by triple knockout, no change in core histone modification was observed (Figure 3.8 A).

To confirm the HILIC result, we compare the phosphorylation levels between WT and 3KO-H1 using pTeH1, the antibody raised against highly phosphorylated *Tetrahymena* H1 (Lu et al., 1994). Surprisingly, this antibody failed to detect any phosphorylation from 3KO-H1 (Figure 3.8 B). To reconcile the difference, we analyzed the H1 purified from WT and 3KO-H1 ES cells by acid-urea PAGE. The results (Figure 3.8C) clearly demonstrated that the remaining H1 in the 3KO-H1 can be phosphorylated to the same extent as WT ES when arrested in mitosis by colchicine treatment. Interestingly, the maximum phosphorylation levels in mouse were five instead of six in human, which can be explained by lacking the S27 (RKS motif) in mouse H1.4 is (Figure 2.11). The reason that pTetH1 failed to see the phosphorylation form in 3KO-H1 is that the crossreactivity of this antibody with mammalian H1 is limited (one of the recognition sites for pTetH1 was pS172-H1.4., described in chapter 4). Therefore, some cautions should be applied for this widely used phospho-specific H1 antibody.

3.7 Conclusions and Discussions

I have made some surveys for H1 variants expression and phosphorylation levels (including how many phosphorylation forms existed and the abundance of these phosphorylation forms) for several cell lines and cells with overexpression or deletion of H1. Several interesting observations have been found: (1) Variants expression differs among human cell lines but H1.2 and H1.4 are the two variants expressed at relative high levels for all human cell lines tested; H1.1 is not detected in human cell lines but present in both mouse 3T3 and ES cells (Table 3.1). (2) The number of phosphorylation sites one H1 variant can obtain during interphase is usually the same as the number of the Ser-containing CDK motifs in that variant with only one exception observed, which is the 3p-H1.4 observed in the TDMS broadband spectrum of asynchronous WI-38 VA13 PCAS. (3) The number of phosphorylation sites one H1 variant can attain as a major form in mitosis is usually the same as the number of the CDK motifs (including both Ser and Thr) in that variant. The one exception for this rule is the S27 in H1.4 which posses RKS motif resembling that of aurora kinase substrate. For the rare form of hyperphosphorylated H1.4, as much as 9 phosphorylations can be achieved but the abundance is as low as 1% of total H1.4. (4) The relative abundant overall phosphorylation is not observed for all cell lines; some cell lines such as HL-60, U937 and HT-29 have relative low phosphorylation (Table 3.1). Importantly, it does not suggest H1 phosphorylation is nonessential since H1 kinase in these cell lines is still active and the fact that H1 phosphorylation is maintained at low levels actually indicate H1 phosphorylation is highly regulated. One of intriguing possibility is another histone modification can substitute roles played by H1 and acK16-H4 might be such candidate since it is abundant in peripheral lymphocyte (Pesavento et al., 2008b) where H1 phosphorylation is particularly low. Actually, it has been reported that no phosphorylated H1 is present in the chromatin containing acetylated H4 (Ryan, 1999). We speculate that only one histone modification that marks the open chromatin

conformation is required as the mechanism underlying this mutually exclusive presence of H1 phosphorylation with H4 acetylation. (5) Abundances of phosphorylation in different H1 variants differ significantly in human cells but much less so in mouse (H1.2-H1.5). Especially all the H1.3 has extremely low or no phosphorylation in all the human cell lines tested. (6) Abundances of phosphorylation in overexpressed H1.4-S183A mutant protein is relative high while H1.4-S173A is extremely low. Intriguingly, both H1.3 and H1.4-S173A proteins share a same feature that they have the hindmost CDK substrate motif (S189 of H1.3 and S187 of H1.4) but lack the motif in the second most C-terminal position (S174 of H1.3 and S173 of H1.4-S173A) (Figure 2.11). This feature suggests the phosphorylatability of one CDK substrate motif in H1 variants is influenced by the sequence in the nearby site. Such low abundant phosphorylation of H1.3 is not observed in mouse since the feature describe here is not conserved in any mouse H1 variant. On the contrary, such crosstalk is not vice versa. Losing the hindmost CDK substrate motif while still having the second most such site, as the example in H1.2 (S173PKK, S187AAK) and H1.4-S187A, has no effect in the phosphorylatability of second most C-terminal site.

To explain low levels of phosphorylation in H1.3 or other H1 in hematopoietic cells in the presence of CDK2, we propose that H1 can only be phosphorylated when it is bound in the chromatin and H1 kinase (CDK2 or other kinase) is targeted to the chromatin. When H1 disassociates from chromatin, it is quickly dephosphorylated. The dephosphorylation has been supported by the observation of increase of H1 phosphorylation when cells were treated with phosphatase inhibitor okadaic acid (Ryan, 1999). However, this model still can not explain the low level phosphorylation of H1.3. Human H1.3 binds chromatin with intermediate affinity among H1 variants, binding loser than H1.4 and H1.5 which have two SPXK motif in the C-terminus but slightly stronger than H1.2 (Th'ng et al., 2005) (multiple reports have demonstrated different binding

affinity for H1 variants, this is the only test involved the human H1.3). Taking the account of the important roles of SPXK motif in DNA binding (Suzuki, 1989), we speculate the conformation caused by the SPXK in the position ~50 amino acid away from the C-terminal is critical for H1 to receive phosphorylation. However, why human cells need a H1 variant that unphosphorylatable in the interphase requires further investigation to reveal.

3.8 References

Contreras, A., T.K. Hale, D.L. Stenoien, J.M. Rosen, M.A. Mancini, and R.E. Herrera. 2003. The dynamic mobility of histone H1 is regulated by cyclin/CDK phosphorylation. *Mol Cell Biol*. 23:8626-36.

Fan, Y., T. Nikitina, J. Zhao, T.J. Fleury, R. Bhattacharyya, E.E. Bouhassira, A. Stein, C.L. Woodcock, and A.I. Skoultchi. 2005. Histone H1 depletion in mammals alters global chromatin structure but causes specific changes in gene regulation. *Cell*. 123:1199-212.

Garcia, B.A., S.A. Busby, C.M. Barber, J. Shabanowitz, C.D. Allis, and D.F. Hunt. 2004. Characterization of phosphorylation sites on histone H1 isoforms by tandem mass spectrometry. *J Proteome Res*. 3:1219-27.

Kratzmeier, M., W. Albig, K. Hanecke, and D. Doenecke. 2000. Rapid dephosphorylation of H1 histones after apoptosis induction. *J Biol Chem*. 275:30478-86.

Kratzmeier, M., W. Albig, T. Meergans, and D. Doenecke. 1999. Changes in the protein pattern of H1 histones associated with apoptotic DNA fragmentation. *Biochem J*. 337 (Pt 2):319-27.

Lennox, R.W., and L.H. Cohen. 1983. The histone H1 complements of dividing and nondividing cells of the mouse. *J Biol Chem*. 258:262-8.

Lindner, H., B. Sarg, and W. Helliger. 1997. Application of hydrophilic-interaction liquid chromatography to the separation of phosphorylated H1 histones. *J Chromatogr A*. 782:55-62.

Lindner, H., B. Sarg, C. Meraner, and W. Helliger. 1996. Separation of acetylated core histones by hydrophilic-interaction liquid chromatography. *J Chromatogr A*. 743:137-44.

Lu, M.J., C.A. Dadd, C.A. Mizzen, C.A. Perry, D.R. McLachlan, A.T. Annunziato, and C.D. Allis. 1994. Generation and characterization of novel antibodies highly selective for phosphorylated linker histone H1 in Tetrahymena and HeLa cells. *Chromosoma*. 103:111-21.

Meergans, T., W. Albig, and D. Doenecke. 1997. Varied expression patterns of human H1 histone genes in different cell lines. *DNA Cell Biol*. 16:1041-9.

Mizzen, C.A., A.J. Alpert, L. Levesque, T.P. Kruck, and D.R. McLachlan. 2000. Resolution of allelic and non-allelic variants of histone H1 by cation-exchange-hydrophilic-interaction chromatography. *J Chromatogr B Biomed Sci Appl*. 744:33-46.

Pesavento, J.J., C.R. Bullock, R.D. LeDuc, C.A. Mizzen, and N.L. Kelleher. 2008a. Combinatorial modification of human histone H4 quantitated by two-dimensional liquid chromatography coupled with top down mass spectrometry. *J Biol Chem*. 283:14927-37.

Pesavento, J.J., C.A. Mizzen, and N.L. Kelleher. 2006. Quantitative analysis of modified proteins and their positional isomers by tandem mass spectrometry: human histone H4. *Anal Chem*. 78:4271-80.

Pesavento, J.J., H. Yang, N.L. Kelleher, and C.A. Mizzen. 2008b. Certain and progressive methylation of histone H4 at lysine 20 during the cell cycle. *Mol Cell Biol*. 28:468-86.

Ryan, C.A. 1999. Phosphorylation of Histone H1 During S Phase in Human Cells. *In* Department of Biology. Vol. Doctor of Philosophy. Boston College.

Sarg, B., W. Helliger, H. Talasz, B. Forg, and H.H. Lindner. 2005. Histone H1 phosphorylation occurs site-specifically during interphase and mitosis. Identification of a novel phosphorylation site on histone H1. *J Biol Chem*.

Suzuki, M. 1989. SPKK, a new nucleic acid-binding unit of protein found in histone. *Embo J*. 8:797-804.

Talasz, H., W. Helliger, B. Puschendorf, and H. Lindner. 1993. G1- and S-phase synthesis of histone H1 subtypes from mouse NIH fibroblasts and rat C6 glioma cells. *Biochemistry*. 32:1188-93.

Talasz, H., W. Helliger, B. Puschendorf, and H. Lindner. 1996. In Vivo Phosphorylation of Histone H1 Variants during the Cell Cycle. *Biochemistry*. 35:1761-1767.

Th'ng, J.P., R. Sung, M. Ye, and M.J. Hendzel. 2005. H1 family histones in the nucleus. Control of binding and localization by the C-terminal domain. *J Biol Chem*. 280:27809-14.

Wisniewski, J.R., A. Zougman, S. Kruger, and M. Mann. 2007. Mass spectrometric mapping of linker histone H1 variants reveals multiple acetylations, methylations, and phosphorylation as well as differences between cell culture and tissue. *Mol Cell Proteomics*. 6:72-87.

3.9 Tables and Figures

Table 3.1

Summary of H1 Variant Expression and Phosphorylation in Different Cell Lines

	% of phos		H1.1	H1.2	H1.3	H1.4	H1.5	$H1^0$
human	high	HeLa S3 [a,b,c,d,e]	-	+++	-	+++	+	+
		WI-38 VA13 [a,b,c,d]	-	+++	++	+++	+	++
		IMR32 [b,c,d]	-	+++	++	+++	+++	+
		HepG2 [b]	-	+++	-	+++	+	+
	low	HL-60 [b,c,d]	-	++	+	++	-	-
		U937 [b,c,d]	-	++	+	++	-	-
		HT-29 [a]	-	++	-	++	++	-
mouse	high	NIH 3T3 [a, c, e]	+	++	++	++	++	+
		ES cell [a, c, e]	+	++	++	++	++	-
		3KO-H1 ES [a, c, e]	+	-	-	-	++	+

a TDMS, b HIC, c SDS-PAGE, d RP-HPLC, e HILIC

- below detection level, + low expression level, ++ medium expression level, +++ high expression level.

Figure 3.1

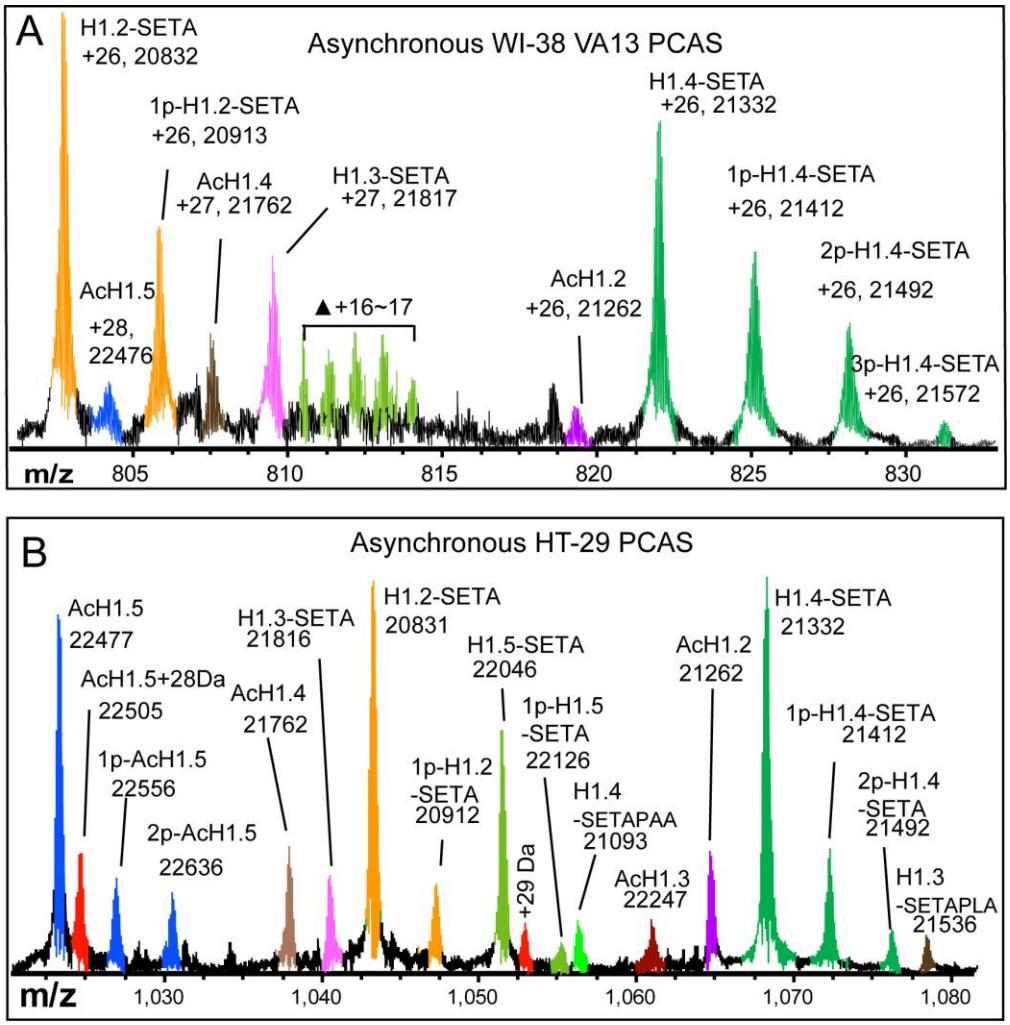

Comparison of H1 Variant Expression and Phosphorylation in Different Cell Lines by FTMS

(A) The mass spectrum of crude H1 purified from asynchronously growing WI-38 VA13 cells. Residues 2-5 (SETA) were lost from majority of forms during electrospray ionization (see text) but missing Met1 and α-N-acetylated at Ser2 were still present in minor forms of H1.2, H1.4 and H1.5. Abundances of phosphorylation for H1.2 and H1.4 were slightly higher to H1 in HeLa and triphosphorylated H1.4 was also observed. No phosphorylation was seen for H1.3. Peaks noted with "▲" had charge from +16 to +17 and were not H1 since mass was lower than any H1 variant.

(B) The mass spectrum of crude H1 purified from asynchronously growing HT-29 cells. Both forms missing Met1 and α-N-acetylated at Ser2 and missing residues 2-5 (SETA) during electrospray ionization (see text) were observed. Percentages of phosphorylation for H1.2, H1.4 and H1.5 were relative low compared with H1 in HeLa. Additional N-terminal fragmented ions, i.e. H1.4-SETAPAA and H1.3-SETAPLA were also observed.

Figure 3.2

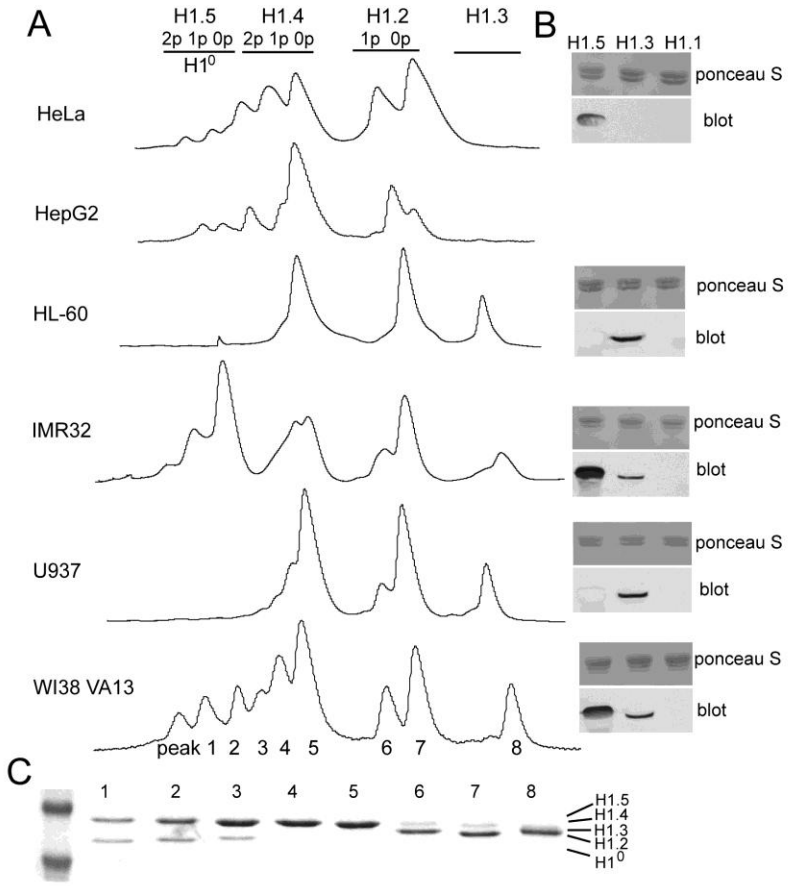

D Relative abudance of expression and phosphorylation levels of H1 variants

	H1.2			H1.3			H1.4			H1.5		
	0p	1p	2p	0p	1p	2p	0p	1p	2p	0p	1p	2p
HeLa	30%	17%	-	-	-	-	20%	16%	12%	3%	2%	-
HepG2	9%	17%	-	-	-	-	41%		5%	17%	6%	6%
HL-60	38%	-	-	15%	-	-	47%	-	-	-	-	-
IMR32	17%	6%	-	5%	2%	-	11%	16%		29%	12%	3%
U937	28%	8%	-	13%	-	-	35%	15%	-	-	-	-
WI38 VA13	16%	9%	-	9%	-	-	23%	14%	7%	*8%*	*9%*	*6%*

Comparison of H1 Variant Expression and Phosphorylation in Different Cell Lines by HIC

(A) Crude H1 prepared from different cell lines was analyzed by Hydrophobic Interaction Chromatography (HIC). PolyPROPYL A column (PolyLC), 100 x 4.6 mm, base = 3 µm spherical silica with 1500 Å diam. Pores, gradient from 2.5 M to 1.5 M $(NH_4)_2SO_4$ in 50 mM ethylendiamine pH7.0, flow rate of 0.8 ml/min. The identity of each peak is noted on the top.

(B) Western blot of crude H1 from different cell lines by H1 variants specific antibody from abcam (H1.1: ab17584, H1.3: ab24174, H1.5: ab24175).

(C) SDS polyacrylamide gel analysis of HIC fractions of H1 from WI-38 VA13 cells.

(D) Abundances of phosphorylation relative to total H1 were quantified by peak area integration in chromatograph from HIC.

Figure 3.3

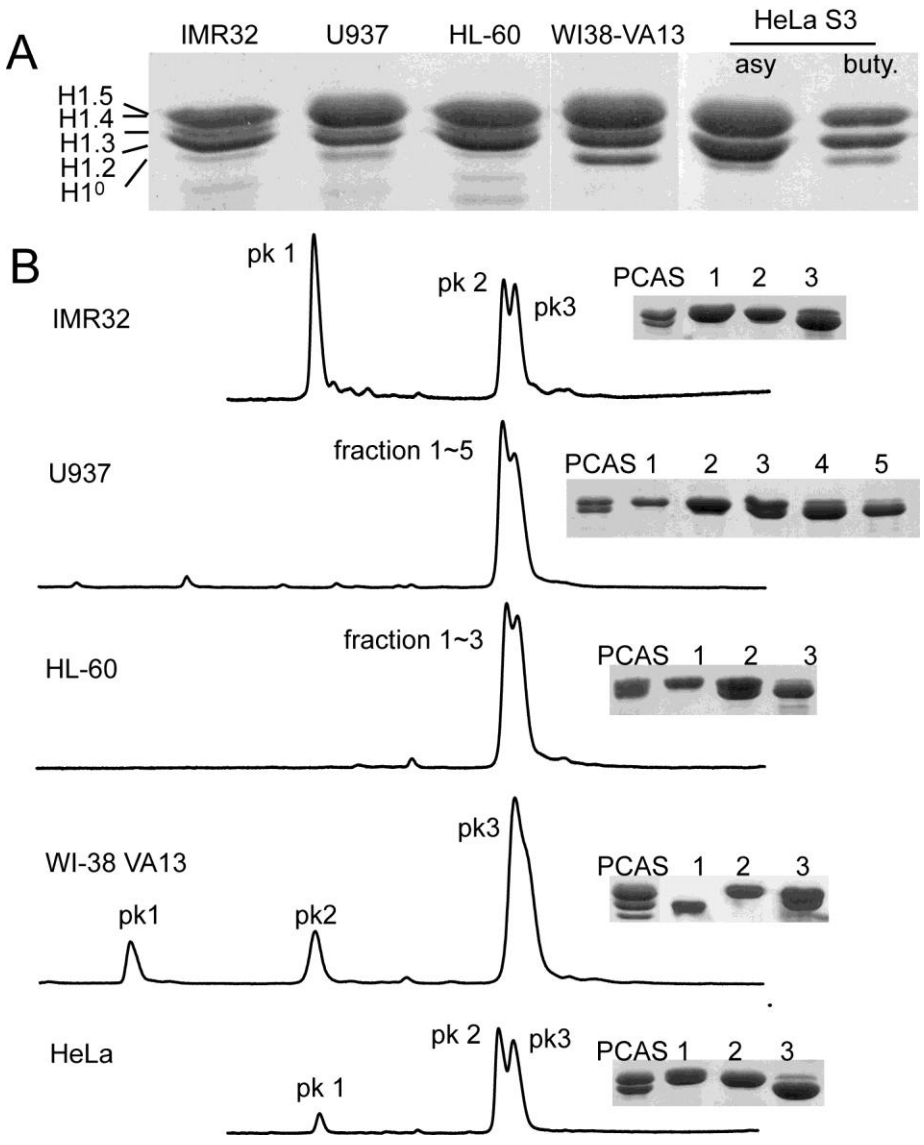

Comparison of H1 Variant Expression in Different Cell Lines by RP-HPLC
(A) SDS polyacrylamide intermediate gel analysis of crude H1 prepared from different cell lines. The relative motilities of H1 variants are shown on the left.
(B) RP-HPLC separation of crude H1 prepared from different cell lines. Vydac 250 x 4.6 mm, C8, flow rate of 0.8 ml/min. Buffer A: 5% ACN, 0.1% TFA, Buffer B: 90% ACN, 0.094% TFA. SDS polyacrylamide gel analysis of recovered peaks or fractions of RP-HPLC is shown on the right. PCAS = crude H1 from asynchronously growing cells.

Figure 3.4

A

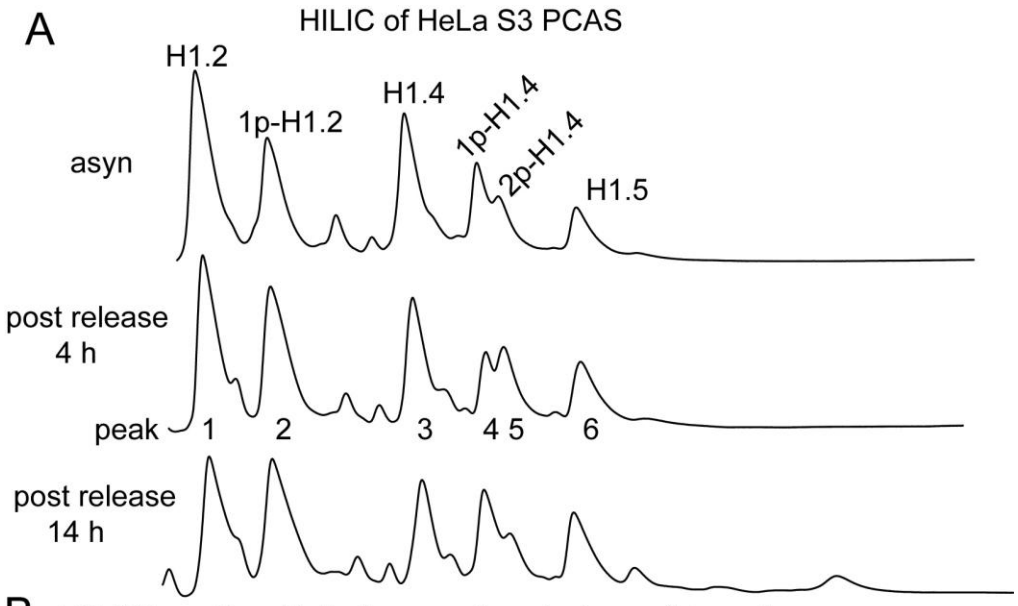

B FTMS broadband intact mass of post release 4 h peaks

	Molecular weight (Da)				
peak	Measured	Predicted	Δm	Variant	Modifications
1	20832.7	20832.6	0	H1.2 -SETA	0 phos
	20862.0	20862.5	0	H1.2(A141T)-SETA	0 phos
2	20913.9	20832.6	80	H1.2 -SETA	1 phos
	20943.5	20862.5	80	H1.2(A141T)-SETA	1 phos
3	21333.3	21332.8	0	H1.4 -SETA	0 phos

C

peak 1
H1.2-SETA

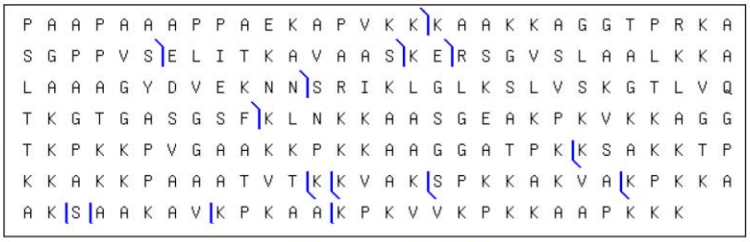

peak 2
pS173-
H1.2-SETA

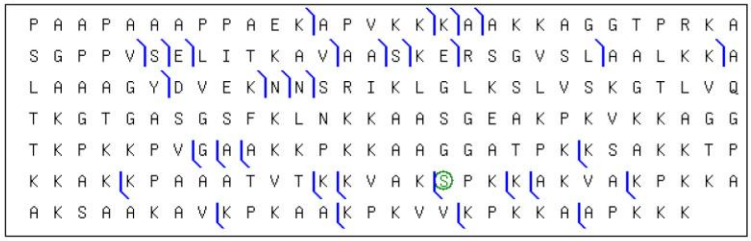

peak 3
H1.4-SETA

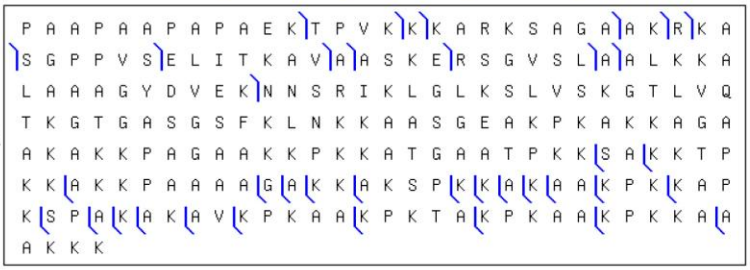

Figure 3.4 (cont.)

Identification of Phosphorylation Sites in H1 Purified by HILIC from Mid S HeLa Cells

(A) Crude H1 prepared from HeLa S3 cells was analyzed by Hydrophilic Interacting Liquid Chromatography (HILIC) using polyCAT A 100x4.6 mm, 3µm, 1500Å. Buffer A: 65% ACN, 20 mM TEA, pH 3.0; Buffer B: 60% ACN, 20 mM TEA, 0.5M $NaClO_4$, pH 3.0. Peaks are numbered according to elution order. Each peak was desalted by TCA precipitation and identified by mass spectrometry.

(B) Intact mass of the components from HILIC peaks in broadband FT-MS was used to deduce the variants identity and phosphorylation levels. Molecular masses are reported for the neutral monoisotopic species.

(C) The sites of phosphorylation identified by direct MS/MS analysis are indicated in the ECD map. Blue "└" represents Z ions from ECD, blue "┐" represents C ions from ECD, the circle around a residue represents phosphorylation in this site.

Figure 3.5

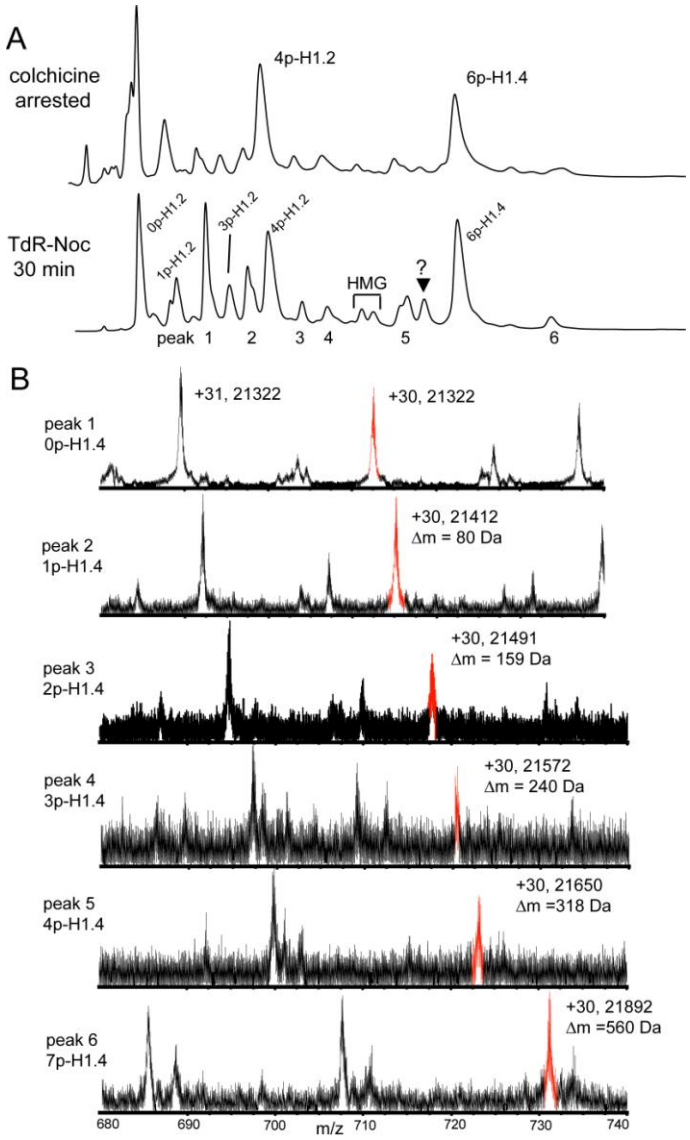

Evidence for a Rare Form of Hyperphosphorylated H1.4 in HeLa Cells

(A) HILIC separation of crude H1 prepared colchicine treated or 30 min release from nocodazole treated HeLa S3 cells. To shorten the treatment time course, 0.5 μg/ml of nocodazole were added to cells released 8 hrs from double thymidine synchronization, after 4.5 hr treatment cells were released to fresh medium to allow the progress of the mitosis for 30 min (TdR-Noc 30 min). All the peaks in TdR-Noc 30 min were analyzed by TDMS and their identity were determined by intact mass. "▼" noted that mass spectrum quality was too bad to determine the identity of the peak.

(B) Broadband mass spectra for the indicated peaks from TdR-Noc 30 min. The main ion species were H1.4-SETA with +31 or +30 charge. The phosphorylation levels in H1.4 were determined by the fold increase of 80 Da in molecule mass.

Figure 3.6

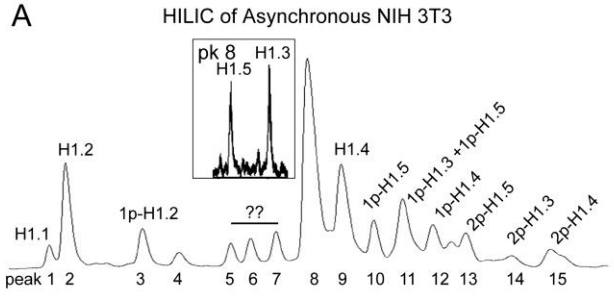

C FTMS broadband of intact mass

peak	Measured	Predicted	Δm	Variant	Modifications
1	21252	21252.7	0	H1.1 -SETA	0 phos
2	20764	20764.5	0	H1.2 -SEAA	0 phos
3	20844	20764.5	80	H1.2 -SETA	1 phos
5	20874		n.d.	n.d.	n.d.
6	20744		n.d.	n.d.	n.d.
7	20703		n.d.	n.d.	n.d.
8	21567	21566.9	0	H1.3 -SETA	0 phos
	22043	22043.2	0	H1.5-SETA	0 phos
9	21445	21444.8	0	H1.4 -SETA	0 phos
10	22123	22043.2	80	H1.5 -SETA	1 phos
11	21646	21566.9	80	H1.3 -SETA	1 phos
	22122	22043.2	80	H1.5-SETA	1 phos
12	21524	21444.8	80	H1.4 -SETA	1 phos
13	22204	22043.2	160	H1.5 -SETA	2 phos
14	21727	21566.9	160	H1.3 -SETA	2 phos
15	21604	21444.8	160	H1.4 -SETA	2 phos

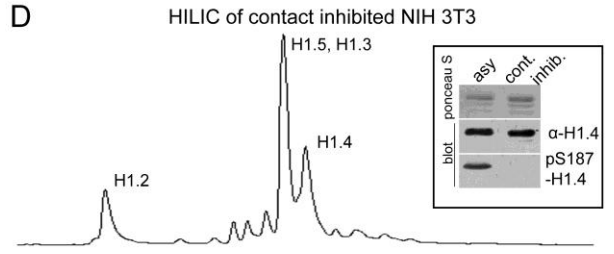

HILIC Analyses of H1 Variant Expression and Phosphorylation in 3T3 Cells

(A) Crude H1 prepared from asynchronous NIH 3T3 cells was analyzed by Hydrophilic Interacting Liquid Chromatography (HILIC) using polyCAT A. Peaks were numbered according to elution order. Each Peak was desalted by TCA precipitation and analyzed by SDS-PAGE and TDMS (panel C).

(B) Peaks numbered in (A) were desalted and analyzed by SDS polyacrylamide gel analysis.

(C) Intact mass of the components from HILIC peaks in broadband FT-MS was used to infer the variants identity and phosphorylation levels. Molecular masses are reported for the neutral monoisotopic species.

(D) HILIC result of crude H1 prepared from contact-inhibited 3T3 cells and the phosphorylation levels in H1.4 was tested by western blot using pS187-H1.4 antibody.

Figure 3.7

A

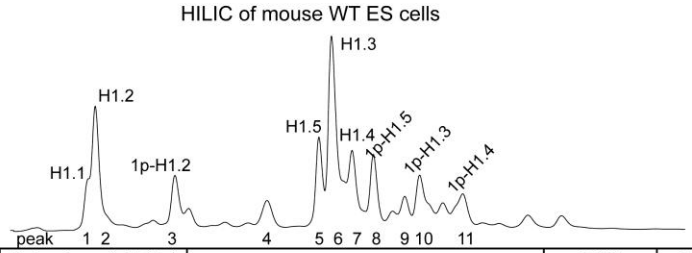

	Molecular weight (Da)					ECD		Mapped
peak	Measured	Predicted	Δm	Variant	Modifications	C ions	Z ions	Sites
2	20764	20764.5	0	H1.2 -SEAA	0 phos	1	4	
3	20845	20764.5	80	H1.2 -SEAA	1 phos	6	4	pS173
4	11677	11476	201	HMGA1	2p + 1ac	14	15	
5	22043	22043.2	0	H1.5 -SETA	0 phos	1	1	
6	21568	21566.9	0	H1.3 -SETA	0 phos	8	6	
7	21444	21444.8	0	H1.4 -SETA	0 phos	11	4	
8	22123	22043.2	80	H1.5 -SETA	1 phos	20	6	pS18

B

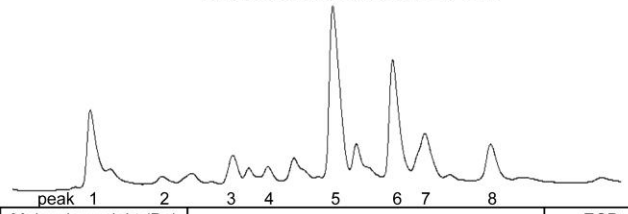

	Molecular weight (Da)					ECD		Mapped
peak	Measured	Predicted	Δm	Variant	Modifications	C ions	Z ions	Sites
1	21252	21252.7	0	H1.1 -SEAA	0 phos	5	13	
	21644	21640.9	24	H1.1	Na adduct			
2	21332	21252.7	80	H1.1 -SETA	1 phos	n.d.		
3	11677	11476	201	HMGA1	2p + 1ac	n.d.		
4	20717	20717.1	0	$H1^0$	0 phos	n.d.		
5	22043	22043.2	0	H1.5 -SETA	0 phos	n.d.		
6	22553	22043.2	122	H1.5	1p+1ac	16	9	N-term Ac pS18
7	22123	22043.2	80	H1.5 -SETA	1p	n.d.		

C

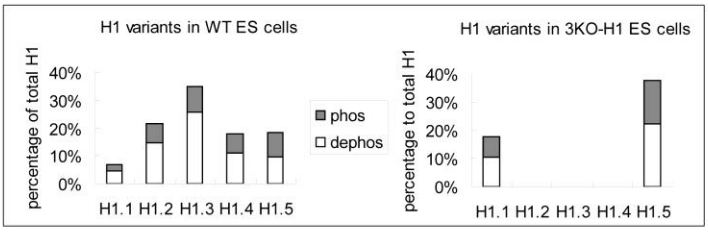

Phosphorylation of the Remaining H1 Variants is Unaltered in H1.2/H1.3/H1.4 Triple Knockout ES Cells

(A, B) Crude H1 prepared from asynchronous wild type mouse ES (WT ES) cells (A) or asynchronous H1.2/H1.3/H1.4 triple knockout ES Cells cells (3KO-H1 ES) (B) were analyzed by Hydrophilic Interacting Liquid Chromatography (HILIC). Peaks are numbered according to elution order and the identification was based on mass spectrometry analysis. The number of C and Z ions identified was listed for MS/MS analysis; otherwise the intact mass was used to identify the variant and the modifications. (C) Relative abundance of phosphorylated and unphosphorylated H1 variants quantified from HILIC for wild type vs. 3KO-H1. The number for 3KO-H1 was corrected for the 50% decrease of H1 stoichiometry (Fan et al., 2005).

Figure 3.8

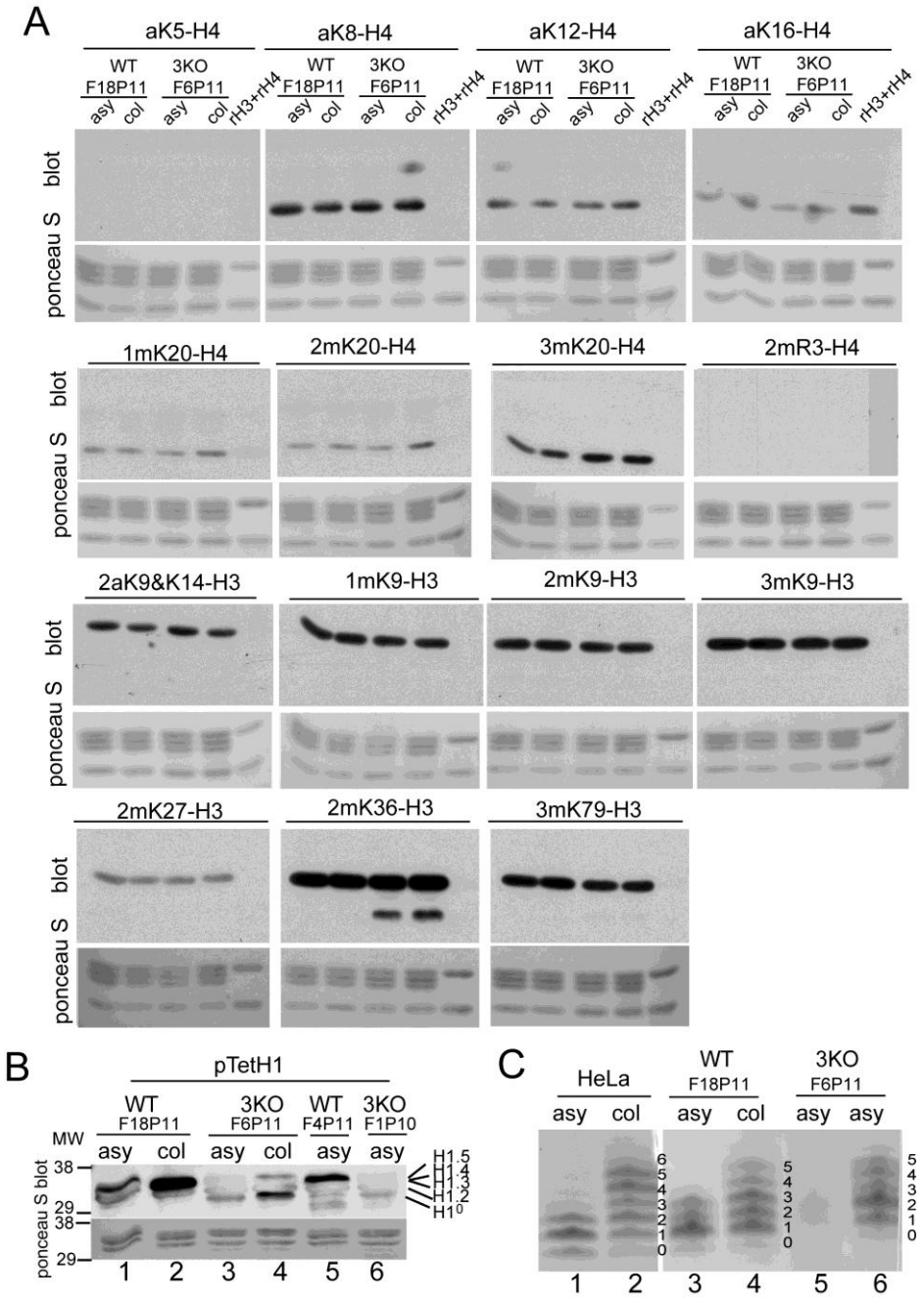

Disruption of Three H1 Variants in Mouse ES Cells Does Not Affect Phosphorylation of the Remaining H1 or Core Histone Modifications

A panel of core histone modification antibodies was used to test the PTMs levels in WT ES vs. 3KO-H1 ES. Recombinant H3 and H4 (rH3+rH4) were used as negative control. Even loading was indicated by ponceau S staining.

(A) pTetH1 antibody was used to monitor the phosphorylation levels in H1.

(B) Acid-Urea PAGE was used to analyze the phosphorylation levels of H1 from WT ES vs. 3KO-H1 ES.

CHAPTER 4 *

NUCLEAR AND NUCLEOLAR H1 PHOSPHORYLATION ASSOCIATED WITH TRANSCRIPTION

*: Some material was adapted from manuscript:

Histone H1 Phosphorylation is Associated with Transcription by RNA Polymerases I and II

Yupeng Zheng, Sam John, James J. Pesavento, Jennifer R. Schultz-Norton, R. Louis Schiltz, Sonjoon Baek, Ann M. Nardulli, Gordon L. Hager, Neil L. Kelleher and Craig A. Mizzen

4.1 Introduction

As discussed in the chapter 1, antibodies have been proven to be an invaluable tool for histone post-translational modifications study, especially in the immunofluorescence (IF) and Chromatin immunoprecipitation (ChIP) study. However lacking the phospho- and site-specific H1 antibodies has become a great obstacle for H1 phosphorylation research, thus we decided to generate these important reagents by ourselves and apply them to IF (chapter 4) and ChIP (chapter 5) study.

4.2 Generation and Characterization of H1 Phosphorylation Site-Specific Antibodies

We used synthetic phosphopeptides coupled to keyhole limpet hemocyanin to generate antisera specific for pS173-H1.2 and pS187-H1.4, the two most abundant interphase phosphorylations in HeLa S3 cells. We also generated antisera against the pS27-H1.4 and pT154-H1.4 M sites. The specificity of these antisera was characterized by immunoblotting, ELISA and immunocytochemical assays. Commercially available antiserum for human pT146-H1.4 and control antisera we generated against unmodified recombinant human H1.4 were also employed.

Synthetic peptide antigens were designed as shown in Figure 4.1 A. Amino acid sequence substitutions within individual H1 variants enabled antisera to be generated which recognize a single site of phosphorylation identical to the respective antigen peptide in just one variant (pS27-H1.4, pT146-H1.4, pS187-H1.4), or at a single site that is completely conserved in just two variants (pT154-H1.2/H1.4 and pS173-H1.2/H1.5).

Immunoblots revealed that the pS27 antisera recognized H1.4 from colchicine-treated cells but not mid-S phase cells (Figure 4.1 B, lanes 1 and 2), confirming our TDMS evidence that H1.4-S27 is phosphorylated exclusively during mitosis. Similarly, H1.4 from colchicine-treated cells, but not mid-S phase cells, was detected by the pT146-H1.4 antisera (Figure 4.1 B, lanes 3 and 4). This is consistent with previous immunocytochemical analyses suggesting that phosphorylation at H1.4-T146 is mitosis-specific (Sarg et al., 2005). The analogous Thr is present in H1.2 and H1.3, but absent from H1.1 and H1.5 (Figure 4.1 A, Figure 2.11). However, it is unlikely that any of the signal in lane 4 (Figure 4.1 B) is attributable to H1.2/H1.3 phosphorylated at this site since the band aligns with H1.4 rather than H1.2 (i.e. the upper band of the major H1 doublet), and since H1.3 is not expressed appreciably in HeLa S3 cells (chapter 2). Moreover, the corresponding epitopes of H1.2 and H1.3 each contain an amino acid substitution expected to diminish antibody binding (Figure 4.1 A). Mitosis-specific phosphorylation was also observed for the pT154 antiserum, raised against a motif that is completely conserved between the H1.2 and H1.4 variants. This antiserum detected H1.2 and H1.4 in samples from colchicine-treated cells but not mid-S phase cells (Figure 4.1 B, lanes 5 and 6). The signals in lane 6 appear to represent T154 phosphorylation primarily in H1.2 and H1.4 since the antiserum failed to recognize H1.5 (a minor species immediately above H1.4), and since the corresponding motifs in H1.1, H1.3 and H1.5 each contain one or more substitutions (Figure 4.1 A).

In contrast, the antisera to pS173-H1.2/H1.5 and pS187-H1.4 recognized H1 from both mid-S phase and colchicine-treated cells in immunoblots. The pS173 antiserum detected a major band aligning with H1.2, and a minor band aligning with H1.5, in both types of samples (Figure 4.1 C, lanes 3 and 4). We presume the latter represents phosphorylation at H1.5-S173 since the phosphopeptide epitope is completely conserved between H1.2 and H1.5, and signals for pS173-H1.5 are expected to be weaker than that

observed for pS173-H1.2 since H1.5 is much less abundant than H1.2 in HeLa S3 cells (chapter 2). The pS187 antisera recognized a single band aligning with H1.4 in both types of samples (lanes 7 and 8). Consistent with ELISA assays performed to assess antisera specificity (Figure 4.2), the signals detected by the pS173 and pS187 antisera are phosphorylation-dependent and specific for the respective sites. Neither antisera recognized purified fractions of non-phosphorylated H1.2/H1.4 (lanes 1, 2, 5 and 6), the pS187 antisera did not cross-react with H1.2, and the pS173 antisera did not cross-react with H1.4 (compare lanes 3, 4, 7 and 8). Moreover, little cross-reactivity with nonhistone proteins was observed for these antisera: a single band corresponding to H1.4 was observed when 2 % SDS extracts of asynchronous or colchicine-treated cells were immunoblotted with the pS187 antisera (Figure 4.1 G, lanes 1, 2, 4 & 5).

We attempted to raise control antisera that would recognize all H1 variants regardless of phosphorylation. Recombinant human H1.4 (rH1.4) expressed in bacteria was used as antigen. The corresponding antisera recognized rH1.4 and HPLC-purified fractions of HeLa H1.4 bearing 0, 1, 2 or 6 phosphorylations with similar affinity in immunoblots (Figure 4.1 D, lanes 3-7). However, it was surprisingly specific for H1.4, displaying little or no binding to purified HeLa H1.2 with 0 or 1 phosphorylations (Figure 4.1 D , lanes 1 & 2), or to variants other than H1.4 from different sources (not shown). The antisera detected a single major band aligning with H1.4 in immunoblots of whole cell extracts from asynchronous (Figure 4.1 G, lanes 3 & 6) and colchicine-treated HeLa cells (not shown), validating the use of this antisera to detect H1.4 regardless of phosphorylation.

Since pTetH1 antisera, which was raised against highly phosphorylated H1 from *Tetrahymena*, was widely used in H1 phosphorylation research, we attempted to identify which sites it can recognize by using the samples with phosphorylation sites already

determined. As shown in Figure 4.1 E, HPLC-purified H1.4-2p (lane 1), H1.4-1p (lane 2), H1.4-0p (lane 3), H1.2-1p (lane 4), H1.2-0p (lane 5), crude histones from asynchronous growing (lanes 6) and colchicine-arrested HeLa S3 cells (lanes 7) were analyzed by immunoblotting with pTetH1. The apparent affinity of the pTetH1 antisera for H1.4-2p phosphorylated at S172 and S187 (lanes 1) was much stronger than that for H1.4-1p phosphorylated at S187 (lane 2), whereas binding to H1.4-0p, H1.2-1p and H1.2-0p were negligible (lanes 6 and 7). These data suggests pTetH1 can recognize pS172-H1.4 but not pS173-H1.2 and pS187-H1.4. We attribute the weak signal observed in H1.4-1p (lane 2) is solely due to the carry over of the H1.4-2p in the chromatograph fraction. However, we were unable to exclude the possibility that the increasing intensity seen in the colchicine-arrested sample is due to the recognition of mitotic specific phosphorylation described in chapter 2. We also tested three antisera that recognize interphase specific phosphorylation with crude histones from MCF-7 cells (Figure 4.1 F). Compared with HeLa cells, the band intensity observed in MCF-7 cells in the upper band aligning with H1.4 and H1.5 increased in immunoblot with pS173-H1.2 specific antisera whereas decreased with pS187-H1.4 specific antisera (lanes 1~3 and 7~9). This observation can be attributed to higher expression level of H1.5 variants in MCF-7 cells. In addition, band intensity in MCF-7 detected by pTetH1 was stronger than that by pS187-H1.4 suggesting pTetH1 also recognizes other phosphorylated H1 in addition to pS172-H1.4 in the interphase cells (lanes 5~7) and it is very likely to be phosphorylation in H1.5. It is also worth noting that no apparent global H1 phosphorylation changes were observed when MCF-7 was treated with 10 nM estradiol for 45 min.

To further compare the specificity of the pS173-H1.2 and pS187-H1.4 antibodies, we employed peptide competition ELISA (Figure 4.2). Specifically, different amount of unmodified, irrelevant phospho- and antigen phospho-peptide were immobilized in the

plate to test the binding of antibodies. In addition, these binding were challenged with no competition, competition with unmodified, irrelevant phospho- and antigen phospho-peptide. As results shown in Figure 4.2, both antibodies reacted well with phosphopeptide but not with unmodified peptide and such reactivity was competed off by the phosphopeptide. It is worth noting that pS187-H1.4 discriminated antigen peptide from irrelevant phosphopeptide better than pS172-H1.2. Taken together, we conclude the specificity of both pS172-H1.2 and pS187-H1.4 is high enough for us to specifically recognize pS173-H1.2 and pS187-H1.4 in the protein for the analyses we want to apply.

4.3 Progressive Phosphorylation of H1 during Cell Cycle

We have determined the dynamic of the H1 phosphorylation abundance in HeLa cells by various techniques including TDMS, HIC (chapter 2) and HILIC (chapter 3). To confirm our results in MCF-7 cells, whole cell extracts from synchronized cells were subjected to western blot with three antisera, namely pT154-H1.2/H1.4, pS173-H1.2/H1.5 and pT187-H1.4. As expected, the signal intensity in pT154 blot was negligible initially and had sharp increase in 10 hrs sample, then steadily decrease and totally disappeared in 16 hrs sample (Figure 4.3). We attributed the detection of pT154 in 12 hrs and 14 hrs sample to the factions of cells exiting mitosis slower than most cells (i.e. lost of synchrony) and thus concluded that this phosphorylation is only present in the mitosis with further evidence from immunofluorescence study described below. For both pS173 and pS187, they increased when cells progressed through S phase, reached the maximum abundance in mitosis and decreased as cells entered the next G1. One interesting phenomena we observed from previous cell cycle study is the slower decrease of 1p-H1.4 compared with 2p-H1.4 and 1p-H1.2 in the G1, which indicates Ser187 in H1.4 might be regulated differently form other I sites. Phosphorylation of Ser187 is present in both 1p-H1.4 and 2p-H1.4 molecules but previous studies only analyzed the behavior of 1p-H1.4. With newly raised pS187 antibody, which recognizes both

1p-H1.4 and 2p-H1.4 forms, we can analyze the behavior of all phosphorylated Ser187 in H1.4 coming from 1p-H1.4 together with 2p-H1.4 molecules. As expected, the signal in the western blot clearly indicated abundance of pS187 remained at higher levels after cells reenter G1 and also maintained at higher levels in early S phase compared with pS173 (Figure 4.3).

To overcome the limitation of cell synchronization and understand when the mitosis specific phosphorylation of H1 appears and disappears, we employed the immunofluorescence study using pT146-H1.4 and pT154-H1.2/H1.4 antisera. As predicted by our previous analysis, both pT146 and pT154 failed to stain the nuclei of interphase HeLa cells above background levels (Figure 4.4 A, B top row). On the contrary, intense staining was observed in condensed chromosomes from prophase and metaphase cells, and such staining started to diminish in anaphase and became very dim in telophase cells (Figure 4.4 A, B). Obviously, such diminish is not the result of losing H1 from chromosome since no diminish in anaphase or telophase was found for total H1 staining (Figure 4.4 C). Very interestingly, less intense staining was also seen in the cytoplasm for both pT146 and pT154 antibodies in mitosis, in addition to the intense staining of condensed chromosome (Figure 4.4 A, B). In fact, similar pattern was also seen for pTetH1 staining (data not shown), which is confirmed by reports of IF and immuneEM study using pTetH1 antibody (Bleher and Martin, 1999; Boggs et al., 2000). By contrast, only condensed chromosome was stained with total H1 antibody (AE-4 monoclonal or α-H1.4 polyclonal that we generate). The observation of hyperphosphorylated H1 localizes to both chromosomes and cytoplasm in M phase suggests that hyperphosphorylation of H1 (6p-H1.4, 4p-H1.2) results in the higher exchange rate between chromatin bound state and nuclear free state. Taken together, these data provide direct evidence to support our conclusion that T146 and T154 are phosphorylated only in mitosis.

4.4 pS173-H1.2/H1.5 and pS187-H1.4 Are Enriched in Nucleoli

To understand the nuclear distribution of interphase specific H1 phosphorylation, we set out confocal microscopy study using the novel phosphospecific antibodies we generated. Confirming the previous result from epifluorescence study, the pT154-H1.2/H1.4 antisera only stained the condensed chromosomes of mitotic HeLa cells (Figure 4.5). In contrast, antisera to pS173-H1.2/H1.5 or pS187-H1.4 stained the chromatin of both interphase and mitotic cells. Interphase cells displayed finely stippled staining that was distributed uniformly throughout the nucleus, together with clusters of more punctate staining in regions poorly stained for DNA that appeared to be nucleoli (Figure 4.5). Staining by the pS173-H1.2/H1.5 and pS187-H1.4 antisera was suppressed by incubation with antigen peptide prior to immunostaining whereas preincubation with the nonphosphorylated peptide had no effect (Figure 4.6). This suggests that both the stippled and punctate types of staining are attributable to phosphorylated H1. In contrast, the general H1.4 (α-H1.4) antisera stained nuclei uniformly in a finely stippled fashion. The punctate nucleolar staining typical of pS173-H1.2/H1.5 and pS187-H1.4 was not observed with the α-H1.4 antisera, and the latter often stained nucleoli less intensely than the surrounding chromatin. Extensive colocalization of fibrillarin with the clustered punctate staining for pS173-H1.2/H1.5 and pS187-H1.4 confirmed that H1 phosphorylated at these sites is enriched in nucleoli (Figure 4.7 A). This suggested the intriguing possibility that pS173-H1.2/H1.5 and pS187-H1.4 may be associated with transcriptionally active rDNA and facilitate transcription by RNA polymerase I. As a first test of this hypothesis, we incubated cells briefly with BrUTP to facilitate selective detection of nascent 45S pre-rRNA transcripts using antibodies to BrdU (Koberna et al., 2002; Olson and Dundr, 2005). As shown in Figure 4.7 B, punctate pS187-H1.4 staining coincided with the centers of Br-UTP incorporation foci. These data support the notion that interphase phosphorylated H1.2 and H1.4 are associated with transcribing rDNA.

The nucleoli of higher eukaryotes contain three distinct ultrastructural elements, the fibrillar center (FC), the dense fibrillar component (DFC) and the granular component (GC) whose relative structure is thought to reflect vectorial organization of major steps in ribosome biogenesis: pre-rRNA transcription, pre-rRNA processing and ribosome assembly on mature rRNA (Hernandez-Verdun, 2006a; Hernandez-Verdun, 2006b; Olson and Dundr, 2005). Both inhibition of pre-rRNA transcription by actinomycin D and perturbation of pre-rRNA processing have been shown to alter nucleolar organization (Jordan et al., 1996; Olson and Dundr, 2005). We investigated how the drug affects the colocalization of pS187-H1.4 with markers for each of these nucleolar compartments. In growing cells, fibrillarin is normally distributed over much of the nucleolar area, localizing primarily to the DFC in a punctate staining pattern that rings FCs. Upon actinomycin D treatment, the FC and DFC dissociate from each other and fibrillarin staining becomes concentrated in a few large foci at the nucleolar periphery. Although there was extensive partial colocalization of pS187-H1.4 and fibrillarin in untreated cells, actinomycin D caused a characteristic change in this relationship (Figure 4.7 D, compare top two rows). Both proteins formed a similar number of foci near the nucleolar periphery, but pS187-H1.4 foci were typically smaller and their centers were shifted relative to those of the fibrillarin foci.

pS187-H1.4 showed extensive colocalization with upstream binding factor (UBF) within the nucleoli of both control and actinomycin D-treated cells (Figure 4.7 D, compare middle two rows). UBF is a positive transcription factor for RNA pol I that normally localizes preferentially to the FC (McStay and Grummt, 2008; Zatsepina et al., 1997). In agreement with previous work, we observed that actinomycin D caused the characteristic punctate UBF staining to coalesce into a few large granules at the nucleolar periphery (Zatsepina et al., 1993). However, in contrast to the results described above for fibrillarin, these UBF foci colocalized completely with the foci formed by

pS187-H1.4 in actinomycin D-treated cells. Actinomycin D had similar effects on staining for RNA pol I (RPA 194, bottom two rows of Figure 4.7 D). Punctate RPA 194 staining localized to the central portions of nucleoli in untreated cells but was concentrated into a few dense clusters at the edge of nucleoli in treated cells. pS187-H1.4 co-localized extensively with RPA 194 before and after actinomycin D treatment. Both UBF and RPA 194 are thought to localize preferentially to the FC in untreated cells (Matera et al., 1994). The persistence of H1.4-S187 phosphorylation and its colocalization with UBF and RPA 194 in foci formed upon actinomycin D treatment are consistent with previous reports that a fraction of these latter proteins remain associated with rDNA under these conditions (Jordan et al., 1996). Taken together, these data suggest that pS187-H1.4 localize largely to the FC or the FC/DFC interface in untreated cells.

4.5 Nucleolar H1 Phosphorylation Appears in G1

We have previously demonstrated that the abundance of phosphorylated H1.2 has significantly decreased from ~30% of total H1.2 in asynchronous cells to ~10% in G1 cells (chapter 2). To investigate the potential difference in staining patterns for phosphorylated H1 in G1, cells prevented from entering S phase by mimosine were stained with pS173-H1.2. Interestingly, both the uniformly distributed nuclear staining and the punctate nucleoli staining were present in the G1 cells but decreased to the similar extent (Figure 4.8 A). More specifically, when the pS173-H1.2 fluorescence intensity profiles were examined in an arbitrary drawn line, which crossed both nuclear and nucleoli regions, the intensity for nuclear and nucleoli in asynchronous cells was roughly 150 and 200 respectively. Such intensity dropped to 100 and 150 for cells arrest in G1 (Figure 4.8 B). This data suggests both nuclear and nucleolar H1 phosphorylations have similar cell cycle regulated dynamics.

To further test when the interphase H1 phosphorylation appears after cells exiting mitosis, mechanical released mitotic cells which were enriched by nocodazole, were replated into fresh medium and stained with pS173-H1.2 antisera after certain amount of time. Strikingly, the nucleolar staining was detected in cells immediately following cytokinesis in the 1 h release sample (Figure 4.9, arrow head and enlarged in the inset, cell stages were indicated by DNA staining and DIC morphology), and cells already in G1 (Figure 4.9 A, arrow). In 2 h release, more nucleolar staining became visible as more cells reentering G1. In 3 h and 10 h release (mid G1 and mid S), the staining was observed in most of the cells and no significant difference staining pattern except increase of overall intensity was observed in 10 hr release when compared with 3 hr release (Figure 4.9 B). Taken together, these data clearly demonstrated interphase specific H1 phosphorylation appears in the early G1 and raises the likelihood that such H1 phosphorylations might involve in ribosome biogenesis and pol II transcription occurring in early G1. However it is not clear whether all the interphase phosphorylations have been erased completely before cytokinesis similar to mitotic specific phosphorylation or some of such phosphorylations actually survive through mitosis.

4.6 Evidence That Nucleolar H1 Phosphorylation is Downstream of mTOR

To further test the possibility that interphase specific H1 phosphorylations are involved in pol I transcription, we tried to compare the fluorescence intensity of pS173-H1.2 in the nucleoli before and after rapamycin treatment, which inhibits the mTOR pathway that regulates ribosome biogenesis (Mayer and Grummt, 2006). Since the fluorescence intensity of both nucleolar and nuclear staining for pS173-H1.4 increase from G1 to S phase with similar extent (Figure 4.8), only comparing cells at the same cell cycle stages can obtain a valid comparison of how rapamycin affect nucleolar H1 phosphorylation. To eliminate the necessary of costaining with cell cycle marker and normalization of the random fluorescence intensity variation, we compare the fluorescence intensity ratio

between nucleolar staining and nuclear staining. Significant decrease of the pS173-H1.2 nucleolar staining was observed for HeLa cells after rapamycin treatment using this quantification scheme (data not shown). To test the effect of rapamycin in nucleolar H1 phosphorylation in a better physiology meaningful model, we chose c2c12 cells which can be differentiated to myotube. We analyzed myoblast cell in two physiology conditions: resting condition and stimulating condition. The first one is growing c2c12 to 100% confluence and maintaining in 2% horse serum for 4 days; the second one is stimulating resting myoblast cells with addition of nutrition by 20% FBS for one day. As shown in Figure 4.10, 20% serum stimulation caused the ratio of nucleolar staining of pS187-H1.4 increased from 13% to 19%. Moreover, such increase was eliminated when stimulated cells were treated with rapamycin in the last 3 hrs of stimulation and this loss of induction was not caused by global decrease of H1 phosphorylation as indicated by western blot from whole cell lysate (Figure 4.10). This result sheds the light on the regulation mechanism of nucleolar H1 phosphorylation. Considering the result that rRNA transcription is not affected when CDKs activity are inhibited (Chapter 5), it suggests that a kinase that not CDKs but downstream of mTOR pathway is the kinase for nucleolar H1 phosphorylation.

4.7 Ligand-Dependent Colocalization of H1 Phosphorylation with ERα

Since the existence of interphase specific H1 phosphorylation in the G1 can not be attributed to the old notion of H1 phosphorylation involving in DNA replication (Ajiro et al., 1981), we decided to test the possibility that H1 phosphorylation involves with pol II transcription in addition to pol I transcription. We first tested our idea by comparing the costaining pattern of pS173-H1.2/H1.5 with ERα in the MCF-7 cells before and after the stimulation of estradiol. As shown in Figure 4.11, the ERα loci became more localized after estradiol stimulation while no visible change of staining pattern was seen for phosphorylated H1. However, the colocalization of ERα and phosphorylated H1

were observed in the estradiol stimulated MCF-7 cells but not in the cells before stimulation and such difference was more obvious in the line profile over an arbitrary drawn line (Figure 4.11). These results have clearly demonstrated the correlation between H1 phosphorylation and transcription by pol I and pol II. We will further investigate this correlation in greater details to specific gene regions by ChIP in chapter 5.

4.8 Materials and Methods

Western Blot

Purified histones or whole cell extract in 2x sample buffer (20 mM Tris pH 8.0, 20 mM EDTA, 2% SDS, 20% glycerol) were separated in 15% SDS-PAGE, transferred to nitorcellulouse membrane using seim-dry transfer apparatus using Towbin's buffer (192 mM glycine, 25 mM Tris, 1.3 mM SDS, 10% methanol) buffer. Membrane was stained with 0.4% ponceau S in 8%TCA and 2% acetic acid, blocked in 5% milk in TBS (20 mM Tris, 150 mM NaCl, pH 7.5) for at least 1 h, incubated with antibodies diluted in TBST (TBS + 01.% Tween) for 2 h, washed 3x in TBST, incubated with HRP-conjugated secondary, followed by another 3 x TBST washes and detected by ECL substrate. Antibodies dilution: crude pS27-H1.4 (rabbit 88) 1:1000, crude pT154-H1.2/H1.4 (rabbit 89) 1:1000, pT146-H1.4 (abcam ab3596) 1: 1000, crude pS173-H1.2 (rabbit UI82) 1: 200, crude pS187-H1.4 (rabbit UI86) 1:5000, pTetH1 1:2000. When primary antibodies from different host were used to reprobe different antigens, membrane can be simply incubated with 5 mM NaN3 + 5% milk in TBS to kill the peroxidase activity before reprobing. If antibodies from same host are desired or same antigen is required to be tested, stripping is necessary and boiling membrane in water for 1 min in microwave is an easy alternative. However, it tends to lose more proteins near the margin of membrane.

ELISA

Coat 96-wll plates with peptide ranging from 0 to 40 ng peptide in sodium carbonate buffer pH 9.6 overnight at 4 °C, block with 1% BSA in PBST (PBS, 0.05% Tween) for 1 h at room temperature. Incubate antibody without or in the presence of unmodified, irrelevant or antigen phosphopeptide at final concentration of 10 μg/ml in PBST for 1 hr at room temperature. Preincubated antibodies were add to the peptide coated wells and incubated for 2 h ar room temperature. Wells were rinsed twice with PBST and diluted HRP-conjugated secondary antibodies were added and incubated for 1 h. Then wells were rinsed twice with PBST and OPD substrate was added for detection by measuring absorbance at 492 nm.

Immunofluorescence Microscopy Staining

The IF staining protocol is described in appendix III. Different fixation procedure was applied for different antibody for best result. For general purpose, cells growing in coverslip was washed in PBS, fixed in 4% PFA in PBS for 12 to 15 min at room temperature, washed in TBST (TBS + 0.1% Tween), permeabilized in 0.2%Triton X-100 in TBS for 10min, washed in TBST again, blocked in 2% NCS + 2% BSA in TBST for 1 hr at room temperature and incubated with primary antibodies diluted in blocking buffer in a humidified chamber for at least 2 hrs. Then coverslip was further washed with TBST, incubated with diluted secondary antibody conjugated with FITC or Cy3 together with 1: 5k diluted TO-PRO-3. However, for some unknown reasons, nucleoli staining of phosphorylated H1 might be lost some time when using PFA in PBS fixation. Alternatively, better nucleoli staining can be achieved by fixation with 4% PFA in CSK (see Appendix III). In addition, temperature also affects the quality of nucleoli staining and it seems shorter fixation and permeabilization at lower temperature such as fixing with 4% PFA in CSK for 10 min followed by permeabilizing with 0.2% Triton X-100 in TBS for 5 min at 17 °C can achieve better result for nucleoli staining. The adverse

effect of fixation with CSK is the cross-reacting of pS187-H1.4 with SR protein in the nuclear speckles.

Antibodies Dilution for Immunofluorescence Microscopy Staining

pT146-H1.4 (Abcam ab3596) 1:1000, pT154-H1.4 crude serum (rabbit 89) 1:1000, pS173-H1.2 crude serum (rabbit UI82) 1:200, pS187-H1.4 affinity purified antibody (rabbit UI86) 1:200, α-H1.4 crude serum (rabbit UI100) 1:200, general H1 (Abcam AE-4) 1:100, fibrillarin (Abcam ab18380) 1:1000, UBF (Santa-Cruz sc-13125) 1:100, RPA194 (Santa-Cruz sc-48385) 1:100, bromo-deoxyuridine (Neomarkers, clone BRD.3) 1:100, ER-α(Santa-Cruz F10) 1:100.

Images Process

Image J Plot Profile function was used to generate line profile values which were then plotted in Excel. Photoshop was used to calculate the fluorescence intensity by multiply mean value by pixel number in the histogram. The nucleoli regions were defined by inverting the selection of the dark region in red channel (fibrillarin staining) using magic wand. Three single cell images scanned using 63x objective in Zeiss LSM510 were used to calculate intensity and the mean value was reported with standard deviation plotted in Excel.

4.9 References

Ajiro, K., T.W. Borun, B.S. Shulman, G.M. McFadden, and L.H. Cohen. 1981. Comparison of the structures of human histone 1A and 1B and their intramolecular phosphorylation sites during the HeLa S-3 cell cycle. *Biochemistry*. 20:1454-1464.

Bleher, R., and R. Martin. 1999. Nucleo-cytoplasmic translocation of histone H1 during the HeLa cell cycle. *Chromosoma*. 108:308-16.

Boggs, B.A., C.D. Allis, and A.C. Chinault. 2000. Immunofluorescent studies of human chromosomes with antibodies against phosphorylated H1 histone. *Chromosoma*. 108:485-90.

Hernandez-Verdun, D. 2006a. The nucleolus: a model for the organization of nuclear functions. *Histochem Cell Biol*. 126:135-48.

Hernandez-Verdun, D. 2006b. Nucleolus: from structure to dynamics. *Histochem Cell Biol*. 125:127-37.

Jordan, P., M. Mannervik, L. Tora, and M. Carmo-Fonseca. 1996. In vivo evidence that TATA-binding protein/SL1 colocalizes with UBF and RNA polymerase I when rRNA synthesis is either active or inactive. *J Cell Biol*. 133:225-34.

Koberna, K., J. Malinsky, A. Pliss, M. Masata, J. Vecerova, M. Fialova, J. Bednar, and I. Raska. 2002. Ribosomal genes in focus: new transcripts label the dense fibrillar components and form clusters indicative of "Christmas trees" in situ. *J Cell Biol*. 157:743-8.

Matera, A.G., K.T. Tycowski, J.A. Steitz, and D.C. Ward. 1994. Organization of small nucleolar ribonucleoproteins (snoRNPs) by fluorescence in situ hybridization and immunocytochemistry. *Mol Biol Cell*. 5:1289-99.

Mayer, C., and I. Grummt. 2006. Ribosome biogenesis and cell growth: mTOR coordinates transcription by all three classes of nuclear RNA polymerases. *Oncogene*. 25:6384-91.

McStay, B., and I. Grummt. 2008. The epigenetics of rRNA genes: from molecular to chromosome biology. *Annu Rev Cell Dev Biol*. 24:131-57.

Olson, M.O., and M. Dundr. 2005. The moving parts of the nucleolus. *Histochem Cell Biol*. 123:203-16.

Sarg, B., W. Helliger, H. Talasz, B. Forg, and H.H. Lindner. 2005. Histone H1 phosphorylation occurs site-specifically during interphase and mitosis. Identification of a novel phosphorylation site on histone H1. *J Biol Chem*.

Zatsepina, O.V., O.A. Dudnic, I.T. Todorov, M. Thiry, H. Spring, and M.F. Trendelenburg. 1997. Experimental induction of prenucleolar bodies (PNBs) in interphase cells: interphase PNBs show similar characteristics as those typically observed at telophase of mitosis in untreated cells. *Chromosoma*. 105:418-30.

Zatsepina, O.V., R. Voit, I. Grummt, H. Spring, M.V. Semenov, and M.F. Trendelenburg. 1993. The RNA polymerase I-specific transcription initiation factor UBF is associated with transcriptionally active and inactive ribosomal genes. *Chromosoma*. 102:599-611.

4.10 Figures

Figure 4.1

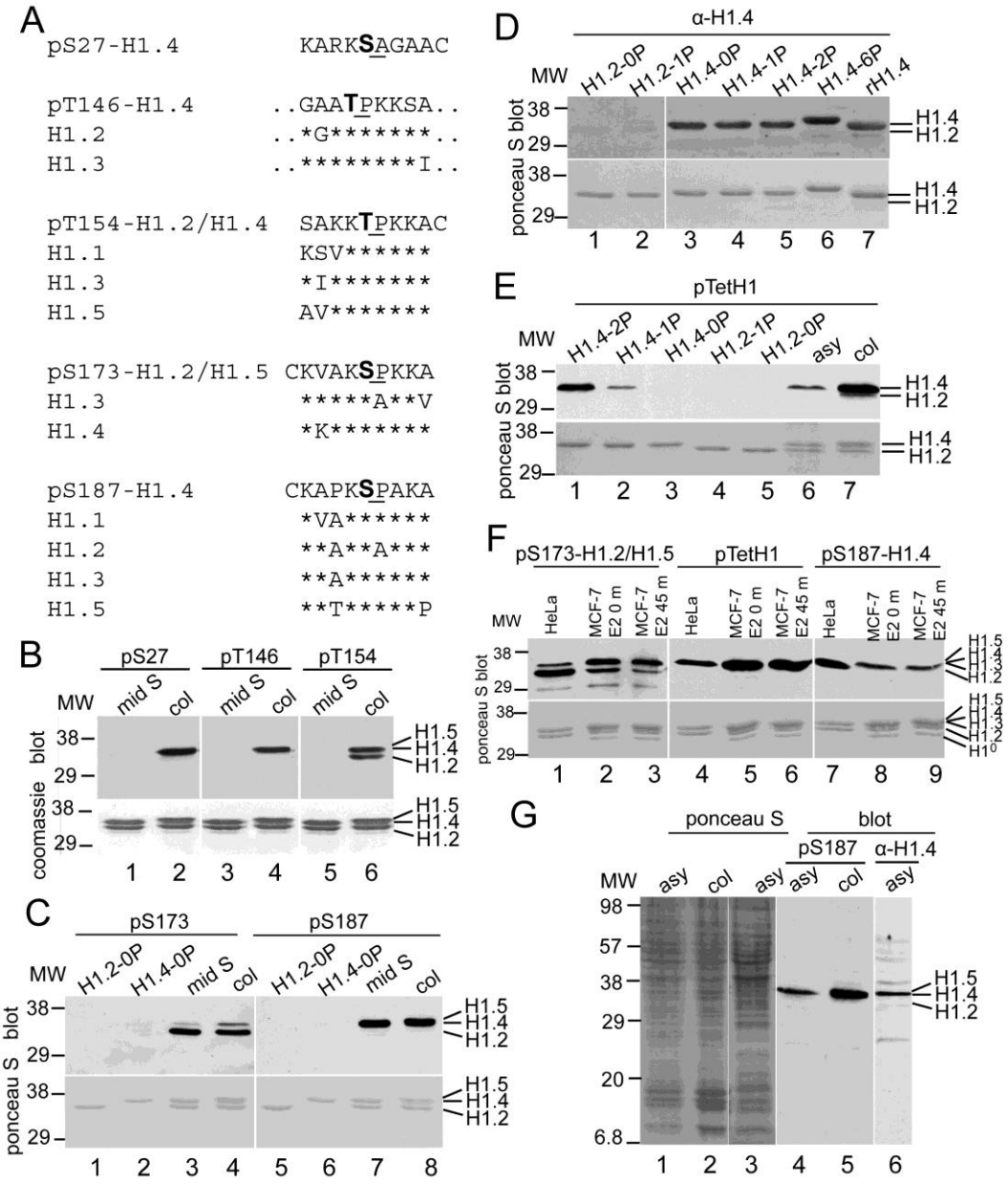

Detection of Individual Mitotic and Interphase Phosphorylations by Highly-Specific Phosphopeptide Antisera

(A) Synthetic peptides representing phosphorylation sites and flanking sequence present in just one (pS27-H1.4, pT146-H1.4, pS187-H1.4) or just two (pT154-H1.2/H1.4, pS173-H1.2/H1.5) human H1 variants were used to generate antisera in rabbits. Phosphorylated residues are underlined. Potentially homologous Ser/Thr-containing motifs in other human H1 variants are shown below each antigen peptide (see also Figure 2.11). Only the core portion of the peptide antigen used by Abcam Inc. to generate antisera to pT146-H1.4 is shown.

Figure 4.1 (cont.)

(B) Crude histones from mid-S phase (lanes 1, 3, 5) and colchicine-arrested HeLa S3 cells (lanes 2, 4, 6) were analyzed by immunoblotting with antisera to pS27-H1.4, pT146-H1.4 or pT154-H1.2/H1.4 (upper panels). Duplicate gels stained with Coomassie Blue confirmed equivalent loading (lower panels). In each case, bands were detected at the expected positions only in colchicine-arrested samples, suggesting that these three sites are phosphorylated exclusively in mitosis.

(C) HPLC-purified nonphosphorylated H1.2 (H1.2-0p, lanes 1 & 5), H1.4-0p (lanes 2 & 6), crude histones from mid-S phase (lanes 3 & 7) and colchicine-arrested HeLa S3 cells (lanes 4 & 8) were analyzed by immunoblotting with antisera to pS173-H1.2/H1.5 or pS187-H1.4 (upper panels). Ponceau S staining of the transfer membranes confirm equivalent loading (lower panels). Both antisera detected bands at the expected positions in mid-S and colchicine-arrested samples, but nonphosphorylated H1.2/H1.4 were not bound. The weak signal apparent for H1.5 in lanes 3 and 4 is consistent with the low abundance of this variant in HeLa cells (described in chapter 2).

(D) HPLC-purified H1.2-0p (lane 1), H1.2-1p (lane 2), H1.4-0p (lane 3), H1.4-1p (lane 4), H1.4-2p (lane 5), H1.4-6p (lane 6) and purified recombinant human H1.4 (rH1.4, lane 7) were analyzed by immunoblotting with antisera (α-H1.4) for total H1.4 that was raised against rH1.4 (upper panels). Ponceau S staining of transfer membranes confirmed equivalent loading (lower panels). The apparent affinity of the α-H1.4 antisera for native H1.4 with defined levels of phosphorylation (lanes 3-6) was similar to that for rH1.4 (lane 7), whereas binding to H1.2 was negligible (lanes 1 and 2).

(E) HPLC-purified H1.4-2p (lane 1), H1.4-1p (lane 2), H1.4-0p (lane 3), H1.2-1p (lane 4), H1.2-0p (lane 5), crude histones from asynchronous growing (lanes 6) and colchicine-arrested HeLa S3 cells (lanes 7) were analyzed by immunoblotting with antisera pTetH1 that was raised against highly phosphorylated *Tetrahymena* H1 (upper panels). Ponceau S staining of transfer membranes confirmed equivalent loading (lower panels). The apparent affinity of the pTetH1 antisera for H1.4-2p with identified phosphorylation sites at S172 and S187 (lanes 1) was much stronger than that for H1.4-1p with identified phosphorylation sites at S187 (lane 2), whereas binding to H1.4-0p, H1.2-1p and H1.2-0p were negligible (lanes 6 and 7).

(F) Crude histones from HeLa S3 (lanes 1, 4, 7), MCF-7 cells without 10 nM E2 treatment (lanes 2, 5, 8) and MCF-7 cells treated with 10 nM E2 for 45 min (lane 3, 5, 9) were analyzed by immunoblotting with antisera to pS173-H1.2, pTetH1 or pTS187-H1.4 (upper panels). Ponceau S staining of transfer membranes confirmed equivalent loading (lower panels).

(G) Whole cell extracts of growing asynchronous (lanes 1, 3, 4, 6) and colchicine-treated cells (lanes 2, 5) were analyzed by immunoblotting with antisera to pS187-H1.4 (lanes 4, 5) or total H1.4 (lane 6). Ponceau S staining of transfer membranes confirmed equivalent loading (lanes 1-3).

Figure 4.2

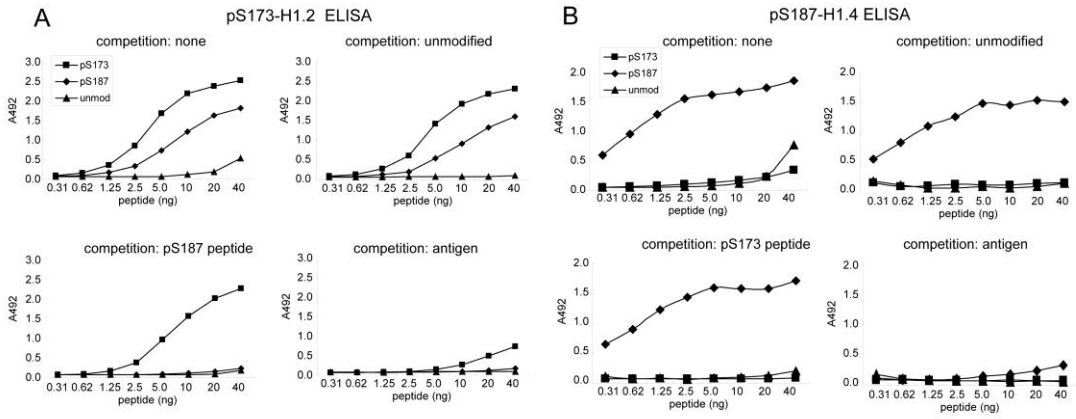

Antigen Preadsorption of the pS173-H1.2 and pS187-H1.4 Antisera Demonstrates Their Specificity in ELISA

(A) Increasing amounts of the pS173-H1.2 (squares), pS187-H1.4 (diamonds), and unmodified S173-H1.2 (triangles) peptides were bound to separate wells of 96 well plates before incubation with antisera to pS173-H1.2 that had been preincubated with no peptide (upper left panel), unmodified S173-H1.2 peptide (upper right), the similar but non-identical pS187-H1.4 peptide (lower left), or the pS173-H1.2 antigen peptide (lower right). The highest affinity binding was observed for the relevant pS173-H1.2 antigen peptide. The relative abilities of the unmodified S173-H1.2 and pS173-H1.2 peptides to compete for this binding indicate that it is phosphorylation-dependent. Intermediate binding affinity was observed for the pS187-H1.4 peptide. This may be attributable to a subpopulation of antibodies since the pS187-H1.4 peptide competed efficiently for this binding without detectably affecting recognition of the relevant pS173-H1.2 peptide.
(B) Same as in (A) except that plates were incubated with antisera to pS187-H1.4 that had been preincubated with no peptide (upper left panel), unmodified S187-H1.4 peptide (upper right), the similar but non-identical pS173-H1.2 peptide (lower left), or the pS187-H1.4 antigen peptide (lower right). The highest affinity binding was observed for the relevant pS187-H1.4 antigen peptide. The relative abilities of the unmodified S187-H1.4 and pS187-H1.4 peptides to compete for this binding indicate that it is phosphorylation-dependent. This antiserum did not show appreciable binding to the irrelevant pS173-H1.2 peptide.

Figure 4.3

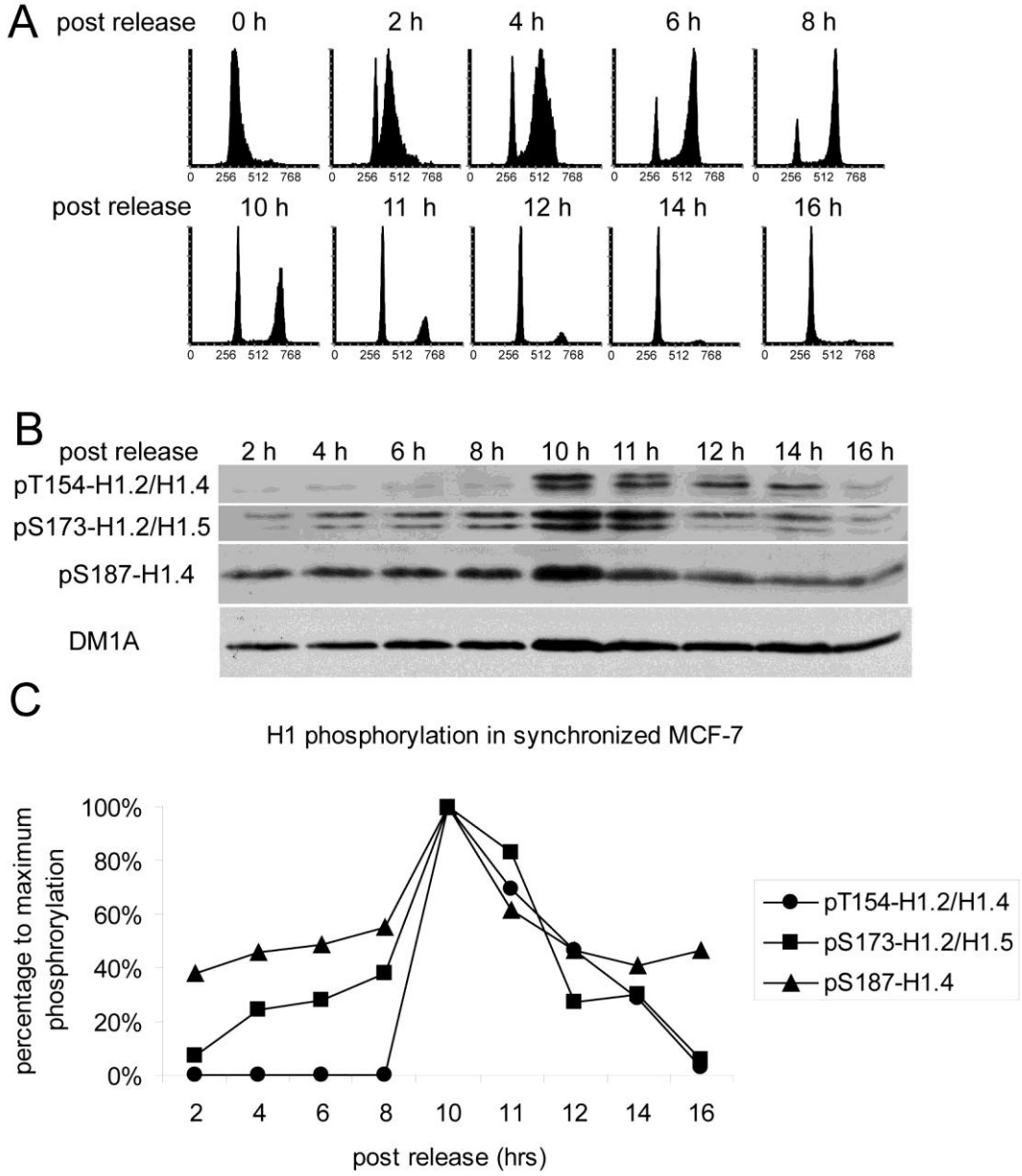

Progressive Phosphorylation of H1 during Cell Cycle

(A) FACS analysis of MCF-7 cells released from double thymidine block at indicated time point.

(B) The H1 phosphorylation levels in synchronized MCF-7 cells were tested by pT154, pS173 and pS187 antibodies using whole cell extracts. Tubulin (DM1A) was used to monitor the loading.

(C) Quantification of the western blot results in B. The intensity of phosphorylated H1 from different time point was plotted as the percentage to the intensity from 10 hrs sample

Figure 4.4

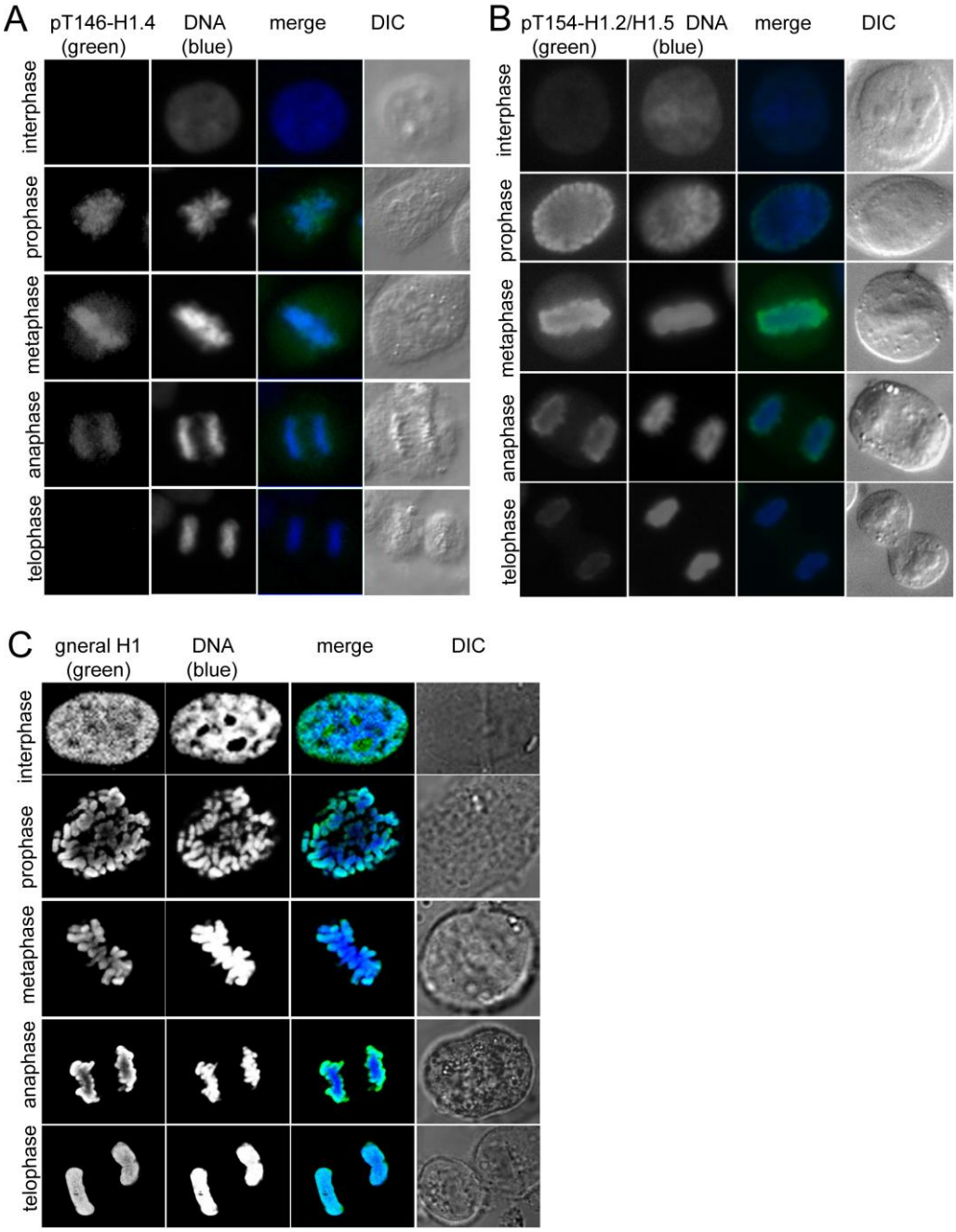

Mitotic Specific Phosphorylation of T146-H1.4 and T154-H1.2/H1.5

(A, B) Asynchronously growing HeLa cells were stained with antisera to pT146-H1.4 or pT154-H1.2/H1.5 and examined by epifluorescence microscopy. DNA was counterstained with DAPI. Cells at different cell cycle staged were determined by DAPI staining and DIC.

(C) Asynchronously growing HeLa cells were stained with general H1 antibody (AE-4) and examined by confocal microscopy. DNA was counterstained with TO-PRO 3.

Figure 4.5

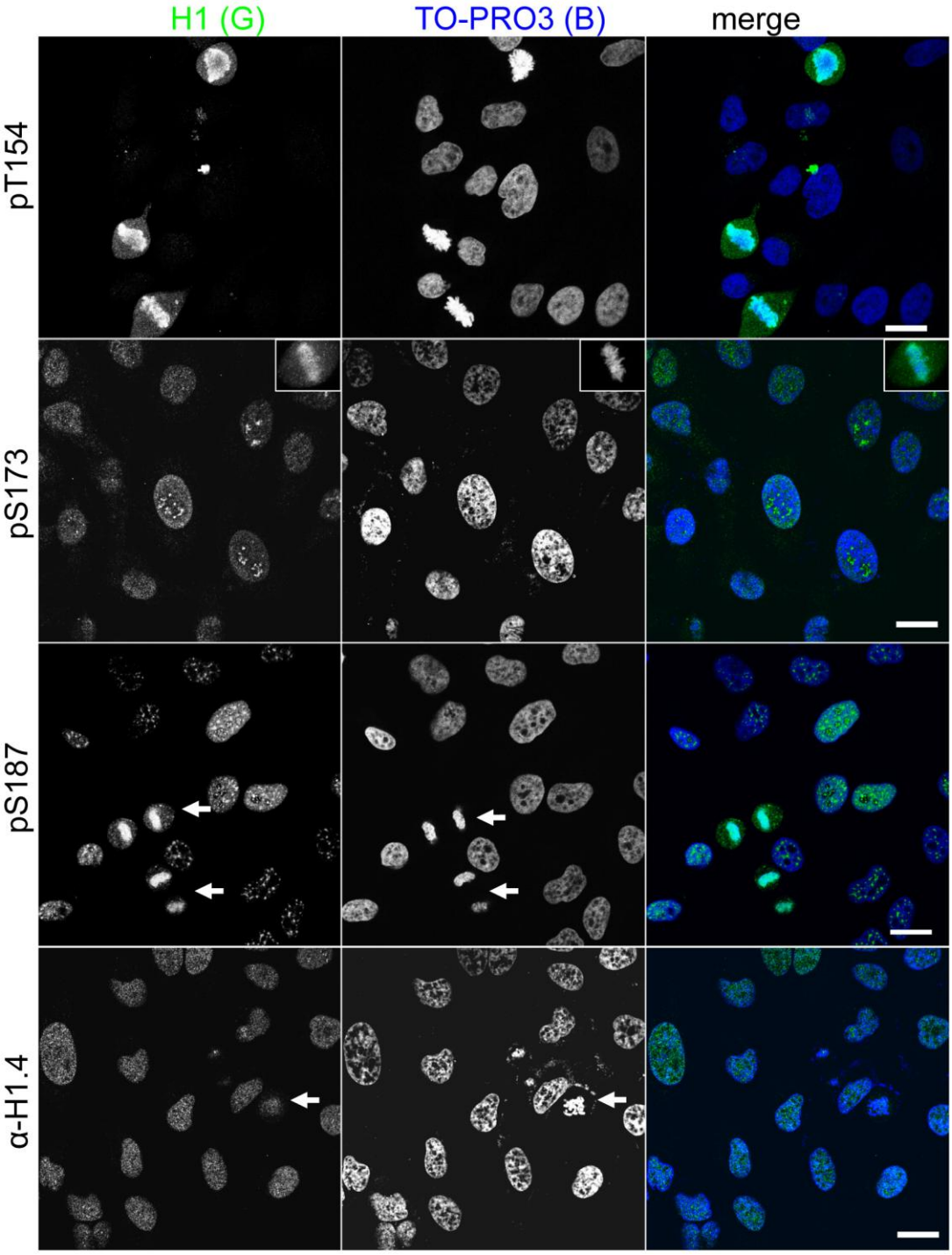

Figure 4.5 (cont.)

Interphase Phosphorylated H1.4 and Total H1.4 Are Localized Distinctly Within Nuclei

Asynchronously growing HeLa cells stained with antisera to pT154-H1.2/H1.4, pS173-H1.2/H.5, pS187-H1.4 or rH1.4 were examined by confocal immunofluorescence microscopy. DNA was visualized using TO-PRO-3. The antisera to pT154-H1.2/H1.4 preferentially stained the condensed chromatin of cells in or near mitosis but did not stain interphase cells appreciably. In contrast, the antisera to pS173-H1.2/H1.5 and pS187-H1.4 stained the nuclei of interphase cells in a stippled pattern and stained the condensed chromatin of mitotic cells (inset for pS173, arrows for pS187). The nucleoli of most interphase cells were conspicuously stained by clusters of punctate pS173 and pS187 staining. The antisera for total H1.4 (α-H1.4) stained interphase nuclei in a finely stippled pattern that was more uniformly distributed than that observed for either pS173 or pS187. In contrast to pS173 or pS187, the pattern of nucleolar staining for total H1.4 resembled that of the surrounding nuclear chromatin but was generally less intense. Clusters of punctate staining for total H1.4 were not observed in interphase cells. Scale bar = 20 microns.

Figure 4.6

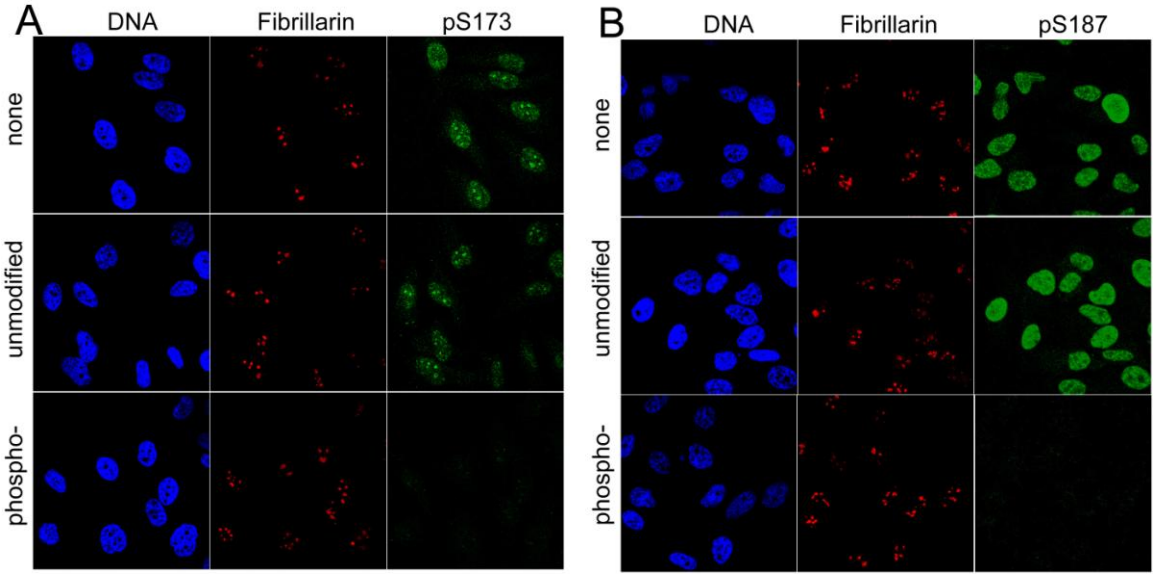

Antigen Preadsorption of the pS173-H1.2 and pS187-H1.4 Antisera Demonstrates Their Specificity in Immunofluorescence Microscopy

(A) Crude antisera to pS173-H1.2/H1.5 was mock-treated (none) or preincubated with the pS173-H1.2/H1.5 antigen peptide (phospho) or the corresponding nonphosphorylated peptide (unmodified) prior to use in staining asynchronous growing HeLa cells. DNA and nucleoli were subsequently stained with TO-PRO-3 and anti-fibrillarin, respectively. (B) As in (A) except that crude antiserum to pS187-H1.4 and the corresponding peptides were used.

Scale bar = 20 microns.

Nuclear and nucleolar staining in both (A) and (B) was significantly reduced following preincubation with the respective phosphopeptide but was unaffected by preincubation with the nonphosphorylated peptide.

Figure 4.7

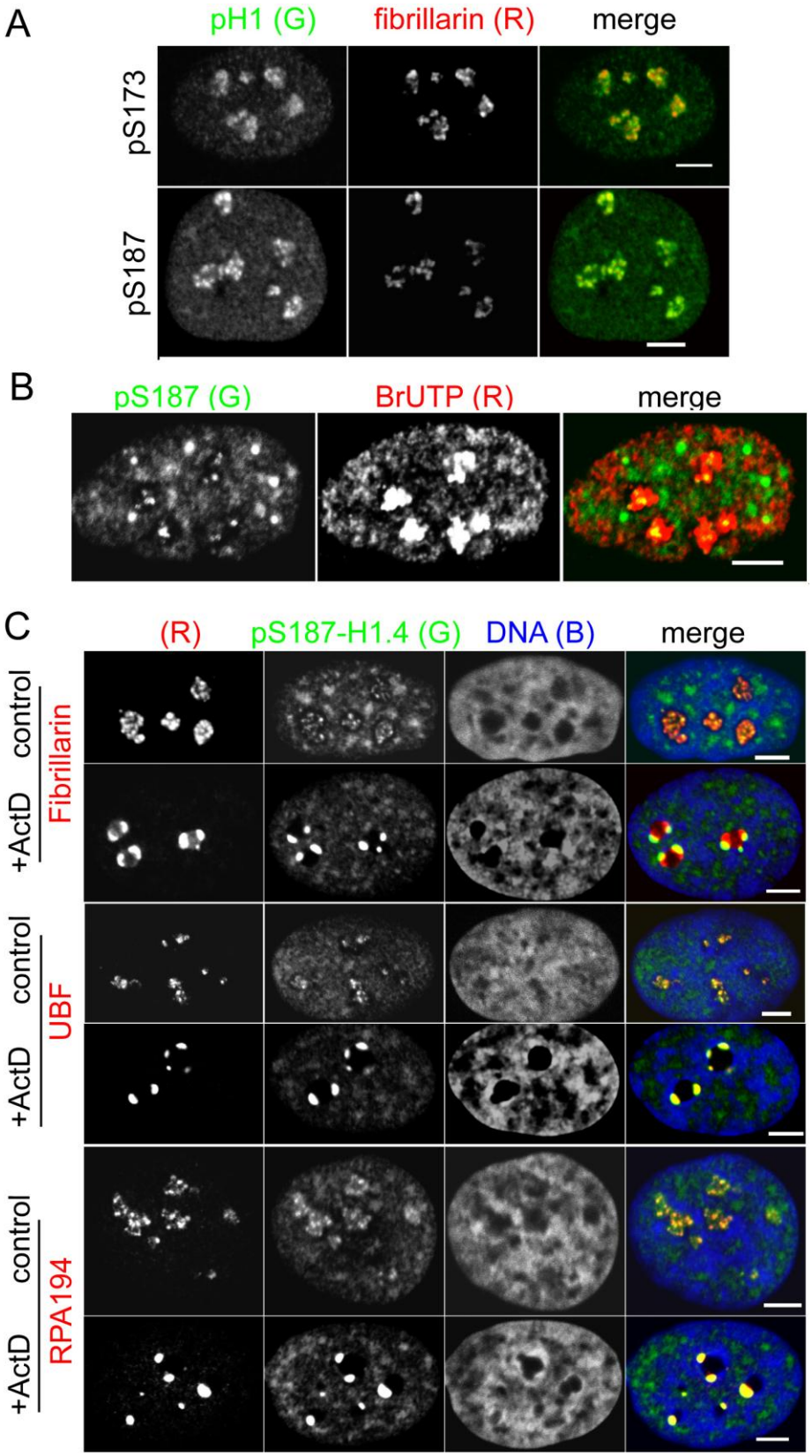
A
pH1 (G)
fibrillarin (R)
merge
pS173
pS187
B
pS187 (G)
BrUTP (R)
merge
C
(R)
pS187-H1.4 (G)
DNA (B)
merge
control
+ActD
Fibrillarin
control
+ActD
UBF
control
+ActD
RPA194

Figure 4.7 (cont.)

Subnuclear Localization of Phosphorylated H1

(A) Asynchronously growing HeLa cells co-stained with antisera to pS173-H1.2/H1.5 or pS187-H1.4 and the nucleolar marker fibrillarin were examined by confocal microscopy. Clusters of punctate staining for pS173-H1.2/H1.5 and pS187-H1.4 overlapped extensively with fibrillarin staining. Scale bar = 5 microns.

(B) Asynchronously growing HeLa cells co-stained with antisera to pS187-H1.4 and monoclonal antibody to BrdU were examined by confocal microscopy after pulse-labeling of nascent transcripts with BrUTP. Br-UTP incorporation co-localized extensively with pS187-H1.4. Scale bar = 5 microns.

(C) Untreated and actinomycin D-treated HeLa cells were co-stained with antibodies to fibrillarin, upstream binding factor (UBF) or the large subunit of RNA polymerase I (RPA194) and pS187-H1.4 prior to confocal microscopy. DNA was visualized using TO-PRO-3. Scale bar = 5 microns.

Figure 4.8

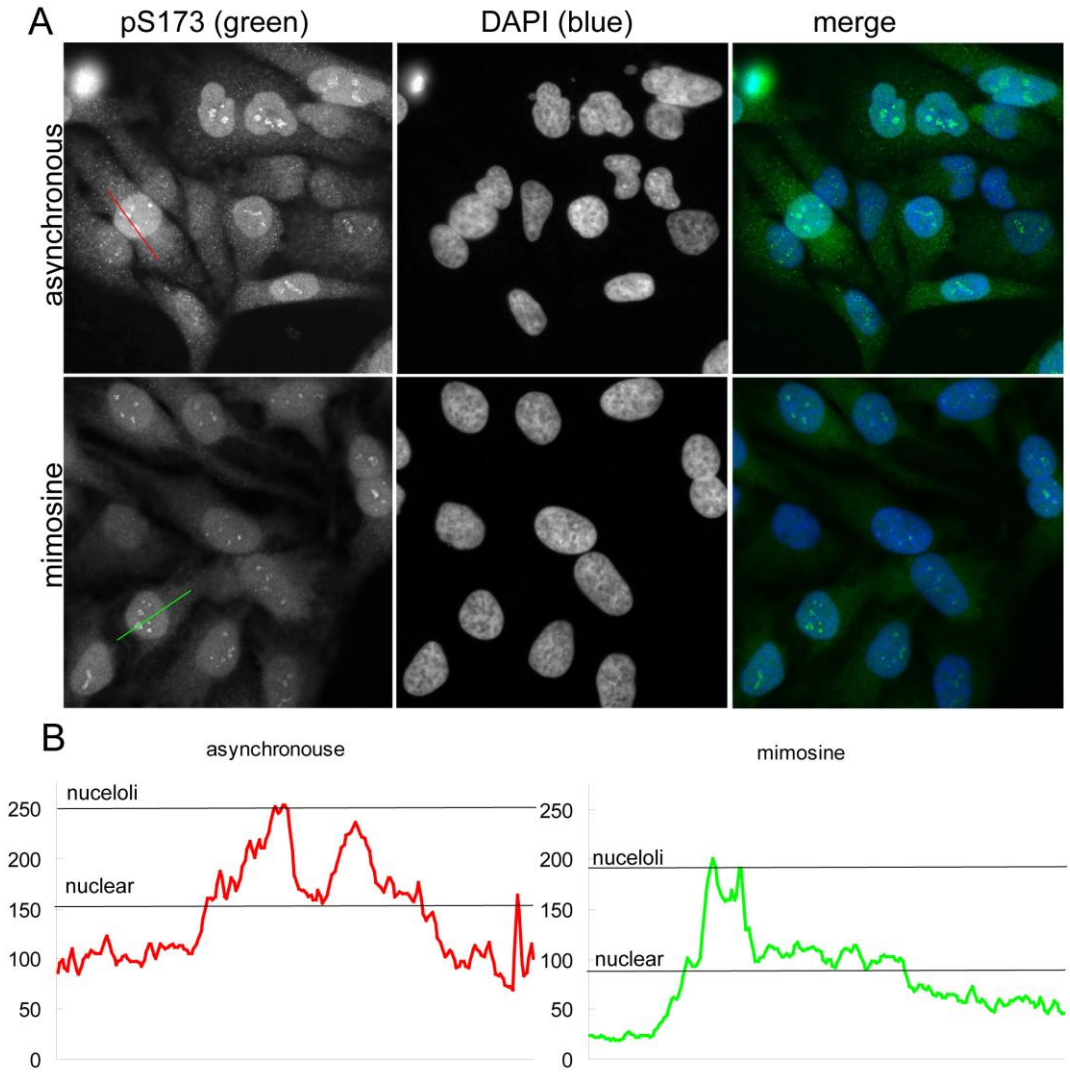

Both Nuclear and Nucleolar H1 Phosphorylation Decrease during G1

(A) Asynchronously growing or mimosine treated HeLa cells stained with antisera to pS173-H1.2/H.5 were examined by epifluorescence microscopy. DNA was visualized using DAPI.

(B) Profiles of pS173 fluorescence intensity along the drawn red line (asynchronous) or green line (mimosine).

Figure 4.9

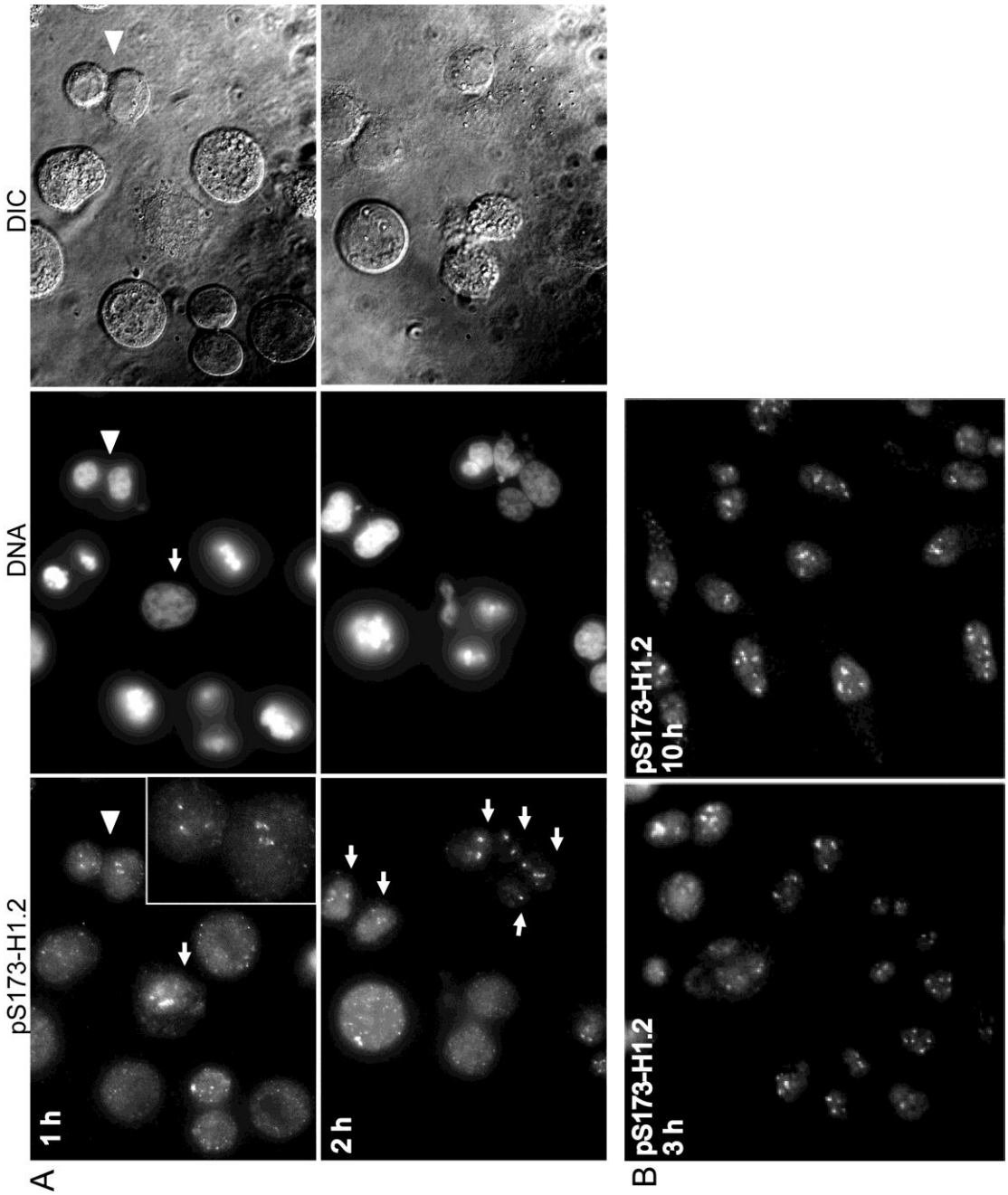

Figure 4.9 (cont.)

H1 Phosphorylation Reappears after Mitosis in Early G1

Mechanical released nocodazole enriched mitotic cells were replated in fresh medium. Cells were fixed after release at indicted time and stained with pS173-H1.2 antisera. Cells remained in mitosis or just entered the next G1 were determined by DAPI staining of DNA and DIC image of cell morphology. Prophase: a bright condensed DAPI staining all over nuclear; Metaphase: a single alignment of bright DAPI staining occupied in the equator; Anaphase: a double alignments of bright DAPI staining presents in a single cells with constriction ring in the formation; Telophase: a double alignments of bright DAPI staining presents in a single cells with 2 daughter cells connected by cytoplasm bridge; Cells just enter next G1: two cells contacted each other without condensed chromatin with rigid DIC pattern contrast to those spread out flatten pattern from cells entered G1 phase longer.

(A) Cells from 1h release, arrow indicates cells in the interphase and arrow head indicates newly divided cells. The pS173-H1.2 nucleolar staining of newly divided cells was enlarged in the inserted panel. pS173-H1.2 nucleolar staining as indicated by arrow in the 2 h release increased compared to 1 h release.

(B) The staining of pS173-H1.2 nucleolar staining appeared in most of cells after 3 h of release and was seen in every cell after 10 h release.

Figure 4.10

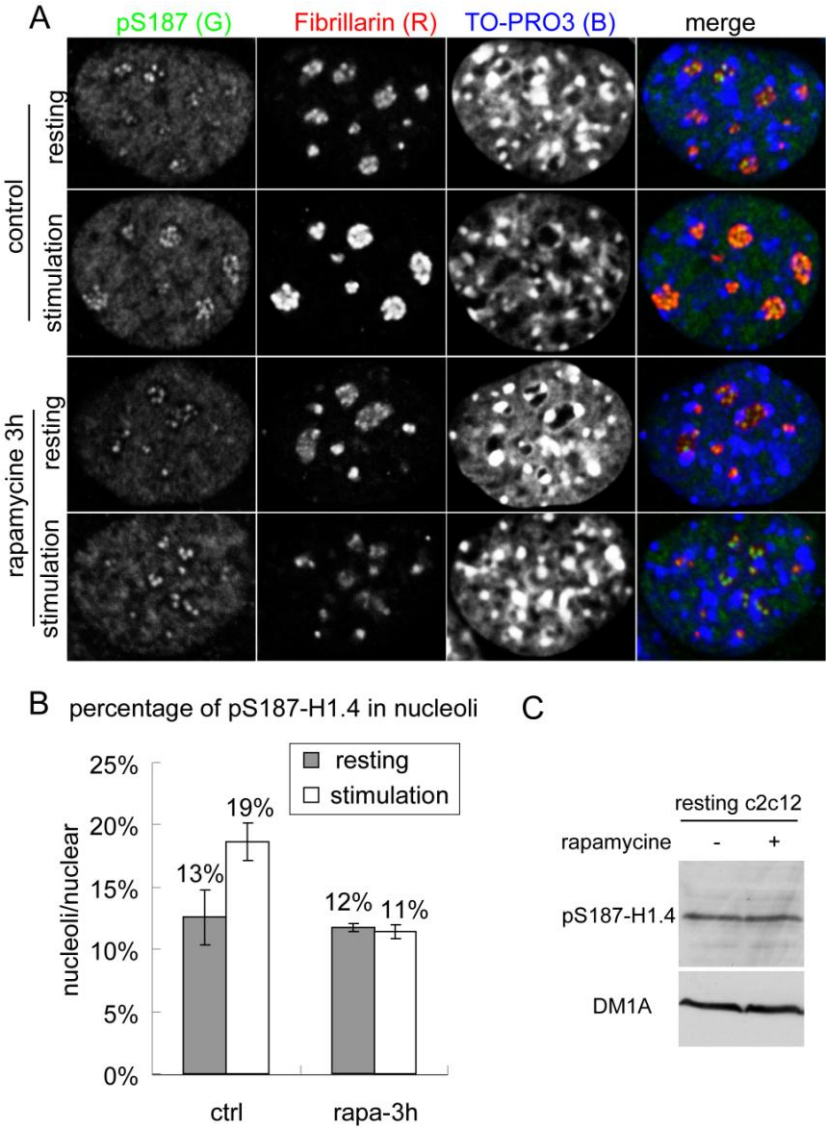

Evidence that Nucleolar H1 Phosphorylation is Downstream of mTOR

(A) c2c12 cells maintained at 2% horse serum were stimulated with 20% FBS without or with the addition of 100 nM rapamycin in the last 3 hrs. Cells were fixed in 4% PFA in CSK for 12 min at room temperature, permeabilized in 0.2 % Triton X-100 in PBS for 15 min. Cells were costained with antisera to pS187-H1.4 and the nucleolar marker fibrillarin were examined by confocal microscopy.

(B) Quantification of the intensity of pS187-H1.4 staining in the nucleoli regions defined by fibrillarin staining over the total intensity of pS187-H1.4 in the nuclear.

(C) The effect of 3 hrs treatment with 100 nM rapamycin in the level of pS187-H1.4 in the resting c2c12 cells were analyzed by western blot by pS187-H1.4 antibody (upper panel). Equivalent loading of whole cell lysate was confirmed by probing with tubulin antibody (DM1A, lower panels).

Figure 4.11

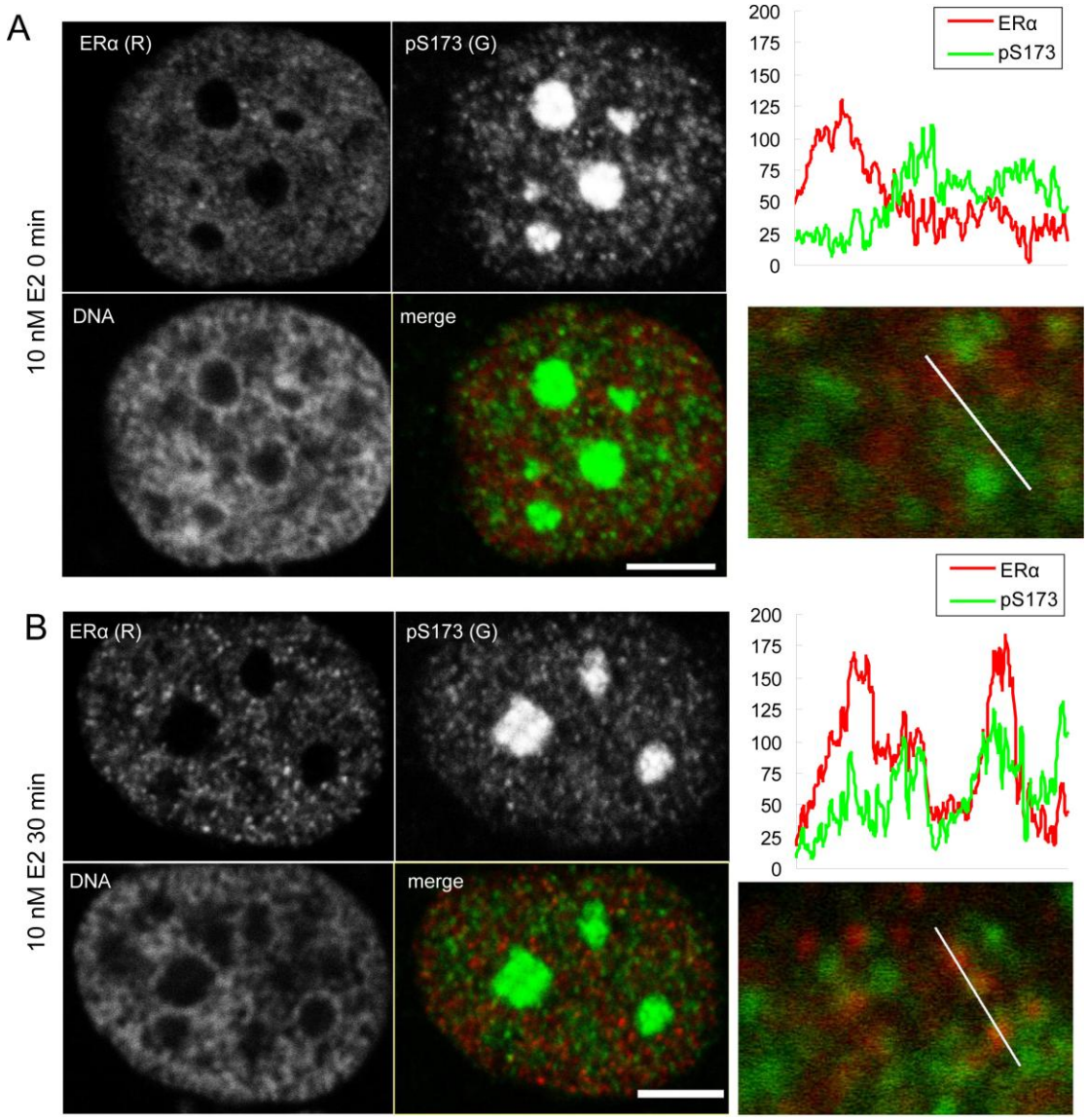

Ligand Dependent Colocalization of H1 Phosphorylation with ERα

Asynchronously growing MCF-7 cells were maintained in 7% charcoal stripped FBS in phenol free DMEM for 3 days before addition of 10 nM E2. Cell treated with ethanol (A) and E2 (B) for 30 min were co-stained with antisera to pS173-H1.2/H1.5 (1:200) and the ERα mAb (Santa Cruz F10, 1:100) and examined by confocal microscopy. Cells were permeabilized in 0.5% Triton X-100 in 4% PFA-CSK for 2 min at room temperature and then further fixed in 4% PFA-CSK for 10 min. The fluorescent intensities of pS173-H1.2/H1.5 (green) and ERα (red) over the arbitrary line drawn across an enlarged area are shown. Scale bar = 5 microns.

CHAPTER 5 *

HISTONE H1 PHOSPHORYLATION ASSOCIATED WITH TRANSCRIPTION BY RNA POLYMERASE I AND II

*: Some material was adapted from manuscript:
Histone H1 Phosphorylation Associated with Transcription by RNA Polymerases I and II
Yupeng Zheng, Sam John, James J. Pesavento, Jennifer R. Schultz-Norton, R. Louis Schiltz, Sonjoon Baek, Ann M. Nardulli, Gordon L. Hager, Neil L. Kelleher and Craig A. Mizzen

5.1 Introduction

Since the discovery of nucleosome, great efforts have been taken to address how elongating RNA-polymerase can transcribe through nucleosomes. Although the mechanism still remains elusive, there is strong evidence that pol II transcription through chromatin is coupled with nucleosome survival at the original position on DNA (Kulaeva et al., 2009). As we discussed in chapter 1.6.1, multiple ChIP experiments have demonstrated H1 is partially depleted upon transcriptional activation in the pol II genes especially in the promoter regions (see review in (Paranjape et al., 1994; Zlatanova and Van Holde, 1992)). The global distribution pattern of H1 along genome has been reported in two recent analyses using ChIP-chip by H1 monoclonal antibody (AE-4) in human cells and DamID in *Drosophila* cells respectively, which is pervasive binding interrupted by thousands of local dips that mostly coincide with TSSs (transcription start site) of active genes and putative regulatory elements (Braunschweig et al., 2009; Krishnakumar et al., 2008).

On the other hand, nucleosomes are believed to be altered or even removed in rDNA transcribed by pol I, possible to cope with the demand of highly active transcription. There are at least three observations to support this notion: first, when the nascent rRNA genes was removed by RNAse, short gap of DNA were visible between polymerase in electron microscopy, indicating lost of nucleosome (Labhart and Koller, 1982); second, MNase digestion revealed nucleosomal repeat and smearing pattern for inactive and

active rRNA gene, respectively (Lucchini et al., 1987); third, two distinct types of ribosomal chromatin were revealed by psoralen crosslink study (Conconi et al., 1989), in which the heavily crosslinked DNA represented nucleosome-free transcribed gene since its accessibility to psoralen whereas the slightly crosslinked DNA represented silent copies containing intact nucleosome organization since its inaccessibility to psoralen. Moreover, the limited run-on in the presence of radioactive precursors demonstrated heavily psoralen crosslinked rDNA represents genes engaged in transcription elongation (Conconi et al., 1989). These evidences were interpreted as absence of nucleosome in active transcribed rRNA genes. However ChIP assay showed histones were still associated with active transcribed rRNA genes in *X. laevis* in embryos at stage 40. In more detail, both H2A and H4 were associated with rDNA in amounts similar to those found for bulk DNA, whilst the content of H1 was reduced to ~50% (Dimitrov et al., 1990). Moreover, observation of histones in active transcribed rRNA genes is not limited in *Xenopus*, H1 is also found in *Drosophila* and *Tetrahymena* rRNA genes (Belikov et al., 1990; Dedon et al., 1991) and yeast H1 is required for maximal pol I processivity during rDNA transcription (Levy et al., 2008). In addition to ChIP approach, direct labeling of histones in immuneEM has identified both H2A/H2B and H1 in the nucleoli for mammalian cells (Raska et al., 1995). Two more recent reports have further demonstrated the association of rDNA with specific PTM of histone: first, pS10-H3 was shown to localize in the fibrillar center in nucleoli by IF and found associated with rDNA by ChIP in the plant (Granot et al., 2009); second, pS10-H3 was correlated with DNA-less region whereas repressive histone marks in the DNA-speckle regions of *Drosophila* rRNA in polytene chromosome spread (Plata et al., 2009). Taken these together with our nucleoli localization of phosphorylated H1 results, we decided to further investigate the correlation between H1 and pol I transcription by ChIP. As we have discussed in chapter 1.8, some interesting correlation between H1 phosphorylation and MMTV transcription has been revealed by ChIP using pTetH1 antibody, thus we also

investigated the correlation between H1 and pol II transcription by our novel phospho-specific antibody.

5.2 pS187-H1.4 Is Preferentially Associated with Active rDNA Promoters

Mammalian cells contain several hundred copies of the rDNA repeat. The proportion of these which are transcriptionally active in individual cells is regulated by mechanisms including histone modifications to match cellular demand for ribosome biogenesis (Lawrence and Pikaard, 2004; McStay and Grummt, 2008; Moss et al., 2007). To investigate whether interphase H1 phosphorylation contributes to this regulation, we used chromatin immunoprecipitation (ChIP) to compare the association of pS187-H1.4 with the rDNA promoter before and after selective inhibition of RNA pol I transcription with 0.05 μg/ml of actinomycin D (Jordan et al., 1996; Olson and Dundr, 2005). The levels of 45S pre-rRNA, normally processed quickly to yield smaller mature rRNA species, were assessed using RT-PCR to provide a semi-quantitative measure of rDNA transcription (James and Zomerdijk, 2004; Murayama et al., 2008). Consistent with the colocalization of Br-UTP incorporation and pS187-H1.4 staining within nucleoli (Chapter 4.5, Figure 4.7 B), ChIP revealed a robust association of pS187-H1.4 with the rDNA promoters in untreated growing HeLa cells (Figure 5.1 A). Strikingly, this association was significantly reduced after 3 hours of actinomycin D treatment (0.05 μg/ml), in concert with a nearly quantitative reduction in the levels of nascent 45S pre-rRNA transcripts (Figure 5.1 B). The reduction in promoter-associated pS187-H1.4 was not attributable to H1 depletion since the level of total H1.4 at the promoter was actually enhanced by actinomycin D treatment (Figure 5.1 A). Since, the global levels of both pS187-H1.4 and total H1.4 were unaffected by actinomycin D under these conditions (Figure 5.1 C), our data reveals that pS187-H1.4 is preferentially associated with the promoters of transcriptionally active rDNA repeats and that this association is regulated dynamically.

5.3 pS187-H1.4 Is Preferentially Associated with Pol II-Transcribed Genes

Data from approaches which did not account for the possible effects of interphase H1 phosphorylation have often suggested that H1 binding is associated with repression of transcription by RNA pol II (Cheung et al., 2002; Kim et al., 2008; Laybourn and Kadonaga, 1991; Lee et al., 2004). In contrast, ChIP analyses employing antiserum to phosphorylated *Tetrahymena* H1 suggest that phosphorylated H1 is required for glucocorticoid-dependent transcription from the MMTV promoter in mammalian cells (Bhattacharjee et al., 2001; Lee and Archer, 1998; Lu et al., 1994). However, the phosphorylated forms of H1 in mammals that can cross-react with this antiserum have not been clearly identified. Nonetheless, given our evidence because that pS187-H1.4 is distributed somewhat differently than total H1.4 and is enriched at active rDNA promoters (Figure 5.1 A), we next investigated whether pS187-H1.4 is involved in regulating gene transcription by RNA polymerase II. We chose to test the association of phosphorylated and total H1 in two constitutively active housekeeping genes and one constantly inactive gene in HeLa cells, i.e. GAPDH and ALDOA for active genes and MyoD for inactive genes. As shown in Figure 5.2, ChIP revealed a robust association of both pS187-H1.4 and total H1.4 around TSSs in both active and inactive genes in growing HeLa cells. Importantly, association of pS187-H1.4 is greater than total H1.4 in active genes whilst opposite relationship is observed in inactive genes. Due to differences in the affinities of the primary antibodies for their respective antigens and primer amplification efficiency in different loci, it is not appropriate to directly compare the ChIP enrichment for different antibodies in same locus or same antibody in different loci. Therefore, at least two different modes can be proposed for gene activation: first, no change for total H1 but increase of abundance of H1 phosphorylation; second, decrease of total H1 concurrent with increase of abundance of H1 phosphorylation. We have shown that the second scenario is what happened for pol I transcription activation in the promoter of rRNA. To further clarify whether similar mechanism is also underlying

the pol II gene activation, we need to compare the H1 association before and after transcription activation in the same locus.

5.4 Induction of Interphase H1 Phosphorylation by Nuclear Hormone Receptors

We used ChIP-qPCR to compare the association of pS187-H1.4 with hormone response elements for the glucocorticoid receptor (GR) in murine 3134 mammary tumor cells and estrogen receptor-alpha (ERα) in human MCF-7 breast cancer cells before and after stimulating cells with the respective ligands (Figure 5.3). 3134 cells carrying multiple copies of the glucorticoid response element (GRE) associated with the murine mammary tumor virus long terminal repeat (MMTV-GRE). Stimulation of 3134 cells with dexamethasone rapidly induced the association of pS187-H1.4 with the MMTV-GRE. The level of pS187-H1.4 at this locus increased by approx. 2.5 fold after 30 minutes of hormone treatment and by more than 3 fold after 60 minutes of treatment (Figure 5.3 A). Similarly, a robust enrichment of pS187-H1.4 was also observed at the GRE of the single copy serum/glucocorticoid regulated kinase (Sgk) gene following hormone treatment (Figure 5.3 B). These data demonstrate that glucocorticoid treatment stimulates the enrichment of interphase phosphorylated H1 at the MMTV-GRE and suggests that phosphorylation of a site resembling H1.4-S187 is likely to have contributed to the hormone-dependent enrichment of phosphorylated H1 described previously for this GRE (Bhattacharjee et al., 2001; Lee and Archer, 1998). They also provide the first evidence that interphase phosphorylated H1 is enriched at the GRE of a single copy natural gene in response to the binding of liganded GR, and suggest that dynamic changes in the association of phosphorylated H1 are likely to be a general feature of the chromatin response to glucocorticoid signaling.

We also compared how the association of ERα and pS187-H1.4 with the estrogen response element (ERE) of the pS2 gene (trefoil factor 1, TFF1) changed in MCF-7 cells

following estradiol treatment (Figure 5.3 C). Both ERα and pS187-H1.4 were markedly enriched at the pS2-ERE after just 15 minutes of estradiol treatment and became further enriched after 45 minutes of treatment. Differences in the affinities of the primary antibodies for their respective antigens preclude comparing the results directly, but the similar nature and time courses of enrichment of ERα and pS187-H1.4 that were observed to converge on this ERE suggest they are tightly-linked events. Taken together, the inducibility of pS187-H1.4 association with the response elements analyzed in Figure 5.3 argues strongly that pS187-H1.4, and possibly other interphase phosphorylated forms of H1, facilitate gene-specific activation of RNA polymerase II transcription by nuclear hormone receptors.

5.5 pS187-H1.4 Marks the Transcribed Regions of Active Genes

In order to gain more precise and complete view of the patterns of pS817-H1.4, we performed ChIP-sequencing to determine the genome wide distribution of pS187-H1.4. A typical result comparing the association of pS187-H1.4 at a gene activated by the glucocorticoid receptor (GR), Irs1, before and after treatment of murine 3134 with dexamethasone, is shown in Figure 5.4 A. Hormone treatment induces the enrichment of pS187-H1.4 along the entire length of the Irs1 gene, starting right at the TSS and extended ~5 kb beyond the 3'UTR. In addition, enrichment of pS187-H1.4 was also observed in the 5' upstream regulatory element locus where GR binds. On the contrary, the levels of pS187-H1.4 at hormone-repressed genes, Tgm2, actually fell compared to untreated cells, whilst the levels of pS187-H1.4 at constantly active genes, Hsp90, were kept at the same levels (Figure 5.4 B, C). Thus, pS187-H1.4 appears to be a novel marker for ongoing transcription by RNA polymerase II.

In summary, pS187-H1.4 is associated with active transcribed gene in the regulatory element and along the whole gene body, starting right at the beginning of TSSs and extended several kb beyond the 3' UTR. In addition, there is no dip for pS187-H1.4

occupancy in the TSSs as reported for total H1 in the active transcribed genes, which suggest more H1 molecules in the TSSs regions are phosphorylated.

5.6 CDK2, CDK8 and CDK9 Are Potential Interphase H1 Kinases but Are Not Required for rRNA Transcription

There are 13 cyclin-dependent kinase (CDKs) based on PSTAIRE motif and 25 cyclin-box-containing proteins in human genome. CDKs play critical roles in multiple cellular activities including, but not limited to, proliferation and transcription. CDK1, CDK2, CDK4 and CDK6 are involved in regulating progression through the G1, S, G2 and M phases of the cell division cycle. In early-mid G1, CDK4 and CDK6 can phosphorylate Rb protein to release the E2F and DP1 transcription factors for the expression of genes required for G1/S transition and S phase progression. During S phase, CDK2/cyclin A phosphorylates various key substrates necessary for DNA replication. Later, CDK1/cyclin B appears and phosphorylates a large set of substrate to trigger the G2/M transition and complete the mitosis (Knockaert et al., 2002). In addition to cell cycle regulation, there are three CDK/cyclin involved in transcription and all are found within larger complex. CDK7/cyclin H (part of the TFIIH) and CDK8/cyclin C (part of mediator) regulate transcription initiation (Akoulitchev et al., 2000; Fisher, 2005) whereas CDK9/cyclinT (core of the p-TEFb) is important for transcription elongation (Wang and Fischer, 2008).

CDK phosphorylation site preferences have been well established as S/TPXK/R, but recent studies have revealed subtle differences in substrate preference. For example, CDK2 has a very strong preference for a basic residue at the position P+3 whereas CDK4 phosphorylates either SPXK/R or SPXX with similar efficiency. In addition, lack of preference for a basic residue at the P+3 residue is also true for CDK7, CDK8 and CDK9, which can phosphorylate the heptad repeats present within the C-terminal domain (CTD) of the RBP1 subunit of pol II (YSPTSPS) (Echalier et al.).

Identifying the kinase for H1 phosphorylation will greatly improve our understanding of how H1 phosphorylation regulates. As discussed in chapter 1.5.2, multiple evidences have indicated CDK2 is the kinase for H1 interphase phosphorylation whereas CDK1 is the kinase for H1 mitosis phosphorylation. However the observation of tight correlation between pS187-H1.4 and transcription suggests other kinase might be involved in H1 phosphorylation at least in G1 when both CDK1 and CDK2 are inactive. In addition, it has been reported that CDK2 is not required for metallothionein transcription activation despite it is necessary for MMTV (Bhattacharjee et al., 2001). To test this hypothesis, we set out to examine whether any other CDKs can modulate the global H1 phosphorylation in interphase by siRNA knocking down single CDK or small molecule inhibitors. Both approaches have their advantages and disadvantages: CDK siRNA approach offers greater specificity but might cause some indirect effects as has been reported that CDK1 or CDK2 knockdown can cause cell cycle defects (Cai et al., 2006); the shorter treatment by CDK specific inhibitor minimizes the indirect effects but the selectivity of CDK inhibitor is not satisfying enough to draw unambiguous conclusion on their own (Karaman et al., 2008).

Before testing the effects on global H1 phosphorylation in the CDK1, 2, 4, 7, 8 and 9 siRNA treated cells, the knockdown efficiencies of siRNA were monitored by RT-PCR and the results indicated a great reduction in the mRNA level after 72 hrs treatment (Figure 5.5 B). Furthermore, the reduction in protein levels for CDK 1, 7 and 9 in the siRNA experiment were confirmed by immunoblot (data not shown). Then the abundance of pS187-H1.4 in the HeLa cells, where individual CDK was knockdown by siRNA, was examined by immunoblot. As expected, pS187-H1.4 was increased in CDK1 siRNA sample since cells were unable to enter mitosis and thus arrested in G2 phase where levels of pS187-H1.4 is much higher than asynchronous (chapter 2, Figure 5.5 A). Similar elevation of pS187-H1.4 has also been observed in FT210 cell line

(CDK1 mutation) when CDK1 was inactivated for as short as 3 hrs at 42 °C (nonpermissive temperature, data not shown). In addition, decrease of pS187-H1.4 in CDK4 siRNA was mostly caused by indirect effects of cell cycle arrest in G1/S, which was corroborated by the observation of no decrease of pS187-H1.4 when CDK4 was inhibited by specific inhibitor CDK4i (Zhu et al., 2003). Consistence with previous studies, abundance of pS187-H1.4 (Figure 5.5 A, C) decreased when CDK2 activity was inhibited by either siRNA or various CDK1/2 drug (purvalanol A, olomoucine II, roscovitine). Interestingly, abundance of pS187-H1.4 decreased in CDK8 and CDK9 siRNA samples but no change was seen in the CDK7 siRNA (Figure 5.5 A). In addition, 3 hrs treatment with CDK9 inhibitor flavopiridol (FLVP) also greatly reduced the global abundance of pS187-H1.4 (Figure 5.5 C). These results raised an interesting possibility that CDK8 and CDK9 are the kinase in transcription machinery that phosphorylates the histone H1 in the ongoing transcribe gene body we observed in ChIP-seq study. Similar role for CDK8 has been reported, which can efficiently phosphorylate serine 10 in H3 in chromatin templates (Knuesel et al., 2009). However, we can not rule out the possibility that decrease in the global phosphorylation of H1 is the indirect consequence of inhibition of H1 kinase transcription. It has been reported inhibition of CDK9 impairs the transcription, whilst inhibition of CDK7, kinase in the TFIIH that is required to initiate transcription, does not impair transcription (Garriga et al.; Kanin et al., 2007). As described in chapter 4.6, the decrease of nucleolar H1 phosphorylation in rapamycin suggests kinase for H1 phosphorylation in rRNA transcription lies in the downstream of mTOR pathway. Since there is no CDKs is known in the signaling pathway of mTOR, we hypothesized CDK is not the kinase for nucleolar H1 phosphorylation and predicted there will be no effects in rRNA transcription when CDKs is inhibited. A shown in Figure 5.5 D, E, none of knockdown of CDKs by siRNA or inhibiting CDKs by drug has significant effects in rRNA transcription, suggesting H1 phosphorylation in rRNA loci might is not involved CDKs.

5.7 Evidence That H1 Phosphorylation Facilitates the Transcriptional Activation of Metallothionein Genes

In order to directly test whether S187 phosphorylation in H1.4 is necessary for the transcription, we designed an experiment to knockdown endogenous H1.2 and H1.4 in the HeLa cells by siRNA first and then express exogenous H1.4 carrying synonymous substitutions in the siRNA targeted region, which made the plasmid resist to siRNA silencing. As reported previously (Dou and Gorovsky, 2000), we then introduced mutations that mimics unphosphorylated (serine to alanine) or phosphorylated status (serine to glutamic acid) in the silencing resisting H1.4 plasmid to directly investigate effects of phosphorylation in H1 in transcription.

We chose metallothionein genes as our model gene since their expression can be easily induced by dexamethasone or metal. As shown in the Figure 5.6 A, hormone induced association of pS187-H1.4 along the entire length of the metallothionein genes was similar to other example we discussed above. The levels of the steady state transcript of MT1A and MT2A were assayed by qRT-PCR for different mutant replacements before and after induction and all the measurements were reported as the relative fold change against the basal level (-$ZnCl_2$) in the control sample. As shown in Figure 5.6 B, robust induction of approx 20-fold increase was seen for MT1A and approx 10-fold increase for MT2A. As expected, inducibility of transcription increased when H1 was knockdown but returned to the same levels when wild type of H1 was introduced into the H1 siRNA cells. These results imply histone H1 acts as repressor in the metallothionein loci and displace of H1 can relieve the repression during induction. In addition, unphosphorylated mimic form of H1 inhibits transcription induction by $ZnCl_2$ whilst phosphorylated mimic form of H1 facilitates such transcription induction (Figure 5.6 B), which suggests H1 phosphorylation is very likely to be the mechanism that causes displacement of H1 for the transcription activation. CDK2 inhibitor purvalanol and CDK9 inhibitor flavopiridol were served as control since CDK2 is not required for MT

transcription as previously reported (Bhattacharjee et al., 2001) and CDK9 inhibition by flavopiridol causes global transcription inhibition (Garriga et al.).

5.8 Conclusions and Discussion

Interphase H1 Phosphorylation and rDNA Transcription

The growth and proliferation of cells is proportional to their capacity for ribosome biogenesis, one of the most energy intensive processes they perform. 45S pre-rRNA synthesis is thought to be limiting for ribosome biogenesis and aspects of chromatin structure including nucleosome positioning, DNA methylation and histone H3 and H4 modifications have all been implicated in determining the transcriptional activity of rDNA repeats (Birch and Zomerdijk, 2008; McStay and Grummt, 2008; Moss et al., 2007). The HMG class protein UBF plays key roles in rDNA transcription. UBF dimers bind rDNA promoters and activate transcription by recruiting SL1/TIF-IB and enhancing PIC formation (McStay and Grummt, 2008; Moss et al., 2007). UBF binding throughout the transcribed portions of rDNA repeats may also affect other aspects of RNA pol I transcription and be involved in maintaining the euchromatic state of rDNA (Moss et al., 2007; O'Sullivan et al., 2002; Sanij and Hannan, 2009; Sanij et al., 2008). UBF competes with H1 for binding to reconstituted mononucleosomes in vitro and depletion of UBF in vivo is associated with a decrease in the proportion of active rDNA repeats and an increase in H1 association with rDNA (Kermekchiev et al., 1997; Sanij et al., 2008). Since rDNA promoter methylation inhibits UBF binding (Santoro and Grummt, 2001), these results suggest a model in which UBF promotes chromatin decondensation of hypomethylated rDNA repeats by limiting the ability of H1 to bind and stabilize higher order chromatin folding. This is consistent with ChIP data that UBF is preferentially associated with hypomethylated rDNA promoters whereas H1 tends to be associated preferentially with methylated promoters (Sanij et al., 2008).

The dependence of pS187-H1.4 and rDNA promoter association on RNA pol I activity (Figure 5.1 A), and the colocalization of pS187-H1.4 with UBF and RNA pol I before and after ActD treatment (Figure 4.7 C), suggest the possibility that H1 kinases are recruited to transcriptionally active/competent rDNA repeats via interactions with UBF or other components of the RNA Pol I machinery. The effect of S187 phosphorylation on H1.4 chromatin binding dynamics could promote rDNA decondensation and transcription by facilitating UBF binding, as suggested by FRAP analyses of GFP-H1 phosphorylation site mutants (Contreras et al., 2003; Hendzel et al., 2004). Moreover, the nucleolar staining observed for pS172-H1.2 suggests that this form may play a similar role, but the poor performance of this antisera in ChIP has precluded testing this hypothesis directly.

Interphase H1 Phosphorylation and Transcriptional Regulation by Nuclear Hormone Receptors

A clear consensus regarding the roles of linker histones in transcriptional regulation mediated by nuclear hormone receptors has remained elusive. Analyses of GR-regulated transcription at the MMTV promoter in different systems suggest that H1 is depleted immediately following hormone stimulation (Belikov et al., 2007; Bresnick et al., 1992), but reassociates with refractory promoters after prolonged hormone treatment (Lee and Archer, 1998), consistent with the notion that H1 generally acts as a repressor. In contrast, overexpression of H1.2 or $H1^{o}$ enhanced basal and hormone-stimulated transcription of stably-integrated MMTV-LTR reporter genes in murine 3T3 cells and prevented repression of these reporters during prolonged hormone stimulation (Gunjan and Brown, 1999). Our data are consistent with the proposal that H1 affects nucleosome positioning or other aspects of MMTV promoter chromatin architecture to facilitate the binding of liganded nuclear hormone receptors, their synergism with transcription factors such as NF1 and AP-1, and the recruitment or activation of kinases which phosphorylate and facilitate H1 displacement following hormone stimulation

(Vicent et al., 2002). Considered together with recent evidence that estradiol stimulates the exchange of HMGB for H1 in the ERE-containing nucleosome of the pS2 gene, and that HMGB is exchanged for H1 at other sites recognized by AP-1 or by other nuclear hormone receptors (Ju et al., 2006), our data suggests that H1.4-S187 phosphorylation promotes nuclear hormone receptor-mediated transcriptional activation by enhancing chromatin access for other regulatory factors.

Interphase H1 Phosphorylation as a Modulator of H1 Binding Dynamics

The predominant expression of H1.2 and H1.4 in HeLa S3 cells, the abundant nature and high specificity of interphase phosphorylation for just one site in H1.2 and just two sites in H1.4, and our evidence that H1.4-S187 phosphorylation facilitates transcription by both RNA polymerases I and II, all imply that interphase H1 phosphorylation at a limited number of specific sites plays a general role in enhancing chromatin access for factors involved in transcription and other chromatin-templated activities. Our data are consistent with evidence from FRAP analyses of GFP-H1 that mutations which mimic constitutive phosphorylation or dephosphorylation of CDK sites enhance or diminish H1 dissociation from chromatin, respectively.

Our evidence that the association of pS187-H1.4 with specific chromatin loci is dynamic also implies that H1 kinases and phosphatases are recruited to these loci in a targeted fashion, presumably via mechanisms similar to those which mediate dynamic locus-specific core histone modification (Berger, 2007). Kinases which mediate interphase H1 phosphorylation *in vivo* have not been directly identified before but several lines of evidence implicate CDK2 (Bhattacharjee et al., 2001; Contreras et al., 2003; Herrera et al., 1996). Our data has suggested CDK8 and CDK9 are very likely the kinase in the transcription machinery that can phosphorylate the H1 which marks the active transcribed gene body and regulatory elements. We had demonstrated H1 phosphorylation is highly dynamic and required constant modulation by kinase and

phosphatase as evidence that H1 phosphorylation greatly decreased when cells were treated with CDK inhibitor for 3 hrs or greatly increased when treated with phosphatase inhibitor okadaic acid (Ryan, 1999). We also found H1 phosphorylation is diminished when treated with protein synthesis inhibitor cycloheximide, which is corroborated by the similar finding reported previously (Ryan, 1999). In addition, the diminishing of H1 phosphorylation caused by cycloheximide can be reverted by proteosome inhibitor (Ryan, 1999), which also implies that H1 phosphorylation requires constant action of kinase.

5.9 Materials and Methods

Cell Culture

3134 cells were maintained as described previously (John et al., 2009). Cells were transferred to 10% charcoal-dextran-treated, heat-inactivated fetal bovine serum for 48 h before treatment with 100 nM dexamethasone. MCF-7 cells were maintained as described previously (Schultz-Norton et al., 2007). Cells were transferred to phenol red-free MEM containing 5% charcoal-dextran-treated calf serum for 72–96 h before treatment with 10 nM estradiol.

Silencing Resistance Plasmid Construction

To prevent transfected plasmid of H1.4 being silenced by siRNA targeting H1.4, four nucleotide synonymous substitutions were introduced to the H1.4-FLAG plasmid including WT, S187A, S187E, S172A+S187A, S172E+S187E within the sequence recognized by H1.4 siRNA (targeting sequence: TC AAG AGC CTG GTG AGC AA). The four underline nucleotides were mutated with following primers: GGT CTC AAG AGC CTG GTC TCA AAG GGC ACC CTG GTG C.

siRNA and Plasmid Transfection

siRNA oligos were introduced to cells using oligofectamine (Invitrogen) using following conditions for 24-well format: 3.0 μl of oligofectamine was added to 12 μl of OPTI-MEM,3.0 μl of 20 μM siRNA oligo was added to 50 μl of OPTI-MEM, two complexes were mixed and incubated for 20 min before added to cells in 2.0 ml 10% FBS DMEM. Plasmids transfection using FuGENE HD (Roche) was found achieving maximum transient expression of histone H1 in pCMV driving pcDNA plasmid in 48 hrs with 7:2 ratio (1.75 μl of FuGENE, 0.5μg of plasmid) in 24-well. Alternatively, 1.0 μl of Lipofectamine 2000 and 0.4 μg of plasmid were used to transfect cells in 24-well plate. 100 μl FuGENE 6 and 30 μg plasmid were first mixed individually to 1.7 ml OPTI-MEM and then combined together for transfection of P150 dish.

Real-time PCR

ChIP products or RT products were quantified by real-time PCR using SYBR Green master mix (Applied Biosystems) following the protocol described in Appendix III. The measured relative amount in ChIP was expressed as percentage to input and further calculated as fold change against no antibody control or folded change against no hormone treatment. The measured relative amount of cDNA was expressed as relative expression unit per μg RNA or further normalized to internal control such as β-actin. Both melting curve and agarose gel electrophoresis were implemented to monitor the amplification specificity. Although gel electrophoresis or melting curve analysis alone may not be 100% reliable, the combination of both should reveal PCR specificity very well. Primers used in the PCR are listed in the Table 5.1.

RT-qPCR

Total RNA was extracted from monolayer of cells in 24-well or 6-well with Trizol (Invitrogen) according to manufacture manual and dissolved in 20~50 μl of TE. The

concentration and the quality of RNA were assayed by UV spectrometry. 1.0 μg of total RNA was used in reverse transcription using SuperScript first-strand synthesis system for RT-PCR (Invitrogen) with random hexamers. Reactions with no reverse transcriptase were also performed together as negative control. The synthesis products were further diluted 20~100x for the real time PCR according to the abundance of transcripts.

5.10 References

Akoulitchev, S., S. Chuikov, and D. Reinberg. 2000. TFIIH is negatively regulated by cdk8-containing mediator complexes. *Nature*. 407:102-6.

Belikov, S., C. Astrand, and O. Wrange. 2007. Mechanism of histone H1-stimulated glucocorticoid receptor DNA binding in vivo. *Mol Cell Biol*. 27:2398-410.

Belikov, S.V., A.R. Dzherbashyajan, O.V. Preobrazhenskaya, V.L. Karpov, and A.D. Mirzabekov. 1990. Chromatin structure of Drosophila melanogaster ribosomal genes. *FEBS Lett*. 273:205-7.

Berger, S.L. 2007. The complex language of chromatin regulation during transcription. *Nature*. 447:407-12.

Bhattacharjee, R.N., G.C. Banks, K.W. Trotter, H.L. Lee, and T.K. Archer. 2001. Histone H1 phosphorylation by Cdk2 selectively modulates mouse mammary tumor virus transcription through chromatin remodeling. *Mol Cell Biol*. 21:5417-25.

Birch, J.L., and J.C. Zomerdijk. 2008. Structure and function of ribosomal RNA gene chromatin. *Biochem Soc Trans*. 36:619-24.

Braunschweig, U., G.J. Hogan, L. Pagie, and B. van Steensel. 2009. Histone H1 binding is inhibited by histone variant H3.3. *Embo J*. 28:3635-3645.

Bresnick, E.H., M. Bustin, V. Marsaud, H. Richard-Foy, and G.L. Hager. 1992. The transcriptionally-active MMTV promoter is depleted of histone H1. *Nucleic Acids Res*. 20:273-8.

Cai, D., V.M. Latham, Jr., X. Zhang, and G.I. Shapiro. 2006. Combined depletion of cell cycle and transcriptional cyclin-dependent kinase activities induces apoptosis in cancer cells. *Cancer Res*. 66:9270-80.

Cheung, E., A.S. Zarifyan, and W.L. Kraus. 2002. Histone H1 represses estrogen receptor alpha transcriptional activity by selectively inhibiting receptor-mediated transcription initiation. *Mol Cell Biol*. 22:2463-71.

Conconi, A., R.M. Widmer, T. Koller, and J.M. Sogo. 1989. Two different chromatin structures coexist in ribosomal RNA genes throughout the cell cycle. *Cell*. 57:753-61.

Contreras, A., T.K. Hale, D.L. Stenoien, J.M. Rosen, M.A. Mancini, and R.E. Herrera. 2003. The dynamic mobility of histone H1 is regulated by cyclin/CDK phosphorylation. *Mol Cell Biol*. 23:8626-36.

Dedon, P.C., J.A. Soults, C.D. Allis, and M.A. Gorovsky. 1991. Formaldehyde cross-linking and immunoprecipitation demonstrate developmental changes in H1 association with transcriptionally active genes. *Mol Cell Biol*. 11:1729-33.

Dimitrov, S.I., V.Y. Stefanovsky, L. Karagyozov, D. Angelov, and I.G. Pashev. 1990. The enhancers and promoters of the Xenopus laevis; ribosomal spacer are associated with histones upon active transcription of the ribosomal genes. *Nucl. Acids Res.* 18:6393-6397.

Dou, Y., and M.A. Gorovsky. 2000. Phosphorylation of linker histone H1 regulates gene expression in vivo by creating a charge patch. *Mol Cell*. 6:225-31.

Echalier, A., J.A. Endicott, and M.E.M. Noble. Recent developments in cyclin-dependent kinase biochemical and structural studies. *Biochimica et Biophysica Acta (BBA) - Proteins & Proteomics*. In Press, Corrected Proof.

Fisher, R.P. 2005. Secrets of a double agent: CDK7 in cell-cycle control and transcription. *J Cell Sci*. 118:5171-5180.

Garriga, J., H. Xie, Z. Obradovic, and X. Grana. Selective control of gene expression by CDK9 in human cells. *J Cell Physiol*. 222:200-8.

Granot, G., N. Sikron-Persi, Y. Li, and G. Grafi. 2009. Phosphorylated H3S10 occurs in distinct regions of the nucleolus in differentiated leaf cells. *Biochimica Et Biophysica Acta-Gene Regulatory Mechanisms*. 1789:220-224.

Gunjan, A., and D.T. Brown. 1999. Overproduction of histone H1 variants in vivo increases basal and induced activity of the mouse mammary tumor virus promoter. *Nucleic Acids Res*. 27:3355-63.

Hendzel, M.J., M.A. Lever, E. Crawford, and J.P. Th'ng. 2004. The C-terminal domain is the primary determinant of histone H1 binding to chromatin in vivo. *J Biol Chem*. 279:20028-34.

Herrera, R.E., F. Chen, and R.A. Weinberg. 1996. Increased histone H1 phosphorylation and relaxed chromatin structure in Rb-deficient fibroblasts. *Proc Natl Acad Sci U S A*. 93:11510-5.

James, M.J., and J.C. Zomerdijk. 2004. Phosphatidylinositol 3-kinase and mTOR signaling pathways regulate RNA polymerase I transcription in response to IGF-1 and nutrients. *J Biol Chem*. 279:8911-8.

John, S., T.A. Johnson, M.H. Sung, S.C. Biddie, S. Trump, C.A. Koch-Paiz, S.R. Davis, R. Walker, P.S. Meltzer, and G.L. Hager. 2009. Kinetic complexity of the global response to glucocorticoid receptor action. *Endocrinology*. 150:1766-74.

Jordan, P., M. Mannervik, L. Tora, and M. Carmo-Fonseca. 1996. In vivo evidence that TATA-binding protein/SL1 colocalizes with UBF and RNA polymerase I when rRNA synthesis is either active or inactive. *J Cell Biol*. 133:225-34.

Ju, B.G., V.V. Lunyak, V. Perissi, I. Garcia-Bassets, D.W. Rose, C.K. Glass, and M.G. Rosenfeld. 2006. A topoisomerase IIbeta-mediated dsDNA break required for regulated transcription. *Science*. 312:1798-802.

Kanin, E.I., R.T. Kipp, C. Kung, M. Slattery, A. Viale, S. Hahn, K.M. Shokat, and A.Z. Ansari. 2007. Chemical inhibition of the TFIIH-associated kinase Cdk7/Kin28 does not impair global mRNA synthesis. *Proceedings of the National Academy of Sciences*. 104:5812-5817.

Karaman, M.W., S. Herrgard, D.K. Treiber, P. Gallant, C.E. Atteridge, B.T. Campbell, K.W. Chan, P. Ciceri, M.I. Davis, P.T. Edeen, R. Faraoni, M. Floyd, J.P. Hunt, D.J. Lockhart, Z.V. Milanov, M.J. Morrison, G. Pallares, H.K. Patel, S. Pritchard, L.M. Wodicka, and P.P. Zarrinkar. 2008. A quantitative analysis of kinase inhibitor selectivity. *Nature Biotechnology*. 26:127-132.

Kermekchiev, M., J.L. Workman, and C.S. Pikaard. 1997. Nucleosome binding by the polymerase I transactivator upstream binding factor displaces linker histone H1. *Mol Cell Biol*. 17:5833-42.

Kim, K., J. Choi, K. Heo, H. Kim, D. Levens, K. Kohno, E.M. Johnson, H.W. Brock, and W. An. 2008. Isolation and characterization of a novel H1.2 complex that acts as a repressor of p53-mediated transcription. *J Biol Chem*. 283:9113-26.

Knockaert, M., P. Greengard, and L. Meijer. 2002. Pharmacological inhibitors of cyclin-dependent kinases. *Trends Pharmacol Sci*. 23:417-25.

Knuesel, M.T., K.D. Meyer, A.J. Donner, J.M. Espinosa, and D.J. Taatjes. 2009. The Human CDK8 Subcomplex Is a Histone Kinase That Requires Med12 for Activity and Can Function Independently of Mediator. *Mol. Cell. Biol.* 29:650-661.

Krishnakumar, R., M.J. Gamble, K.M. Frizzell, J.G. Berrocal, M. Kininis, and W.L. Kraus. 2008. Reciprocal Binding of PARP-1 and Histone H1 at Promoters Specifies Transcriptional Outcomes. *Science*. 319:819-821.

Kulaeva, O.I., D.A. Gaykalova, N.A. Pestov, V.V. Golovastov, D.G. Vassylyev, I. Artsimovitch, and V.M. Studitsky. 2009. Mechanism of chromatin remodeling and recovery during passage of RNA polymerase II. *Nat Struct Mol Biol*. 16:1272-1278.

Labhart, P., and T. Koller. 1982. Structure of the active nucleolar chromatin of Xenopus laevis Oocytes. *Cell*. 28:279-92.

Lawrence, R.J., and C.S. Pikaard. 2004. Chromatin turn ons and turn offs of ribosomal RNA genes. *Cell Cycle*. 3:880-3.

Laybourn, P.J., and J.T. Kadonaga. 1991. Role of nucleosomal cores and histone H1 in regulation of transcription by RNA polymerase II. *Science*. 254:238-45.

Lee, H., R. Habas, and C. Abate-Shen. 2004. MSX1 cooperates with histone H1b for inhibition of transcription and myogenesis. *Science*. 304:1675-8.

Lee, H.L., and T.K. Archer. 1998. Prolonged glucocorticoid exposure dephosphorylates histone H1 and inactivates the MMTV promoter. *Embo J*. 17:1454-66.

Levy, A., M. Eyal, G. Hershkovits, M. Salmon-Divon, M. Klutstein, and D.J. Katcoff. 2008. Yeast linker histone Hho1p is required for efficient RNA polymerase I processivity and transcriptional silencing at the ribosomal DNA. *Proc Natl Acad Sci U S A*. 105:11703-8.

Lu, M.J., C.A. Dadd, C.A. Mizzen, C.A. Perry, D.R. McLachlan, A.T. Annunziato, and C.D. Allis. 1994. Generation and characterization of novel antibodies highly selective for phosphorylated linker histone H1 in Tetrahymena and HeLa cells. *Chromosoma*. 103:111-21.

Lucchini, R., U. Pauli, R. Braun, T. Koller, and J.M. Sogo. 1987. Structure of the extrachromosomal ribosomal RNA chromatin of Physarum polycephalum. *J Mol Biol*. 196:829-43.

McStay, B., and I. Grummt. 2008. The epigenetics of rRNA genes: from molecular to chromosome biology. *Annu Rev Cell Dev Biol*. 24:131-57.

Moss, T., F. Langlois, T. Gagnon-Kugler, and V. Stefanovsky. 2007. A housekeeper with power of attorney: the rRNA genes in ribosome biogenesis. *Cell Mol Life Sci*. 64:29-49.

Murayama, A., K. Ohmori, A. Fujimura, H. Minami, K. Yasuzawa-Tanaka, T. Kuroda, S. Oie, H. Daitoku, M. Okuwaki, K. Nagata, A. Fukamizu, K. Kimura, T. Shimizu, and J. Yanagisawa. 2008. Epigenetic Control of rDNA Loci in Response to Intracellular Energy Status. *Cell*. 133:627-639.

O'Sullivan, A.C., G.J. Sullivan, and B. McStay. 2002. UBF binding in vivo is not restricted to regulatory sequences within the vertebrate ribosomal DNA repeat. *Mol Cell Biol*. 22:657-68.

Olson, M.O., and M. Dundr. 2005. The moving parts of the nucleolus. *Histochem Cell Biol*. 123:203-16.

Paranjape, S.M., R.T. Kamakaka, and J.T. Kadonaga. 1994. ROLE OF CHROMATIN STRUCTURE IN THE REGULATION OF TRANSCRIPTION BY RNA-POLYMERASE-II. *Annual Review of Biochemistry*. 63:265-297.

Plata, M.P., H.J. Kang, S. Zhang, S. Kuruganti, S.J. Hsu, and M. Labrador. 2009. Changes in chromatin structure correlate with transcriptional activity of nucleolar rDNA in polytene chromosomes. *Chromosoma*. 118:303-22.

Raska, I., M. Dundr, K. Koberna, I. Melcak, M.C. Risueno, and I. Torok. 1995. Does the synthesis of ribosomal RNA take place within nucleolar fibrillar centers or dense fibrillar components? A critical appraisal. *J Struct Biol*. 114:1-22.

Ryan, C.A. 1999. Phosphorylation of Histone H1 During S Phase in Human Cells. *In* Department of Biology. Vol. Doctor of Philosophy. Boston College.

Sanij, E., and R.D. Hannan. 2009. The role of UBF in regulating the structure and dynamics of transcriptionally active rDNA chromatin. *Epigenetics*. 4:374-82.

Sanij, E., G. Poortinga, K. Sharkey, S. Hung, T.P. Holloway, J. Quin, E. Robb, L.H. Wong, W.G. Thomas, V. Stefanovsky, T. Moss, L. Rothblum, K.M. Hannan, G.A. McArthur, R.B. Pearson, and R.D. Hannan. 2008. UBF levels determine the number of active ribosomal RNA genes in mammals. *J Cell Biol*. 183:1259-74.

Santoro, R., and I. Grummt. 2001. Molecular mechanisms mediating methylation-dependent silencing of ribosomal gene transcription. *Mol Cell*. 8:719-25.

Schultz-Norton, J.R., K.A. Walt, Y.S. Ziegler, I.X. McLeod, J.R. Yates, L.T. Raetzman, and A.M. Nardulli. 2007. The deoxyribonucleic acid repair protein flap endonuclease-1 modulates estrogen-responsive gene expression. *Mol Endocrinol*. 21:1569-80.

Vicent, G.P., R. Koop, and M. Beato. 2002. Complex role of histone H1 in transactivation of MMTV promoter chromatin by progesterone receptor. *J Steroid Biochem Mol Biol*. 83:15-23.

Wang, S., and P.M. Fischer. 2008. Cyclin-dependent kinase 9: a key transcriptional regulator and potential drug target in oncology, virology and cardiology. *Trends Pharmacol Sci*. 29:302-13.

Zhu, G., S.E. Conner, X. Zhou, C. Shih, T. Li, B.D. Anderson, H.B. Brooks, R.M. Campbell, E. Considine, J.A. Dempsey, M.M. Faul, C. Ogg, B. Patel, R.M. Schultz, C.D. Spencer, B. Teicher, and S.A. Watkins. 2003. Synthesis, structure-activity relationship, and biological studies of indolocarbazoles as potent cyclin D1-CDK4 inhibitors. *J Med Chem*. 46:2027-30.

Zlatanova, J., and K. Van Holde. 1992. Histone H1 and transcription: still an enigma? *J Cell Sci*. 103 (Pt 4):889-95.

5.11 Tables and Figures

Table 5.1

Oligonucleotide Primers Used

ChIP					
loci		primer	acession number	amplified region	product length
rDNA promoter	for	GTGGCTGCGATGGTGGCGTTTT	HSU13369	-152..-23	130 bp
	rev	TGCCGACTCGGAGCGAAAGA			
GAPDH	for	AAGGAGAGCTCAAGGTCAG	NM_002046	145..282	138 bp
	rev	GAGTAGGGACCTCCTGTTTC			
ALDOA	for	AGGAAGGAAATCCAGGTTAG	NM_000034	440..541	102 bp
	rev	AATGTCGAGTAAATGCCCTA			
MyoD	for	GCCAGCACTTTGCTATCTAC	NM_002478	-111..14	125 bp
	rev	CGACAGTAGCTCCATATCCT			
MMTV GRE	for	TTTCCATACCAAGGAGGGGACAGTG			
	rev	CTTACTTAAGCCTTGGGAACCGCAA			
Sgk GRE	for	CTTCCCTTATCCAGCATGTCTTGTG		1 kb downstream	98 bp
	rev	TGCATCGTGCAATCTGTGGC			
pS2 ERE	for	CCCGTGAGCCACTGTTGTC	NM_007344	-390..-293	96 bp
	rev	CCTCCCGCCAGGGTAAATAC			

qRT-PCR					
gene		primer	acession number	amplified region	product length
pre-rRNA	for	GAACGGTGGTGTGTCGTTC	HSU13369	851..980	130 bp
	rev	GCGTCTCGTCTCGTCTCACT			
BACT	for	ATCGTCCACCGCAAATGCTTCTA	NM_001101	1189..1293	105 bp
	rev	AGCCATGCCAATCTCATCTTGTT			
MT1A	for	CTCGAAATGGACCCCAACT	NM_005946	68..286	219 bp
	rev	ATATCTTCGAGCAGGGCTGTC			
MT2A	for	CCGACTCTAGCCGCCTCTT	NM_005953	63..321	259 bp
	rev	GTGGAAGTCGCGTTCTTTACA			
H1.2	for	ACACCGAAGAAAGCGAAGAA	NM_005319	460..576	117 bp
	rev	AGCCTTAGCAGCACTTTTGG			
H1.4	for	CTCAAGAGCCTGGTGAGCA	NM_005321	250..373	124 bp
	rev	CGCCTGCCTTTTTAGCCTTA			
H1.4-flag-SR	for	CGAAGGCCAAAGCAGTTAAA	N/A	N/A	108 bp
	rev	GTACCGGATCCGTCGACTT			

Table 5.1 (cont.)

conventional RT-PCR					
gene	primer		acession number	amplified region	product length
CDK1	for	CTGGGGTCAGCTCGTTACTC	NM_001786	655..970	326 bp
	rev	CCATTTTGCCAGAAATTCGT			
CDK2	for	CATTCCTCTTCCCCTCATCA	NM_001798	527..829	303 bp
	rev	CGAGTCACCATCTCAGCAAA			
CDK7	for	GGCTCTGGACGTGAAGTCTC	NM_001799	91..436	346 bp
	rev	GGCTTTGATGTGTGATGGTG			
CDK8	for	AGGCTATGCAGGACCCCTAT	NM_001260	1009..1321	313 bp
	rev	GGATAGGCAGCATGTGGATT			
CDK9	for	AGGGACATGAAGGCTGCTAA	NM_001261	540..901	362 bp
	rev	ACCAGCTCCAGCTTTTCGTA			
GAPDH	for	TGGCGTCTTCACCACCAT	NM_002046	399..1077	679 bp
	rev	CACCACCCTGTTGCTGTA			

siRNA oligo			
histone H1.2/H1.4	sense	UCAAGAGCCUGGUGAGCAAUU	NM_001786
	antisense	UUGCUCACCAGGCUCUUGAUU	
CDK1	sense	CAAACGAAUUUCUGGCAAAUU	NM_033379
	antisense	PUUUGCCAGAAAUUCGUUUGUU	
CDK2	sense	GAAACAAGUUGACGGGAGAUU	NM_052827
	antisense	PUCUCCCGUCAACUUGUUUCUU	
CDK7	sense	GAUGACUCUUCAAGGAUUAUU	NM_001799
	antisense	PUAAUCCUUGAAGAGUCAUCUU	
CDK8	sense	CGUCAGAACCAAUAUUUCAUU	NM_001260
	antisense	PUGAAAUAUUGGUUCUGACGUU	
CDK9	sense	UAUAACCGCUGCAAGGGUAUU	NM_001261
	antisense	PUACCCUUGCAGCGGUUAUAUU	
CDK4	pool of 4 target-specific 20-25 nt siRNAs (sc-29261)		NM_000075

Figure 5.1

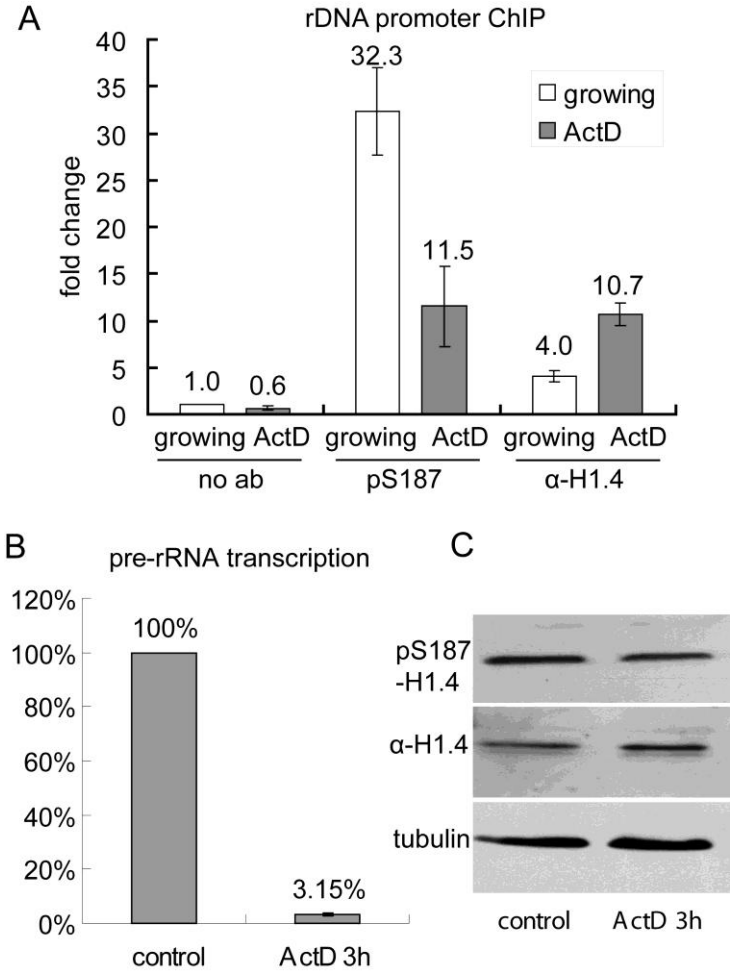

Interphase Phosphorylated H1.4 is Preferentially Associated With Transcriptionally Active rDNA

(A) The relative levels of pS187-H1.4 and total H1.4 at the 45S pre-rRNA promoter following treatment of asynchronously growing HeLa cells with actinomycin D (50 ng/ml, 3 hours) was compared to that of untreated cells using ChIP-qPCR. The data are expressed as fold change relative to immunoprecipitations performed without primary antibody from untreated cells.

(B) The levels of the 45S pre-rRNA transcript assayed by RT-PCR after three hours of treatment with actinomycin (3 hours at 50 ng/ml) are shown relative to untreated cells. The data were normalized according to β-actin expression.

(C) The global phosphorylation abundance at S187 was monitored by western blot using pS187-H1.4 antibody. Total H1.4 and tubulin were served as loading control.

Figure 5.2

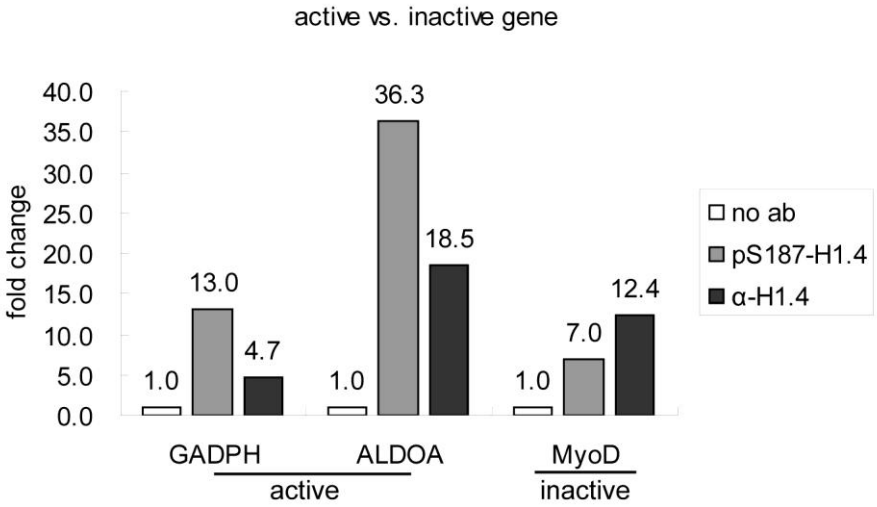

Interphase Phosphorylated H1.4 is Preferentially Associated with Transcriptionally Active Genes

The relative levels of pS187-H1.4 and total H1.4 at the housekeeping genes and inactive genes in HeLa cells were measured using ChIP-qPCR. The data are expressed as fold change relative to immunoprecipitations performed without primary antibody.

Figure 5.3

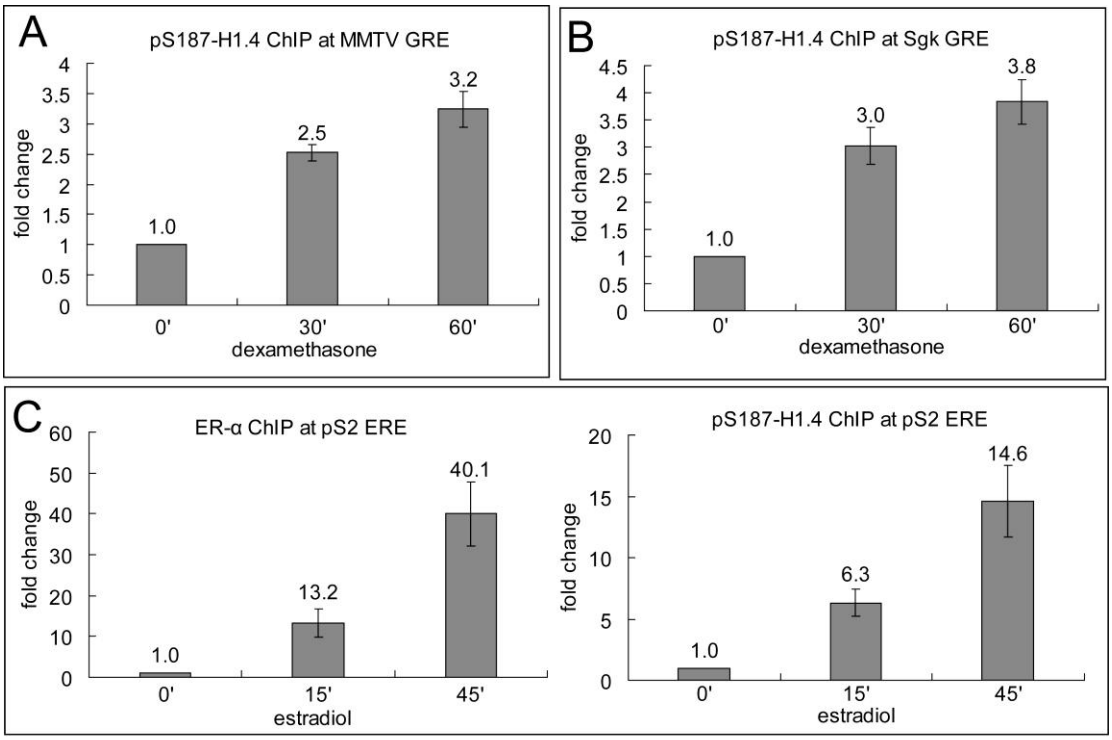

Nuclear Hormone Receptors Induce Enrichment of Interphase Phosphorylated H1.4 at Their Response Elements

(A) The association of pS187-H1.4 with the GRE of the MMTV-LTR array in 3134 cells was assessed by ChIP-qPCR before and after dexamethasone stimulation.

(B) The association of pS187-H1.4 with the GRE of the single copy Sgk gene in 3134 cells was assessed by ChIP-qPCR before and after dexamethasone stimulation.

(C) The association of ER-α and pS187-H1.4 with the ERE of the TFF1 gene in MCF-7 cells was assessed by ChIP qPCR before and after estradiol stimulation.

The data in panels A, B and C are normalized to the signal obtained for each antibody prior to hormone stimulation.

Figure 5.4

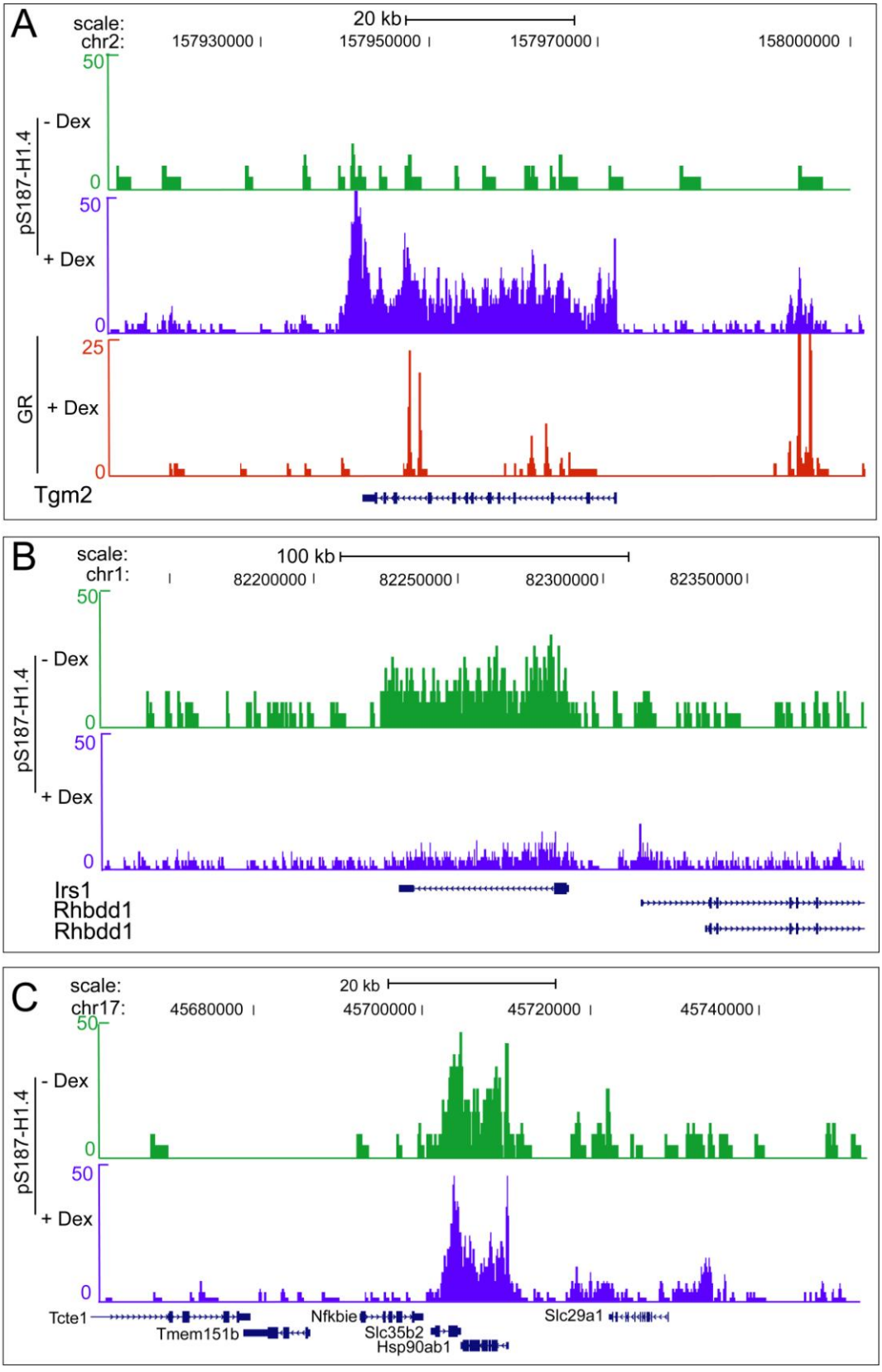
A
scale:
20 kb
chr2:
157930000
157950000
157970000
158000000
50
- Dex
0
pS187-H1.4
50
+ Dex
0
25
GR
+ Dex
0
Tgm2
B
scale:
100 kb
chr1:
82200000
82250000
82300000
82350000
50
- Dex
0
pS187-H1.4
50
+ Dex
0
Irs1
Rhbdd1
Rhbdd1
C
scale:
20 kb
chr17:
45680000
45700000
45720000
45740000
50
- Dex
0
pS187-H1.4
50
+ Dex
0
Tcte1
Tmem151b
Nfkbie
Slc35b2
Hsp90ab1
Slc29a1

Figure 5.4 (cont.)

Examples of Enrichment of pS187-H1.4 Revealed by Genome Wide Analysis

A. Hormone treatment induces the enrichment of pS187-H1.4 along the entire length of the hormone activated gene, Tgm2, starting right at the TSS and extending ~5 kb beyond the 3'UTR. In addition, enrichment of pS187-H1.4 was also observed in the 5' upstream regulatory element locus where GR binds.

B. The levels of pS187-H1.4 at hormone-repressed genes, Tgm2, fell compared to untreated cells. The association of pS187-H1.4 with genes before hormone treatment starts right at the TSS and extends ~1 kb beyond the 3'UTR.

C. The levels of pS187-H1.4 at constantly active genes, Hsp90, are kept at the constant levels. The association of pS187-H1.4 with genes in both before and after hormone treatment starts right at the TSS and extends ~2 kb beyond the 3'UTR.

Figure 5.5

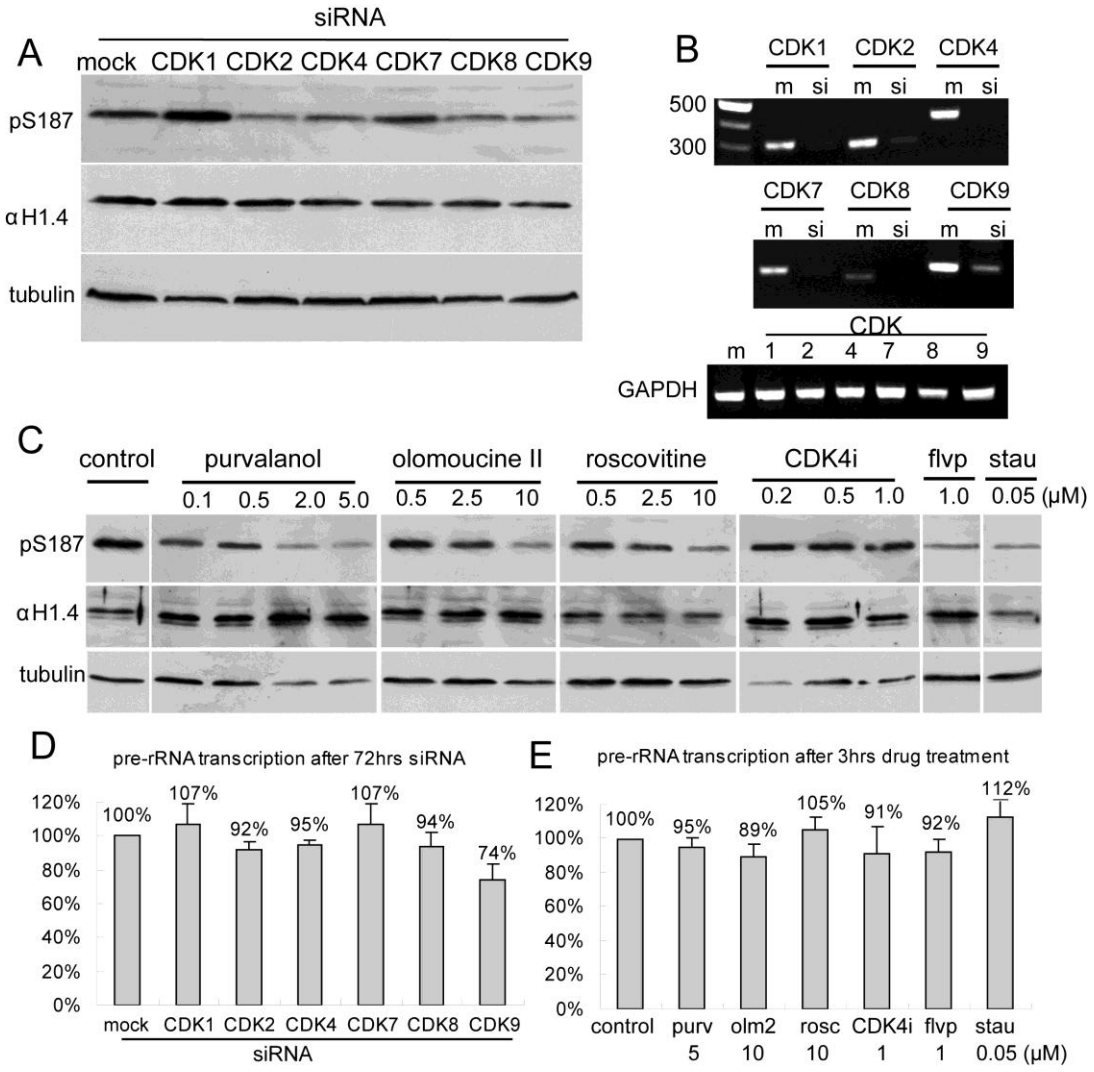

CDK2, CDK8 and CDK9 Are Potential H1 Kinases But Are Not Required For Pol I Transcription

(A) The global phosphorylation abundance at S187 in HeLa cells after CDKs knocked down by siRNA was monitored by western blot using pS187-H1.4 antibody. Total H1.4 and tubulin were served as loading control. Sample = cells lysate in 2x SDS sample buffer

(B) The mRNA expression level of CDKs after siRNA treatment was monitored by RT-PCR. GAPDH was served as loading control. (m: mock, si: siRNA)

(C) The global phosphorylation abundance at S187 was monitored by western blot using pS187-H1.4 antibody. Total H1.4 and tubulin were served as loading control.

(D) The levels of the 45S pre-rRNA transcript were assayed by qRT-PCR after expressions of CDKs were knocked down by siRNA.

(E) The levels of the 45S pre-rRNA transcript were assayed by qRT-PCR after CDKs activities were inhibited by specific CDK inhibitors.

Figure 5.6

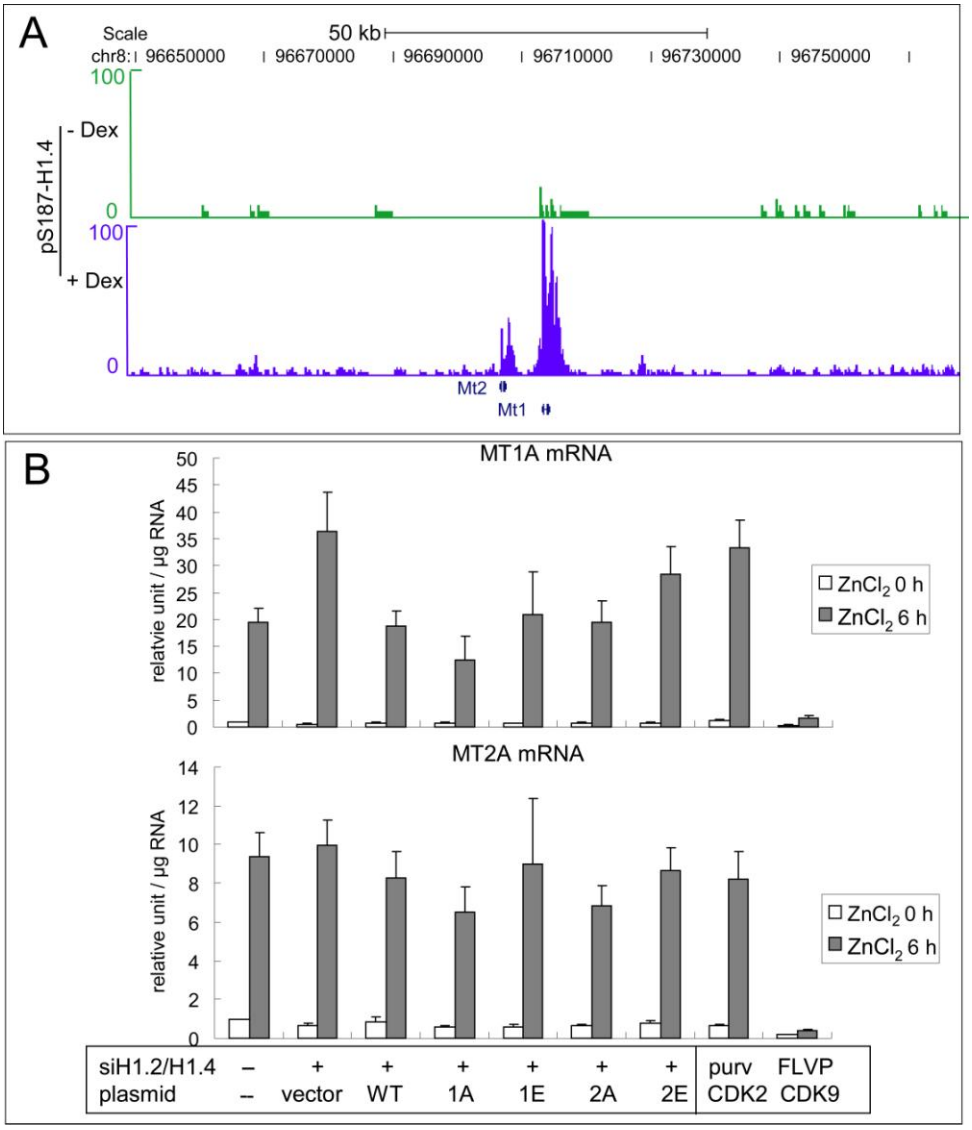

H1 Phosphorylation Is Necessary for Transcription Activation of Metallothionein

(A) Hormone treatment (-/+ 100 nM dexamethasone) induces the enrichment of pS187-H1.4 along the entire length of the metallothionein genes. The association starts right at the TSSs for both MT1 and MT2, extends ~2 kb beyond the 3'UTR of MT1 and ~1 kb beyond the 3'UTR of MT2.

(B) Endogenous H1.2 and H1.4 in HeLa cells are knocked down by siRNA for 72 hrs and were replaced with different mutants for 48 hrs. Cells were stimulated with 200 µM $ZnCl_2$ for 6 hrs. The inhibitors were also included for 6 hrs with 5.0 µM purvalanol A and 1.0 µM flavopiridol. The levels of the steady state transcript of MT1A and MT2A were assayed by qRT-PCR for different mutant replacements.

APPENDIX A

A.1 Optimization of RP-HPLC for Histone H1 Separation

We have found the condition of RP-HPLC using acetonitrile as organic modifier and TFA as ion-paring agent in mobile phase is unable to resolve most of H1 variants as indicated in Figure 3.3. We have demonstrated H1 variants from HeLa S3 are remarkably simple with only two major forms of H1.2 and H1.4 (chapter 2). Thus, we decided to use total H1 purified from HeLa S3 cells in our optimization efforts. As shown in Figure A.1 A, two partially resolved peaks were obtained in standard condition of RP-HPLC. First, the degree of separation was analyzed by TDMS and mass spectrum was shown in Figure A.1 E, demonstrated both H1.2 and H1.4 are present in the partially separated peak 2. Then we tried to improve the resolution of H1 variants in RP-HPLC with different organic modifier as well as ion pairing agent (Delgado et al., 2003; Shibue et al., 2005). Unfortunately, no better resolution was obtained with either isopropanol/methanol as organic modifier (Figure A.1 B, C, D) or perchlorate anion as ion-pairing agent (Figure A.1 F). Although it has been reported H1.2 and H1.4 can be separated in RP-HPLC when isopropanol gradient was used in 1 M pyridine-formic acid (pH 5) at 50 ℃ (Ohe et al., 1986), running at elevated temperature is not a good option for us. Therefore RP-HPLC is not a good chromatograph method for H1 separation.

A.2 Optimization of HIC for Histone H1 Separation

The facts that HIC is not able to fully resolve phosphorylated H1 down to the baseline and $H1^0$ is overlapped with 2p-H1.4 (Figure A.2 A) motivated us to optimize the conditions. Crude H1 purified from asynchronous and colchicine arrested HeLa S3 cells are used for the test. Low pH was first tested to see whether it might change the conformation of H1 to benefit the separation. It turned out only two peaks was resolved when pH < 6, which suggested even the slight decrease of charge in phosphate group will

compromise the separation (Figure A.2 A). We theorized better resolution can be achieved at higher pH since the negative charge in the phosphate increase at higher pH and indeed both phosphorylated H1.2 and H1.4 was better separated at pH 8.0 (Figure A.2 A). However, the slight improvement did not outweigh the inconvenience of column life shortening under basic condition (silica beads dissolve in basic solution). Therefore we tested different salt/buffer and column with different material but no improvement was found. It is worthy of noting that polyPROPYL A with spherical silica having 1000 Å diam. pores was not able to resolve phosphorylated H1 while the same stationary phase immobilized in silica with 1500 Å diam. pores was able to resolve the phosphorylated H1 (Figure A.2 D)

A.3 Optimization of HILIC for Histone H1 Separation

Despite the well separation of H1 variants and their phosphorylation forms achieved by HIC, the significant changes in the baseline limits its ability to resolve minor forms. Such changes is caused by the great changes in the refractive index of the mobile phase resulted from marked change in salt concentration necessary to separate H1 in HIC. HILIC is a good choice among the alternative approaches to overcome this limitation. When the weak cation exchanger polyCAT A column under predominant organic mobile phase, the hydrophilic interactions will be superimposed on the electrostatic effects and thus resolve solutes that differ in polarity but not charge. The condition for HILIC running at neutral pH (nHILIC) developed by Mizzen has successfully resolve the nonallelic H1 variants (Mizzen et al., 2000) whereas the condition running at acidic pH (aHILIC) developed by Lindner is able to resolve different phosphorylation forms from RP-HPLC purified H1.5 (Lindner et al., 1997). As described in chapter 3, we have determined the identity of most peaks for the total H1 separated by aHILIC in the mass spectrometry analyses (Figure 3.7). However, H1.3, H1.4 and H1.5 turned out to elute closely together before their phosphorylation forms. When total H1 from asynchronous

HeLs S3 was tested using the nHILIC, better resolution was found for variants as indicated by the separation of H1.2 polymorphism we discovered in HeLa S3 cells (H1.2 eluted earlier than H1.2-A142T in both H1.2-0p and H1.2-1p fractions). The determination of identity for each peak was based on the relative abundance of each form we identified previously by mass spectrometry analysis (Figure A.3 A). However, retention of H1 in the nHILIC condition was too strong, which was demonstrated by the proteins carried from one run with injection of total H1 to the three following washes with no injection (Figure A.3 B). This retention problem prevents us from using nHILIC for routine analysis of mammalian H1.

In recent years, several new stationary phases have been applied for HILIC approaches (Boersema et al., 2008). Among them, the weak anion exchanger PolyWAX has been used to retain phosphopeptide through hydrophilic interaction (Alpert, 2008). Such new separation technique is termed electrostatic repulsion-hydrophilic interaction chromatography (ERLIC). Two different interaction modes will happen when phosphorylated H1 was running in polyWAX with predominantly organic mobile phase: first, the positively charged H1 will retain through hydrophilic interaction even if they have the same charge as the stationary phase; second, phosphate group in the H1 can interact with stationary phase through electrostatic interaction. To test whether we can improve H1 separation by exploiting the repulsion effects, total H1 from asynchronous HeLa S3 was separated by HILIC with polyWAX column using the condition indicated in the Figure A.3 C. However, only five peaks were partially resolved demonstrating this technique was not suitable for H1 separation with current condition.

A.4 Optimization of CZE for Histone H1 Separation

CZE has been demonstrated to be well suited for resolving histone H1 (Kratzmeier et al., 1999; Lindner et al., 1993; Mizzen and McLachlan, 2000) with great sensitivity.

However, the migration order of H1 variants established in a species usually can not apply to other species appropriately due to the sequence divergence in the H1 variants among species. In addition, the buffer concentration and composition also influence migration order and resolution of H1 variants (Lindner, 2008).

To establish a good running condition of CZE for H1, total H1 from asynchronous growing HeLa S3 was used to test several conditions since the relative abundance of all H1 variants and their phosphorylation forms in HeLa S3 has been well characterized by us. In order to increase the difference causing by phosphorylation, we decided to run at the pH 2.5 instead of pH 2.0 (Lindner et al., 1993) and we found 10 fold increase of HPMC to 0.2% was necessary to block the histone-wall interaction caused by the electrostatic attraction between negatively charged silanol and positively charged H1. Five peaks were obtained using the condition described in the Figure A.4 A. To determine the identity of these peaks, RP-HPLC purified recombinant H1.4 (rH1.4) was spiked in the total H1 from HeLa S3 and was found eluting earlier than all human H1 (Figure A.4 B), which was very likely caused by the N-terminal acetylation of H1 in mammal cells.

Addition of sodium perchlorate has been demonstrated to be able to improve the resolution of H1 variants (Lindner et al., 1993) possibly by increasing α-helix content as suggested by circular dichroism (CD) spectroscopy study (Mizzen et al., 2000). To prevent the electrical current from collapsing when using the high ionic strength buffer containing $NaClO_4$, 25 μm ID tube was used to replace 50 μm ID tube. The six peaks separated with this condition and their relative abundance was shown in the Figure A.4 C. Compared to the known relative abundance, the predicted identity for each peak was also listed in the Figure A.4 C.

A.5 References

Alpert, A.J. 2008. Electrostatic repulsion hydrophilic interaction chromatography for isocratic separation of charged solutes and selective isolation of phosphopeptides. *Anal Chem*. 80:62-76.

Boersema, P.J., S. Mohammed, and A.J. Heck. 2008. Hydrophilic interaction liquid chromatography (HILIC) in proteomics. *Anal Bioanal Chem*. 391:151-9.

Delgado, S., M.C. Garcia, M.L. Marina, and M. Torre. 2003. Influence of the organic modifier and the ion-pairing agent in the mobile phase on the separation of soya bean proteins by perfusion liquid chromatography. Analysis of commercial dairylike soya bean products using multivariate techniques. *Journal of Separation Science*. 26:1363-1375.

Kratzmeier, M., W. Albig, T. Meergans, and D. Doenecke. 1999. Changes in the protein pattern of H1 histones associated with apoptotic DNA fragmentation. *Biochem J*. 337 (Pt 2):319-27.

Lindner, H., B. Sarg, and W. Helliger. 1997. Application of hydrophilic-interaction liquid chromatography to the separation of phosphorylated H1 histones. *J Chromatogr A*. 782:55-62.

Lindner, H., M. Wurm, A. Dirschlmayer, B. Sarg, and W. Helliger. 1993. Application of high-performance capillary electrophoresis to the analysis of H1 histones. *ELECTROPHORESIS*. 14:480-5.

Lindner, H.H. 2008. Analysis of histones, histone variants, and their post-translationally modified forms. *ELECTROPHORESIS*. 29:2516-2532.

Mizzen, C.A., A.J. Alpert, L. Levesque, T.P. Kruck, and D.R. McLachlan. 2000. Resolution of allelic and non-allelic variants of histone H1 by cation-exchange-hydrophilic-interaction chromatography. *J Chromatogr B Biomed Sci Appl*. 744:33-46.

Mizzen, C.A., and D.R. McLachlan. 2000. Capillary electrophoresis of histone H1 variants at neutral pH in dynamically modified fused- silica tubing. *ELECTROPHORESIS*. 21:2359-67.

Ohe, Y., H. Hayashi, and K. Iwai. 1986. Human spleen histone H1. Isolation and amino acid sequence of a main variant, H1b. *J Biochem*. 100:359-68.

Shibue, M., C.T. Mant, and R.S. Hodges. 2005. The perchlorate anion is more effective than the trifluoroacetate anion as an ion-pairing reagent for reversed-phase chromatography of peptides. *Journal of Chromatography A*. 1080:49-57.

A.6 Figures

Figure A.1

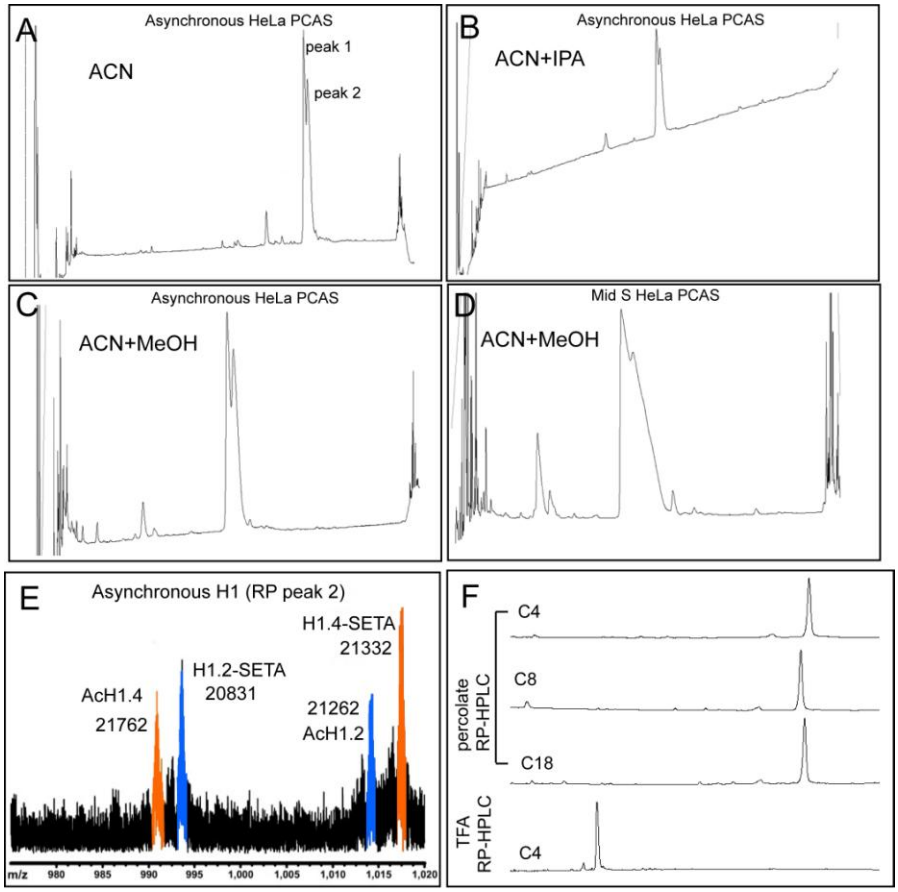

Optimization of RP-HPLC for for Histone H1 Separation

(A-D) Compare the separation of Histone H1 with RP-HPLC using different mobile phase. ES industries Chromega MC18 analytical column, 25 cm x 4.6 mm, 1000 Å diam. pores, flow rate of 0.8 ml/min. (A) Buffer A: 5% ACN, 0.1% TFA, Buffer B: 90% ACN, 0.094% TFA, gradient: 20%-40% in 140 min. (B) Buffer A: 5% ACN, 0.1% TFA, Buffer B: 40% ACN+20% IPA, 0.094% TFA, gradient: 55%-95% in 140 min. (C, D) Buffer A: 5% ACN, 0.1% TFA, Buffer B: 40% ACN+20%MeOH, gradient: 0.094% TFA gradient: 55%-75% in 140 min

(E) The mass spectrum of H1 from partially separated peak 2 in RP-HPLC, blue: H1.2, orange: H1.4.

(F) Compare the separation of Histone H1 using Vydac RP column with different length of carbon base under percolate modified condition, Buffer A: 20% ACN, 0.1 M $NaClO_4$, 10 mM phosphate, pH 2.35; Buffer B: 60% ACN, 0.1 M $NaClO_4$, 10 mM phosphate, pH 2.5.

Figure A.2

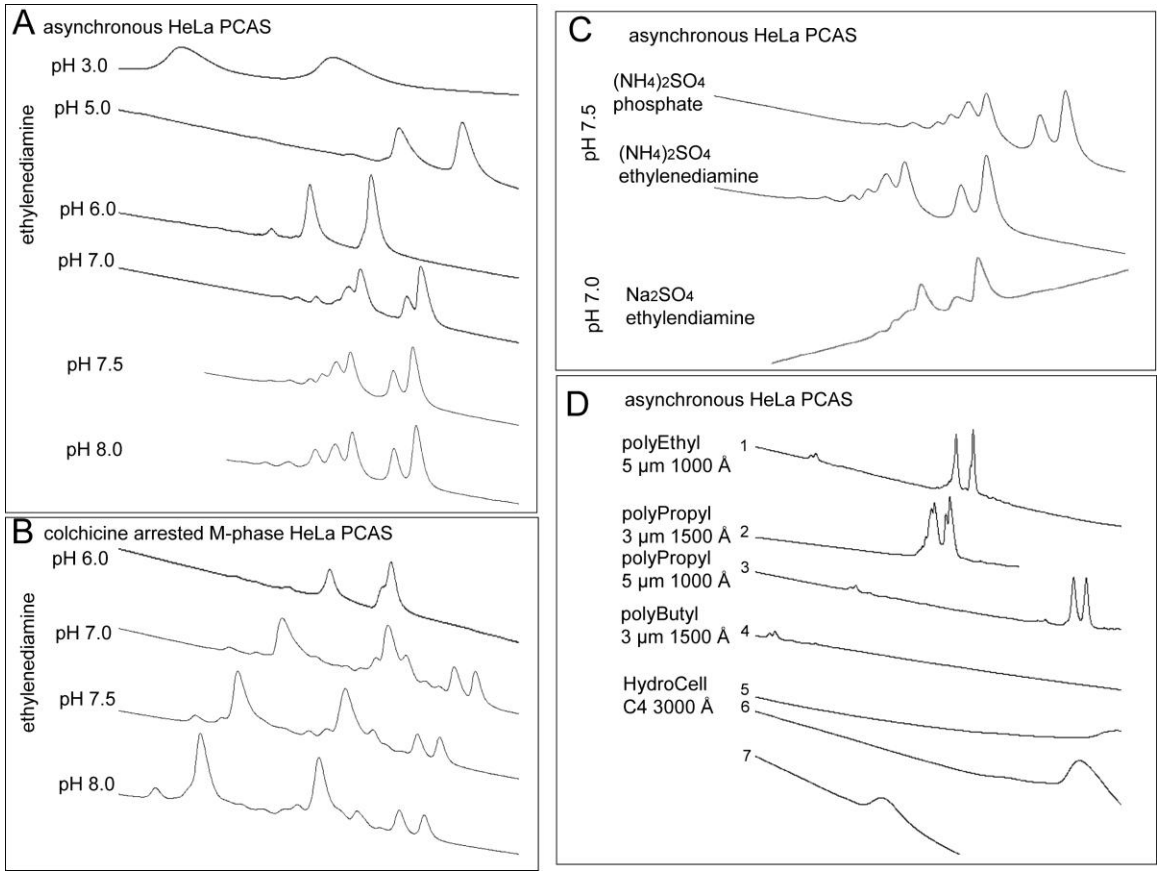

Optimization of HIC for Histone H1 Separation

Crude H1 prepared from HeLa S3 cells was analyzed by Hydrophobic Interaction Chromatography (HIC). PolyPROPYL A column (PolyLC), 100 x 4.6 mm, base = 3 µm spherical silica with 1500 Å diam. Pores, gradient: 1% B per min, flow rate of 0.8 ml/min.

(A, B, C) Effects of different pH or buffer were compared for H1 from asynchronous or colchicine arrested M phase. Ethylenediamine buffer: gradient from 2.5 M to 1.5 M $(NH_4)_2SO_4$ in 50 mM ethylendiamine, phosphate buffer: gradient from 2.0 M to 0 M $(NH_4)_2SO_4$ in 40 mM sodium phosphate.

(D) Effects of different columns (listed on the left) were compared. 1~5: gradient from 2.5 M to 1.5 M $(NH_4)_2SO_4$ in 50 mM ethylendiamine pH7.0; 6: gradient from 2.0 M to 0 M $(NH_4)_2SO_4$ in 40 mM sodium phosphate, pH7.0; 7: gradient from 2.3 M to 0 M $(NH_4)_2SO_4$ in 80 mM sodium phosphate + 20% MeOH, pH7.0.

Figure A.3

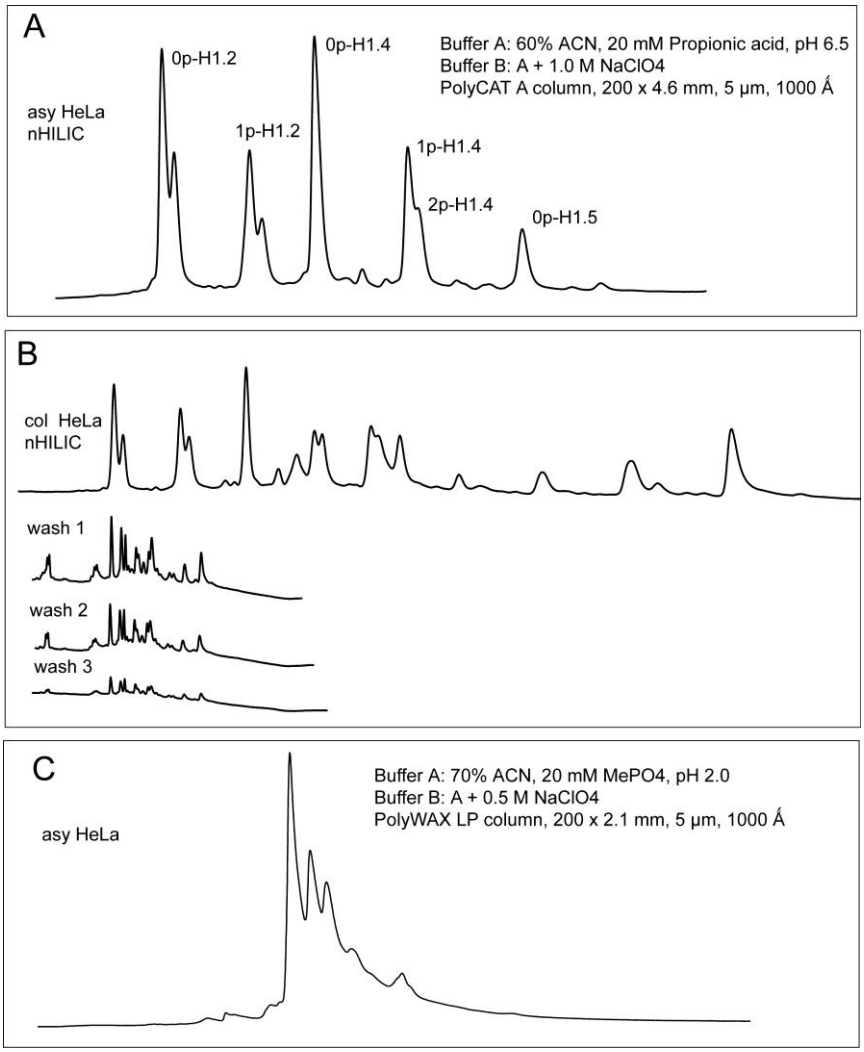

Optimization of HILIC for Histone H1 Separation

(A) Total H1 from asynchronous HeLa S3 was separated in the neutral pH by HILIC (nHILIC) using the condition noted in the figure. Compared with aHILIC (A: 70% ACN, 15 mM TEA / H_3PO_4 pH 3.0; B: A + 0.68 M $NaClO_4$), nHILIC achieved better resolution for variants as indicated by the separation of H1.2 polymorphism we discovered in HeLa cells (H1.2 eluted earlier than H1.2-A142T in both H1.2-0p and H1.2-1p fraction)

(B) Retention of H1 in the nHILIC condition was too strong to elute. Top panel: a nHILIC run of total H1 from colchicine arrested HeLa S3 with a shallow gradient; bottom panel: three washes following one run in the top panel using a fast gradient of 0-100% B in 30 min.

(C) Total H1 from asynchronous HeLa S3 was separated by HILIC using the polyWAX column and the condition noted in the figure.

Figure A.4

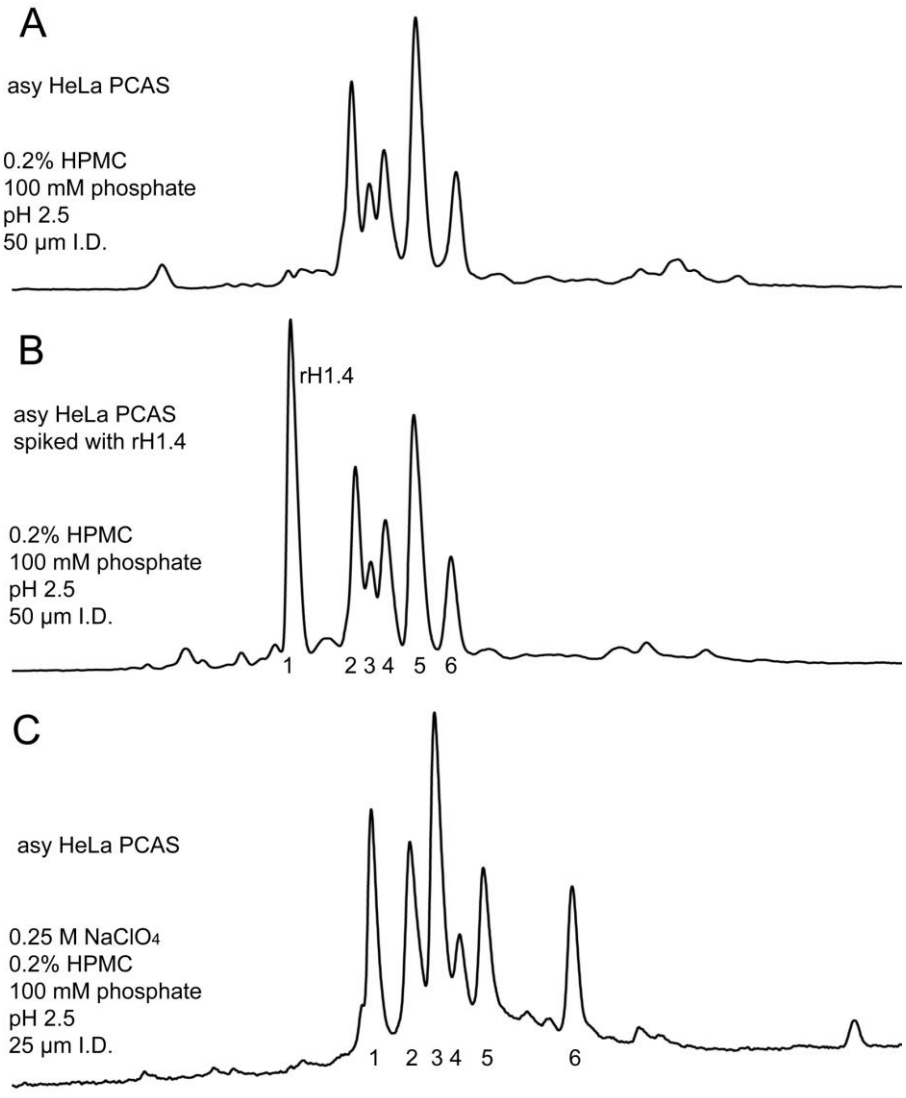

relative abudance and prediction

pk 1	pk 2	pk 3	pk 4	pk 5	pk 6
21%	19%	29%	6%	12%	13%
0p-H1.4	1p-H1.4	0p-H1.2	?	2p-H1.4	1p-H1.2

Optimization of CZE for Histone H1 Separation

Uncoated fused silica capillary with length of 60 cm, 50 cm to window and inner diameter as indicated was used in Beckman P/ACE System MDQ system under following conditions: temperature, 20 ℃; voltage, 12 kV; separation time, 40 min; sample injection by pressure, 2 psi; injection time, 10 s; absorbance detection at 200 nm. HPMC: hydroxypropylmethylcellulose

APPENDIX B

B.1 Histone H1 Phosphorylation in *Drosophila*

Before we started to investigate H1 phosphorylation in HeLa cells, we first tried to map the H1 phosphorylation sites in *Drosophila melanogaster* S2 cells since there is only a single H1 variant in *Drosophila*. The rationale is to take the advantage of single variant in order to establish the TDMS method for H1 analysis. In fact, we were able to obtain nice broadband for RP-HPLC purified H1 from *Drosophila* S2 cells. As shown in Figure B.1 A, up to 2 phosphorylations could be added to *Drosophila* H1 and the abundance of phosphorylation was relative high, with un-, mono- and diphosphorylated H1 accounting roughly ~20%, 50% and 30% of total H1. Due to some technique difficulties, we were unable to identify phosphorylation sites except localizing the phosphorylation sites to the N-terminal in the MS/MS analysis by ECD.

To test whether the levels and the abundance of phosphorylation in *Drosophila* H1 will increase like mammalian during mitosis, S2 cells were treated with 5 μM colchicine for 20 hrs but no increase of phosphorylation were observed in the mass spectrum (Figure B.1 A). However, we later found out 30 μM colchicine of colchicine is necessary to arrest S2 cells, which was much higher than the 1μM concentration we used for mammalian cells (Lemos et al., 2000). Thus whether phosphorylation in *Drosophila* H1 increases in mitosis remained unknown yet. The insufficient arrest was also evidenced by the absence of obvious increase of pS10-H3 intensity in the histone purified from colchicine treated S2 cells (Figure B.1 C). Although the 26.2 kDa *Drosophila* H1 is slightly heavier than human H1.4 (21.7 kDa), they ran to the similar position in the SDS-PAGE. However *Drosophila* H1 ran significantly slower than human H1 in acid urea PAGE and only two bands was visible for there different phosphorylation forms which was different from human H1 (addition of every phosphorylation resulted in a band up shifting, 0 to 6-p of H1 was indicated as 0~6 in Figure B.1 D).

Recent mass spectrometry mapping of the *Drosophila* H1 purified from embryo at different ages has localized the phosphorylations to the first 10 amino acid and identified

a monophosphorylated form with major site located at S10 and some minor site possible at S1 or S3. In addition, two subpopulations were found for diphosphorylated forms, one was mapped to S10 together with T7 or S8, another was mapped to S10 together with S1 or S3 (Villar-Garea and Imhof, 2008) (Figure B.1 E). The authors could not distinguish between S1 and S3 phosphorylation and T7 and S8 phosphorylation. These data demonstrated *Drosophila* H1 is phosphorylated to the moderately levels with relative high abundance in the interphase despite lacking CDK substrate motif (S/T)PXZ (where X is any amino acid and Z a basic amino acid).

B.2 Targeted H1 Phosphorylation during Transcriptional Activation

Belmont lab has developed a powerful tool that able to visualize the effects of transcription factor at a targeted chromatin locus. In this system, multiple copies of lacO/ DHFR vector were stably integrated and amplified in CHO cell. When LacI-GFP or LacI-GFP derivative in trans was provide in this derivative cell line (A03_1 cells), a homogenously staining region (HSR) can be visualized (Tumbar and Belmont, 2001). We have demonstrated phosphorylated H1 is partially colocalized with ERα after estradiol stimulation, which suggests H1 phosphorylation might play roles in the transcription activation. However, the fact that ERα is all over the nucleus make it difficult to determine which loci are actually transcribed without doing RNA FISH. Thus we decided to take advantage of CHO system by studying the phosphorylated H1 patterns in the presence of transcription activator.

To identify which H1 antibody can be used in CHO cells, whole cell lysate from CHO was used to test a panel of antibodies. Among them, pS173-H1.2 and α-H1.4 turned out to be able to react with H1 in CHO cells (Figure B.2 A). CHO cell line harboring integrated lacO repeats (A03_1) was fist transient transected with dlacI-EGFP control vector or dlacI-EGFP-VP16 plasmid, and then subjected to immunofluorescence staining of pS173-H1.2 and GFP. As expected, lacO repeat locus remained closed as indicated by a small dot-like staining of GFP when no transcription activator was targeted to the locus. By contrast, such locus became open as indicated by dramatic decondensation staining of GFP when VP16 fusion protein was targeted to the loci (Figure B.2 B). Importantly,

phosphorylated H1 was observed in the open chromatin (Figure B.2 B, C). Thus this preliminary data suggests H1 phosphorylation is present in the transcription activated loci.

To further test whether present of H1 phosphorylation in the transcription activation loci is the result of recruitment of H1 kinase, we decided to perform histone H1 kinase assay from immunoprecipitated ERα. Although we successfully pulled down ERα from MCF-7 cells (Figure B.3 B), no kinase activity was found in the immunoprecipitate as indicated by no CPM reading above the background in either recombinant H1.4 or peptide substrate (Figure B.3 A). Nonetheless, we believed it was not sufficient to disprove the hypothesis of kinase being recruited to the activated transcription loci for the phosphorylation of H1. It is possible that the interaction between kinase and ERα is transient and thus difficult to capture or H1 kinase is recruited by other component in the transcription machinery for ERα transactivation. Actually, it has been reported that CDK2 is recruited to the MMTV array upon hormone stimulation (Stavreva and McNally, 2006). Taken this result with our evidence that association of phosphorylated H1 in the MMTV array increases after dexamethasone treatment, it is reasonable to propose H1 is phosphorylated by targeted kinase.

B.3 What is the Role of H1 Phosphorylation in DNA Replication?

As described in chapter 1.9, the observation that H1 phosphorylation increases as cells transverse S phase has led to the speculation that H1 phosphorylation plays some roles in DNA replication near 30 years ago(Ajiro et al., 1981). However the direct evidence has not been reported until 5 years ago (Alexandrow and Hamlin, 2005). Once we obtained the good phosphospecific H1 antibody, we started to test this old speculation with IF staining of BrdU labeled cells. Very soon, we found out the conventional protocol requiring 2 N HCl treatment to denature the DNA for the recognition of BrdU antigen was not compatible with phosphorylated H1 staining since the acid extraction of basic H1 disrupted phosphorylated H1 staining pattern. Therefore, we used the DNAse I digestion to expose BrdU antigen. Using this approach, a partial colocalization for pS173-H1.2 or pS187-H1.4 with BrdU was found (Figure B.4 A, B), i.e. not all phosphorylated H1 were colocalized with BrdU and vice versa. Since H1 phosphorylation involves some other

processes such as transcription, thus it is reasonable that not all H1 phosphorylation are colocalized with BrdU. On the other hand, not all BrdU loci colocalized with phosphorylated H1 was a surprise to us. Does it indicated H1 phosphorylation only function in a short lived process right after replication firing? In other word, only those replication loci firing not long before the end of BrdU labeling (stop by fixation) will have phosphorylated H1. To solve this problem, we can label cells with shorter pulse of BrdU but it requires better imaging technique since DNAse I is not very efficient to expose the antigen thus signal from 30 min of labeling is already very weak. Another possibility for the partial colocalization observed is caused by chance since both BrdU foci and H1 phosphorylation foci are abundant and distributed all over the nuclear. To test this possibility, we rotated the green channel left for 90 degree and similar colocalization pattern were still observed indicated some of the staining do come by chance (Figure B.4 C). Taken these data together, whether H1 phosphorylation is involved in DNA replication remained unclear. As discussed in chapter 3, the relative abundant phosphorylation in HeLa seems not necessary for the cell survival. Hence it is reasonable to argue that fair amount of phosphorylation foci we visualized might not actively participated in any of cellular process. It might be wise to choose cells with relative low percentage of phosphorylation for immunofluorescence study of DNA replication.

B.4 Interphase Phosphorylation Diminishes Chromatin Binding by H1

Salt extraction has been adopted to investigate the association of structural proteins with chromatin as an alternative to FRAP experiments (Meshorer et al., 2006). Having the phosphospecific H1 antibody, we can directly measure the relative amount of phosphorylated H1 in the salt extraction fractions. As shown in Figure B.5, isolated nuclei were incubated with different concentration of $(NH_4)_2SO_4$ and the H1 being extracted to the supernatants or remained in the pellet were recovered by acid extraction and separated in SDS-PAGE. The amount of total H1.4 was measured by commassie blue stain while amount of phosphorylated H1.4 was monitored by western blot using pS187-H1.4. All measurements of both total H1.4 and pS187-H1.4 were normalized as percentage to the intensity from pellet with no salt extraction. This experiment clearly

demonstrated phosphorylated H1 is much easier to extract, as 80% of phosphorylated H1 was released from chromatin while only 40% of total H1 were released at 250 mM $(NH_{4)2}SO_4$ (Figure B.5). These data are consistence with the predication that phosphorylation in H1 increase its dynamic from FRAP (Contreras et al., 2003) study.

B.5 References

Ajiro, K., T.W. Borun, and L.H. Cohen. 1981. Phosphorylation states of different histone 1 subtypes and their relationship to chromatin functions during the HeLa S-3 cell cycle. *Biochemistry*. 20:1445-1454.

Alexandrow, M.G., and J.L. Hamlin. 2005. Chromatin decondensation in S-phase involves recruitment of Cdk2 by Cdc45 and histone H1 phosphorylation. *J. Cell Biol*. 168:875-886.

Contreras, A., T.K. Hale, D.L. Stenoien, J.M. Rosen, M.A. Mancini, and R.E. Herrera. 2003. The dynamic mobility of histone H1 is regulated by cyclin/CDK phosphorylation. *Mol Cell Biol*. 23:8626-36.

Lemos, C.L., P. Sampaio, H. Maiato, M. Costa, L.V. Omel'yanchuk, V. Liberal, and C.E. Sunkel. 2000. Mast, a conserved microtubule-associated protein required for bipolar mitotic spindle organization. *EMBO J*. 19:3668-82.

Meshorer, E., D. Yellajoshula, E. George, P.J. Scambler, D.T. Brown, and T. Misteli. 2006. Hyperdynamic plasticity of chromatin proteins in pluripotent embryonic stem cells. *Dev Cell*. 10:105-16.

Stavreva, D.A., and J.G. McNally. 2006. Role of H1 phosphorylation in rapid GR exchange and function at the MMTV promoter. *Histochemistry and Cell Biology*. 125:83-89.

Tumbar, T., and A.S. Belmont. 2001. Interphase movements of a DNA chromosome region modulated by VP16 transcriptional activator. *Nat Cell Biol*. 3:134-9.

Villar-Garea, A., and A. Imhof. 2008. Fine Mapping of Posttranslational Modifications of the Linker Histone H1 from Drosophila melanogaster. *PLoS ONE*. 3:e1553.

B.6 Figures

Figure B.1

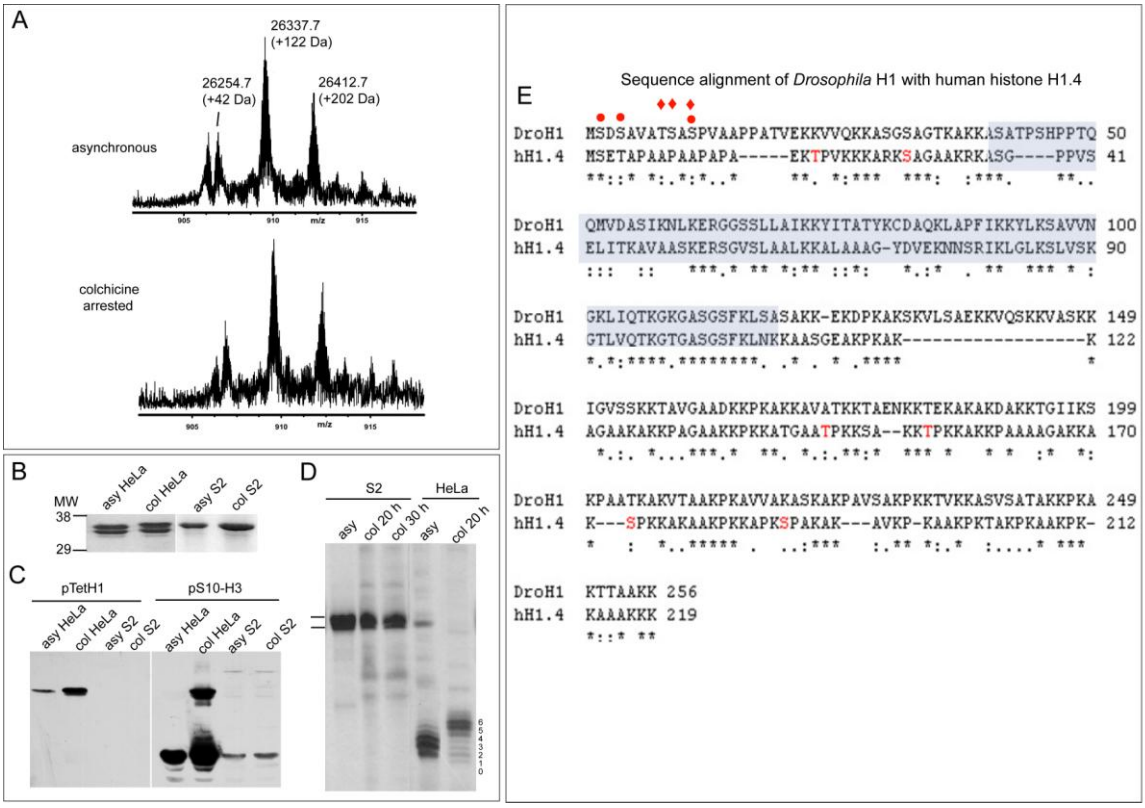

H1 Phosphorylation in Drosophila S2 Cells

(A) The mass spectrum of RP-HPLC purified H1 from asynchronously growing or colchicine arrested *Drosophila* S2 cells. Missing Met1 and α-N-acetylated at Ser2 were present in H1. Phosphorylation levels were inferred from the difference between the molecular mass measured and the value predicted for the unmodified H1. Molecular masses are reported for the neutral monoisotopic species. Abundance of phosphorylation for H1 was not increased in the cells treated with 5 μM colchicine.

(B) SDS polyacrylamide gel analysis of H1 from asynchronous or colchicine treated HeLa S3 or *Drosophila* S2 cells (1 μM for HeLa, 5 μM for S2). Molecular weight standards (MW) in kilodaltons are shown on the left.

(C) Total H1 purified from asynchronous or colchicine treated HeLa S3 or *Drosophila* S2 cells in were analyzed by immunoblotting with antisera of pTetH1 or pS10-H3.

(D) Acid urea polyacrylamide gel analysis of H1 from asynchronous or colchicine treated HeLa S3 or *Drosophila* S2 cells

(E) Sequence alignment of *Drosophila* H1 and human H1.4 variant. Globular domain in H1.4 was indicated by blue shade. Monophosphorylation of *Drosophila* H1 was mapped to S1, S3 or S10 (red circle) and diphosphorylation was mapped to S10 plus T7/S8 or S10 plus S1/S3 (red diamond) according to the MALDI-TOF analysis from *Villar-Garea et al.* (Villar-Garea and Imhof, 2008).

Figure B.2

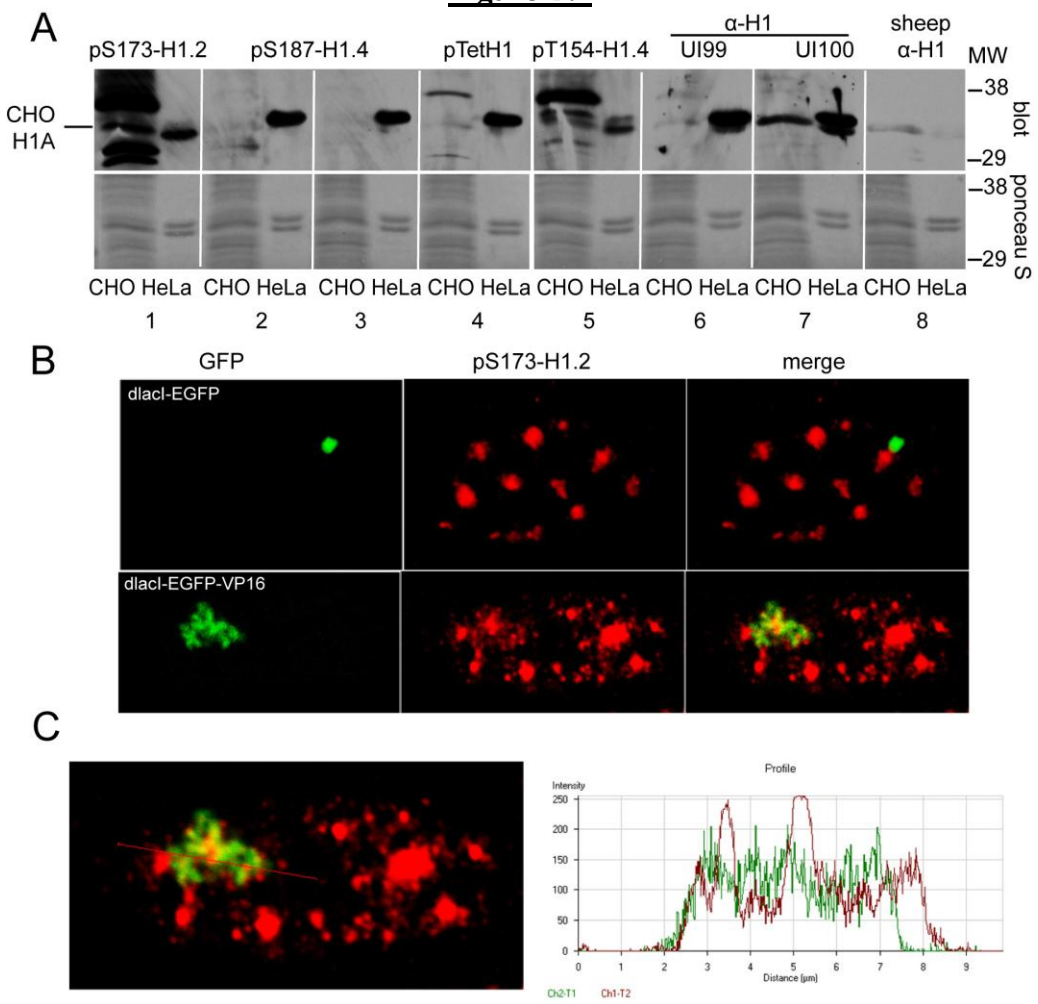

Targeted H1 Phosphorylation is Associated With Chromatin Decondensation In Vivo

(A) Whole cell lysate from CHO were used to test which antibody can be used to study H1 in CHO cells. PCAS from HeLa was used as control. 1. pS173-H1.2 (rabbit UI82 crude serum) 1:200, 2. pS187-H1.4 (rabbit UI86 crude serum) 1: 5k, 3. pS187-H1.4 (affinity purified, 0.5 µg/ml), 4. pTetH1 1:1k, 5. pT154-H1.4 (rabbit 89 crude serum) 1:500, 6. αH1.4 (rabbit UI99 crude serum) 1:1k, 7. αH1.4 (rabbit UI100 crude serum) 1:1k, 8. sheep αH1 1:1k

(B) CHO cell line carrying integrated lacO repeats was transient transfected with dlacI-EGFP control vector or dlacI-EGFP-VP16 plasmid and subjected to immunofluorescence staining of pS173-H1.2 and GFP.

(C) Profile of partial colocalization of pS173-H1.4 in the open chromatin of lacO repeat over the arbitrarily drawn line. (red: pS73-H1.2, green: EGFP-VP16)

Figure B.3

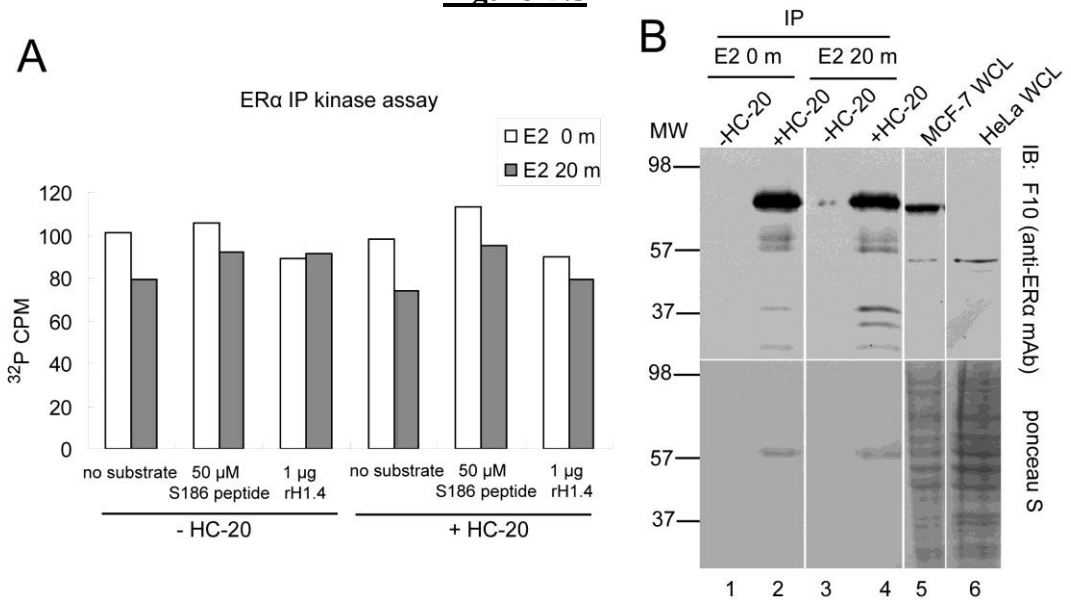

Evidence That H1 Kinase Activity is Not Associated With Liganded ER *In Vivo*

(A) MCF-7 cells received no estradiol treatment (E2 0 m) or 10 nM E2 treatment for 20 min (E2 20 m) were lysed in lysis buffer (50 mM HEPES pH 7.6, 150 mM NaCl. 5 mM EDTA, 10% glycerol, 10 mM NaF, 1 mM Na3VO4, 1% NP-40, 0.2 mM AEBSF, 50 nM microcystein). ERα was immunoprecipitated from cell lysate with or without rabbit polyclonal antibody against ERα (HC-20). The immunoprecipitate was added to 50 μl of substrate in the kinase reaction buffer (20 mM HEPES pH 7.6, 1 mM EGTA, 1 mM DTT, 5 mM $MgCl_2$, 10 mM ATP, 0.1 μCi/μl ^{32}P-γATP). The reactions were incubated at 30 °C for 30 min. 10 μl of reaction mixture was spot onto phosphocellulose P81 paper. The air dried P81 paper was washed 5 x with 0.75 % phosphoric acid, transferred to 4 ml scintillation tube with 2 ml scintillation cocktail. ^{32}P in different reactions was measured by scintillation counter.

(B) The immunoprecipitate with or without antibody before and after E2 stimulation were eluted with SDS sample buffer and were subjected to western blot to confirm the successful immunoprecipitation of ERα. Whole cell lysate from MCF-7 expressing ERα and HeLa cells lacking ERα were served as positive and negative control, respectively.

Figure B.4

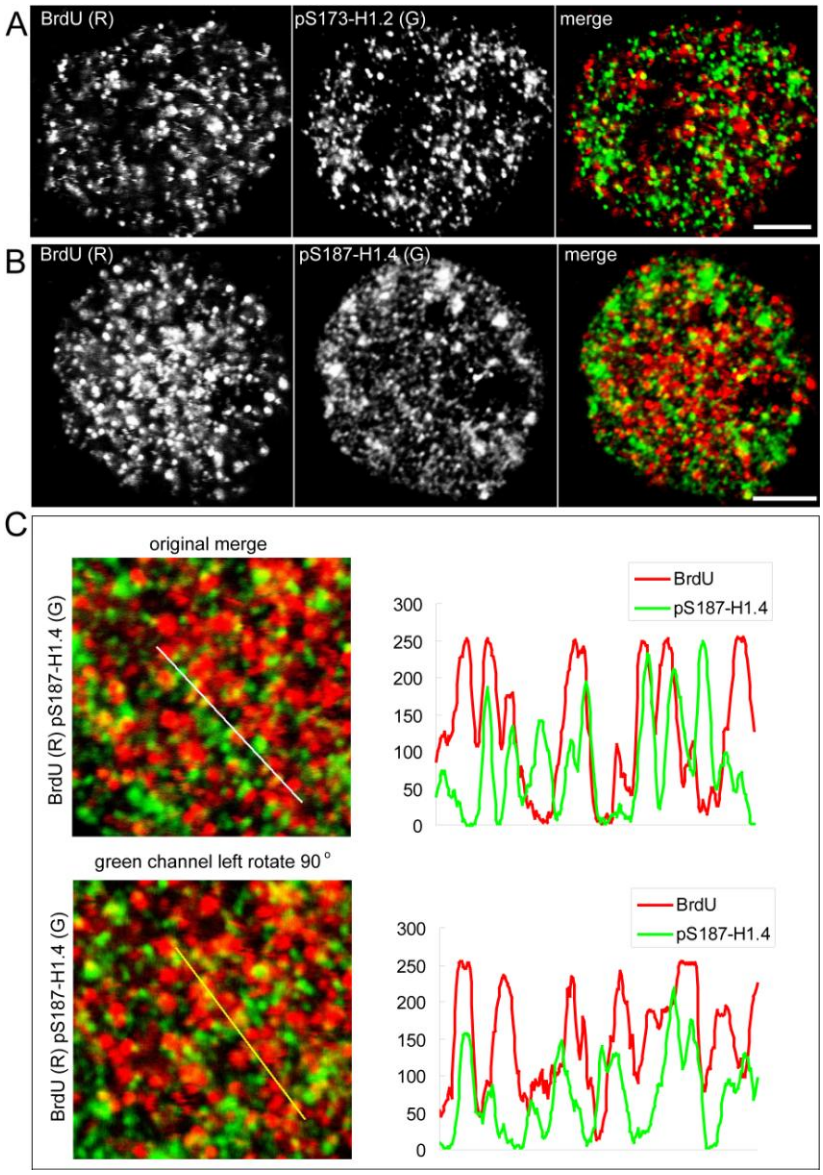

Analysis of the Colocalization of H1 Phosphorylation with Newly Synthesized DNA
(A, B) HeLa cells were labeled with 10 μM BrdU for 30 min then fixed by 4% PFA in PBS for 10 min and permeabilized in 0.2% Trion-X 100 in PBS for 3 min. Cells were incubated with DNAse I with diluted antibody in digestion solution (30 mM Tris pH 8.0, 0.3 mM $MgCl_2$, 0.5 mM β-Me, 0.2 U/μl DNAse I) at 37 °C for 1 h. After incubation with secondary antibody at room temperature for 1 h, images were collected by Zeiss LSM 510 using 63 x objective. (Scale bar = 5 μm)
(C) Upper panel: enlarged portion from merged image in B was shown; lower panel: the green channel (pS187-H1.4 staining) was rotated counterclockwise 90^o before merging with red channel. The profiles over the arbitrarily drawn line were shown.

Figure B.5

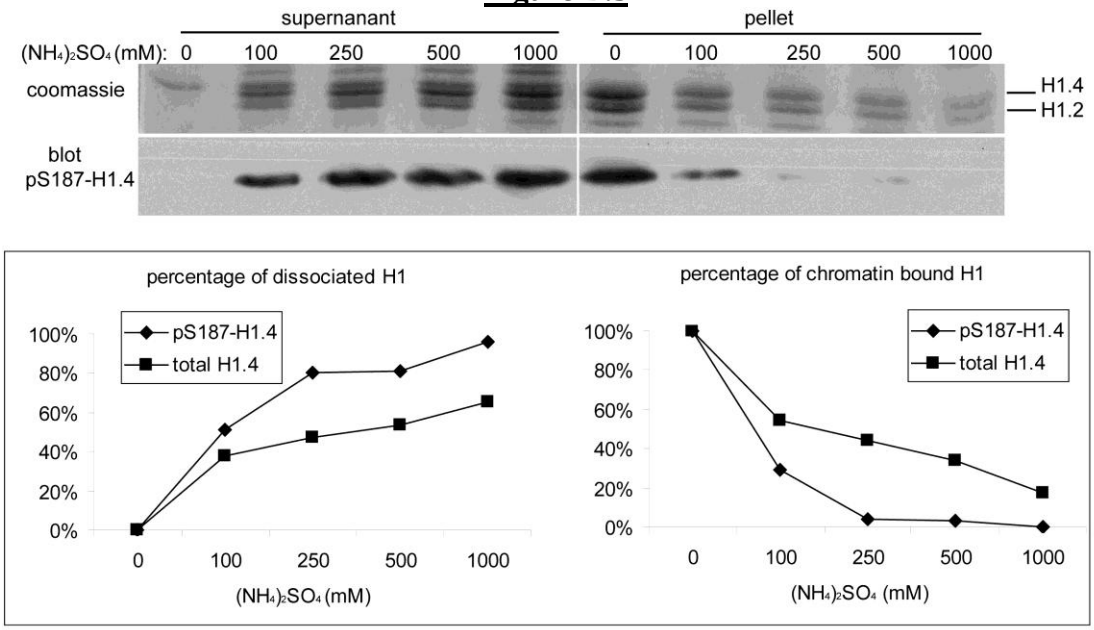

Interphase Phosphorylation Diminishes Chromatin Binding by H1
Isolated nuclei from HeLa S3 were resuspended in Buffer B (15 mM HEPES pH 7.9, 60 mM KCl, 15 mM NaCl, 0.34 mM sucrose, 10% glycerol) and incubated with different $(NH_4)_2SO_4$ concentrations (100–1000 mM) at 4 ℃ for 30 min. Both supernatants and 0.4 N H_2SO_4 acid extraction of pellet from salt extraction were precipitated with 20% TCA and separated in 15% SDS-PAGE. Amount of H1.4 was quantified from Coomassie blue staining of gel and amount of pS187-H1.4 was quantified from western blot. All values were normalized as the percentage to intensity from no salt extracted pellet.